

SELF-ORGANIZED CRITICALITY AS A
NEURODYNAMICAL CORRELATE OF
CONSCIOUSNESS:

A neurophysiological approach to measure states of
consciousness based on EEG-complexity features



Dissertation
zur Erlangung des Doktorgrades
der Humanwissenschaften
(Dr. sc. hum.)

der
Fakultät für Medizin
der Universität Regensburg

vorgelegt von
Nike Walter
aus
Braunschweig
im Jahr
2022

SELF-ORGANIZED CRITICALITY AS A
NEURODYNAMICAL CORRELATE OF
CONSCIOUSNESS:

A neurophysiological approach to measure states of
consciousness based on EEG-complexity features



Dissertation
zur Erlangung des Doktorgrades
der Humanwissenschaften
(Dr. sc. hum.)

der
Fakultät für Medizin
der Universität Regensburg

vorgelegt von
Nike Walter
aus
Braunschweig
im Jahr
2022

Dekan: Prof. Dr. Dirk Hellwig

Betreuer: *Prof. Dr. Thilo Hinterberger*

Tag der mündlichen Prüfung: 26.08.2022

Zusammenfassung

Die Theorie der selbst-organisierten Kritikalität als neurodynamisches Korrelat des Bewusstseins: Ein neurophysiologischer Ansatz zur Messung von Bewusstseinszuständen anhand EEG-basierter Komplexitätsparameter

Hintergrund und Zielsetzung

Diese Arbeit basiert auf der Hypothese, dass der aus der Physik stammende theoretische Ansatz der selbstorganisierten Kritikalität auf die neuronale Dynamik des menschlichen Gehirns angewendet werden kann. Aus der Perspektive der Bewusstseinsforschung ist dies besonders attraktiv, da die kritische Gehirndynamik eine Nähe zu einem Phasenübergang impliziert, der mit optimierten Informationsverarbeitungsfunktionen sowie dem größten Repertoire an Konfigurationen verbunden ist, die ein System während seiner zeitlichen Entwicklung durchläuft. Daher könnte die selbstorganisierte Kritikalität als neurodynamisches

Korrelat für das Bewusstsein dienen, das die Möglichkeit bietet, empirisch überprüfbare neurophysiologische Indizes abzuleiten, die zur Charakterisierung und Quantifizierung von Bewusstseinszuständen geeignet sind. Ziel dieser Arbeit war es, die Anwendbarkeit der selbstorganisierten Kritikalität als hypothetisches Korrelationsmaß für das Bewusstsein experimentell zu untersuchen. Zu diesem Zweck sollten auf der Grundlage der Analyse von drei 64-Kanal-EEG-Datensätzen die folgenden Forschungsfragen beantwortet werden:

(i) Lassen sich auf der Ebene des EEGs Signaturen selbstorganisierter Kritikalität in Form einer skalenfreien Verteilung neuronaler Lawinen und des Vorhandenseins temporaler Autokorrelationen (LRTC) in der Amplitude neuronaler Oszillationen finden?

(ii) Sind Kritikalitätsmerkmale geeignet, um Bewusstseinszustände im Spektrum des Wachseins zu differenzieren?

(iii) Kann die neuronale Dynamik durch mind-body Interventionen in Richtung des kritischen Punktes eines Phasenübergangs verschoben werden, der mit einer optimierten Informationsverarbeitungsfunktion verbunden ist?

(iv) Kann eine eindeutige Beziehung zu anderen nichtlinearen Komplexitätsmerkmalen und Leistungsspektraldichteparametern identifiziert werden?

(v) Spiegeln EEG-basierte Kritikalitätsmerkmale individuelle Persönlichkeitsmerkmale wider?

Material und Methoden

Studie (1): Reanalyse: Dreißig meditationserfahrene Teilnehmer (Durchschnittsalter 47 Jahre, 11 Frauen/19 Männer, Meditationserfahrung von mindestens 5 Jahren Praxis oder mehr als 1000 Stunden Gesamtmeditationszeit) wurden mit 64-Kanal-EEG während einer Sitzung gemessen, die aus einem aufgabenfreien Ruhezustand, einer Lesebedingung und drei Meditationsbedingungen

(gedankenlose Leere, Präsenz und fokussierte Aufmerksamkeit) bestand.

Studie (2): 64-Kanal-EEG wurde von 34 Teilnehmern (Durchschnittsalter $36,3 \pm 13,4$ Jahre, 24 Frauen/10 Männer) vor, während und nach einer professionellen Klangschalenmassage aufgezeichnet. Darüber hinaus wurden psychometrische Daten erhoben, darunter die Absorptionskapazität, definiert als die Fähigkeit Aufmerksamkeitsressourcen für sensorische und imaginative Erfahrungen einzusetzen, gemessen mit der Tellegen-Absorptionsskala (TAS-D), subjektive Veränderungen des Körpergefühls, des emotionalen Zustands und des mentalen Zustands (CSP-14) sowie die Phänomenologie des Bewusstseins (PCI-K).

Studie (3): Elektrophysiologische Daten (64 Kanäle von EEG, EOG, EKG, Hautleitwert und Atmung) wurden von 116 Teilnehmern (Durchschnittsalter $40,0 \pm 13,44$ Jahre, 83 Frauen/ 33 Männer) – in Zusammenarbeit mit dem Institut für Psychologie, Bundeswehruniversität München -während eines

aufgabenfreien Ruhezustands aufgezeichnet. Das individuelle Level der sensorischen Verarbeitungssensibilität wurde mit der High Sensitive Person Scale (HSPS-G) bewertet.

Die Datensätze wurden mit Analysewerkzeugen aus der Theorie der selbstorganisierten Kritikalität (trendbereinigende Fluktuationsanalyse, neuronale Lawinenanalyse), nichtlinearen Komplexitätsalgorithmen (Multiskalenentropie, fraktale Dimension nach Higuchi) und der Leistungsspektraldichte analysiert. In Studie 1 und 2 wurden die Aufgabenbedingungen kontrastiert und die Effektstärken mit einem gepaarten zweiseitigen t-Test verglichen. Die t-Werte wurden anhand der Falscherkennungsrate für multiples Testen korrigiert. Zur Berechnung der Korrelationen zwischen den EEG-Merkmalen wurde die Spearman-Rangkorrelation verwendet, nachdem mit dem Shapiro-Wilk-Test festgestellt worden war, dass die Verteilung nicht für parametrische Tests geeignet war. Darüber hinaus wurde in Studie 1 eine Diskriminanzanalyse durchgeführt, um die

Klassifizierungsleistung der EEG-Merkmale zu bestimmen. Hier wurden eine partielle Kleinst-Quadrat-Regression (Englisch: Partial Least Squares Regression) und eine Analyse der Grenzwertoptimierungskurve (Englisch: receiver operating characteristic, ROC) angewandt. Um festzustellen, ob die EEG-Merkmale individuelle Charaktereigenschaften widerspiegeln, wurde das individuelle Level der Absorptionskapazität (Studie 2) und der sensorischen Verarbeitungssensibilität (Studie 3) mit den EEG-Merkmalen unter Verwendung der Spearman-Rangkorrelation korreliert.

Ergebnisse

Signaturen selbstorganisierter Kritikalität in Form einer skalenfreien Verteilung neuronaler Lawinen und zeitlichen Autokorrelationen (LRTCs) in der Amplitude neuronaler Oszillationen wurden in drei verschiedenen EEG-Datensätzen nachgewiesen. Sowohl EEG-Kritikalität als auch Komplexitätsmerkmale waren geeignet,

unterschiedliche Bewusstseinszustände zu charakterisieren. In Studie 1 zeigten alle drei meditativen Zustände im Vergleich zum Ruhezustand signifikant reduzierte Autokorrelationen mit moderaten Effektgrößen (Präsenz: $d = -0,49$, $p < .001$; gedankenlose Leere: $d = -0,37$, $p < .001$; und fokussierte Aufmerksamkeit: $d = -0,28$, $p = .003$). Der kritische Exponent war geeignet, um zwischen fokussierte Aufmerksamkeit und Präsenz zu unterscheiden ($d = -0,32$, $p = .02$). In Studie 2 änderten sich die Kritikalitätsparameter im Verlauf des Experiments signifikant, wobei die Werte eine Verschiebung in Richtung des kritischen Regimes während der Klangbedingung suggerieren. Beide Analysen des ersten und zweiten Datensatzes ergaben, dass der kritische Exponent signifikant negativ mit Werten der Entropie, dem aus der trendbereinigende Fluktuationsanalyse resultierenden Skalierungsexponenten, der das Ausmaß der zeitlichen Autokorrelationen angibt, sowie der fraktalen Dimension nach Higuchi in jeder Bedingung korreliert war. Darüber hinaus wurde

festgestellt, dass der kritische Skalierungsexponent signifikant negativ mit dem Persönlichkeitsmerkmal der Absorption korreliert (Spearman's $\rho = -0,39$, $p = .007$), während ein Zusammenhang zwischen der kritischen Dynamik und dem Level der sensorischen Verarbeitungssensitivität nicht nachgewiesen werden konnte (Studie 3).

Schlussfolgerung

Die Ergebnisse dieser Arbeit legen nahe, dass die neuronale Dynamik durch das Phänomen der selbstorganisierten Kritikalität reguliert wird. EEG-basierte Kritikalitätsmerkmale erwiesen sich als sensitiv, um experimentell induzierte Veränderungen des Bewusstseinszustandes zu erfassen. Darüber hinaus wurde ein eindeutiger Zusammenhang mit weiteren nichtlinearen Maßen, die den Grad der neuronalen Komplexität - in Form von statistischer Selbstähnlichkeit - bestimmen, festgestellt. Somit scheint die selbstorganisierte Kritikalität als Korrelate für das Bewusstsein geeignet zu sein, mit dem Potential Bewusstseinszuständen zu quantifizieren

und zu charakterisieren. Die Übereinstimmung des Modells mit den derzeit einflussreichsten Theorien auf dem Gebiet der Bewusstseinsforschung wird diskutiert.

Schlüsselwörter

Selbstorganisierte
Bewusstseinskorrelate, neuronale
Phasenübergang, Komplexität,
Informationsverarbeitung,
Hochsensibilität, EEG

Kritikalität,
Dynamik,
optimale
Meditation,

Abstract

Self- organized criticality as a neurodynamical correlate of consciousness:

A neurophysiological approach to measure states of consciousness based on EEG-complexity features

Background and Objectives

This thesis was based on the hypothesis that the physics-derived theoretical framework of self-organized criticality can be applied to the neuronal dynamics of the human brain. From a consciousness science perspective, this is especially appealing as critical brain dynamics imply a vicinity a phase transition, which is associated with optimized information processing functions as well as the largest repertoire of configurations that a system explores throughout its temporal evolution. Hence, self-organised criticality could serve as a neurodynamical correlate for consciousness, which provides the possibility of deriving empirically testable neurophysiological indices suitable to

characterise and quantify states of consciousness. The purpose of this work was to experimentally examine the feasibility of the self-organized criticality theory as a correlate for states of consciousness. Therefore, it was aimed at answering the following research questions based on the analysis of three 64 channel EEG datasets:

- (i) Can signatures of self-organized criticality be found on the level of the EEG in terms of scale-free distribution of neuronal avalanches and the presence of long-range temporal correlations (LRTC) in neuronal oscillations?
- (ii) Are criticality features suitable to differentiate state of consciousness in the spectrum of wakefulness?
- (iii) Can the neuronal dynamics be shifted towards the critical point of a phase transition associated with optimized information processing function by mind-body interventions?
- (iv) Can an explicit relationship to other nonlinear complexity features and power spectral density parameter be identified?

(v) Do EEG-based criticality features reflect individual temperament traits?

Material and Methods

(1): Re-analysis: Thirty participants highly proficient in meditation (mean age 47 years, 11 females/19 males, meditation experience of at least 5 years practice or more than 1000 h of total meditation time) were measured with 64-channel EEG during one session consisting of a task-free baseline resting, a reading condition and three meditation conditions, namely thoughtless emptiness, presence monitoring and focused attention.

(2): 64-channel EEG was recorded from 34 participants (mean age 36.0 ± 13.4 years, 24 females/10 males) before, during and after a professional singing bowl massage. Further, psychometric data was assessed including absorption capacity defined as the individual's capacity for engaging attentional resources in sensory and imaginative experiences measured by the Tellegen-Absorption Scale (TAS-

D), subjective changes in in body sensation, emotional state, and mental state (CSP-14) as well as the phenomenology of consciousness (PCI-K).

(3): Electrophysiological data (64 channels of EEG, EOG, ECG, skin conductance, and respiration) was recorded from 116 participants (mean age 40.0 ± 13.4 years, 83 females/ 33 males) – in collaboration with the Institute of Psychology, Bundeswehr University Munich - during a task-free baseline resting state. The individual level of sensory processing sensitivity was assessed using the High Sensitive Person Scale (HSPS-G).

The datasets were analysed applying analytical tools from self-organized criticality theory (detrended fluctuation analysis, neuronal avalanche analysis), nonlinear complexity algorithms (multiscale entropy, Higuchi's fractal dimension) and power spectral density. In study 1 and 2, task conditions were contrasted, and effect sizes were compared using a paired two-tailed t-test calculated across participants, and features. T-values were corrected for multiple testing using false discovery rate. To

calculate correlations between the EEG features, Spearman's rank correlation was applied after determining that the distribution was not appropriate for parametric testing by the Shapiro-Wilk test. In addition, in study 1, a discrimination analysis was carried out to determine the classification performance of the EEG features. Here, partial least squares regression and receiver operating characteristics analysis was applied. To determine whether the EEG features reflect individual temperament traits, the individual level of absorption capacity (study 2) and sensory processing sensitivity (study 3) was correlated with the EEG features using Spearman's rank correlation.

Results

Signatures of self-organized criticality in the form of scale-free distribution of neuronal avalanches and long-range temporal correlations (LRTCs) in the amplitude of neural oscillations were observed in three distinct EEG-datasets. EEG criticality as well as complexity features were suitable to characterise

distinct states of consciousness. In study 1, compared to the task-free resting condition, all three meditative states revealed significantly reduced long-range temporal correlation with moderate effect sizes (presence monitoring: $d = -0.49$, $p < .001$; thoughtless emptiness: $d = -0.37$, $p < .001$; and focused attention: $d = -0.28$, $p = .003$). The critical exponent was suitable to differentiate between focused attention and presence monitoring ($d = -0.32$, $p = .02$). Further, in study 2, the criticality features significantly changed during the course of the experiment, whereby values indicated a shift towards the critical regime during the sound condition. Both analyses of the first and second dataset revealed that the critical exponent was significantly negatively correlated with the sample entropy, the scaling exponent resulting from the DFA denoting the amount of long-range temporal correlations as well as Higuchi's fractal dimension in each condition, respectively. In addition, the critical scaling exponent was found to be significantly negatively correlated with the trait absorption (*Spearman's* $\rho = -0.39$, $p = .007$), whereas an

association between critical dynamics and the level of sensory processing sensitivity could not be verified (study 3).

Conclusion

The findings of this thesis suggest that neuronal dynamics are governed by the phenomena of self-organized criticality. EEG-based criticality features were shown to be sensitive to detect experimentally induced alterations in the state of consciousness. Further, an explicit relationship with nonlinear measures determining the degree of neuronal complexity was identified. Thus, self-organized criticality seems feasible as a neurodynamical correlate for consciousness with the potential to quantify and characterize states of consciousness. Its agreement with the current most influencing theories in the field of consciousness research is discussed.

Keywords: Self-organised criticality, correlates of consciousness, neural dynamics, phase transition,

complexity, optimal information processing,
meditation, sensory processing sensitivity, EEG

Table of Contents

1. Introduction	7
1.1 Altered States of Consciousness: History, definitions and measures.....	7
1.2 Measuring the brain's complexity.....	24
1.2.1 Dynamical systems and attractors.....	28
1.2.2 Self-similarity of the EEG	33
1.2.3 Higuchi's fractal dimension	37
1.2.4 Multiscale entropy.....	44
1.3 Self-organized criticality.....	53
1.3.1 Experimental findings and functional benefits.....	61
1.3.2 Detrended fluctuation analysis	68
1.3.3 Neuronal avalanches	72
1.3.4 Clinical relevance	75
2. Research questions and Aims	82
3. Material and Methods.....	88
3.1: Mediation states	88
3.1.1 Data acquisition and participants	88
3.1.2 EEG data processing.....	91
3.1.3 Merging of topographic brain regions	98

3.1.4 Comparison between conditions	99
3.1.5 Statistics.....	99
3.2 Singing bowl experience.....	102
3.2.1 Data acquisition and participants	102
3.2.2 EEG data processing.....	105
3.2.3. Comparison between conditions	106
3.2.4 Statistics.....	106
3.3 Sensory processing sensitivity.....	108
3.3.1 Data acquisition and participants	108
3.3.2 EEG Data processing	109
3.3.3 Statistics.....	110
4. Results	112
4.1 Meditation states	112
4.1.1 Kruskal-Wallis Test.....	112
4.1.2 Global comparisons of complexity parameter	116
4.1.3 Local comparisons.....	122
4.1.4 Complexity, criticality, and spectral features for each condition	138
4.1.5 Correlations between complexity, criticality, and spectral features.....	144
4.1.6 Discrimination analysis	151

4.2 Singing bowl experience.....	156
4.2.1 Kruskal-Wallis Test.....	156
4.2.2 Global comparisons.....	157
4.2.3 Local comparisons.....	161
4.2.4 Complexity, criticality, and spectral features for each condition	167
4.2.5 Correlations between complexity, criticality, and spectral features.....	172
4.2.6 Phenomenological data	176
4.3 Sensory processing sensitivity.....	180
4.3.1 Correlations between sensory processing sensitivity, complexity, criticality, and spectral features	180
4.3.2 Differences in frequency power spectra, complexity, and criticality features between highly sensitive and not sensitive participants	182
5. Discussion.....	187
5.1 The neurophysiology of meditative states	189
5.2 Effects of a singing bowl experience	201
5.3 Criticality and sensory processing sensitivity.....	207
5.4 Self-organized criticality as a neurodynamical correlate of consciousness	211
5.4.1 Consciousness as an order parameter.....	212

5.4.2 Oscillatory synchrony.....	215
5.4.3 Coordination dynamics	225
5.4.4 The global workspace theory	228
5.4.5 The integrated information theory	232
5.5 Limitations.....	240
6. Summary	249
7.a Appendix I: t-statistics	255
7.b Appendix II: Questionnaires	270
8. References	279
9. List of acronyms, figures, and tables	335

1. Introduction

*“If the doors of perception were cleansed
every thing would appear to man as it is, infinite.*

*For man has closed himself up,
till he sees all things thro’ narrow chinks of his cavern.”*

William Blake, The Marriage of Heaven and Hell

1.1 Altered States of Consciousness: History, definitions and measures

Understanding and defining consciousness has challenged thinkers, philosophers, and scientist for decades. Nowadays, with the development of greater spatial and temporal resolution of neuroimaging methods, allowing to investigate neural correlates of states consciousness more deeply, consciousness research is reflourishing. However, as the contemporary philosopher David Chalmers puts it: “Consciousness poses the most baffling problems in the science of the mind. There is nothing that we know more intimately than conscious experience, but there is nothing harder to explain” [1, p. 200]. Therefore, no all-encompassing universally

agreed definition on consciousness exists and distinguishing often blurred lines between ordinary waking consciousness, the tip of the iceberg and alterations from it, the wide realms beneath, depicts a challenge. In the literature, consciousness has often been associated with wakefulness [2] and was defined by Searle (1993) as “those subjective states of sentience or awareness that begin when one awakes in the morning from a dreamless sleep and continue throughout the day until one goes to sleep at night or falls into a coma, or dies, or otherwise becomes, as one would say, ‘unconscious.’” [3, p. 312]. Accordingly, from the clinical perspective, unconsciousness is described as the “absence of perception of self and environment [4]. However, importantly, being awake does not necessarily imply to be conscious [5]. Keeping in mind that any definition would be tentative at best, for the scope of this thesis, consciousness will be referred to the first-person perspective filled with qualia and sensual experience, the subjective awareness of both internal and external phenomena [6]. In this context,

consciousness corresponds to the capacity of any kind of experience, “a concept that is upstream to further distinctions, such as those between levels, those between global states of consciousness (e.g. the distinction between dreaming and wakeful consciousness), and those between local states of consciousness characterized in terms of specific conscious contents or phenomenal character” [7].

While the specific modulation of states of consciousness has already been utilized by ancient culture since prehistoric times [8], Western psychology opened up to this field of research in the beginning of the 20th century, when William James made the pioneering statement in his lectures on the varieties of religious experience that “our normal waking consciousness, rational consciousness as we call it, is but one special type of consciousness, whilst all about it, parted from it by the filmiest of screens, there lie potential forms of consciousness entirely different. We may go through life without suspecting their existence; but apply the requisite stimulus, and at a touch they are there in all their

completeness, definite types of mentality which probably somewhere have their field of application and adaptation. No account of the universe in its totality can be final which leaves these other forms of consciousness quite disregarded“ [9, pp. 378-378]. During that time psychology was mainly influenced by behaviourism concentrating on operant and classical condition to modify behaviour based on work from Ivan Pavlov [10], John B. Watson [11] and B. F. Skinner [12]. Also, psychoanalysis was driving the field established by Sigmund Freud [13], who believed that an individual’s personality had three components affected by unconscious processes. Out of Freud’s theories, a number of schools developed in Europe, such as the ‘individual psychology’ by Alfred Adler [14], the ‘will therapy’ by Otto Rank [15] and the theory of the collective unconsciousness and archetypes by Carl Jung [16]. In the early 1950s a third force called humanistic psychology arose highlighting the human potential including higher functions of the psyche and qualities empathy and love. This was mainly initiated by Carl Rogers, who

revolutionized psychotherapy with his client-centered approach [17] and Abraham Maslow, who elaborated on his prominent hierarchy of needs, a model including the concept of self-actualization, a development towards personal growth, fulfilment, appreciation of life and the realization of one's abilities [18]. Within the zeitgeist of the late 60s, shaped by revolutionary cultural movements in the United States and a growing interest in Eastern spiritual systems, Maslow replaced the top of his hierarchy of human needs with the motivational level of self-transcendence [19]. In the same stance, Arnold M. Ludwig wrote in 1966: "Beneath man's thin veneer of consciousness lies a relatively uncharted realm of mental activity, in nature and function of which have neither systematically explored nor adequately conceptualized", firstly coining the term Altered States of Consciousness (ASC), which set a cornerstone for research into the spectrum in which experience may be organized. In this work, he defined ASCs as "any mental state(s), induced by various physiological, psychological, or

pharmacological maneuvers or agents, which can be recognized subjectively by the individual himself (or by an objective observer of the individual) as representing a sufficient deviation in subjective experience of psychological functioning from certain general norms for that individual during alert, waking consciousness" [20, p.225]. A year later, a small working group of psychologists aimed at "creating a new psychology that would honour the entire spectrum of human experience, including various non-ordinary states of consciousness" [21, p. 3]. Subsequently, the Association of Transpersonal Psychology was launched in 1967, also founding the Journal of Transpersonal Psychology [19]. Transpersonal psychology was devoted to higher order development. Lajoie and Shapiro executed a review of 40 definitions published during the first two decades of the beginning of transpersonal psychology concluding that it "is concerned with the study of humanity's highest potential, and with the recognition, understanding, and realization of unitive, spiritual, and transcendent states of consciousness"

[22, p.91]. Proceeding, Charles T. Tart collected existing work in this domain with the purpose “to make this a respectable field of investigation” and emphasized “that one could scientifically approach altered states of consciousness” for which he provided the following definition: “An altered state of consciousness for a given individual is one in which he clearly feels a qualitative shift in his pattern of mental functioning, that is, he feels not just a quantitative shift (more or less alert, more or less visual imagery, sharper, duller, etc.), but also that some quality or qualities of his mental processes are different” [23, pp 1 and 8]. Further, Tart used the term discrete states of consciousness defined as “a unique, dynamic pattern or configuration of psychological structures” [24, p.5]. Tart also pointed out that Western psychology tends to assume that “a healthy personality is one which allows the individual to be well-adjusted in terms of his culture” [25, p.86]. Thus, according to Walsh, the implementation of Eastern therapy drawn from Buddhist, Hindu and Taoist knowledge systems in the domain of

transpersonal psychology can “change the deeper beliefs underlying collective pathology that keep us identified with an erroneous self-sense, trapped at conventional levels of development, and unaware of the true nature of our mind and identity” He further states that “our ordinary state of mind is considerably more dysfunctional, uncontrolled and underdeveloped than we usually recognize. This results in an enormous amount of unnecessary personal, interpersonal and social suffering...it is possible to train and develop the mind beyond conventionally recognized limits and thereby overcome the usual dysfunction and lack of control. This can enhance happiness, wellbeing, and psychological capacities to remarkable degrees “[26, p.6]. Also, for Stanislav Grof, who focused on what he calls “technologies of the sacred” such as psychedelic drugs and specific breathing methods [27], the term altered states reflects the belief of mainstream psychiatrists “that only the everyday state of consciousness is normal and that all departures from it without exception represent

pathological distortions of the correct perception of reality and have no positive potential" [21, p.5]. Clarifying that "Transpersonal psychology is interested in a significant subgroup of these states that have heuristic, healing, transformative and even evolutionary potential", he coined the term "holotropic" state, literally translated as "oriented towards wholeness" [21, p.5, 19].

In the early 90s, G. William Farthing characterized ASC as "a drastic change in the overall patterns of subjective experience, which is accompanied by major differences in the cognitive as well as physiological functions. For typical examples we can consider here such states as sleeping, hypnagogic and hypnotic states, a variety of meditative, mystical and transcendent experiences, and all of the psychedelic states of consciousness induced by drugs, etc" [28, pp.202-203]. Additionally, he structured his explanations in the following points: i) ASCs are not merely changes in the content of consciousness; ii) ASCs involve a changed pattern of subjective experience, not merely a change in one

aspect or dimension of consciousness; iii) ASCs are not necessarily recognized by the individual at the time that they are happening; they may be inferred afterwards; iv) ASCs are relatively short-term, reversible conditions; v) ASCs are identified by comparison to the individual's normal waking state of consciousness; vi) The essence of a state of consciousness is the individual's pattern of subjective experience, not his or her overt behavior or psychological response. Following the attempts to categorize ASCs, Fischer mapped a variety of conscious states on a perception-hallucination-meditation continuum, differentiating between ergotropic and trophotropic arousal. While the first describes aroused, hyperaroused up to ecstatic states, the latter refers to tranquil and hypoaroused states [29]. Other authors conceptualized ordinary and ASC as a function of arousal and absorption [30]. In their work "psychobiology of altered states of consciousness" Vaitl and colleagues highlighted that a valid overarching model for ASCs is missing and remarked domains associate with alterations of

consciousness classified by the method of induction. Here, the categories span from spontaneously occurring (states of drowsiness, daydreaming, hypnagogic states, sleep and dreaming, near-death experiences), physically and physiologically induced (extreme environmental conditions such as pressure or temperature, starvation and diet, sexual activity and orgasm, respiratory manoeuvres), psychologically induced (sensory deprivation, homogenization, and overload, rhythm-induced trance, relaxation, meditation, hypnosis, biofeedback), to disease induced (psychotic disorders, coma and vegetative state, epilepsy) and pharmacologically induced [31]. Also, it has been argued that ASC share certain features regardless of their induction method [32]. Whereas the concept of altered states of consciousness is still under an ongoing debate [33, 34], much effort has been done to develop measures to assess the subjective experience of perceptual alterations. For instance, in 1995 a series of 11 experiments containing different induction methods was compiled on 1133 probands

in six countries to test the hypothesis that ASC have major dimension in common regardless of their induction. Here, a phenomenological approach was used applying the Abnormal Mental States (ABZ) questionnaire. Psychometric results revealed three shared dimensions, namely “oceanic boundlessness”, “dread of ego dissolution” and “visionary restructuralization” [35, 36]. From there on, the original version from Dittrich and colleagues was revised and refined [37] and a variety of different questionnaires were developed such as the Phenomenology of Consciousness Inventory (PCI) [38], the Mystical Experience Questionnaire [39] or the Ego-Dissolution Inventory [40]. For a comparison between the phenomenological descriptions of differently induced ASCs, the Altered States Database has been introduced recently, extracting data from a specified set of standardized questionnaires [41]. Whereas the above-mentioned metrics assess the subjective experience as a multidimensional phenomenon including domains such as perception, imagery or working memory,

core characteristics of an ASC experiences can be summarized as an joint alteration in the experience of space and time [42, 43], a “sense of timelessness and spacelessness” [44]. Importantly, however, ASC should not be based on changes in phenomenal consciousness per se [34] and neurophenomenological research programs were launched to bridge the gap between first- and third person approaches [45, 46]. Hence, to measure ASC, besides determining individual pattern in psychometric data, features of electrophysiological data underlying the induced altered state have to be characterized (Figure 1). On the search of electrophysiological markers for consciousness multiple neurobiological theories were proposed [47–50]. Especially, the attempt of unrevealing the “neural correlates of consciousness (NCC) paved the way for scientific approaches to consciousness as based on the premise that phenomenal experience is entailed by neuronal activity in the brain [51]. Thus, the obstacle of the hard problem, which describes the obstacle of the qualia of subjective experience, the

philosophical question of ‘what it is like” [52] has not been hindered progress in consciousness research anymore [53].

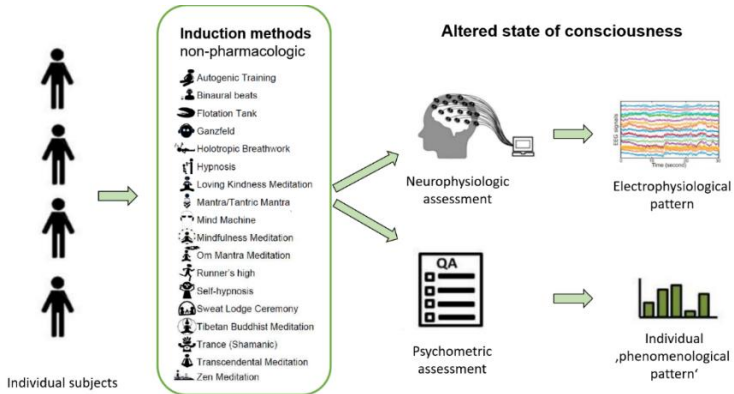


Figure 1: Neuroscientific approach to measure altered states of consciousness. To associate phenomenological changes to underlying neuronal mechanisms, ASCs can be induced experimentally. For this, besides substance-based approaches, a variety of non-pharmacological induction methods such as breathing techniques, meditation practices or sensory deprivation can be utilized. By investigating phenomenological states and electrophysiological patterns simultaneously, subjective experience can be mapped onto brain functions. Comparisons across studies capturing a broad range of ASC experiences may lead to the identification of common structures shared by differently induced ASCs. Modified from [54].

A huge body of literatures exists correlating changes in oscillatory brain activity with ASC [31]. Several candidate neurophysiological parameters were investigated, comprising for instance frequency-specific synchronization across different brain areas, local gamma response and event-related potentials such as the contingent negative variation or the P3b component. However, most of them have proved illusory [55]. For example, it has been observed that gamma synchrony increases during non-rapid eye movement (NREM) sleep, anaesthesia or seizures [56, 57] and the P3b was shown to have a low sensitivity regarding the discrimination of vegetative and minimally conscious states [58–60]. Thus, decades of research on the physical substrate of consciousness did not lead to an agreement on the topic [7]. Therefore, one of the most compelling topics in consciousness sciences still remains finding a reliable biomarker capturing states of consciousness. In other words, computational measures that successfully quantify global brain states from electrophysiological data are required as

indices of consciousness [61]. Also, instead of solely describing correlations, such markers should be embedded in functional frameworks explaining the mechanisms underlying changes in the state of consciousness [31]. In the literature, there is a consensus that consciousness relates to neural dynamical complexity, which can be assessed with quantitative measures [2, 62, 51, 55, 63]. Accordingly, novel indices capturing the degree of differentiation (the repertoire of different firing patterns) and integration (neural activity behaving as a single entity) could be applied and ASC can be approximated as the results of quantitative changes in the level of complexity [64, 55]. Investigating markers suitable to capture how neural signals combine, dissolve, and reconfigure over time would be of special interest not only, although especially in the field of psychotherapy research. Psychological and psychosomatic interventions aim at modifying a patient's mindset, i.e. the emotional and cognitive disposition or the embodied self-perception. Therefore, a broad range of techniques enabling a

modification of the state of consciousness found their way in therapeutical practice [65]. For instance, the concept of mindfulness has been incorporated into a number of evidenced-based clinical interventions [66, 67]. It is assumable that changes in neuronal complexity patterns occur in the course of therapeutic processes and measures could be useful for the evaluation of effectiveness [68]. Further, from a clinical perspective, such analytical tools could be important for advances in diagnosis paving the way for determining generalizable fingerprints of disorders of consciousness [63].

In the following I will outline basic principles underlying the umbrella term “chaos and complexity” and introduce methods based on the dynamical system approach to capture brain state activity on multiple spatial-temporal scales. In particular, I will elaborate on the concept of self-organized criticality (SOC), originally stemming from physics. This model will be adapted to the brain dynamics and the usefulness of criticality measures as general gauges of information processing and potential classifiers for

discriminating global states of consciousness will be investigated.

*"The mind as a whole is self-similar
no matter whether it refers to the large or the small."*

Anaxagoras, Fragment No. 12 (456 BC)

1.2 Measuring the brain's complexity

In a special issue of the journal *Science* for its 125th anniversary in the year 2005, scientific knowledge gaps were addressed with 125 questions, which have not yet been solved. The most fundamental was "What is the universe made of?", followed by "What is the biological basis of consciousness?" [69]. Thus, answering elementary questions such as "How are those myriads of elements and interactions coordinated together in complex living creatures?" or "How does coherent behaviour emerge out of such a soup of highly heterogeneous components?" as already posed in 1944 by Schrödinger [70] is still contemporary. With the aim of finding general principles, that could underlie the large-scale

organization of biological complexity, approaches from Statistical Physics have been transferred and adapted to investigate living organisms [71]. Especially in neuroscience, the understanding of how the interaction of billions of neurons coordinated across multiple scales produces emergent phenomena such as cognition, behaviour and consciousness has been inspired researchers to incorporate interdisciplinary perspectives.

A prominent non-invasive electrophysiological technique to measure electrical activity arising from the brain is the electroencephalography (EEG). This method records voltage fluctuations on the scalp associated with neuronal ionic current representing the summation of inhibitory and excitatory postsynaptic potentials. Given its high temporal resolution in a millisecond range, the EEG is beneficial in the evaluation of dynamic neuronal functioning. Historically, the first EEG recording was performed by Richard Caton, a British physician, in 1875, who recorded electrical activity in rabbits and monkeys. Half a century later, in 1929, the Germany

psychiatrist Hans Berger used EEG in human [72, 73]. Until the 1980s, EEG signals were registered on paper tape allowing for an interpretation of frequency of EEG waves by counting pen sways per seconds. With the introduction of computers enabling numerical registration of EEG-signals, spectral analysis methods such as the fast Fourier transform (FFT) and wavelet transforms were developed, converting the signal in the frequency domain [74]. Hitherto these linear methods have been the “gold standard” in the analysis of electrophysiological data, characterizing the signal according to the five major brain rhythms (Table 1). Also, diverse correlations with cortical functions were observed [75]. However, for unveiling the functional role of these rhythms in major cognitive functions such as attention and multi-modal coordination, the classification solely based on the frequency range has been shown to be too simple [76].

Table 1: EEG spectral bands.

Rhythm	Frequency range [Hz]
delta (δ)	1-4
theta (θ)	4-8
alpha (α)	8-12
beta (β)	12-30
gamma (γ)	>30

Nowadays, the dynamical system approach has become widespread in neuroscience and a fair amount of research suggests that nonlinear methods are more appropriate for EEG-analysis [77, 78, 79 80]. Indeed, linear approaches rely on the assumption of stationary, whereas real biological time series are nonstationary, meaning that statistical properties such as its mean value, standard deviation, or correlation function change with time. Hence, these may yield faulty results. Whereas the dynamical system approach found its way into research and academic training [78], these methods have not yet been implemented into everyday clinical practice [81].

1.2.1 Dynamical systems and attractors

A dynamical system depicts a model that determines the evolution in time solely based on the initial state, hence, implying that the system has memory. A variety of dynamical systems exist. For instance, there are linear systems, showing a relation between causes and effects. There also are nonlinear systems, in which small causes may have large effects. If quantities of the systems are preserved over time, nonlinear systems are termed conservative, whereas dissipative systems are thermodynamically open [77]. Mathematically dynamical systems are described by a coupled set of first-order ordinary differential equations [82]:

$$\frac{d\vec{x}}{dt} = \vec{F}(\vec{x}(t)) \quad (1)$$

where the vectors \vec{x} are the dynamical variables of the system evolving in continuous time. For detailed mathematical background the reader is referred to the work by Henry and colleagues (2001) as well as Kantz and Schreiber (2004) [83, 82]. Accordingly, the variables describe the state of a system. Each

possible state of a dynamical system can be represented by a point in a so-called phase space, an abstract multidimensional space. A sequence of points $x(t)$ solving the equations is termed a trajectory of the dynamical system. In cases of dissipative systems, the trajectory will converge to a subset of the phase space with proceeding time. The subspace is termed attractor as it 'attracts' trajectories from all possible initial conditions [77].

Hereby, attractors can vary in their form. For instance, in linear deterministic dissipative systems the attractor is a simple point in state space (point attractor). The repertoire of nonlinear system dynamics also includes limit cycles, which represent closed loops corresponding to periodic dynamics, torus attractors corresponding to quasi-periodic dynamics as well as strange or chaotic attractors corresponding to deterministic chaos. A famous example for the latter is the Lorenz attractor as depicted in Figure 2 defined by the following

equations: $\frac{dx}{dt} = \sigma(y - x)$, $\frac{dy}{dt} = x(p - z) - y$ and $\frac{dz}{dt} = xy - \beta z$ [84]:

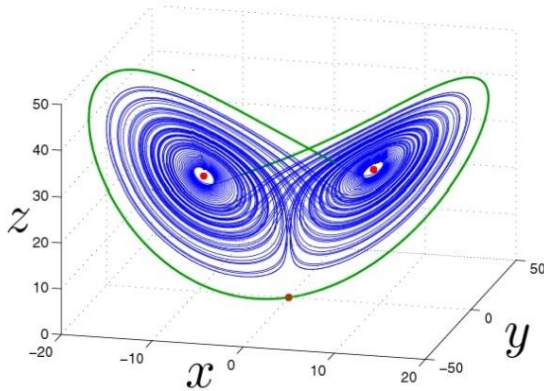


Figure 2: Numerical visualization of the Lorenz attractor as example of a three-dimensional nonlinear dynamical systems which shows chaotic behaviour with the parameters $p = 28$, $\sigma = 10$, $b = \frac{8}{3}$. Modified from [85].

To characterize the dynamics of a nonlinear system several techniques are used. For instance, the dimension of the attractor can be captured in degrees of freedom or the ‘complexity’ of the dynamics. In cases of point attractors this would be zero and for limit cycles one, whereas a torus would have an integer dimension in accordance to the number of

superimposed periodic oscillations. A strange or chaotic attractor would yield a fractal dimension, a non integer number (e.g. 2.16) [77]. In general, biological systems are dissipative and thermodynamically open, exchanging entropy with the environment [86]. This accounts also for the brain, which has the capacity to form strange attractor with fractal properties [87].

Further, in dynamical systems such as the brain, attractors can coexist [88]. In cases of one or more attractors in the dynamical structure of a system, the condition is termed bi- or multistability [89]. The systems' coordination can be changed by different mechanisms. The first is called bifurcation and describes a modulation of a control parameter on which the "attractor landscape" is based on beyond a critical threshold. In case neural networks these could include for instance the balance between excitation and inhibition dependent of certain concentration of neurotransmitters [90]. Secondly, perturbation, noise or energy can transiently destabilize the coordination dynamics and cause a

system to lose a pre-existing attractor (Figure 3A) [89]. Additionally, dynamical system can be metastable, meaning that there are no attractors in such regime, however, some traces of fixed points are still present, which are sometimes called ‘ghost’ attractors [91, 88]. These are successively visited in the time course, whereby no input or energy expenditure is required (Figure 3B) [89].

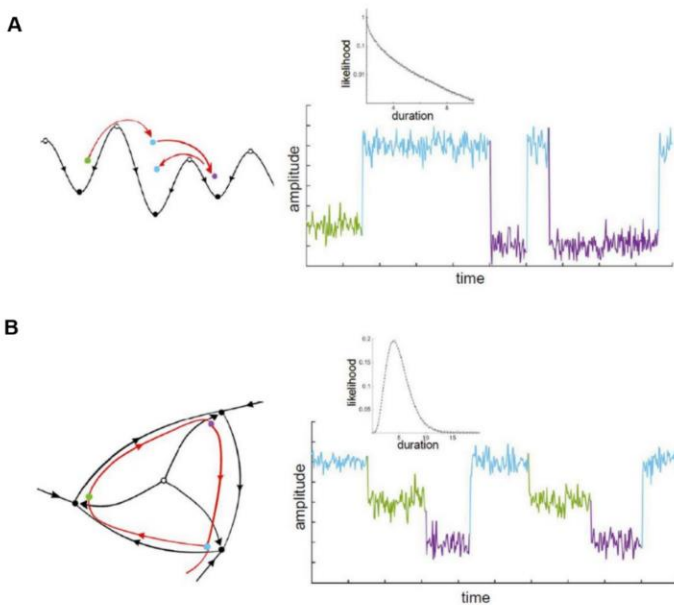


Figure 3: Coordinated system dynamics. (A) Multistable systems can switch between attractors. As the system is briefly

dwelling in each attractor basin, time series are characterized by long-tailed distributions (here shown on a logarithmic scale). (B) Metastable systems do not have attractors, rather a sequence of unstable fixed points and time series are associated with gamma distributions (here shown in linear coordinates). Modified from [92].

1.2.2 Self-similarity of the EEG

Generally, fractal geometry is associated with Euclidian objects, which reflect iterative processes, i.e. procedural repetitions and recursion, incorporating the previous state of the system as the input of a new iteration. Hence, these are dividable into identical segments, each reduced by a scaling factor (Figure 4). Such self-similarity cannot only be defined geometrically, but also statistically. Statistical self-similarity is also indicated with the term self-affinity [93]. Moreover, fractal behaviour is not only evident in space, but also in the time domain [94].

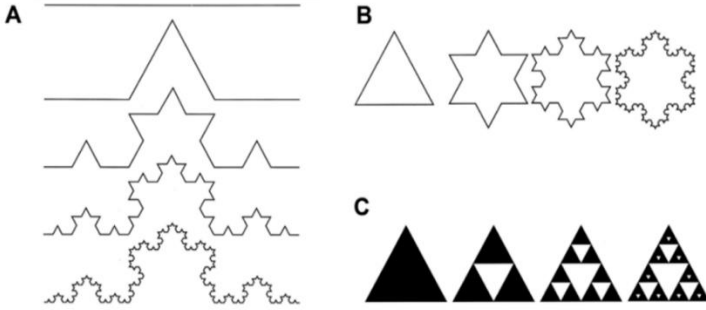


Figure 4: Examples of geometrically self-similar fractals. (A) The Mandelbrot set. (A) the curve and (B) the snowflake described by Niels F.H. von Koch. (C) shows the Sierpinski triangle. Modified from [93].

For instance, the time evolution of a dynamical system is represented by the time series $X(t)$. Specified over a time interval T , the mean signal $\bar{X}(t)$ is governed by:

$$\bar{X}(t) = \frac{1}{T} \int_0^1 X(t) dt \quad (2)$$

Further, the time series can be described in the frequency domain f , represented by the amplitude $A(f, T)$, which is given by the Fourier transform of $X(t)$:

$$A(f, T) = \int_{-\infty}^{\infty} X(t) e^{2\pi i f t} dt \quad (3)$$

The power spectral density is given by:

$$s(f) = \lim_{T \rightarrow \infty} \frac{1}{T} |A(f, T)|^2 \quad (4)$$

In case of a fractal time series, the power spectrum obeys a power law:

$$s(f) \propto \frac{1}{f^\beta} \quad (5)$$

where f the frequency and β the spectral exponent [95]. Historically, the case of $\beta= 0$ was called white noise, according to the fact that its power spectral density is the same at all frequencies within a fixed bandwidth. Statistically, white noise depicts an uncorrelated process. The case $\beta= 1$ is referred to as pink noise and $\beta= 2$ is termed Brownian noise, also known as red noise, which is a highly correlated process (Figure 5). Importantly, in contrast to periodic phenomena, which would generate characteristic peaks in the power spectrum, a time series with $1/f$ power spectrum has no characteristic time scale. Therefore, fluctuations of a $1/f$ process would appear similar under temporal magnification such as fractal shapes remain identical in the spatial

domain. As a power-law function is indicative of scale-invariance, the arrhythmic brain activity contributing to this $1/f$ slope has been termed “scale-free brain activity” [96, 97].

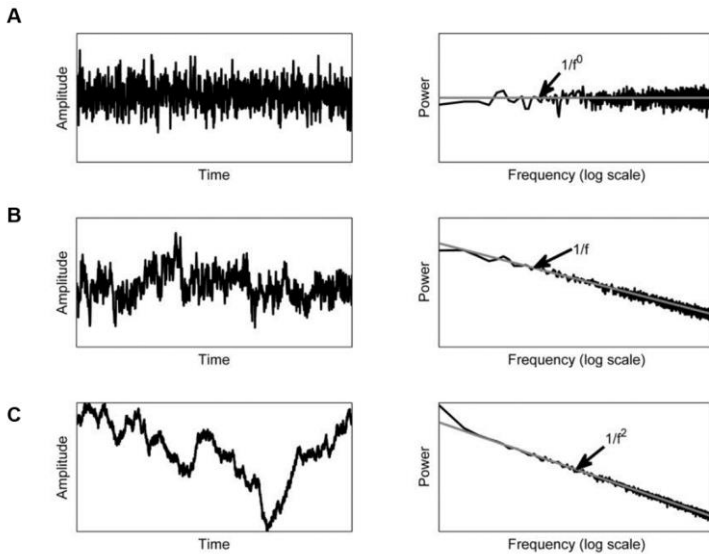


Figure 5: Examples of noise processes. (A) white noise, (B) pink noise, (C) Brownian noise. Adapted from [98].

Several algorithms exist to extract complexity features from electrophysiological data [7, 99]. In this thesis, I will focus on two algorithms, namely Higuchi’s fractal dimension and the multiscale

entropy analysis, which are described in the following.

1.2.3 Higuchi's fractal dimension

As mentioned above dynamical systems such as the brain can exhibit attractors with fractal properties. Most approaches characterizing attractors of nonlinear systems rely on the reconstruction of the systems dynamics in state space by a procedure called embedding [100], such as, for example, the calculation of the correlation dimension D_2 [101] or the Lyapunov exponents [102]. However, the reconstruction of the phase space from a given observation in time is accompanied by time consumption as surrogate data testing is essential to justify conclusions and involves pitfalls such as biases by autocorrelation effects in the time series [77]. Therefore, algorithms were developed to calculate the fractal dimension directly in the time domain allowing to examine systems dynamic without reconstructing the attractor. Among existing algorithms such as Katz's [103] or Petrosian's

method [104], Higuchi's fractal dimension (HFD) depicts the most accurate one [105, 106]. Originally introduced in 1988 as a nonlinear approach originating from chaos theory to capture natural phenomena such as the earth's changing magnetic field [105], the measure has been implemented over time in biological and medical research. Nowadays, HFD is widely applied in basic and clinical neurophysiological research to measure the complexity of neuronal activity in different neurophysiological conditions [107]. The algorithm constructs k new time series for $m = 1, 2, \dots, k$ from a starting time series of N samples: $y(1), y(2), \dots, y(N)$:

$$y_k^m: y(m), y(m+k), y(m+2k), \dots, y\left(m + \text{int}\left(\frac{N-m}{k}\right)k\right) \quad (6)$$

where m indicates the initial time sample, k denotes the time interval and $\text{int}(r)$ is integer part of a real number r .

As an illustration, for $k = 4$ and $N = 1000$, the algorithm produces 4 times series [108]:

$$\begin{aligned}
 y_{41}: & y(1), y(5), y(9), \dots, y(997), \\
 y_{42}: & y(2), y(6), y(10), \dots, y(998), \\
 y_{43}: & y(3), y(7), y(11), \dots, y(998), \\
 y_{44}: & y(4), y(8), y(12), \dots, y(1000),
 \end{aligned} \tag{7}$$

Then, the average length $L_m(k)$ of each of the time series y_k^m is computed as follows:

$$L_m(k) = \frac{1}{k} \left[\frac{N-1}{\text{int}\left(\frac{N-m}{k}\right)k} \left(\sum_{i=1}^{\text{int}\left(\frac{N-m}{k}\right)} |y(m+ik) - y(m+(i-1)k)| \right) \right] \tag{8}$$

where N indicates the total length of the original data series. $\frac{N-1}{\text{int}\left(\frac{N-m}{k}\right)k}$ is a normalization factor. The calculation is repeated for k ranging from 1 to k_{max} , resulting in a sum of average lengths $L(k)$:

$$L(k) = \frac{1}{k} \sum_{m=1}^k L_m(k) \quad (9)$$

A fractal curve follows the relationship

$$L(k) \sim k^{-HFD} \quad (10)$$

Hence, when plotting $\log(L(k))$ against $\log\left(\frac{1}{k}\right)$, HFD can be estimated as the slope using a least squares linear best fitting procedure:

$$HFD = \frac{n \sum(x_k y_k) - \sum x_k \sum y_k}{n \sum x_k^2 - (\sum x_k)^2} \quad (11)$$

Where $y_k = \log(L(k))$, $x_k = \log\left(\frac{1}{k}\right)$, $k = k_1, k_2, \dots, k_{max}$, and n depicts the number of k values for which the linear regression is calculated ($2 \leq n \leq k_{max}$).

Numerical values of HFD have the lower and upper limits of 1 and 2, respectively. Considering a curve that represents the amplitude of a given time series signal as a function of time on a 2D plane, a simple

curve has a dimension equal 1 and a plane has a dimension equal 2. HFD can be imaged as a measure of the “degree of filling out” the plane by the curve and hence, its complexity [80]. Accordingly, HFD close to one would represent a smooth curve with low complexity, whereas HFD=2 would correspond to complex curve, such as white noise practically filling 100% of the plane. Hereby, the fractal dimension of a time series is related to the spectral exponent β :

$$\beta = 5 - 2HFD \quad (12)$$

It has been shown that if $1 \leq \beta \leq 3$, then $HFD = (5 - \beta)/2$ with the established limits if $\beta \rightarrow 0$ then $HFD \rightarrow 2$ and if $\beta \rightarrow 3$ then $HFD \rightarrow 1$ [105, 95]. Important to note, HFD gives no information of the systems nature generating the signal, e.g., it is not determinable whether the system behaves deterministic, chaotic or stochastic. Instead, HFD depicts a tool to demonstrate relative changes in the signals' complexity, for instance, before and after an intervention [80; 74].

The choice of this algorithm is motivated by several studies, showing that the HFD is promising for the discrimination of states of consciousness. For instance, it has been used to measure the depth of sedation in intensive care unit [109], showing that HFD values decrease with the depth of anaesthesia [110]. In the context of anaesthesia it has been found that HFD is accurate in estimating the bispectral index (BIS), a method which quantifies the degree of phase coupling between EEG components [111]. It has been concluded that HFD depicts an even more promising method for the assessment of anaesthesia depth [112], especially in combination with other measures such as the burst suppression ratio [113]. Further, it has been effectively used for the discrimination between sleep stages [114], even using a single EEG channel [115], as well as between sleep and propofol induced EEG spindles [116]. In the context of diseases, already over a decade ago, HFD has been applied in neurophysiology for the detection of epileptic seizure, providing better temporal resolution than

spectral analysis [117]. Especially in combination with other nonlinear features, HFD is suitable for epileptiform EEG analysis [118] and has been implemented in the development of diagnostic tools such as an automated classifier [119]. Further, it has been shown that HFD values are suitable serving as a biomarker for early detection of Alzheimer's disease (AD) as the EEG signal of AD patients reveals significantly reduced HFD values in the parietal areas [120], as well as in temporal-occipital regions [121]. Staudinger and Polikar achieved a diagnostic accuracy of 78 % for AD, training a support vector machine with HFD combined with features of several nonlinear signal complexity measures [122]. Additionally, it is suggested that HFD is suitable to discriminate between normal and hypnotic states, as well as between relaxation and imagination tasks [123]. It was shown that HFD revealed differences between internal vs. external percepts and discriminates external visual from auditory percepts [124]. Also, HFD provided better results than linear measures as part of a system for

classification of subject's hypnotic susceptibility [125] and a real-time fractal dimension based algorithm has been proposed for the recognition of emotions inducted via sound stimuli [126].

1.2.4 Multiscale entropy

Another approach to calculate the complexity of a time series are entropy measures. Generally, the entropy of a single discrete random variable is a measure of its average uncertainty. Multiple mathematical methods exist such as Shannon's entropy [127] or the Kolmogorov-Sinai entropy [128, 129]. However, the latter is limited in use of estimating the entropy of time series of finite length [130]. In 1991, Pincus introduced a parameter termed approximate entropy A_E , which applies for the analysis of "real-world" time series [131]. This has further been modified and termed sample entropy S_E , which allows an estimation less depending on the time series length describing the complexity more accurate with better consistency [132, 133]. The parameter S_E has been defined by Richman and

Moorman, starting from the definition of the K_2 entropy, a lower bound of the Kolmogorov-Sinai entropy, suggested by Grassberger and Procaccia [129, 132]:

$$S_E(m, r) = \lim_{N \rightarrow \infty} - \ln \frac{B^{m+1}(r)}{B^m(r)}, \quad (13)$$

estimated by the statistic:

$$S_E(m, r, N) = - \ln \frac{B^{m+1}(r)}{B^m(r)} \quad (14)$$

where N = data points of the time series $\{x(i)|1 \leq i \leq N\}$, and m = length of the vector sequences $X_m(i) = [x(i), x(i + 1), \dots, x(i + m - 1)]$, $1 \leq i \leq N - m + 1$. r depicts the tolerated distance level, a percentage of the standard deviation serving as a similarity criterion. $B^m(r)$ defines the probability that other vectors are similar to vector $X_m(i)$ matching for m points, i.e., the number of vectors satisfying $d[X_m(i), d[X_m(j), \leq r$, where d is the Euclidean distance and thus, that any two vectors are within r of each other:

$$B^m(r) = \frac{1}{N - m} \sum_{i=1}^{N-m} B_i^m(r) \quad (15)$$

To illustrate the function of the algorithm, a simulated time series $u[1], \dots, u[N]$ is shown in Figure 6. Here, a two-component template sequence $(u[1], u[2])$ and a three-component template sequence $(u[1], u[2], u[3])$ are considered. The number of sequences matching these template sequences are calculated. In this example, the number would yield 2 for the two-component template sequence $(u[13], u[14]$ and $u[43], u[44])$ and one for the three-component template sequence $(u[43], u[44], u[45])$. This procedure is then repeated for the next template sequences $(u[2], u[3]$ and $u[2], u[3], u[4])$, respectively. The number of matching sequences are summed up and added to the previous value. The calculations are repeated for all possible sequences $(u[3], u[4], u[5]), \dots, (u[N - 2], u[N - 1], u[N])$.

Finally, S_E is determined as the natural logarithm of the ratio between the total number of two-component template matches and the number of three-component- template matches. Hence the parameter reflects the probability that sequences that match

each other for the first data point will also match for the next point [130].

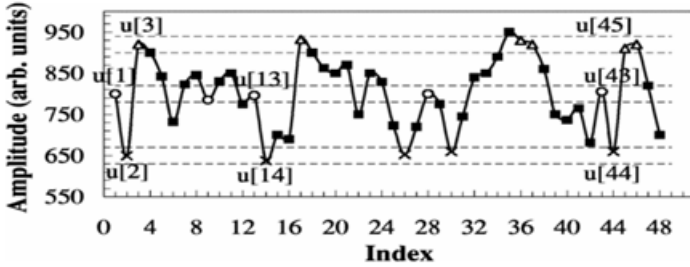


Figure 6: Simulated time series to illustrate the procedure of calculation the sample entropy for the case $m = 2$ and a given positive real value r [130].

This algorithm, however, was shown to assign a higher value of entropy to pathologic time series that are assumed to represent less complexity compared to time series derived from healthy participants [134, 135]. Costa and colleagues suggested that such misleading results might be explainable by the fact, that these measures are based on a single scale [135] and advanced the algorithm further terminating the introduced methods multiscale entropy. Given a one-dimensional discrete time series $\{x_1, \dots, x_i, \dots, x_N\}$ of length N , the multiscale entropy

algorithm is based on the construction of a consecutive coarse-grained time series $\{\gamma^{(\tau)}\}$, determined by the scale factor τ [130]. Here, the original times series is divided into windows of the length τ and data points are averaged for each window according to:

$$\gamma_j^{(\tau)} = \frac{1}{\tau} \sum_{i=(j-1)\tau+1}^{j\tau} x_i, \quad 1 \leq j \leq N/\tau. \quad (16)$$

Then, the entropy measure S_E is calculated for each course-grained time series (Figure 7) and plotted [130]. For $\tau = 1$, the time series $\{\gamma^{(1)}\}$ is the original time series. The length of each coarse-grained time series is equal to the original time series divided by the scale factor τ [130].

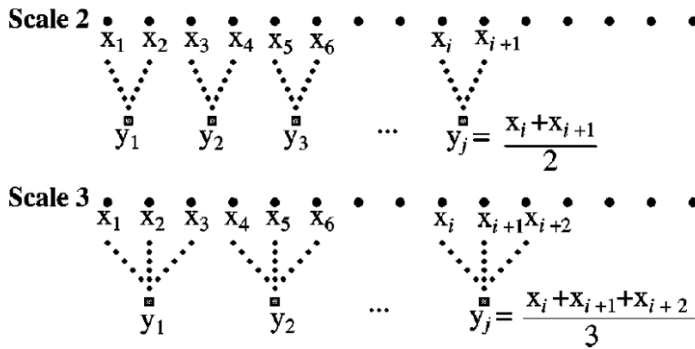


Figure 7: Schematic illustration of the coarse-gaining procedure. Adapted from [130].

As S_E values are based on a lower probability of repeated sequences in the data, higher values represent more complexity. For instance, higher scale one entropy values are representative of white noise series compared to $1/f$ time series (Figure 8).

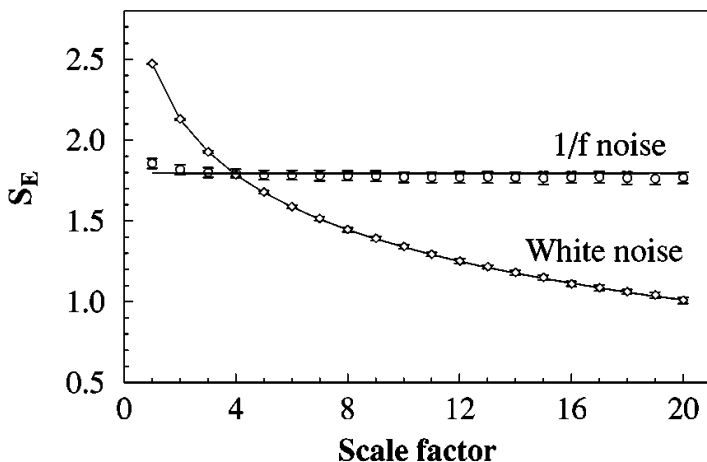


Figure 8: MSE analysis of simulated white and 1/f noise time series. The value of the sample entropy is plotted against the scale factor, which specifies the number of data points averaged to obtain each element of the coarse-grained time series [130].

The MSE analysis was chosen as several studies demonstrated that the MSE is useful for quantifying neural complexity in the context of states of consciousness [136]. For instance, Miskovic and colleagues showed significant MSE changes across the human sleep cycle in the EEG [137]. Also, in one study MSE values were used as input data to train an artificial neural network for monitoring the depth of anaesthesia during surgery. The effectiveness of this

proposed new index was analysed by correlation analysis with the bispectral index (BIS), indicating an accurate and robust measurement of the depth of anaesthesia [138]. Regarding the potential of MSE values as biomarkers in the context of disease, Takahashi et al. recorded resting state EEG data of drug-naïve schizophrenia patients pre- and post-treatment with antipsychotics. In comparison to healthy controls, patients showed higher complexity in fronto-centro-temporal brain regions. After antipsychotic treatment the signal complexity decreased to healthy control subject levels selectively in fronto-central regions, highlighting the usefulness of MSE to identify abnormal temporal dynamics [139]. Further, MSE was used to distinguish EEG data derived from Alzheimer's disease patients and age- and sex-matched healthy controls. Here, significant negative correlations between the sample entropy averaged over all scales factors and cognitive decline as assessed with the Mini-Mental State Examination were reported [140]. A link between MSE values and memory

consolidation was also proposed by other studies [141]. As an example, significant MSE differences were reported in a visual memory task, which involved making the executive decision of remembering or forgetting the visual stimuli. Hereby, greater complexity in the prefrontal and frontal lobe was observed, when participants intentionally memorized a visual scene [142].

However, to understand the complexity of brain activity and its function, a comprehensive theoretical framework is required describing the multitude of interaction of billions of neurons. In the following I will elaborate on the concept of self-organized criticality, which has originally been introduced as an explanation of ubiquitous $1/f$ noise [143]. In recent years, the hypothesis arose that self-organized criticality is a fundamental property of neural systems [144]. As described in the following, the theory states that the brain state space dynamics self-organize towards a phase transition, an attractor termed the critical state. This premise is especially compelling, as the critical state has been associated with optimal

information processing functions [145] and has been handled as promising for quantifying consciousness [146].

*“Who could ever calculate the path of a molecule?
How do we know that the creations of worlds
are not determined by falling grains of sand?”
Victor Hugo, les Misérables*

1.3 Self-organized criticality

Self-organized criticality, in the sense of statistical physics, is defined as a specific type of behavior, seen when a system undergoes a phase transition. During a phase transition, macroscopic properties of the system, termed the order parameters, change as a function of a so-called control parameter. For example, when water gets boiled, a phase transition from liquid to a vaporous phase occurs. Here, the order parameter would reflect the phase’s entropy (such as water or vapor), whereas the control parameter is the temperature. Modifying the control parameter gradually changes the order parameter

until a specific point, at which the values of the order parameter vary abruptly. Graphically, phase transitions are either marked by a discontinuity of the phase diagram (a jump of the order parameter) or by a point of non-differentiability reflected as a sharp corner. The latter is termed a continuous second order phase transition, which allows the system to be poised exactly between two phases. In that case the system is in the critical state, residing between two qualitative distinct types of behavior such as ordered and disorder. A system at criticality is therefore sometimes referred to as on the “edge of chaos”. If the control parameter is below the critical value, the state is called subcritical, whereas values above the critical state results in a supercritical state [147, 144, 148]. Systems in a critical state show complex behavior with inherent characteristics such as scale-invariance meaning that no scale in time or space dominates the behavioral pattern. This mode is reflected by spatial and temporal correlations scaling of a power law over several orders of magnitude. Hence, these give rise to self-similar fractal-like

structure over many scales [149]. Power laws refer to a probability density function expressed by $p(x) = Cx^{-\alpha}$, for $x > x_0$ and α denoting the scaling exponent. The scale invariance is shown when power laws are plotted logarithmically, indicated as a straight line: $\log(f(x)) = \log C - \alpha \log(x)$. Multiplying the plotted coordinate units of such a graph with a common factor is not resulting in any change of the slope $-\alpha$. A zooming in or zooming out produces a similar slope with a constant scaling exponent. For an illustration of the phenomenon, the two-dimensional Ising model, a classic example of the ferromagnetic-paramagnetic second-order phase transition is considered (Figure 9).

The Ising model consists of a lattice in a piece of iron, whereby each site of the lattice corresponds to a dipole moment. Below the so-called Curie point ($T_c=1043\text{ K}$), iron is magnetized even in the absence of an external field. Here, nearest neighbour interactions dominate and almost all spins of the electrons are aligned in the same direction yielding an ordered state, which creates a net magnetization.

However, with increasing temperature, the thermal fluctuations dominate the tendency to align. Spins are pointed in different directions resulting in a more disordered state. At $T > T_c$ permanent magnetic characteristics get lost, and iron becomes paramagnetic. During the critical phase at T_c where order and disorder is balanced, the correlation length, reflecting statistical correlations between any pair of elements in the systems, is maximized. Further, the averaged correlation length Γ follows a power law: $\Gamma \sim (T - T_c)^{-\xi}$, with the critical exponent $\xi > 0$. Also, the order parameter of the system at criticality can be described with power laws. For instance, the magnetization M is governed by: $M \sim (T - T_c)^{-\beta}$, with $\beta > 0$. [147, 150, 148].

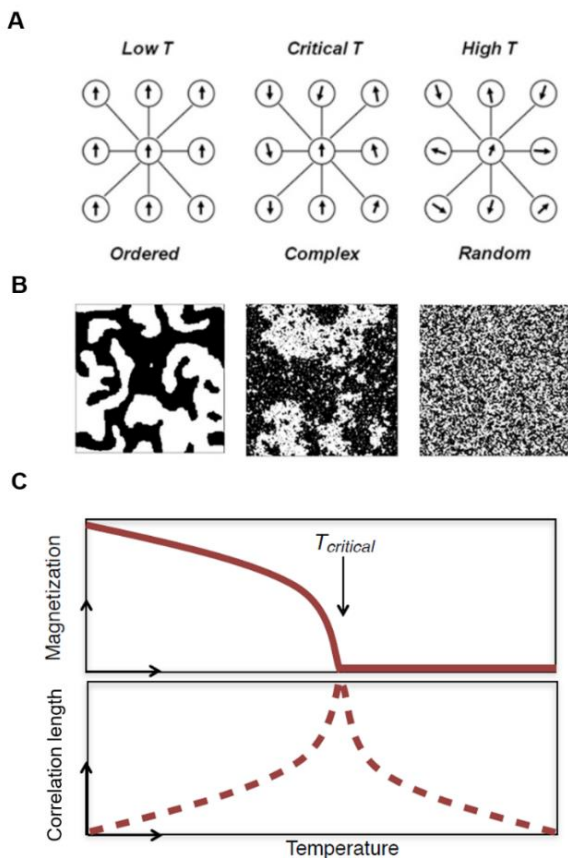


Figure 9: (A) Diagram of the spins in the Ising model in an ordered state at low temperature, a complex state at critical temperature and a disordered state at high temperature, adapted from [150]. (B) Simulation of a 2D Ising model with length = 256 in subcritical, critical and supercritical states as temperatures increases from left to right panels. Black areas

reflect a spin pointed up and white square represent spins down, adapted from [148]. (C) modified from [151].

Alan Turing was probably the first one speculating that the brain could be in a critical regime in his seminal paper on the topic of artificial intelligence written in 1950 [152]. This was around the same time when Donald Hebb (1949) formulated his theory on cell assembly formation as a principle of cortical functions, often summarized as “Cells that fire together wire together ”[153]. A decade later advances in explaining the principles of self-organization and nonequilibrium phase transitions such as Herman Haken’s pioneering work on synergetics and Stuart Kauffmann’s investigations paved the way for the understanding the brain in terms of a complex system [154–156]. Back then, the potential equivalence between neuronal networks and systems exhibiting a phase transition such as cellular automata, binary lattices evolving iteratively, was highlighted [157]. The field further progressed, when Christopher Langton, one of the founders of the field of artificial life, published an approach to

parametrize the space of cellular automata. In his work, Langton (1990) showed the occurrence of a phase transition between highly ordered, deterministic and highly disorder, chaotic dynamics. Further, he outlined that the vicinity of the transition point supported optimal processing, transmission and storage of information [158] (Figure 10).

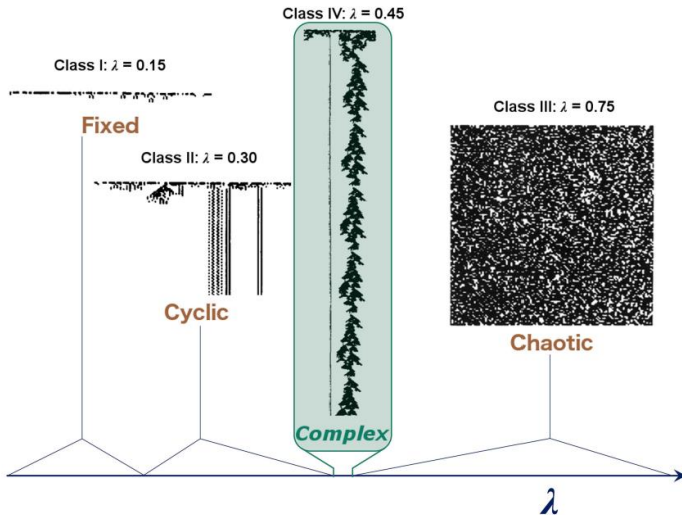


Figure 10: A binary cellular automaton represents an n -dimensional array of binary cells. The states are update synchronously in discrete time steps, whereby each state $t+1$ depends on the state of the cells at time t . Langton (1990) identified different classes corresponding to different dynamical

regimes characterized by the ratio of transitions to an arbitrary state selected as the “quiescent state” (parameter λ). Class IV depicts a transitional state analogous to complex behavior arising in the critical regime. Taken from Heiney et al (2021), adapted from Langton (1990) [149, 158].

This so-called “computation at the edge of chaos” [159, 160], was in accordance with theories from Per Bak, who pioneered the science of self-organised criticality, promoting critical phase transitions as an ubiquitous mechanisms to generate complexity, ubiquitous $1/f$ noise and the preponderance of fractal structures in nature. In his book “How nature works” he uses the canonical example of a sand pile [143]. The sandpile model, which is analogous to a cellular automata, randomly placing chips on a finite grid, describes the process of a random positioning of sand grains on a pile. This results in a slope, which builds up until it reaches a specific, critical threshold value, the transition point. At this point the system is out of balance and from here on, the dropping of more sand grains leads to an avalanche. During an avalanche the site collapses transferring sand into

the adjacent site, extending their slope. This dynamic was found to be governed by power laws [161]. Importantly, the concept of criticality as proposed by Bak, Tang and Wiesenfeld fundamentally differs from the critical point at phase transitions in equilibrium statistical mechanics as no tuning of a parameter, for instance temperature, is required. Hence, the critical point is an attractor, to which the system self-organized, whereby the scaling properties are insensitive to the parameters of the model [161].]

However, after a rapid increase of publications in this field in the 1990s, interest slowly receded [144]. Hence, the conjecture of critical brain dynamics has come a long way before it was only recently put to experimental testing ground and revived [162].

1.3.1 Experimental findings and functional benefits

In vitro cultures exhibit spontaneous dynamical activity, brief bursts of activity followed by longer intervals of quiescence [163]. In 2003, Beggs and Plenz hypothesized that the propagation of activity in networks of cortical neurons is describable by

equations that govern cascades indicative of a state of self-organized criticality. In their study, they recorded spontaneous negative local field potentials (LFP) of mature organotypical cultures and acute slices of rat cortex using a multielectrode array [164]. Indeed, the propagation of synchronized LFP followed a power law with a scaling exponent of $-3/2$ as it would be predicted from a network of globally coupled nonlinear threshold elements [165]. The authors termed this new mode of network activity “neuronal avalanches” [164, 166]. Subsequently, avalanches were investigated in superficial layers of rat prefrontal cortex [167] and during development of cortical layer 2/3 [168]. Authors showed that nested beta/gamma oscillations organized as neuronal avalanches during up-states, which required an activation of the dopamine D_1 receptor [168]. Homeostatic regulation of avalanche dynamic and the role of the excitation/inhibition (E/I) balance was then studied in a series of experiments, selectively blocking excitatory and inhibitory synaptic transmission by pharmacological means [169].

Further, *in vivo* experiments confirmed power law statistic and spontaneous activity in form of neuronal avalanches in cats under anaesthesia [170, 171], in awake monkeys [170, 172] and in rats traversing the wake-sleep cycle [173]. First signatures of criticality in the human brain were reported by Linkenkaer-Hansen and colleagues, who focused on the temporal fluctuations employing a method called detrended fluctuation analysis (DFA) and reported scale-free temporal statistics in EEG data [174]. One more step towards evidencing criticality was achieved when Shriki and colleagues analysed resting-state brain activity from 124 participants using magnetoencephalography (MEG). Here, large deflections at single MEG sensors were identified and analysed as cascades. The authors reported that cascade size distribution obeyed power laws with an exponent of $-3/2$ at timescales where the branching parameter was close to 1. A scaling and coarse graining of the sensor array did not change this relationship [175]. Using intracranial depth recordings in humans it was further shown that

avalanche distributions follow a power law, whereby these differed between states of vigilance with larger and longer avalanches during rapid eye movement (REM) sleep [176]. Interestingly, Priesemann and colleagues analysed highly parallel spike recordings from animals and LFP from human, suggesting that the dynamic is self-organized towards a slightly subcritical brain state [177]. The authors suggest that potential advantages may be a safety margin from supercriticality and developed methods to precisely quantify the distance to the critical point [178, 179]. Subsequently, spatial critical dynamics were also described in whole brain functional neuroimaging (fMRI) data [180].

Such studies provided proof-of-principle that SOC could be a unifying framework to understand complex patterns of activity in the brain and, by extension, cognition, behaviour and consciousness [92]. Work on criticality in physical systems suggest that systems in a critical state exhibit optimal computational properties [92] and it has been shown that critical dynamics in the brain would be

equivalently accompanied by functional benefits [145]. SOC implies a balanced signal propagation, which can have important implications for the dynamics of neural networks. Such balance is based on the likelihood that one spike causes each other neuron to fire and can be captured by the branching parameter σ , which is defined as the ratio of descendants, the number of events in a temporal interval t and the ancestors, the number of events in the following interval $t+1$ (Figure 11) [181, 145, 182]. Accordingly, experimental evidence suggest that critical dynamics emerge when excitation and inhibition is balanced [183–185]. Importantly, the balance between independence and interdependence among neurons is fundamental for the transmission and processing of information [186]. Computational advantages of criticality have been demonstrated in neural network models and empirical recordings. For instance, it has been shown that that the dynamic range of a neural network is maximized at a critical point [187, 188], which has also been suggested by an in vitro experiments

manipulating cultures pharmacologically close to criticality [189] as well *in vivo* recordings from rats [190]. Further, optimal information transmission, storage and capacity has been reported in neuronal models at criticality [191–193], *in vivo* [194] and in animal studies [195]. Importantly, the observed scale-free patterns close to a critical point of a phase transition imply the largest variability and thus, the largest number of configurations and repertoire of possible brain states [151].

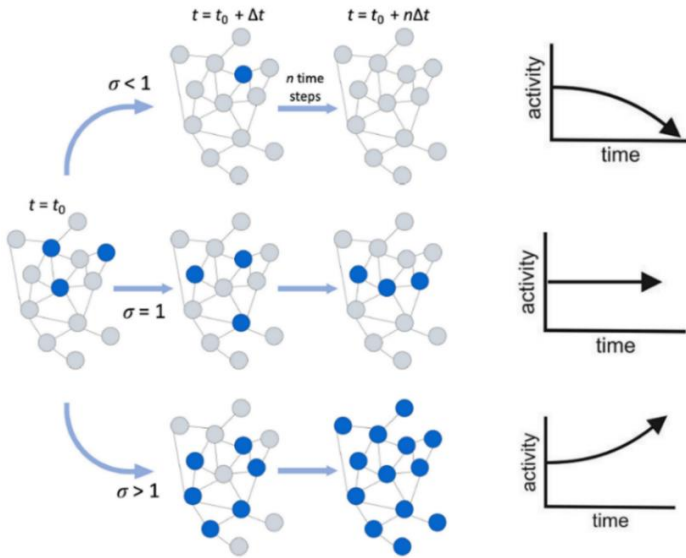


Figure 11: Schematic illustration of the branching ratio. Adapted from [149] and [181]. Blue nodes represent active ones and gray nodes are inactive. The middle regime of $\sigma = 1$ corresponds to the critical state, in which activity is self-sustained. The case of $\sigma < 1$ corresponds to a subcritical state in which activity will die out over time. A supercritical state is indicated by a $\sigma > 1$, in which activity will increase with time.

To summarise, key experimental observations in support of the criticality hypothesis are (i) neuronal avalanches with power law distribution and (ii) long-range temporal correlations in the amplitude of

neural oscillations [196]. These can be determined by analytical metrics as described in the following.

1.3.2 Detrended fluctuation analysis

The detrended fluctuation analysis (DFA) depicts a prominent method to quantify the scale-free nature of physiological time series by estimating long-range temporal correlations (LRTC), the scale-free decay of temporal (auto)correlations. The algorithm captures fluctuations of the signal at different time scales determining the statistical self-affinity of a signal [197–199]:

$$Y(Lt) \equiv L^H Y(t) \quad (17)$$

where $Y(Lt)$ and $Y(t)$ are values of a 1-dimensional process at time windows of length Lt and t , respectively. L depicts the Window length factor and H denotes the Hurst parameter, a dimensionless estimator of self-affinity. The algorithm consists of two steps (Figure 12). First, the data series $x(t)$ is shifted by the mean of the time series $\langle y \rangle$ and cumulatively summed:

$$x(t) = \sum_{k=1}^t [y(k) - \langle y \rangle] \quad (18)$$

Then, the signal profile is divided into a set of non-overlapping separate time “boxes” of various sizes Δn . Subsequently, in each segmentation the data is locally fit to a polynomial $y_{\Delta n}(k)$. The local polynomial trends fit within each box are subtracted and the root-mean-square of the residuals $F(\Delta n)$ (“fluctuations”) is calculated:

$$F(\Delta n) = \sqrt{\frac{1}{N} \sum_{k=1}^N [y(k) - y_{\Delta n}(k)]^2} \quad (19)$$

Subsequently, the mean fluctuation per window size is plotted against the window size on a logarithmic scale. The scaling exponent α is estimated as the slope of the least-squares fit line. The resulting DFA exponent α can be interpreted as an estimation of the Hurst parameter. If $0 < \alpha < 0.5$, the process is of a stationary nature, exhibits anti-correlations and has a memory. In the case of $0.5 < \alpha < 1$, the process is

stationary, exhibits positive correlations and has a memory. A random process with no memory is governed by $\alpha = 0.5$, whereas when $1 < \alpha < 2$, then the process is non-stationary, meaning that the signal's statistical characteristics change with time [199]. Stationary processes can be modelled as fractional Gaussian noise with $H = \alpha$ and non-stationary processes can be modelled as fractional Brownian motion with $H = \alpha - 1$ [200].

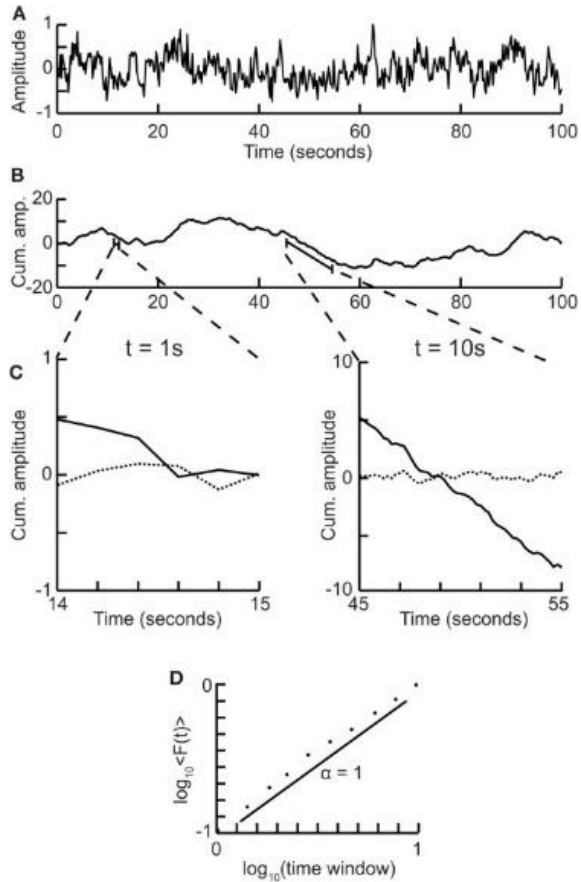


Figure 12: Stepwise explanation of the detrended fluctuation analysis. (A) shows an original time series taken from a $1/f$ signal sampled at 5 Hz with a duration of 100 s. (B) The cumulative sum of the time series. (C) Removal of the linear trend from the signal for each time window. (D) Plot of the mean fluctuation per window size against window size on a

logarithmic scale. In this example the scaling exponent is $\alpha=1$, estimated as the slope of the best fit line. Adapted from [199].

1.3.3 Neuronal avalanches

For the neuronal avalanche analysis, the time series is first z-scored. Then, a certain threshold is applied and negative and positive excursions beyond the threshold are identified as concrete event (Figure 13A,B) [201]. Subsequently, the time series is discretized with time bins of the duration Δt . Neuronal avalanches are defined as a contiguous sequence of time bins of activity preceded, ending with at least one time bin of quiescence [175].

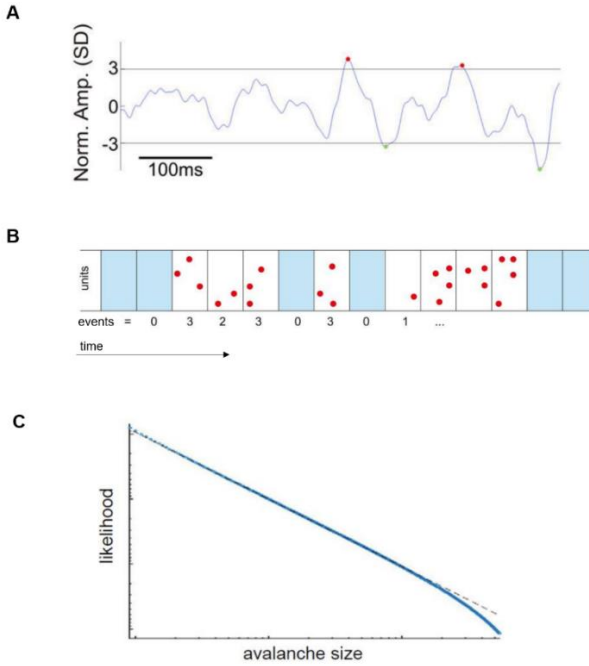


Figure 13: (A) Schematic illustration of the event identification process. Adapted from [175]. (B) Avalanche definition. Neuronal avalanches are defined as a contiguous sequence of time bins of activity preceded, ending with at least one time bin of quiescence. Modified from [202]. (C) Probability distribution of the relationship between size and likelihood of avalanches shown in double logarithmic coordinates. At criticality a scale-free process yields a power law relationship with a critical exponent of $-3/2$. Adapted from [92].

A hallmark that a neural network operates near a critical point is given by a power law scaling of avalanche size distribution ($f_s(S)$) (Figure 13B), duration distribution ($f_d(T)$) and average size conditioned on given duration data ($\langle S \rangle(T)$). The resulting critical scaling exponents τ, α and $\sigma v z$ show a relationship according to [203, 204]:

$$f_s(S) \propto S^{-\tau} \quad (20)$$

$$f_d(T) \propto T^{-\alpha} \quad (21)$$

$$\langle S \rangle(T) \propto T^{\frac{1}{\sigma v z}} \quad (22)$$

$$\frac{\alpha - 1}{\tau - 1} = \frac{1}{\sigma v z} \quad (23)$$

Another method for establishing criticality involves investigating the averaged, scale-invariant profiles of cortical fluctuations. Typically, avalanche shapes are inverted parabolas, depicting fractal copies of each other when different avalanche sizes are examined. Hence, in a critical state mean temporal profiles of avalanches should be identical across scales, e.g. long duration avalanches are supposed to have the

same scaled mean shape as short avalanches (Figure 14) [203].

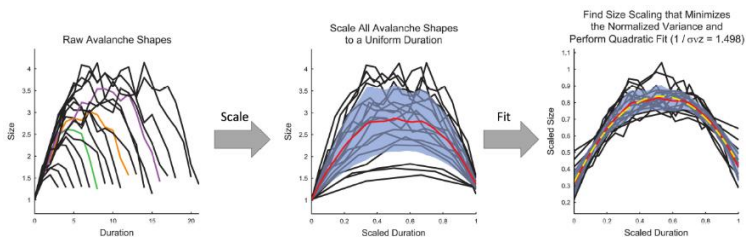


Figure 14: Shape collapse procedure [149]. First, raw avalanche shapes are determined by averaging the profile of all avalanches with a given duration. Then, the avalanches are scaled to a uniform length and finally, the scaling parameter is estimated by using a quadratic polynomial. Adapted from [201].

1.3.4 Clinical relevance

The concept of combining consciousness and criticality is promising for a wide range of clinical applications (Figure 15) [148]. For instance, findings suggest that criticality-based markers could potentially be used to assess the depth of anaesthesia [205]. An analysis of long-range temporal correlations (LRTC) combined with spectral data successfully differentiated between

wakefulness from induced unconsciousness. The authors suggesting that the loss of consciousness may be accompanied with an increase in regularity and a decrease in network repertoire limiting cognitive processing [206]. Further, signatures of criticality were applied to predict, localize, and characterize epileptic seizures. Whereas some studies identified power-law distribution during seizure intervals [207–209], others report a deviation from critical dynamics [210, 211]. Additionally, a few studies investigated criticality in neurodegenerative diseases such as Alzheimer’s disease (AD). Findings suggest that criticality inspired markers such as the level of autocorrelations and synchronization as well as differences in the power-law exponent in the frontal and pre-frontal lobes may be beneficial for disease monitoring and the diagnostic evaluation of early-onset [212]. Whereas in AD patients a scale-free distribution of spontaneous fluctuations was maintained, Parkinson disease has been suggested to represent a situation of departure from a critical state, whereby motor symptom severity was found to

be positively correlated with the scaling exponent of an adaption of the detrended fluctuation analyses (DFA) [213]. As criticality implies optimal information capacity and transmission in models [193], the role of criticality in aspects of attention, cognition and learning has also been a topic of investigation. As an example, it has been shown that power law scaling decreases with increased cognitive load in a MEG study of children with high-functional autism, who underwent executive function tasks [214]. Further studies suggested that focused cognitive tasks induce subcritical dynamics [215]. In contrast, an EEG study of 210 neurotypical adults undergoing an object recognition tasks demonstrated that variation in $1/f$ noise robustly predicted cognitive processing speed [216]. Suggesting that critical state dynamics are important for language acquisition, Dimitriadis *et al.* carried out a MEG study of children with reading difficulties. Here, temporal correlations decreased in the left temporoparietal region at rest compared to a age and IQ matched control group [217]. In line with these findings, increased LRTC positively correlated

with language score was demonstrated in a high-density EEG study of neurotypical children [218]. Also, high intelligence has been associated with near-criticality dynamics in a resting-state as shown in a recent functional magnetic resonance imaging (fMRI) study of neurotypical adults with varying IQ scores [219]. Furthermore, criticality-based markers were used to improve the understanding of psychiatric conditions. For instance, in one study MEG was recorded from patient with major depressive disorder (MDD) and healthy controls during an eyes-closed resting state. The magnitude of temporal correlations over the left-temporo-central region was suitable to predict severity of depression assessed with the Hamilton Depression Rating Scale. In comparison to controls, patients with MDD exhibit absent LRTC in the theta frequency band, which was interpreted as a possible underlying defect in limbic-cortical networks [220]. The latter could not be confirmed in an EEG study of patients with MDD, whereas increased LRTC scaling exponents were correlated positively with depression

severity. Here, the authors concluded that rumination and psychomotor retardation may be the reason for the persistence of LRTC [221]. Also, higher LRTC scaling exponents were shown in patients with MDD at baseline compared to healthy controls in EEG data. The strength of LRTC decreased after an intervention consisting of stress reduction training or mindfulness training in both cohorts [222]. Other studies examined whether alterations in LRTC during sleep could be a signature of depression reporting no statistical significant differences through the sleep stages [223, 224]. Regarding schizophrenia and schizoaffective disorders, an attenuation of LRTC scaling exponents was found in alpha and beta frequency bands compared to healthy controls in an EEG study indicating decreased temporal correlation and precision [225]. These results have been confirmed in other studies [226] and have been associated with the 'disconnection hypothesis', considering that the core symptoms of schizophrenia are related to aberrant connectivity between distinct brain regions [227, 228]. Interestingly, first studies

with healthy participants provided evidence that neurofeedback can restore critical brain dynamics. It has been speculated that neurofeedback alters excitation associated with increases in temporal improvement and hence, could balance psychiatric conditions, which have been characterized by decreased LRTC [229, 230]. In summary, the concept of criticality has several domains of clinical application. While criticality-based markers are not yet part of clinical routine and despite some controversies, these could prove beneficial in diagnosis, prognosis or treatment of a variety of diseases and may pave an important avenue of future research for understanding brain-related disorders and the relationship between neural and cognitive flexibility [148].

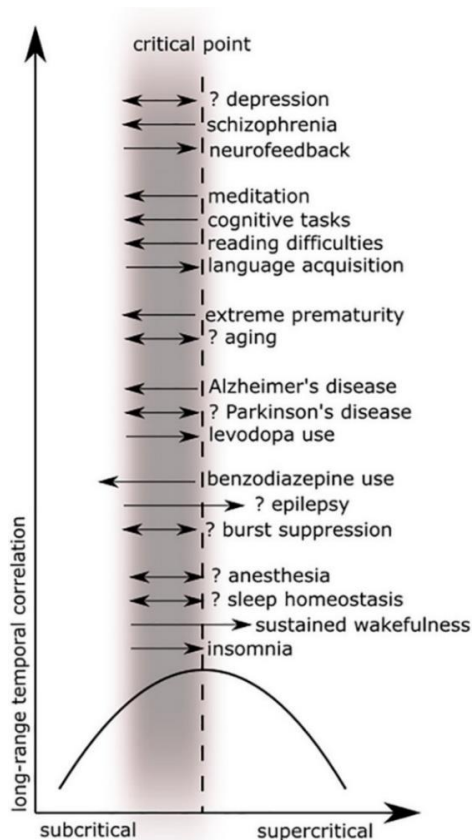


Figure 15: Illustration of long-range temporal correlations (LRTC) as a function of criticality in different conditions. Adapted from [231] and [148]. The grey area represents the physiological range of brain dynamics. Black arrays show the deviations towards a subcritical regime (left) or a supercritical regime (right) according to findings in the literature [148]. Double arrays imply contradictory evidence for both increases and decreases in LRTC.

2. Research questions and Aims

1. *Can signatures of self-organized criticality be found on the level of the EEG?*

For this purpose, electrophysiological data (64-channel EEG) will be analyzed in respect to the key experimental observations in support of the criticality hypothesis: (1) neuronal avalanches with power law distribution, (2) long-range temporal correlations (LRTCs) in the amplitude of neural oscillations. To note, in this thesis I will not aim at answering whether the brain is critical, rather than outline possible interpretations of experimental results. Many studies have been conducted and controversies emerged. To date, there is no study enabling to confirm or disprove the criticality hypothesis in neuronal networks. However, with this research, I aim to contribute to the expanding field suggesting

features of criticality to quantify consciousness.

- II. *Are criticality features suitable to differentiate states in the spectrum of wakeful consciousness and to characterize electrophysiological correlates of altered states of consciousness?*

The framework of self-organized criticality seems promising for developing physiological markers of consciousness alterations. However, to identify their potential utility in monitoring neurophysiological changes in response to interventions as well as diagnostics, it has to be shown that EEG-based criticality parameters are suitable to sufficiently differentiate mental states in the spectrum of wakelfulness. First, this will be tested on an EEG dataset of professional meditators performing three distinct meditative tasks. Second, it will be

investigated whether the measures are suitable to reflect state changes in the temporal course of a relaxation process.

III. Can critical dynamics be induced by psychophysical (mind-body) interventions?

Critical dynamics are associated with brain activity tuned towards optimized information processing functions, such as input susceptibility, maximized dynamic range, storage capacity and computational power. In other words, the optimal brain state. Here, criticality measures are proposed as general gauges of information processing. At the same time, findings suggest that psychological self-regulation techniques such as mindful focused attention during meditation enhance allocation of attentional resources and thereby, information processing capacities. However, how critical dynamics relate to cognitive function is poorly understood. Therefore, I aim at testing

whether altered states of consciousness, here specifically induced by distinct meditation tasks and a vibroacoustic relaxation process represent neuronal activity exhibiting dynamics closer the critical point of a phase transition compared to a baseline task-free condition.

IV. Can an explicit relationship to other nonlinear complexity features power spectral density parameter be identified?

This thesis is based on the contemporary proposal that consciousness represents a dynamic process of self-sustained coordinated brain-scale activity of simultaneous integration and differentiation and thus, might be quantifiable by the degree of neural complexity. Whereas self-organized criticality can be seen as a theoretical framework for the emergence of complex patterns of activity in the brain, to date, the

relationship between complexity and criticality in neural systems has not been determined experimentally. Therefore, besides applying analytical tools from criticality theory to EEG data recorded during meditative tasks and a relaxation process as well as sampled from a cohort with different levels of sensory processing sensitivity, also nonlinear methods to quantify neural complexity, namely fractal dimension analysis, and multiscale entropy analysis will be used. In addition, the standard methods using spectral decomposition will be applied to the datasets. The resulting EEG-based features will then be evaluated with respect to their comparability in the discrimination of brain states. In this stance, correlations between criticality and complexity measures as well as spectral data will be analysed.

V. *Do EEG-based complexity and criticality features reflect individual temperament traits?*

For this purpose, it will be determined whether EEG complexity and criticality features correlate with the temperament traits absorption defined as the individual's capacity for engaging attentional resources in sensory and imaginative experiences (study 2) as well as the individual level of sensory processing sensitivity (study 3).

3. Material and Methods

3.1: Mediation states

3.1.1 Data acquisition and participants

An EEG data set, which has been recorded and previously analysed by T. Hinterberger in the spectral domain was used for reanalysis [232]. Data were recorded from 30 participants (mean age 47 years, 11 females/19 males) with a meditation experience of at least 5 years practice or more than 1000 h of total meditation time. On average, participants had meditated for 20 years and 6498 hours. Participants were associated with different kinds of spiritual traditions. For instance, six participants were Zen Buddhist monks in Japan. Based on these backgrounds, the subjects developed an individual 'idiosyncratic' meditation style.

Data were recorded using a 72-channels QuickAmp amplifier system (BrainProducts GmbH, Munich, Germany). EEG was measured with a 64-channel ANT Waveguard electrode cap (ANT B.V., Enschede, The Netherlands) with active shielding

and Ag/AgCl electrodes, which were arranged according to the international 10/10 system with grounding at the participant's shoulder. To note, the data was provided by Prof. Dr. Hinterberger for a re-analysis.

The experimental procedure started with an initial 15 min baseline resting, including 5min with eyes open, 5 min with eyes closed and 5 min silently reading a neutral text from a book or a computer screen. Then, after a short break, participants were asked to meditate in their own preferred style (idiosyncratic meditation) for 20- 30 min. Next, three specific meditative tasks were instruction lasting 2 min each (Figure 16). These were in accordance to classification categories established by Travis and Shear [233].

- i) presence monitoring (instruction: "Try to be in a state of high presence at the place you are in this room at each moment of time.")

- ii) thoughtless emptiness (instruction: “Try to maintain the state of emptiness from all thought as well as possible.”)
- iii) focused attention (instruction: “Direct your attention on a spot in the middle of the forehead above your eyes.”)

Instructions were spoken by the same experimenter. Participants kept their eyes closed during the meditation tasks. Afterwards, all meditators reported that they were able to reach and maintain the instructed mental states [234, 232].

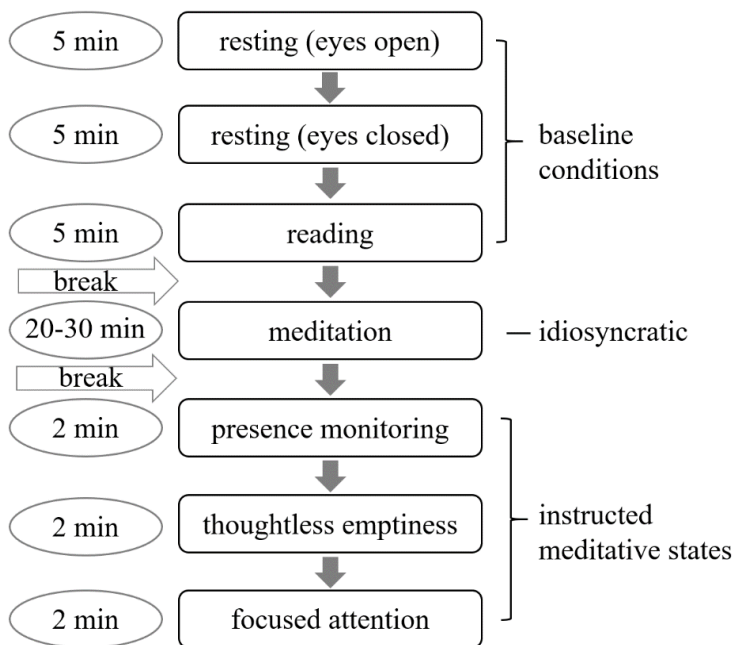


Figure 16: Experimental procedure. Modified from [232].

3.1.2 EEG data processing

Matlab (MathWorks, Natick, USA) was used for data processing. Data was sampled at 250 samples/sec in a range from DC to 70 Hz with a notch filter at 50 Hz. After detrending the 64 EEG channels, a correction for eye movement was done using a linear correction algorithm, which detects eye blinks as well

as movement events and uses those periods for determining a correction factor for each channel. Then, the EOG was multiplied with this factor and subtracted from the EEG. The efficiency of the algorithm was previously demonstrated [235]. Subsequently, the following analysis tools were applied to the data as described in the following.

Power spectral density (PSD): A power spectrum time series was calculated using the Fast Fourier Transform (FFT) for the following frequency bands:

- Delta: 1-3.5 Hz
- Theta: 4-7.5
- Alpha1: 8-10
- Alpha2: 10.5-12 Hz
- Beta1: 12.5–15 Hz
- Beta2: 15.5–25 Hz
- Gamma1: 25.5–45 Hz
- Global: 1–45 Hz

To obtain a measure of the power spectral density (PSD) FFT values were squared and all FFT bins within a frequency band range were averaged. EEG PSD was calculated for each participant, task, electrode, and frequency band.

Neuronal avalanches: For the neuronal avalanche analysis the NCC toolbox was used [201]. First, the signal from each electrode was z-scored. A threshold of ± 3 SD was applied [175]. Negative and positive excursions beyond the threshold were identified as concrete events. The time series obtained from each electrode was discretized with time bins of the duration $\Delta t = 5$ s. Neuronal avalanches are defined as a contiguous sequence of time bins of activity preceded, ending with at least one time bin of quiescence. Avalanche properties were determined using the function `avprops.m`, which calculates the duration T (number of active time bins), the size S (total number of events) as well as the shape (number of events at each time at each time bin). The average size given duration distribution ($\langle S \rangle(T)$) was

calculated using the built in function `sizegivdurwls.m`, which computes the scaling parameter SNZ and standard deviation using the weighted least squares method (see equations (20 to (23) [203, 204]. Mean temporal profiles of avalanche shapes were calculated using the function `avgshapes.m` and an avalanche shape collapse has been performed (`avshapecollapse.m`), determining the shape collapse scaling parameter [201]. Subsequently, differences between the value of the obtained critical exponent SNZ and the shape collapse scaling parameter were calculated, as these should be identical for brain dynamics operating in a critical regime [204]. The resulting variable was termed $SNZdiff$.

Detrended fluctuation analysis: To estimate long-range temporal correlations (LRTC), detrended fluctuation analysis (DFA) was used, an algorithm which, captures fluctuations of the signal at different time scales determining the statistical self-affinity of a signal [199]. Here, an algorithm described by

Colombo and colleagues (2016) was used [231]. First, the cumulative sum of the time series was calculated. Then, the signal profile was divided into a set of non-overlapping separate time “boxes” of length t . Subsequently, local polynomial trends fit within each box were subtracted and the root-mean-square of the residuals was calculated. Here, the detrend order, specifying the degree of polynomials was set to 2. The local detrending was repeated for 50 automatically determined box sizes and the power-law relationship between root-mean-square fluctuations and box sizes was determined by means of regression. The resulting exponent was termed α (see equations (18)(19)).

Fractal dimension: As a measure of signal complexity in the time domain the algorithm proposed by Higuchi was applied to calculate the fractal dimension (see equations (6, and 8 to (11) [105]. The value of k_{max} , the maximum number of sub-series composed from the original, can be determined by examining the data and plotting the fractal dimension over a range

of k . For k greater than k_{max} the fractal dimension plateaus, reaching a saturation point [107]. In this work that was the case for $k_{max} = 5$.

Multiscale entropy: The multiscale entropy was calculated using an algorithm described by Costa and colleagues (2005), which is based on the construction of a coarse-grained time series by averaging the data points within non-overlapping windows (see equations (13 to (16) [130]. For the template length m a value of 2 was chosen and the similarity criteria r was set to 0.2. MSE was measured for six different time scales (sf= 1, 3, 5, 7, 10, 20) over 5s time windows.

For an overview, the workflow is visualized in Figure 17.

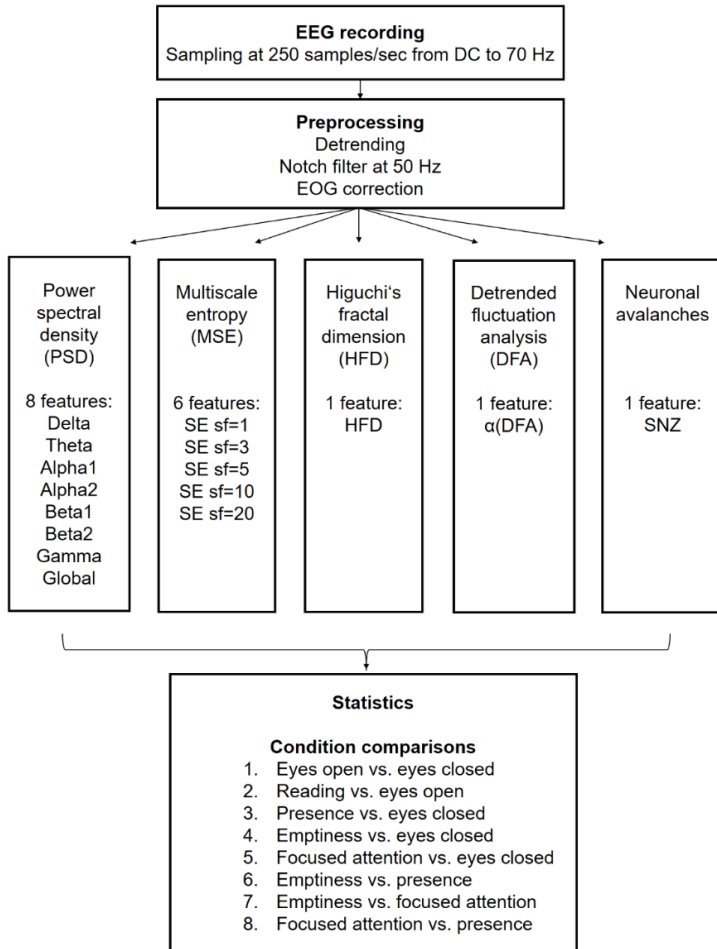


Figure 17: Scheme of the analysis workflow. PSD= power spectral density, DFA= detrended fluctuation analysis, HFD= Higuchi's fractal dimension, MSE= multiscale entropy, SE= sample entropy, sf=scale factor.

3.1.3 Merging of topographic brain regions

After calculation of complexity, criticality and spectral features, the 64-channel data was merged into the 13 topographic brain regions prefrontal (PF), left frontal (Fl), right frontal (Fr), frontal (Fz), central (Cz), left central (Cl), right central (Cr), left temporal (Tl), right temporal (Tr), parietal (Pz), left parietal (Pl), right parietal (Pr) and occipital (O) (Figure 18).

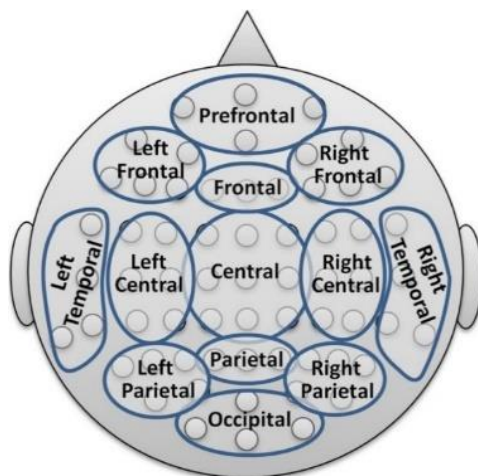


Figure 18: Reduction scheme into 13 major topographic regions. Adapted from [232].

3.1.4 Comparison between conditions

Due to high individual differences, the idiosyncratic meditation task was excluded in the analysis. Hence, the following six comparisons were calculated:

1. Eyes open vs. eyes closed
2. Reading vs. eyes open
3. Presence vs. eyes closed
4. Emptiness vs. eyes closed
5. Focused attention vs. eyes closed
6. Emptiness vs. presence
7. Emptiness vs. focused attention
8. Focused attention vs. presence

3.1.5 Statistics

To determine whether the resulting features are significantly influenced by the task condition, a Kruskal-Wallis-Test was calculated for the temporal means of each feature averaged over electrodes, participants, and conditions.

For state comparison on a global level, effect sizes defined as standardized mean differences (Cohen's d) were estimated according to Cohen (1988) [236]:

$$d = \frac{x_1 - x_2}{\sqrt{(s_1^2 + s_2^2)/2}} \quad (24)$$

With x_1 and x_2 being the mean PSD value or mean complexity/criticality feature, respectively and s_1 and s_2 the estimated variances.

Effect sizes of all participants were submitted to a paired two-tailed t-test calculated across participants, and features. Considering 17 extracted EEG features and 11 comparisons, this results in 187 variables. The t-values were corrected for multiple testing using false discovery rate (FDR) adjustment, which gives the proportion of false discoveries among all discoveries [237]. FDR was applied across conditions and features.

For a detailed analysis, estimated effect sizes were compared with a paired two-tailed t-test calculated across participants for each of the 13 topographic areas, complexity, criticality and spectral features, respectively. T-values were corrected using FDR adjustment over brain regions, conditions, complexity, criticality and spectral features.

To calculate correlations between the features, Spearman's rank correlation was applied after determining that the distribution was not appropriate for parametric testing by the Shapiro-Wilk test. Correlations were calculated from the median of the time series across participants after averaging over channels for each condition, respectively.

To analyze the classification performance, partial least squares regression as a cross between multiple linear regression and principal component analysis was chosen. Basically, partial least squares regression is an iterative process used to exploit fundamental relations between two matrices X and Y [238]. Here Y reflected the conditions and X the EEG features (function `plsregress.m`). Then, receiver operating characteristics (ROC) analysis was applied and the area under the curve (AUC) was determined [239].

The level of significance was set at $p < 0.01$.

3.2 Singing bowl experience

3.2.1 Data acquisition and participants

Electrophysiological data (64 channels of EEG, EOG, ECG, skin conductance, and respiration) was recorded from 34 participants (mean age 36.03 \pm 13.43 years, 24 females/ 10 males). The study was approved by the institutional ethics committee of the University Clinic of Regensburg according to the Helsinki Convention (file number: 20-1995-101). All gave their informed consent according to the university ethics standards and filled in an introductory questionnaire assessing demographical data and prior experiences concerning singing bowl massages as well as altered states of consciousness. Further psychometric data was assessed using the Tellegen-Absorption Scale (TAS-D) [240]. After the recording, participants ensued the PCI-K, a modified German version of the Phenomenology of Consciousness Inventory [38] and the CSP-14 [241].

TAS-D: The Tellegen-Absorption Scale (TAS-D) contains 34 true/false self-report items [240]. High

levels of internal reliability and test-retest reliability were reported [242]. The absorption capacity (i.e. the individual's capacity for engaging attentional resources in sensory and imaginative experiences) is measured by the sum of "true" responses and has been suggested to be an effective predictor of outcomes in mind-body interventions [243].

PCI-K: The Phenomenology of Consciousness (PCI) [38] is a self-report measure to quantify states of consciousness associated with a specific stimulus condition. Originally, the questionnaire consists of 53 items, grouped into the following 12 major and 14 minor dimensions. The items, including five Reliability Item Pairs, were rated on a 7-point Likert scale on a continuum between two poles. The internal consistency has been validated with an alpha coefficients between 0.69 and 0.92, [38]. Here, a modified version of the PCI has been applied (PCI-K), reducing the number of items to 27, taking at least one question of the above-mentioned dimensions.

CSP-14: The CSP-14 allows for the assessment of changes in body sensation, emotional state and

mental state consisting of three factor, namely (1) Integration, (2) Balance and (3) Vitality [241] The questionnaire contains 14 items, which are rated on a scale ranging from -3 to +3.

Electrophysiological data was recorded using a 72 channels QuickAmp amplifier system (BrainProducts GmbH, Munich, Germany). EEG was measured with a 64-channel ANT Waveguard electrode cap (ANT B.V., Enschede, The Netherlands) with active shielding and Ag/AgCl electrodes, which were arranged according to the international 10/10 system.

The experimental procedure started with an initial 10 min baseline resting, including 5 min with eyes open and 5 min with eyes closed. Then, a singing bowl massage was conducted by professionals trained according to the Peter Hess®-method with a duration of 20 minutes. Afterwards 10 min of silence were given to integrate the experience. Directly after a second resting state took place, during which participants kept their eyes closed for 5 min and

subsequently opened their eyes for 5 min (Figure 19). This final resting phase will be termed postresting in the following. During the whole procedure participants lay comfortably on a massage table.

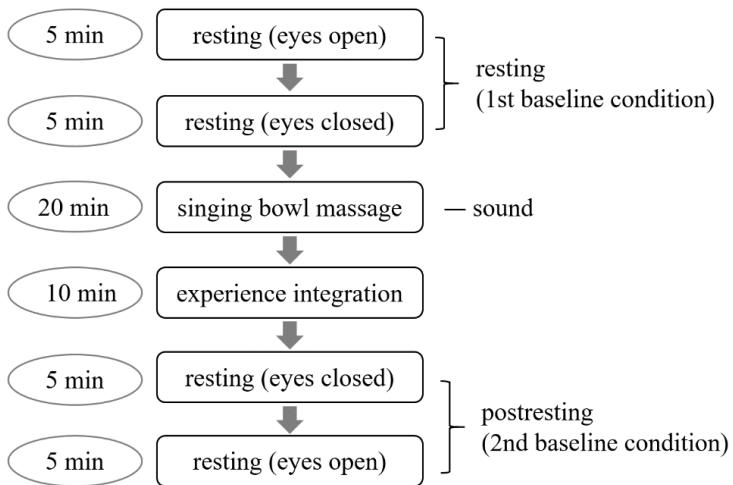


Figure 19: Experimental procedure.

3.2.2 EEG data processing

Matlab (MathWorks, Natick, USA) was used for data processing. Data was sampled at 250 samples/sec in a range from DC to 70 Hz with a notch filter at 50 Hz. After detrending the 64 EEG channels, a

correction for eye movement was done using a linear correction algorithm as described previously [235]. Then, the power spectral density, the neuronal avalanche analysis, the detrended fluctuation analysis, the fractal dimension analysis and the multiscale entropy analysis were applied as described in the preceding chapter “EEG data processing” under study 1. Topographic brain regions were merged according to Figure 18.

3.2.3. Comparison between conditions

The following three phases of the experimental course were compared:

1. sound vs resting
2. postresting vs. sound
3. postresting vs. resting

3.2.4 Statistics

For comparison on a global level, effect sizes defined as standardized mean differences (Cohen’s d) were estimated according to equation (24). Then, a paired two-tailed t-test was calculated across participants for each complexity, criticality and spectral feature,

respectively. T-values were corrected for multiple testing using false discovery rate (FDR) adjustment [237] across conditions and complexity, criticality and spectral features.

For a detailed analysis, estimated effect sizes were compared with a paired two-tailed t-test calculated across participants for each of the 13 topographic areas, complexity and criticality features as well as frequency bands, respectively (Figure 18). T-values were corrected using FDR adjustment over brain regions, conditions, and EEG features.

To calculate correlations between the EEG features, Spearman's rank correlation was applied after determining that the distribution was not appropriate for parametric testing by the Shapiro-Wilk test. Correlations were calculated from the mean of the time series across participants after averaging over channels for each condition, respectively.

To evaluate whether the EEG features reflect the individual level of trait absorption, Spearman's rank correlation was applied determining relations

between the EEG features and the TAS-D summary score.

Significance was set at $p < 0.01$.

3.3 Sensory processing sensitivity

3.3.1 Data acquisition and participants

Electrophysiological data (64 channels of EEG, EOG, ECG, skin conductance, and respiration) was recorded from 116 participants (mean age 39.95 ± 13.43 years, 83 females/ 33 males). The measurements took place in a laboratory of the department of Clinical Psychology and Psychotherapy, Bundeswehr University Munich. Before the recording all participants filled in the questionnaire 'High Sensitive Person Scale' (HSPS-G) [244].

HSPS-G: The HSPS-G (HSP scale, original version Aron & Aron, 1997 [245]; German version Konrad & Herzberg, 2017 [244]) is a 26-item self-reported questionnaire that measures the degree of sensitivity in a 5-point Likert rating scale ("0" does not apply at all - "4" applies completely) (Appendix II). For this

purpose, the measurement instrument is divided into the subscales of *Ease of Excitation* (EOE), *Aesthetic Sensitivity* (AES), and a *Low Sensory Threshold* (LST). The HSPS-G was normed and standardized on individuals from the general population and was found to have good reliability (Cronbach's α of .93 to .95) [244].

Electrophysiological data was recorded using a 72 channels QuickAmp amplifier system (BrainProducts GmbH, Munich, Germany). EEG was measured with a 64-channel ANT Waveguard electrode cap (ANT B.V., Enschede, The Netherlands) with active shielding and Ag/AgCl electrodes, which were arranged according to the international 10/10 system. The experimental procedure consisted of a 10 min baseline resting, including 5 min with eyes open and 5 min with eyes closed.

3.3.2 EEG Data processing

Matlab (MathWorks, Natrick, USA) was used for data processing. Data was sampled at 250 samples/sec in a range from DC to 70 Hz with a notch filter at 50

Hz. After detrending the 64 EEG channels, a correction for eye movement was done using a linear correction algorithm as described previously. Then, the power spectral density, the neuronal avalanche analysis, the detrended fluctuation analysis, the fractal dimension analysis and the multiscale entropy analysis were applied as described the chapter “EEG data processing” in study 1 of this thesis.

3.3.3 Statistics

To calculate correlations between the EEG features and the HSPS-G summary score as well as subscales, Spearman’s rank correlation was applied after determining that the distribution was not appropriate for parametric testing by the Shapiro-Wilk test. Correlations were calculated from the mean of the time series across participants. Then, according to a latent class analysis performed by Lionetti et al. determining a frequency distribution of approximately 30% in the low-sensitivity, 40% in the medium-sensitivity and 30% in the high-sensitivity group, the cohort was grouped in regard to the HSPS-G summary score into highly sensitive (77-

104) and not sensitive (0-43) participants [246]. EEG features were compared between the two groups applying a Wilcoxon signed-rank test. Significance was set at $p < 0.05$.

4. Results

4.1 Meditation states

4.1.1 Kruskal-Wallis Test

To test whether features of criticality, neuronal complexity and power spectra were significantly influenced by the task conditions, a Kruskal-Wallis-Test was performed. The analysis revealed a significant main effect for state on a $p < 0.001$ level concerning SE sf=1, SE sf=7, SE sf=10, SE sf=20, DFA and SNZ. For the power spectral density, significant effects were found for delta and alpha 1 (Table 2, Figure 20). However, when calculating the Kruskal-Wallis- Test only over the meditation conditions, no significant effect for state was observed (Table 3, Figure 21).

Table 2: Chi-Square values for each complexity, criticality and spectral feature resulting from the Kruskal-Wallis-Test calculated over all conditions. ** $p < .001$, * $p < .01$

	Chi square	p-value
Delta	39.02**	<0.001
Theta	10.22	0.069
Alpha 1	21.87**	<0.001
Alpha 2	17.02*	0.005
Beta 1	1.28	0.937
Beta 2	1.93	0.858
Gamma	18.32*	0.003
Global	5.89	0.217
SE sf=1	56.82**	<0.001
SE sf=3	18.41*	0.003
SE sf=5	7.16	0.209
SE sf=7	42.89**	<0.001
SE sf=10	64.48**	<0.001
SE sf=20	24.06**	<0.001
HFD	20.13*	0.001
α (DFA)	43.17**	<0.001
SNZ	53.42**	<0.001

Table 3: Chi-Square values for each complexity, criticality and spectral feature resulting from the Kruskal-Wallis-Test calculated over the three meditation conditions.

	Chi square	p-value
Delta	0.424	0.809
Theta	0.050	0.976
Alpha 1	1.170	0.5572
Alpha 2	0.385	0.825
Beta 1	0.3543	0.938
Beta 2	0.933	0.659
Gamma	0.451	0.798
Global	0.564	0.754
SE sf=1	1.481	0.477
SE sf=3	1.172	0.556
SE sf=5	1.184	0.553
SE sf=7	0.127	0.939
SE sf=10	2.226	0.329
SE sf=20	0.161	0.923
HFD	0.760	0.684
α (DFA)	0.454	0.797
SNZ	1.482	0.477

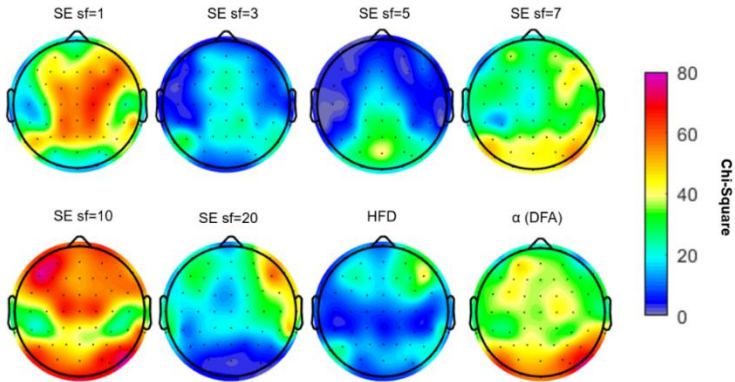


Figure 20: Topographical maps of chi-square values resulting from the Kruskal-Wallis test over all conditions for the complexity and criticality features.

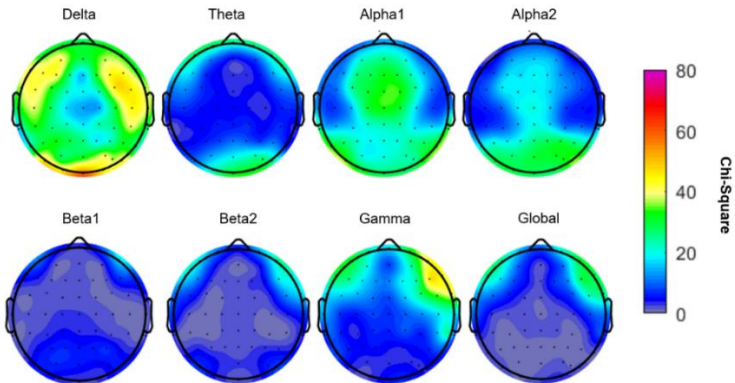


Figure 21: Topographical maps of chi-square values resulting from the Kruskal-Wallis test over all conditions for the spectral bands.

4.1.2 Global comparisons of complexity parameter

For state comparisons, effect sizes were estimated for each complexity and criticality feature and frequency band. Significant differences were determined by a two-tailed t-test corrected for multiple comparisons by the false discovery rate.

The resting state with eyes open was associated with higher complexity in comparison to resting with eyes closed. Here, largest effect size was found for SE sf=1 ($d= 1.47$) and SE sf=10 ($d= 0.93$), whereby the HFD yielded a low effect size ($d= 0.33$). The DFA as an index of long-range temporal correlations (LRTC) was significantly higher in the eyes open resting condition with moderate effect size ($d= 0.73$), whereas the critical scaling exponent was reduced compared to eyes closed with a large effect size ($d= -0.96$). Further, alpha 1 and alpha 2 decreased during eyes open compared to eyes closed with small to moderate effect sizes ($d= -0.58$ and $d= -0.37$).

Compared to resting with eyes open, the reading condition further increased the neuronal complexity

as captured by SE sf=1, SE sf=3, SE sf=7, SE sf=10 and HFD. Regarding the spectral data, an increase in the theta band and a decrease in alpha 1 and alpha 2 was found.

For the presence meditation condition, the increase of SE sf=1 and HFD did not reach statistical significance. However, LRTC were decreased shown by the DFA exponent yielding a medium effect size ($d = -0.49$) in comparison to resting with eyes closed. Delta, and theta band PSD were significantly reduced with a small effect size ($d = -0.33$; $d = -0.22$). In contrast comparing emptiness with the eyes closed resting state resulted in slightly higher complexity with a small effect size as shown by the HFD ($d = 0.23$), whereby less LRTC were measured with the DFA, also with a small effect size ($d = -0.37$). Delta ($d = -0.38$), theta ($d = -0.25$) and beta 1 band PSD ($d = -0.12$) were reduced. A similar pattern was observed in the comparison focused attention vs. eyes closed. Here, the neuronal complexity was higher as captured by SE sf=1 ($d = 0.61$) and SE sf=3 ($d = 0.48$) with moderate effect sizes. The DFA and

the critical exponent were reduced with small effect sizes ($d = -0.28$ and $d = -0.26$). Further, a decrease in delta ($d = -0.36$) and theta band power ($d = -0.21$) was observed, whereas gamma band power was significantly enhanced ($d = 0.32$).

Contrasting the meditation states against each other revealed slightly higher complexity in emptiness compared to presence, whereas the global PSD was lower ($d = -0.28$). Also, alpha 1, alpha 2, beta 1, beta 2 band power was reduced. However, in comparison with the focused attention meditation, the state of emptiness was associated with reduced complexity according to SE $sf=1$ ($d = -0.33$) and SE $sf=3$ ($d = -0.24$) as well as reduced gamma band power ($d = -0.28$). Also, focused attention was characterized by higher complexity compared to presence as captured by SE $sf=1$, SE $sf=3$, SE $sf=5$, SE $sf=7$ and SE $sf=10$, whereas alpha 1 band power was significantly lower during focused attention compared to presence ($d = -0.27$). Also, here, the SNZ was lower during focused attention yielding a small effect size of $d = -0.32$ (Figure 22, Figure 23, Table 4, Table 5).

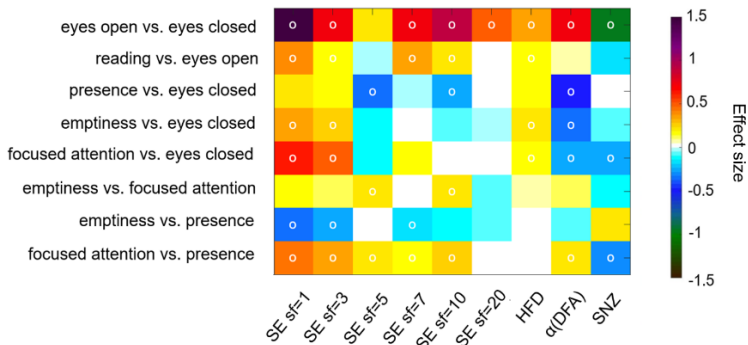


Figure 22: Color-coded differences of complexity parameters shown as effect sizes (Cohen's d) of the meditation task comparisons on a global level averaged over all electrodes. Fields marked with a white circle were significant on the 0.05 level after FDR adjustment.

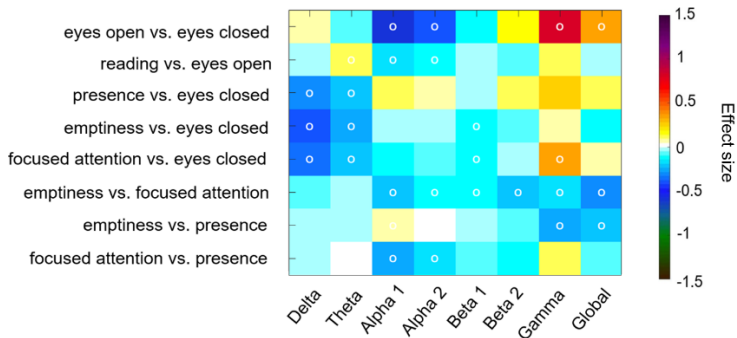


Figure 23: Color-coded differences of power spectral density shown as effect sizes (Cohen's d) of the task comparisons on a global level averaged over all electrodes. Fields marked with a

white circle were significant on the 0.01 level after FDR adjustment over conditions and frequency bands.

Table 4: Values of the effect size and p-values resulting from the comparison between conditions. All p-values were corrected for multiple comparison.

ES (p-value)	SE sf=1	SE sf=3	SE sf=5	SE sf=7	SE sf=10	SE sf=20	HFD	α (DFA)	SNZ
Eyes open vs eyes closed	1.467 (.000)	.720 (.000)	.197 (.342)	.711 (.000)	.930 (.000)	.511 (.000)	.323 (.000)	.727 (.000)	-.972 (.000)
Reading vs eyes open	.382 (.005)	.187 (.003)	-.008 (.086)	.365 (.010)	.197 (.002)	.029 (.276)	.152 (.005)	.076 (.013)	-.175 (.050)
Presence vs eyes closed	.209 (.246)	.154 (.266)	-.336 (.002)	-.020 (.858)	-.244 (.007)	.025 (.833)	.146 (.056)	-.487 (.000)	.026 (.565)
Emptiness vs eyes closed	.348 (.006)	.268 (.006)	-.121 (.110)	.001 (.868)	-.048 (.483)	-.030 (.453)	.231 (.001)	-.369 (.000)	-.077 (.875)
Focused attention vs eyes closed	.610 (.000)	.483 (.000)	-.123 (.130)	.165 (.077)	.046 (.543)	.033 (.635)	.182 (.017)	-.276 (.003)	-.262 (.005)
Emptiness vs presence	.145 (.138)	.128 (.053)	.210 (.003)	.015 (.656)	.196 (.003)	-.051 (.247)	.080 (.231)	.135 (.049)	-.102 (.453)
Emptiness vs focused attention	-.332 (.006)	-.244 (.007)	.000 (.051)	-.166 (.008)	-.098 (.092)	-.066 (.105)	.037 (.691)	-.089 (.101)	.210 (.065)
Focused attention vs presence	.452 (.011)	.367 (.006)	.202 (.028)	.179 (.024)	.277 (.005)	.006 (.969)	.031 (.883)	.228 (.007)	-.321 (.020)

Table 5: Values of the effect size and p-values resulting from the comparison between conditions. All p-values were corrected for multiple comparison.

ES (p-value)	Delta	Theta	Alpha 1	Alpha 2	Beta 1	Beta 2	Gamma	Global
Eyes open vs eyes closed	.088 (.168)	-.082 (.309)	-.582 (.000)	-.377 (.000)	-.094 (.069)	.145 (.118)	.799 (.000)	.375 (.002)
Reading vs eyes open	-.037 (.301)	.096 (.039)	-.171 (.007)	-.132 (.000)	-.019 (.478)	-.062 (.243)	.095 (.484)	-.004 (.969)
Presence vs eyes closed	-.327 (.000)	-.220 (.002)	.138 (.086)	.085 (.141)	-.017 (.669)	.103 (.108)	.237 (.075)	.134 (.272)
Emptiness vs eyes closed	-.377 (.000)	-.248 (.000)	-.045 (.448)	-.035 (.542)	-.116 (.070)	-.079 (.103)	.069 (.517)	-.129 (.199)
Focused attention vs eyes closed	-.360 (.000)	-.214 (.006)	-.116 (.171)	-.064 (.451)	-.103 (.061)	.003 (.792)	.335 (.003)	.065 (.526)
Emptiness vs presence	-.053 (.077)	-.031 (.297)	-.191 (.002)	-.120 (.005)	-.101 (.000)	-.192 (.000)	-.177 (.001)	-.282 (.000)
Emptiness vs focused attention	-.017 (.555)	-.035 (.235)	.077 (.050)	.032 (.492)	-.013 (.716)	-.079 (.099)	-.279 (.004)	-.203 (.002)
Focused attention vs presence	-.036 (.272)	.005 (.933)	-.270 (.002)	-.151 (.009)	-.087 (.035)	-.110 (.183)	.0113 (.416)	-.070 (.579)

4.1.3 Local comparisons

In general, the detailed topographical analysis of the different states illustrated in Figure 24 reveals highest effect sizes in the comparison eyes open vs. eyes closed, whereby seven of the eight analyzed EEG features showed significance in all 13 brain areas. The sample entropy sufficiently discriminates the four comparisons eyes open vs. eyes closed, reading vs. eyes open, emptiness vs. eyes closed and emptiness vs. focused attention. SE $sf=3$ showed significance in all 13 brain areas regarding the comparisons eyes open vs. eyes closed and emptiness vs. eyes closed, whereby SE $sf=7$ distinguishes eyes open vs. eyes closed and reading vs. eyes open. SE $sf=5$ as the only one not showing significance in the brain areas prefrontal and right central regarding the comparison eyes open vs. eyes closed, however, differentiates the comparisons presence vs. eyes closed and emptiness vs. presence in all brain regions. For SE $sf=10$ only in the comparison eyes open vs. eyes closed significant effect size differences could be found in all brain

areas. Though, reading vs. eyes open and presence vs. eyes closed were distinguishable in 12 brain areas except of the left frontal and the right temporal region, respectively. SE $sf=20$ revealed significant effect sizes in the comparison eyes open vs. eyes closed in all regions and discriminated readings vs. eyes open in 10 areas, whereas presence vs. eyes closed only showed significant results in the left temporal area and emptiness vs. eyes closed only right central. HFD sufficiently differentiates eyes open vs. eyes closed as well as emptiness vs. eyes closed in all areas. For the comparison reading vs. eyes open effect sizes reached significance in 11 areas and for presence vs. eyes closed in 8 areas, whereas emptiness vs. presence and emptiness vs. focused attention seem not to be discriminable by the fractal dimension. The scaling exponent resulting from the DFA distinguishes eyes open vs. eyes closed, presence vs. eyes closed and emptiness vs. eyes closed in all brain regions. Taken together, the sample entropy seems the best for the discrimination of the distinct states with 66 significant differences

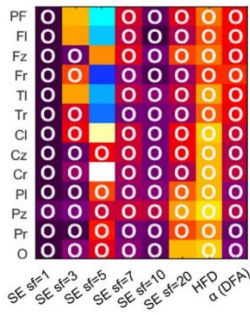
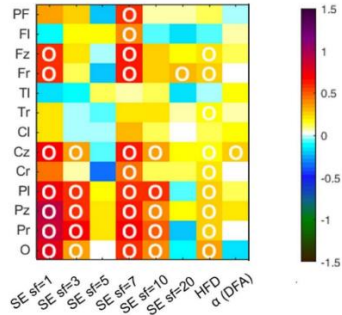
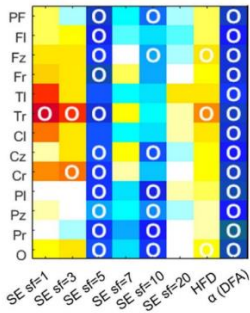
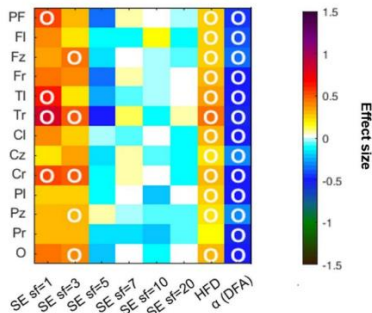
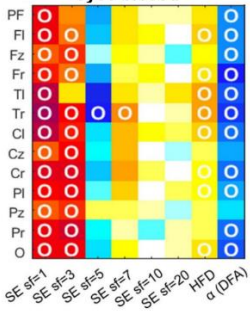
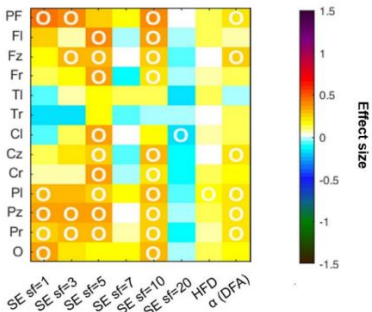
summed up for all comparisons, whereas the DFA gives 60 significant brain areas and the HFD 45 (Figure 25, Figure 26).

Regarding the frequency bands, the comparison between eyes open vs. eyes closed revealed only one significant difference in effect size for the delta band in the prefrontal area, whereas effects for the theta band were found for the frontal and central area. Alpha 1 and alpha 2 discriminated the conditions in all 13 brain areas. Beta 1 showed significances in the occipital and parietal areas as well as central and frontal, whereas beta 2 also sufficiently discriminated the two states in the occipital and parietal, temporal prefrontal and frontal areas. For the gamma band, significant effects were revealed for all 13 topographical regions, except for occipital. On a global frequency band, the resting state task were distinguishable in the prefrontal, the left and right frontal, the temporal, the left central and central area. Contrasting reading with eyes open mainly resulted in significant effects regarding the alpha 1 and alpha 2 band power. The theta and the

gamma band differentiated the conditions in the occipital and right parietal regions, whereby theta also revealed an effect in the left parietal region and gamma in the central parietal region. Beta 1 only showed a significance in the parietal region, whereas beta 2 sufficiently discriminated the tasks in the left central and left temporal area. On a global level, the comparison of effect sizes was only significant in the occipital and left temporal region. Comparing the presence meditation with the eyes closed resting state resulted in significant differences in all 13 brain areas regarding the delta and theta band. Alpha 1 and alpha2 both distinguished the tasks in the right parietal region, whereby the latter also showed a significance in the occipital region. Beta 1 did not show a significance in the occipital region. Beta 1 was not suitable to discriminate the states, whereas for beta 2 significant differences could be observed in the right and left parietal region as well as in the right temporal area. Main effects for the gamma band were found in the left and right temporal region. On a local level, only the right temporal area was significantly different. Emptiness vs. eyes closed

revealed a similar pattern for the delta and theta band with significant differences in effect size in all brain areas. Both alpha bands were not suitable to discriminate the states. Beta 1 was superior compared to beta 2, with significant effects in the occipital, left and central parietal, central, frontal and prefrontal areas. The latter distinguished the conditions in the parietal, the central and frontal region. Gamma was only able to discriminate the tasks in the right temporal region, whereas on a global level discriminability was given in the parietal and central area. The meditation conditions presence and emptiness showed significant differences in the right and left temporal as well as in the right frontal regions in the delta band, whereas no significance was observed for the theta band. In the alpha 1 band, all areas were distinguishable. This was also the case for the alpha 2 band, except for the frontal region. Beta 1 discriminated 11 of the 13 areas and beta 2 revealed significant differences in all regions apart from the prefrontal and left frontal area. The same pattern was observed on a global

level, whereas differences in the gamma band were only found for the right and central parietal, the central, the right temporal and the right frontal region. Contrasting emptiness and focused attention showed mainly effects for the gamma band, with significances in the occipital, prefrontal, central, left temporal, left frontal and prefrontal area. On a global frequency band, the conditions were suitable discriminated in the right parietal, the right and left central, the left temporal as well as the left frontal region. Neither the delta, alpha 1 nor beta 1 band were able to sufficiently distinguish the tasks. A difference in the theta band was only observed in the right temporal area, whereas alpha 1 was distinct in the occipital, left and right parietal as well as the central and frontal region (Figure 25, Figure 27).

A eyes open vs. eyes closed**B** reading vs. eyes open**C** presence vs. eyes closed**D** emptiness vs. eyes closed**E** focused attention vs. eyes closed**F** emptiness vs. presence

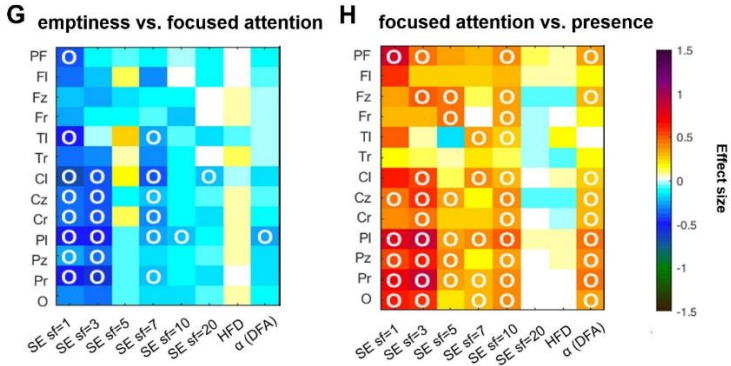
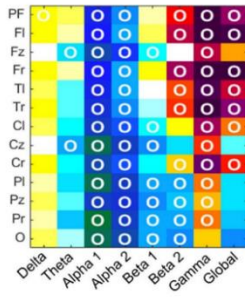
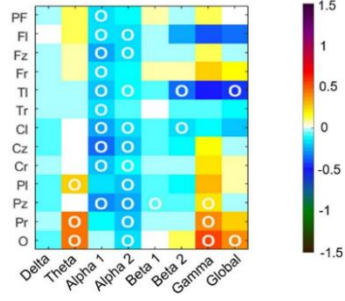


Figure 24: Color-coded feature differences shown as effect sizes (Cohen's d) resulting from the task comparisons. (A) Comparison between eyes open and eyes closed, (B) reading vs. eyes open, (C) presence vs. eyes closed, (D) emptiness vs eyes closed, (E) focused attention vs. eyes closed, (F) emptiness vs. presence, (G) emptiness vs focused attention, (H) focused attention vs. presence. T-tests were calculated from each participant for each location and complexity parameter. Fields marked with a white circle were significant on the 0.05 level after FDR adjustment.

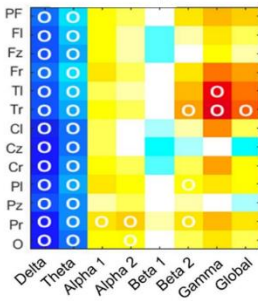
A eyes open vs. eyes closed



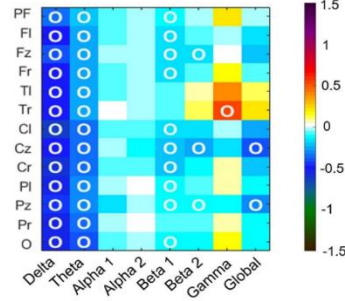
B reading vs. eyes open



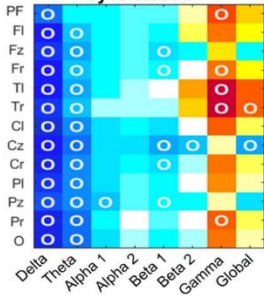
C presence vs. eyes closed



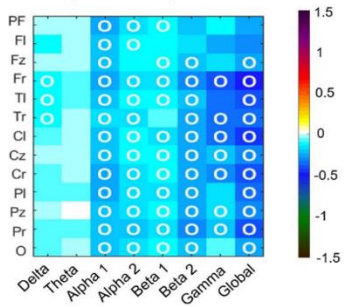
D emptiness vs. eyes closed



E focused attention vs. eyes closed



F emptiness vs. presence



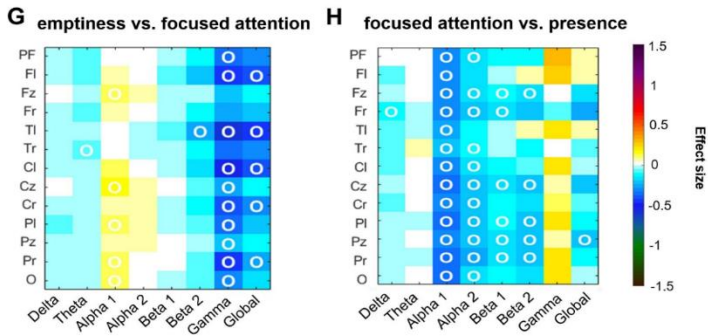
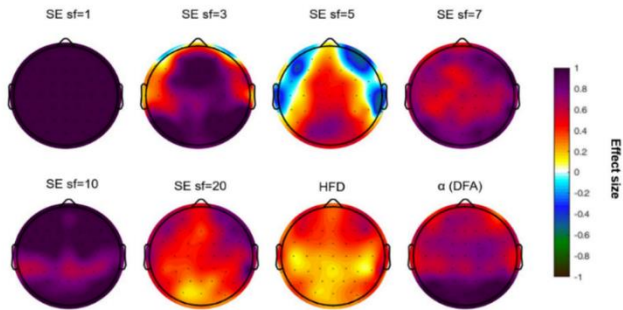
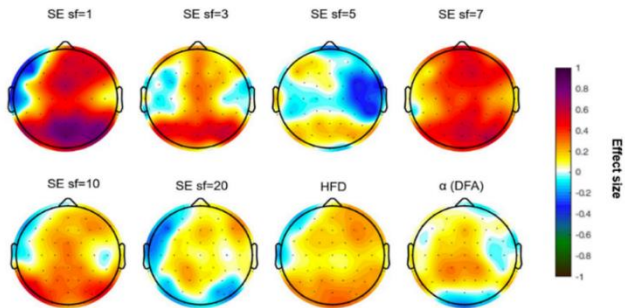


Figure 25: Color-coded power spectral density differences shown as effect sizes (Cohen's d) resulting from the task comparisons. (A) Comparison between eyes open and eyes closed, (B) reading vs. eyes open, (C) presence vs. eyes closed, (D) emptiness vs eyes closed, (E) focused attention vs. eyes closed, (F) emptiness vs. presence, (G) emptiness vs focused attention, (H) focused attention vs. presence. T-tests were calculated from each participant for each location and complexity parameter. Fields marked with a white circle were significant on the 0.05 level after FDR adjustment.

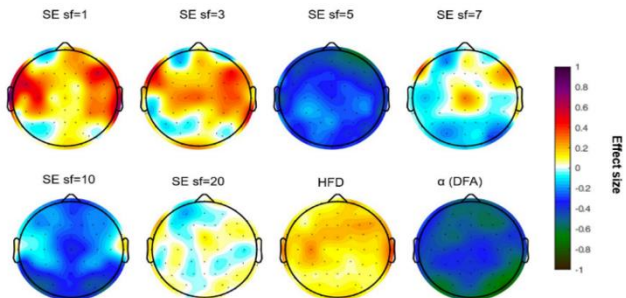
A eyes open vs. eyes closed



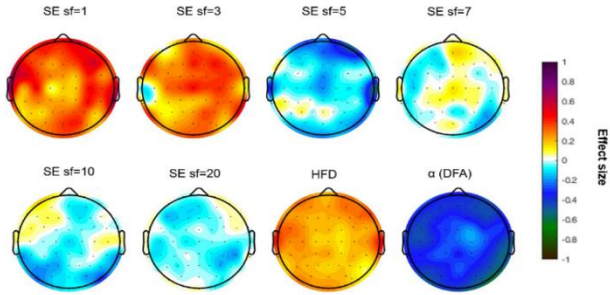
B reading vs. eyes open



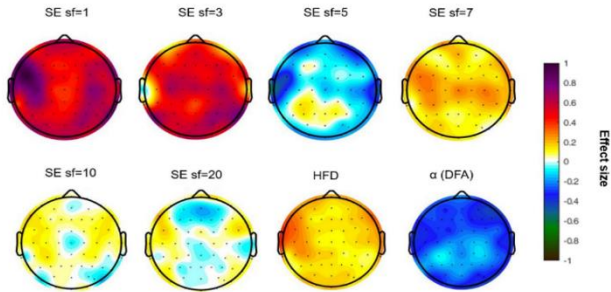
C presence vs. eyes closed



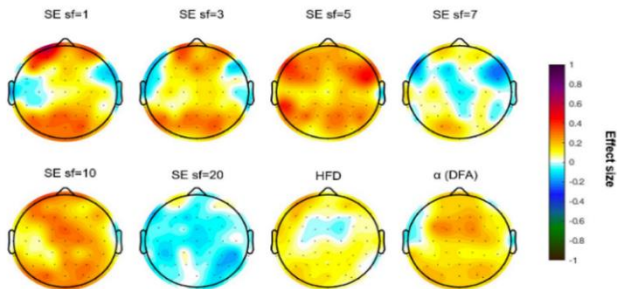
D emptiness vs. eyes closed



E focused attention vs. eyes closed



F emptiness vs. presence



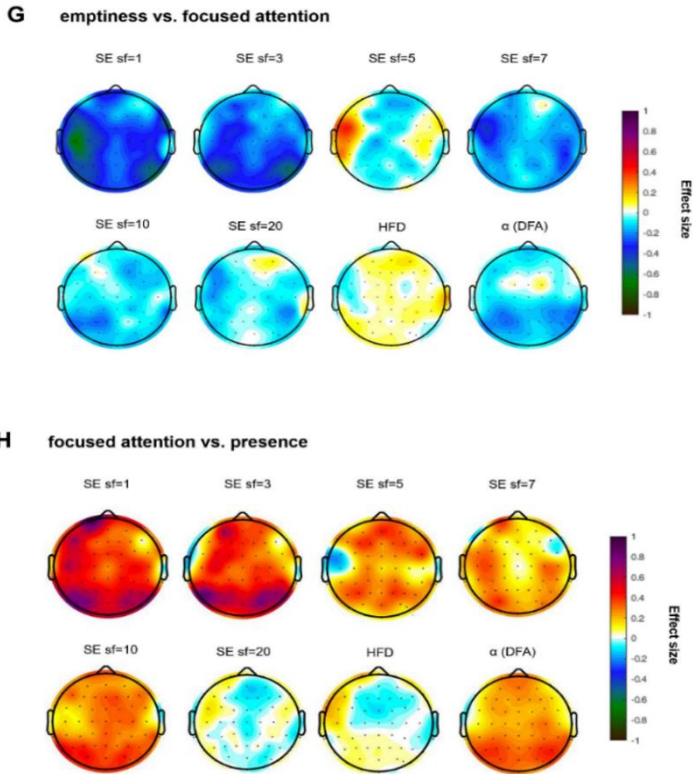
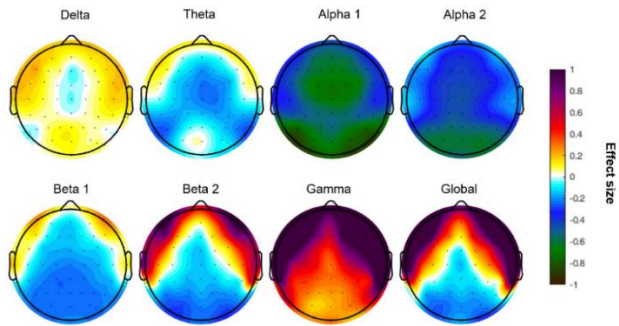
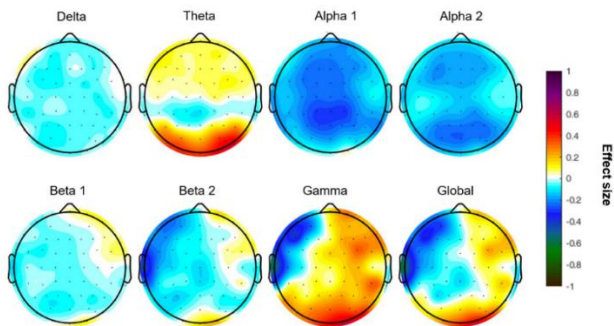


Figure 26: Topographical maps of differences in the effect sizes calculated for each complexity and criticality feature, respectively. (A) Comparison between eyes open and eyes closed, (B) reading vs. eyes open, (C) presence vs. eyes closed, (D) emptiness vs eyes closed, (E) focused attention vs. eyes closed, (F) emptiness vs. presence, (G) emptiness vs focused attention, (H) focused attention vs. presence.

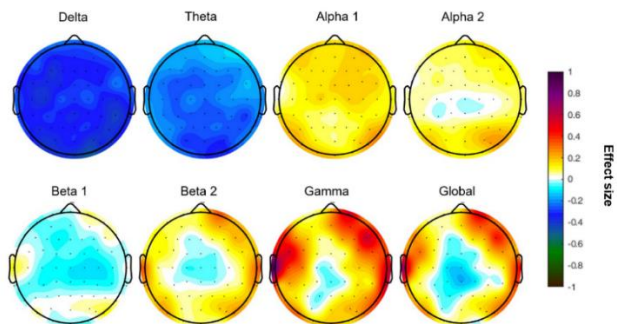
A eyes open vs. eyes closed



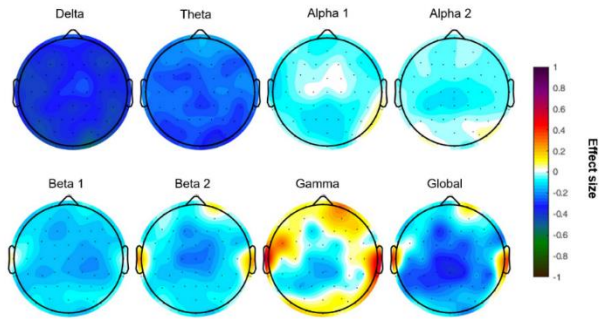
B reading vs. eyes open



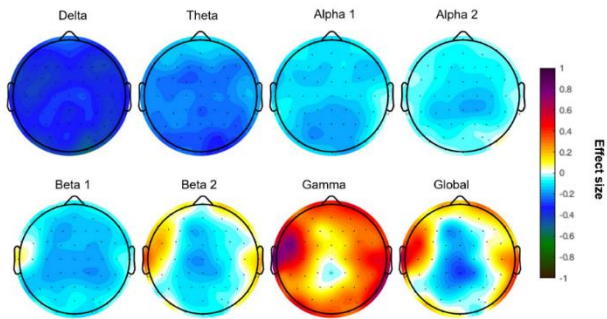
C presence vs. eyes closed



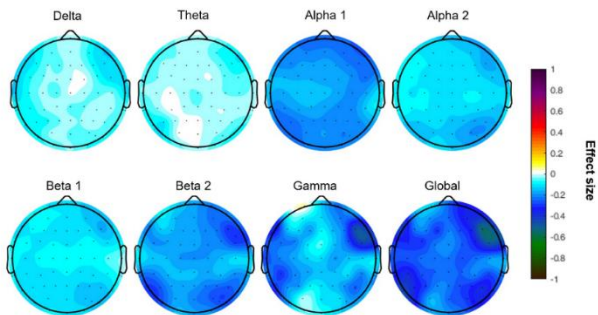
D emptiness vs. eyes closed



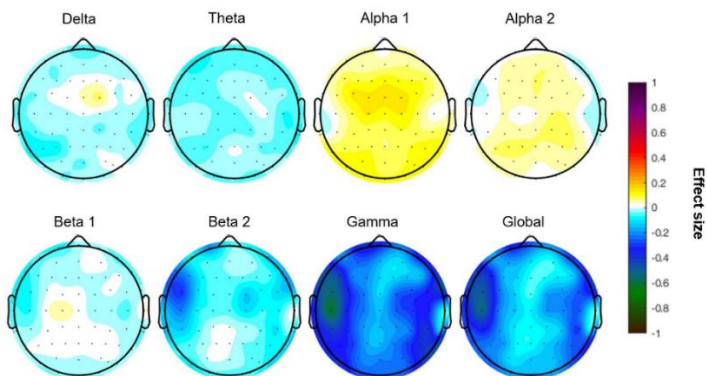
E focused attention vs. eyes closed



F emptiness vs. presence



G emptiness vs. focused attention



H focused attention vs. presence

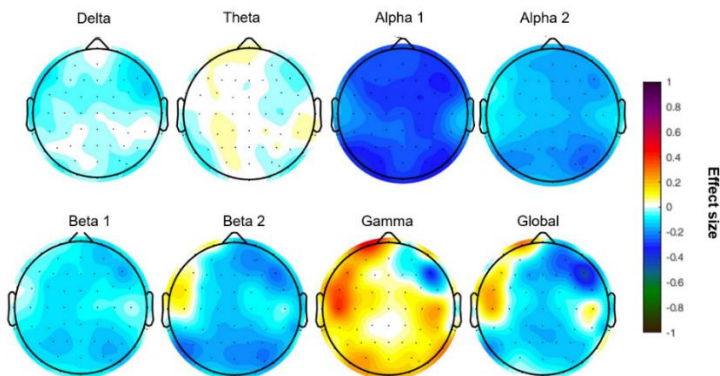


Figure 27: Topographical maps of differences in the effect sizes calculated for each frequency band, respectively. (A) Comparison between eyes open and eyes closed, (B) reading

vs. eyes open, (C) presence vs. eyes closed, (D) emptiness vs eyes closed, (E) focused attention vs. eyes closed, (F) emptiness vs. presence, (G) emptiness vs focused attention, (H) focused attention vs. presence.

4.1.4 Complexity, criticality, and spectral features for each condition

For the sample entropy and HFD higher mean values are observed for the individual meditation and the tasks presence, emptiness and focused attention in comparison to the resting condition with eyes closed, whereby the scaling exponent resulting from the DFA declined (Figure 28, Figure 29A and B). The critical exponent showed the lowest values for the conditions eyes open (1.371 ± 0.09) and reading (1.352 ± 0.07) (Figure 29C). Accordingly, the differences between the critical exponent resulting from the neuronal avalanches analysis and the scaling parameter obtained from the shape collapse function (SNZdiff) were closest to zero in the conditions eyes open (0.429 ± 0.218) and reading (0.322 ± 0.196) (Figure 29D). Regarding the power

spectral density, delta was slightly reduced in the meditation conditions. However, differences were small. For instance, lowest power was found for emptiness (4.868 ± 0.147) compared to highest power for the condition eyes open (5.059 ± 0.130). Theta activity did not show a clear trend. Alpha 1 and alpha 2 were lowest during the reading condition (4.381 ± 0.230 and 4.358 ± 0.273) with highest value in during the presence meditation task (4.821 ± 0.553 and 4.653 ± 0.373). Neither beta 1 nor beta 2 activity revealed differences between the conditions. Gamma was slightly increased in the reading condition (3.701 ± 0.275) (Figure 30).

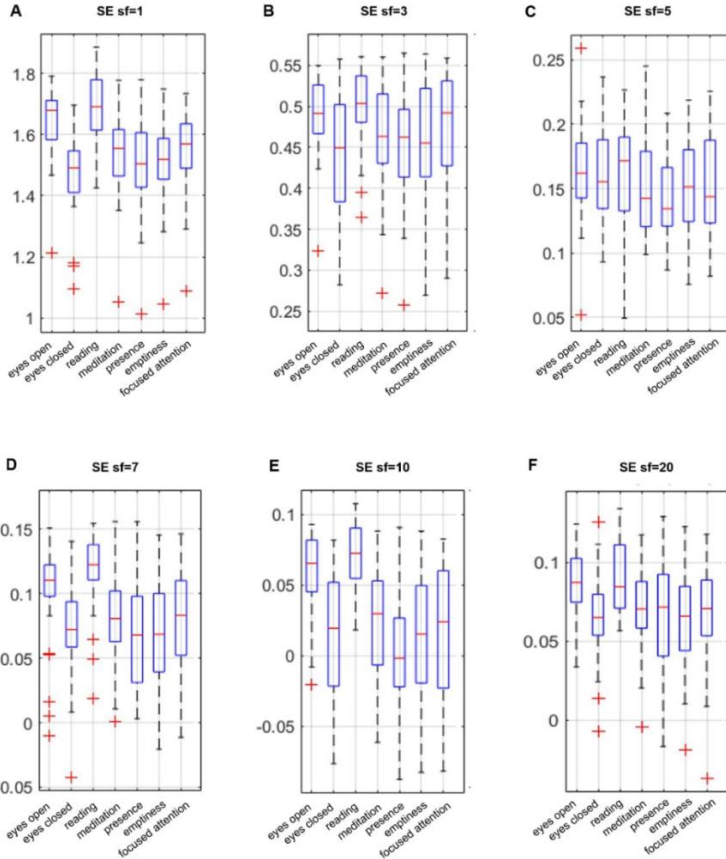


Figure 28: Resulting sample entropy (SE) values for the distinct scale factors (sf) are shown for each condition (A-F).

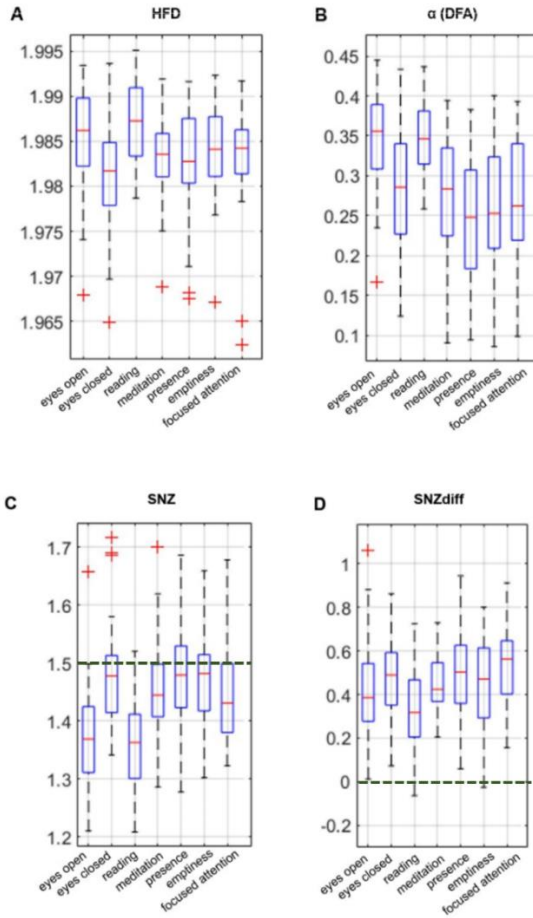
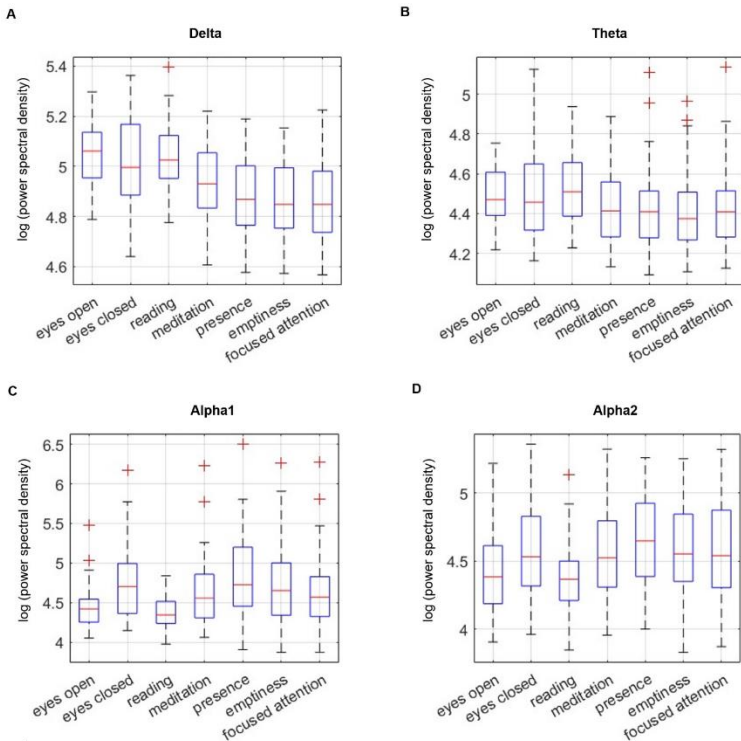


Figure 29: (A) Resulting Higuchi fractal dimension (HFD) values are shown for each condition. (B) Values from exponent resulting from detrended fluctuation analysis (DFA) are illustrated. (C) The critical exponents obtained from the

neuronal avalanches analysis are shown for each condition. The hypothetical value is illustrated by the dark green dotted line. (D) SNZdiff depicts the difference between the critical exponent resulting from the neuronal avalanches analysis and the scaling parameter obtained from the shape collapse function for each condition, respectively. The hypothetical value is illustrated by the dark green dotted line.



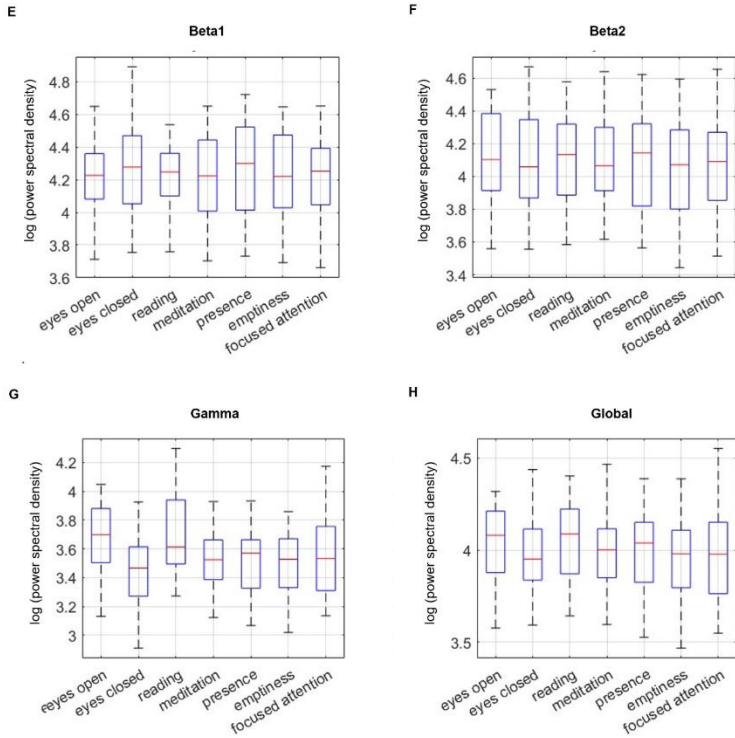


Figure 30: Power spectral density for each frequency band and condition, respectively. (A) shows the delta band, (B) the theta band, (C) alpha 1, (D) alpha 2, (E) beta 1, (F) beta 2, (G) the gamma band and (H) results on a global level.

4.1.5 Correlations between complexity, criticality, and spectral features

Further, correlations were calculated from the mean of the time series across participants after averaging over channels for each condition, respectively (Table 6-Table 11). Here, it becomes evident that the SNZ was significantly negatively correlated with the sample entropy, the scaling exponent resulting from the DFA as well as the HFD in each condition. Thus, the correlation seems to be condition independent. The scaling exponent from the DFA showed highest negative correlations with the alpha 1 and alpha 2 frequency bands.

Table 6: Spearman correlations of complexity and spectral parameter from the mean of the time series of the condition eyes open across participants after averaging over channels; n=30. **p<0.001, *p<0.01

rho	SE	SE sf=3	SE sf=5	SE sf=7	SE sf=10	SE sf=20	HFD	α (DFA)	SNZ
Delta	0.11**	0.08**	-0.15**	0.24**	0.20**	0.18**	0.01	0.32**	-0.01
Theta	0.05	0.03	-0.18**	0.12**	0.00	-0.11**	0.00	-0.07*	0.03
Alpha1	-0.05	-0.13**	-0.33**	-0.18**	-0.32**	-0.21**	0.06	-0.55**	0.18**
Alpha2	-0.03	-0.19**	-0.44**	-0.23**	-0.30**	-0.09**	0.18**	-0.58**	0.13**
Beta 1	0.19**	-0.18**	-0.46**	0.05	-0.10**	0.19**	0.39**	-0.40**	-0.01
Beta 2	0.41**	-0.19**	-0.38**	0.18**	0.05	0.43**	0.59**	-0.33**	-0.13**
Gamm a	0.76**	0.27**	-0.52**	0.48**	0.35**	0.56**	0.72**	-0.14**	-0.19**
Global	0.55**	0.07	-0.50**	0.32**	0.18**	0.43**	0.60**	-0.26**	-0.11**
SE	1.00	0.51**	-0.37**	0.69**	0.61**	0.74**	0.83**	0.09**	-0.35**
SE sf=3	0.51**	1.00	-0.26**	0.60**	0.31**	0.16**	0.13**	0.33**	-0.03
SE sf=5	-0.37**	-0.26**	1.00	-0.37**	0.10**	-0.19**	-0.35**	0.35**	0.01
SE sf=7	0.69**	0.60**	-0.37**	1.00	0.34**	0.56**	0.44**	0.38**	-0.30**
SE sf=10	0.61**	0.31**	0.10**	0.34**	1.00	0.48**	0.41**	0.51**	-0.21**
SE sf=20	0.74**	0.16**	-0.19**	0.56**	0.48**	1.00	0.72**	0.29**	-0.38**
HFD	0.83**	0.13**	-0.35**	0.44**	0.41**	0.72**	1.00	-0.19**	-0.37**
α (DFA)	0.09**	0.33**	0.35**	0.38**	0.51**	0.29**	-0.19**	1.00	-0.15**
SNZ	-0.35**	-0.03	0.01	-0.30**	-0.21**	-0.38**	-0.37**	-0.15**	1.00

Table 7: Spearman correlations of complexity and spectral parameter from the mean of the time series of the condition eyes closed across participants after averaging over channels; n=30. **p<0.001, *p<0.01

rho	SE	SE sf=3	SE sf=5	SE sf=7	SE sf=10	SE sf=20	HFD	α (DFA)	SNZ
Delta	0.12**	0.05	-0.17**	0.21**	0.17**	0.12**	0.01	0.20**	0.01
Theta	-0.03	0.02	-0.10**	0.06	-0.11**	-0.28**	-0.02	-0.25**	0.10
Alpha1	-0.09**	-0.14**	-0.22**	-0.11**	-0.29**	-0.29**	0.10**	-0.54**	0.26**
Alpha2	-0.03	-0.19**	-0.35**	-0.15**	-0.21**	-0.15**	0.21**	-0.54**	0.26**
Beta 1	0.19**	-0.21**	-0.47**	0.10**	-0.10**	0.09**	0.42**	-0.48**	0.05**
Beta 2	0.42**	-0.25**	-0.44**	0.26**	0.07*	0.35**	0.62**	-0.39**	-0.16**
Gamma	0.76**	0.19**	-0.64**	0.56**	0.42**	0.52**	0.72	-0.17**	-0.35**
Global	0.56**	0.01	-0.57**	0.40**	0.24**	0.36**	0.62**	-0.30**	-0.20**
SE	1.00	0.39**	-0.56**	0.76**	0.67**	0.75**	0.82**	0.09**	-0.56**
SE sf=3	0.39**	1.00	-0.25**	0.53**	0.27**	0.06*	-0.01	0.31**	-0.17**
SE sf=5	-0.56**	-0.25**	1.00	-0.54**	-0.17**	-0.37**	-0.56**	0.23**	0.22**
SE sf=7	0.76**	0.53**	-0.54**	1.00	0.39**	0.59**	0.52**	0.25**	-0.47**
SE sf=10	0.67**	0.27**	-0.17**	0.39**	1.00	0.58**	0.42**	0.47**	-0.44**
SE sf=20	0.75**	0.06*	-0.37**	0.59**	0.58**	1.00	0.66**	0.36**	-0.49**
HFD	0.82**	-0.01	-0.56**	0.52**	0.42**	0.66**	1.00	-0.29**	-0.43**
α (DFA)	0.09**	0.31**	0.23**	0.25**	0.47**	0.36**	-0.29**	1.00	-0.19**
SNZ	-0.56**	-0.17**	0.22**	-0.47**	-0.44**	-0.49**	-0.43**	-0.19**	1.00

Table 8: Spearman correlations of complexity and spectral parameter from the mean of the time series of the reading condition across participants after averaging over channels; n=30. **p<0.001, *p<0.01

rho	SE	SE sf=3	SE sf=5	SE sf=7	SE sf=10	SE sf=20	HFD	α (DFA)	SNZ
Delta	0.02	0.10**	-0.14**	0.05	0.18**	-0.03	-0.10**	0.12**	0.03
Theta	-0.15**	0.02	-0.27**	-0.06	-0.05	-0.37**	-0.24**	-0.25**	0.21**
Alpha1	-0.44**	-0.15**	-0.37**	-0.49**	-0.56**	-0.56**	-0.42**	-0.77**	0.56**
Alpha2	-0.41**	-0.26**	-0.47**	-0.55**	-0.48**	-0.27**	-0.27**	-0.62**	0.46**
Beta 1	-0.06	-0.18**	-0.48**	-0.12**	-0.33**	0.00	0.13**	-0.40**	0.02
Beta 2	0.06*	-0.19**	-0.37**	0.01	-0.41**	0.16**	0.26**	-0.39**	-0.05
Gamma	0.48**	0.43**	-0.46**	0.27**	-0.03	0.26**	0.37**	-0.14**	-0.11**
Global	0.19**	0.13**	-0.51**	0.06	-0.23**	0.08**	0.19**	-0.35**	0.04
SE	1.00	0.73	0.05	0.78**	0.53**	0.63**	0.78**	0.56**	-0.50*
SE sf=3	0.73**	1.00	-0.11**	0.55**	0.46**	0.20**	0.31**	0.35**	-0.15**
SE sf=5	0.05	-0.11**	1.00	-0.04	0.29**	0.13**	0.04	0.45**	-0.19**
SE sf=7	0.78**	0.55**	-0.04	1.00	0.46**	0.53**	0.62**	0.62**	-0.59**
SE sf=10	0.53**	0.46**	0.29**	0.46**	1.00	0.16**	0.24**	0.78**	-0.33**
SE sf=20	0.63**	0.20**	0.13**	0.53**	0.16**	1.00	0.67**	0.52**	-0.60**
HFD	0.78**	0.31**	0.04	0.62**	0.24**	0.67**	1.00	0.39**	-0.56**
α (DFA)	0.56**	0.35**	0.45**	0.62**	0.78**	0.52**	0.39**	1.00	-0.59**
SNZ	-0.50**	-0.15**	-0.19**	-0.59**	-0.33**	-0.60**	-0.56**	-0.59**	1.00

Table 9: Spearman correlations of complexity and spectral parameter from the mean of the time series of the presence meditation condition across participants after averaging over channels; n=30. **p<0.001, *p<0.01

rho	SE	SE sf=3	SE sf=5	SE sf=7	SE sf=10	SE sf=20	HFD	α (DFA)	SNZ
Delta	0.05	0.15**	-0.17**	0.09**	0.22**	-0.06	-0.10**	0.16**	0.07*
Theta	-0.08**	0.09**	-0.30**	0.02	-0.03	-0.37**	-0.14**	-0.21**	0.13**
Alpha1	-0.40**	-0.19**	-0.36**	-0.47**	-0.62**	-0.49**	-0.19**	-0.77**	0.36**
Alpha2	-0.39**	-0.25**	-0.51**	-0.52**	-0.54**	-0.24**	-0.11**	-0.68**	0.47**
Beta 1	-0.07*	-0.19**	-0.51**	-0.13**	-0.42**	0.01	0.23**	-0.51**	0.14**
Beta 2	0.06*	-0.23**	-0.39**	-0.04	-0.48**	0.16**	0.36**	-0.51**	0.02
Gamma	0.46**	0.38**	-0.50**	0.24**	-0.11**	0.22**	0.46**	-0.26**	-0.10**
Global	0.19**	0.10**	-0.54**	0.04	-0.30**	0.07*	0.31**	-0.45**	0.05
SE	1.00	0.71**	0.01	0.76**	0.50**	0.58**	0.72**	0.45**	-0.44**
SE sf=3	0.71**	1.00	-0.19**	0.58**	0.44**	0.16**	0.27**	0.34**	-0.17**
SE sf=5	0.01	-0.19**	1.00	-0.10**	0.31**	0.10**	-0.03	0.45**	-0.20**
SE sf=7	0.76**	0.58**	-0.10**	1.00	0.45**	0.47**	0.46**	0.56**	-0.46**
SE sf=10	0.50**	0.44**	0.31**	0.45**	1.00	0.15**	0.13**	0.81**	-0.29**
SE sf=20	0.58**	0.16**	0.10**	0.47**	0.15**	1.00	0.57**	0.42**	-0.41**
HFD	0.72**	0.27**	-0.03	0.46**	0.13**	0.57**	1.00	0.12**	-0.40**
α (DFA)	0.45**	0.34**	0.45**	0.56**	0.81**	0.42**	0.12**	1.00	-0.43**
SNZ	-0.44**	-0.17**	-0.20**	-0.46**	-0.29**	-0.41**	-0.40**	-0.43**	1.00

Table 10: Spearman correlations of complexity and spectral parameter from the mean of the time series of the emptiness meditation condition across participants after averaging over channels; n=30. **p<0.001, *p<0.01

rho	SE	SE sf=3	SE sf=5	SE sf=7	SE sf=10	SE sf=20	HFD	α (DFA)	SNZ
Delta	0.05	0.15**	-0.17**	0.09**	0.22**	-0.06	-0.10**	0.16**	0.07*
Theta	-0.08**	0.09**	-0.30**	0.02	-0.03	-0.37**	-0.14**	-0.21**	0.13**
Alpha1	-0.40**	-0.19**	-0.36**	-0.47**	-0.62**	-0.49**	-0.19**	-0.77**	0.36**
Alpha2	-0.39**	-0.25**	-0.51**	-0.52**	-0.54**	-0.24**	-0.11**	-0.68**	0.47**
Beta 1	-0.07*	-0.19**	-0.51**	-0.13**	-0.42**	0.01	0.23**	-0.51**	0.14**
Beta 2	0.06*	-0.23**	-0.39**	-0.04	-0.48**	0.16**	0.36**	-0.51**	0.02
Gamma	0.46**	0.38**	-0.50**	0.24**	-0.11**	0.22**	0.46**	-0.26**	-0.10**
Global	0.19**	0.10**	-0.54**	0.04	-0.30**	0.07*	0.31**	-0.45**	0.05
SE	1.00	0.71**	0.01	0.76**	0.50**	0.58**	0.72**	0.45**	-0.44**
SE sf=3	0.71**	1.00	-0.19**	0.58**	0.44**	0.16**	0.27**	0.34**	-0.17**
SE sf=5	0.01	-0.19**	1.00	-0.10**	0.31**	0.10**	-0.03	0.45**	-0.20**
SE sf=7	0.76**	0.58**	-0.10**	1.00	0.45**	0.47**	0.46**	0.56**	-0.46**
SE sf=10	0.50**	0.44**	0.31**	0.45**	1.00	0.15**	0.13**	0.81**	-0.29**
SE sf=20	0.58**	0.16**	0.10**	0.47**	0.15**	1.00	0.57**	0.42**	-0.41**
HFD	0.72**	0.27**	-0.03	0.46**	0.13**	0.57**	1.00	0.12**	-0.40**
α (DFA)	0.45**	0.34**	0.45**	0.56**	0.81**	0.42**	0.12**	1.00	-0.43**
SNZ	-0.44**	-0.17**	-0.20**	-0.46**	-0.29**	-0.41**	-0.40**	-0.43**	1.00

Table 11: Spearman correlations of complexity and spectral parameter from the mean of the time series of the focused attention meditation condition across participants after averaging over channels; n=30. **p<0.001, *p<0.01

rho	SE	SE sf=3	SE sf=5	SE sf=7	SE sf=10	SE sf=20	HFD	α (DFA)	SNZ
Delta	0.15**	0.16**	-0.17**	0.20**	0.22**	0.04	-0.05	0.19**	-0.06*
Theta	0.03	0.17**	-0.26**	0.08**	-0.02	-0.31**	-0.11**	-0.18**	0.05
Alpha1	-0.29**	-0.09**	-0.41**	-0.40**	-0.60**	-0.47**	-0.17**	-0.76**	0.35**
Alpha2	-0.30**	-0.20**	-0.53**	-0.47**	-0.58**	-0.21**	-0.09**	-0.71**	0.40**
Beta 1	0.03	-0.11**	-0.54**	-0.10**	-0.41**	0.02	0.26**	-0.51**	0.02
Beta 2	0.14**	-0.17**	-0.39**	-0.02	-0.42**	0.16**	0.35**	-0.49**	-0.08**
Gamma	0.51**	0.40**	-0.52**	0.24**	-0.09**	0.17**	0.42**	-0.29**	-0.12**
Global	0.28**	0.16*	-0.53**	0.07	-0.26**	0.06*	0.30**	-0.44**	-0.03
SE	1.00	0.65**	-0.06*	0.73**	0.50**	0.51**	0.72**	0.37**	-0.43**
SE sf=3	0.65**	1.00	-0.24**	0.54**	0.38**	0.05	0.20**	0.24**	-0.11**
SE sf=5	-0.06*	-0.2**4	1.00	-0.10**	0.33**	0.07*	-0.08**	0.47**	-0.26**
SE sf=7	0.73**	0.54**	-0.10**	1.00	0.46**	0.42**	0.47**	0.53**	-0.43**
SE sf=10	0.50**	0.38**	0.33**	0.46**	1.00	0.19**	0.18**	0.81**	-0.30**
SE sf=20	0.51**	0.05	0.07*	0.42**	0.19**	1.00	0.50**	0.40**	-0.40**
HFD	0.72**	0.20**	-0.08**	0.47**	0.18**	0.50**	1.00	0.09**	-0.42**
α (DFA)	0.37**	0.24**	0.47**	0.53**	0.81**	0.40**	0.09**	1.00	-0.38**
SNZ	-0.43**	-0.11**	-0.26**	-0.43**	-0.30**	-0.40**	-0.42**	-0.38**	1.00

4.1.6 Discrimination analysis

To determine the discrimination accuracy, ROC analysis was applied. Regarding the frequency bands, highest accuracy was found for the gamma band (0.83-0.98) followed by the global PSD (0.78-0.96) (Table 12). The sample entropy was slightly superior to the HFD and DFA analysis in discriminating the meditation conditions (0.86-0.90 vs. 0.73-0.75 and 0.74.-0.77) (Table 17). This was also reflected when plotting the ROC curve two-dimensional with the false positive rate on the x-axis and the true positive rate on the y-axis and calculating the area under the curve (AUC) (Table 14, Table 15).

Table 12: Accuracy of classification of the frequency bands determined by partial least square regression and ROC analysis.

Accuracy	Delta	Theta	Alpha1	Alpha2	Beta 1	Beta 2	Gamma	Global
eyes open vs. eyes closed	0.68	0.70	0.74	0.71	0.70	0.83	0.94	0.91
reading vs. eyes open	0.66	0.68	0.66	0.65	0.66	0.79	0.90	0.87
presence vs. eyes closed	0.71	0.64	0.65	0.63	0.68	0.77	0.92	0.89
emptiness vs. eyes closed	0.72	0.65	0.63	0.63	0.66	0.75	0.90	0.86
focused attention vs. eyes closed'	0.73	0.66	0.63	0.63	0.67	0.77	0.91	0.88
emptiness vs. presence	0.62	0.61	0.62	0.62	0.63	0.68	0.84	0.78
emptiness vs. focused attention	0.62	0.61	0.62	0.61	0.64	0.70	0.83	0.78
focused attention vs. presence	0.63	0.62	0.65	0.64	0.67	0.75	0.88	0.83
presence vs. reading	0.74	0.75	0.81	0.78	0.76	0.89	0.97	0.96
emptiness vs. reading	0.75	0.75	0.79	0.76	0.75	0.90	0.98	0.96
focused attention vs. reading	0.75	0.76	0.77	0.75	0.74	0.90	0.97	0.96

Table 13: Accuracy of the complexity and criticality features in classification determined by partial least square regression and ROC analysis.

Accuracy	SE	SE sf=3	SE sf=5	SE sf=7	SE sf=10	SE sf=20	HFD	α (DFA)
eyes open vs. eyes closed	0.94	0.94	0.92	0.91	0.89	0.88	0.78	0.84
reading vs. eyes open	0.92	0.91	0.89	0.90	0.85	0.84	0.76	0.78
presence vs. eyes closed	0.91	0.92	0.88	0.89	0.83	0.84	0.75	0.79
emptiness vs. eyes closed	0.90	0.91	0.89	0.87	0.80	0.83	0.74	0.78
focused attention vs. eyes closed'	0.92	0.93	0.90	0.89	0.81	0.85	0.74	0.76
emptiness vs. presence	0.86	0.89	0.86	0.85	0.79	0.82	0.73	0.74
emptiness vs. focused attention	0.86	0.90	0.88	0.88	0.79	0.82	0.73	0.76
focused attention vs. presence	0.90	0.92	0.90	0.89	0.83	0.84	0.75	0.77
presence vs. reading	0.97	0.98	0.97	0.97	0.95	0.93	0.87	0.92
emptiness vs. reading	0.98	0.98	0.97	0.97	0.95	0.94	0.86	0.92
focused attention vs. reading	0.98	0.96	0.97	0.96	0.94	0.92	0.86	0.91

Table 14: Values of the area under the curve (AUC) for ROC analysis for the frequency bands.

Area under the ROC curve	Delta	Theta	Alpha1	Alpha2	Beta 1	Beta 2	Gamma	Global
eyes open vs. eyes closed	0.73	0.75	0.79	0.76	0.76	0.89	0.97	0.95
reading vs. eyes open	0.69	0.72	0.70	0.69	0.71	0.85	0.94	0.92
presence vs. eyes closed	0.76	0.69	0.68	0.68	0.73	0.83	0.95	0.93
emptiness vs. eyes closed	0.78	0.70	0.66	0.67	0.70	0.81	0.94	0.91
focused attention vs. eyes closed'	0.78	0.70	0.67	0.67	0.72	0.82	0.95	0.92
emptiness vs. presence	0.65	0.64	0.65	0.64	0.66	0.73	0.89	0.84
emptiness vs. focused attention	0.65	0.64	0.64	0.64	0.67	0.75	0.88	0.83
focused attention vs. presence	0.66	0.65	0.69	0.68	0.71	0.81	0.92	0.88
presence vs. reading	0.81	0.81	0.85	0.83	0.82	0.94	0.98	0.98
emptiness vs. reading	0.81	0.81	0.83	0.82	0.81	0.95	0.99	0.98
focused attention vs. reading	0.81	0.81	0.82	0.80	0.80	0.95	0.99	0.98

Table 15: Values of the area under the curve (AUC) for ROC analysis for the complexity parameter.

Area under the ROC curve	SE	SE sf=3	SE sf=5	SE sf=7	SE sf=10	SE sf=20	HFD	α (DFA)
eyes open vs. eyes closed	0.96	0.97	0.95	0.95	0.93	0.92	0.81	0.87
reading vs. eyes open	0.94	0.95	0.94	0.94	0.90	0.90	0.80	0.82
presence vs. eyes closed	0.94	0.96	0.92	0.92	0.86	0.87	0.79	0.84
emptiness vs. eyes closed	0.94	0.95	0.93	0.91	0.83	0.88	0.78	0.82
focused attention vs. eyes closed'	0.95	0.97	0.94	0.93	0.85	0.89	0.77	0.80
emptiness vs. presence	0.89	0.93	0.90	0.89	0.83	0.86	0.74	0.77
emptiness vs. focused attention	0.89	0.92	0.91	0.92	0.82	0.86	0.74	0.79
focused attention vs. presence	0.93	0.95	0.93	0.93	0.86	0.87	0.78	0.80
presence vs. reading	0.98	0.99	0.99	0.98	0.97	0.97	0.90	0.94
emptiness vs. reading	0.99	0.99	0.98	0.98	0.97	0.97	0.89	0.94
focused attention vs. reading	0.98	0.98	0.99	0.98	0.96	0.96	0.88	0.94

4.2 Singing bowl experience

4.2.1 Kruskal-Wallis Test

A Kruskal-Wallis-Test was performed to analyse whether criticality, neuronal complexity and power spectra were significantly influenced by the course of the experiment. No significant main effect was found (Table 16).

Table 16: Chi-Square values for each complexity, criticality and spectral features resulting from the Kruskal-Wallis-Test.

	Chi square	p-value
SE sf=1	2.05	.360
SE sf=3	0.25	.884
SE sf=5	0.38	.828
SE sf=7	0.21	.899
SE sf=10	0.84	.656
SE sf=20	1.22	.544
HFD	2.34	.311
α (DFA)	0.15	.927
SNZ	4.23	.120
Delta	0.32	.853

Theta	0.051	.975
Alpha 1	0.01	.998
Alpha 2	0.18	.912
Beta 1	0.20	.905
Beta 2	0.68	.713
Gamma	0.92	.632
Global	0.57	.750

4.2.2 Global comparisons

For a comparison between the three conditions, effect sizes were estimated for each complexity and criticality feature as well as frequency band. Significant differences were determined by a two-tailed t-test corrected for multiple comparisons by the false discovery rate. Comparing the distinct phases of the course of the singing bowl massage experiment, statistically significant differences in the effect size of the complexity measures are only found for the HFD exponent in the condition postresting vs. resting ($d = -.11$). However, the critical scaling exponent was suitable to discriminate all three

conditions sound vs. resting ($d = .21$), postresting vs. sound ($d = .38$) and postresting vs. resting ($d = .14$) (Figure 31, Table 17).

The comparison of frequency bands for the experimental tasks on a global level revealed that there was less significant overall EEG power during the sound condition compared to the first resting state ($d = -.30$). The decrease of EEG activity was specifically significant for the frequency bands alpha 2 ($d = -.17$), beta 1 ($d = -.16$), beta 2 ($d = -.24$), and gamma ($d = -.35$). The comparison between the second resting state and the sound condition revealed a decrease in the beta 2 ($d = -.15$) and the gamma frequency band ($d = -.06$). Hence, further reduction in global EEG power was observed during the second resting states compared to the first resting state ($d = -.46$), also with significant effects for alpha 2 ($d = -.21$), beta 1 ($d = -.14$), beta 2 ($d = -.40$) and gamma ($d = -.21$) (Figure 32, Table 18).

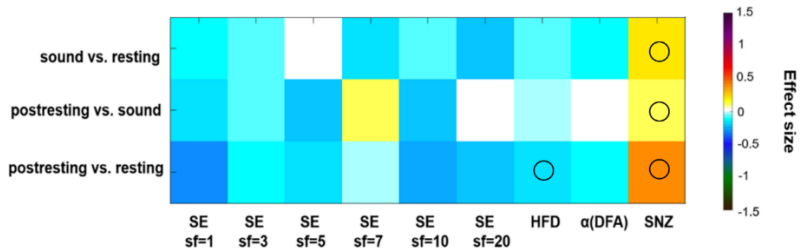


Figure 31: Color-coded differences of complexity and criticality features shown as effect sizes (Cohen's d) of the comparisons between the phases of the experiment on a global level averaged over all electrodes. Fields marked with a black circle were significant on the 0.05 level after FDR adjustment.

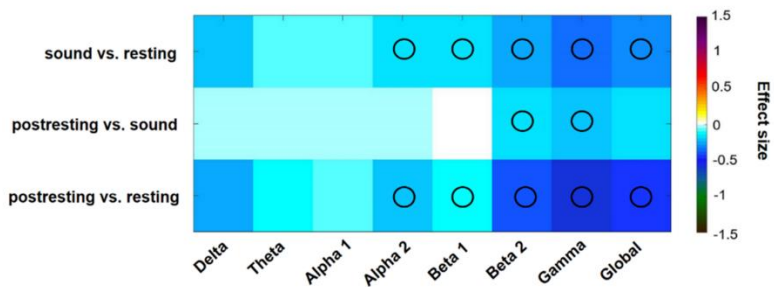


Figure 32: Color-coded differences of power spectral density shown as effect sizes (Cohen's d) of the task comparisons on a global level averaged over all electrodes. Fields marked with a black circle were significant on the 0.05 level after FDR adjustment over conditions and frequency bands.

Table 17: Values of the effect size and p-values resulting from the comparison of complexity and criticality features between the three phases of the experiment. All p-values were corrected for multiple comparison.

ES (p-value)	SE sf=1	SE sf=3	SE sf=5	SE sf=7	SE sf=10	SE sf=20	HFD	α (DFA)	SNZ
Sound vs. resting	-.060 (.645)	-.006 (.997)	.051 (.401)	-.057 (.581)	-.025 (.920)	-.071 (.461)	-.050 (.300)	-.105 (.219)	.211 (.007)
Postresting vs. sound	-.156 (.329)	-.073 (.731)	-.150 (.876)	.081 (.952)	-.085 (.508)	.015 (.661)	-.045 (.008)	.076 (.510)	.140 (.033)
Postresting vs. resting	-.206 (.430)	-.079 (.792)	-.079 (.264)	.038 (.597)	-.101 (.325)	-.055 (.756)	-.113 (.695)	-.040 (.678)	.376 (.000)

Table 18: Values of the effect size and p-values resulting from the comparison of frequency band power between the three phases of the experiment. All p-values were corrected for multiple comparison.

ES (p-value)	Delta	Theta	Alpha 1	Alpha 2	Beta 1	Beta 2	Gamma	Global
Sound vs. resting	-.206 (.052)	-.073 (.392)	-.06 (.376)	-.173 (.003)	-.156 (.002)	-.238 (.005)	-.348 (.001)	-.296 (.002)
Postresting vs. sound	-.026 (.982)	-.013 (.995)	-.020 (.794)	-.022 (.719)	.022 (.325)	-.145 (.002)	-.056 (.000)	-.154 (.06)
Postresting vs. resting	-.239 (.053)	-.113 (.291)	-.08 (.221)	-.208 (.010)	-.136 (.006)	-.396 (.000)	-.206 (.004)	-.460 (.000)

4.2.3 Local comparisons

In the comparison sound vs. resting the scale factors 1, 3, 5, 7, and 10 of the MSE did not yield significant differences in the effect size. Highest effect sizes were found for the SE $sf=20$ in the occipital and left central region. The HFD effect size were only significant different in the occipital area, whereas the DFA showed significances in the prefrontal, left frontal, right frontal, left temporal and central brain region. Comparing the second resting state with the sound phase, the sample entropy showed the lowest

effect size in the right temporal region. For the SE $sf=5$ significant differences were observed in the left temporal, left central and left parietal area, whereas the SE $sf=10$ discriminated the conditions in the right temporal, left central and right central region. Neither the scaling exponent resulting from the DFA nor the HFD yielded big effect sizes. The comparison of the second resting state with the first resting state showed highest effect size differences in the left temporal, right temporal and left central area for the sample entropy. Here, the HFD yielded significant differences in 7 brain areas, whereas the scaling exponent from the DFA was not able to discriminate the conditions on the local level (Figure 33). Regarding the frequency bands, for the comparison sound vs. resting, highest effect sizes were found in the right temporal, the left temporal and left central area in the beta 2, gamma and the global frequency band. The gamma band yielded statistically significant differences in all brain areas, whereas theta and alpha 1 were not able to discriminate the two phases of the course of the experiment.

Comparing the second resting state with the sound phase, resulted also in highest effect sizes in the beta 2, gamma and the global frequency band with significant differences in all brain regions. A similar picture was observed contrasting the second with the first resting state (Figure 34). Topographical plots of the condition comparisons are shown in Figure 35 and Figure 36.

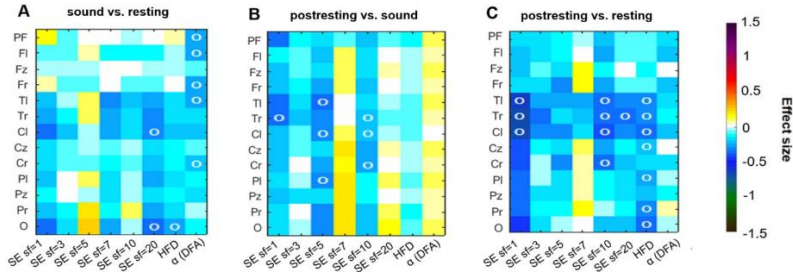


Figure 33: Color-coded complexity and criticality feature differences shown as effect sizes (Cohen's d) resulting from the task comparisons (A-C). T-tests were calculated from each participant for each location and complexity parameter. Fields marked with a white circle were significant on the 0.05 level after FDR adjustment.

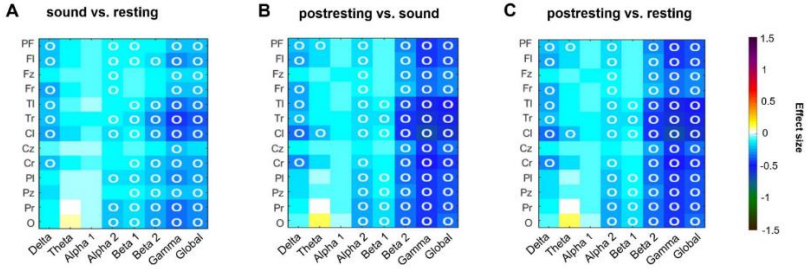


Figure 34: Color-coded power spectral density differences shown as effect sizes (Cohen's d) resulting from the task comparisons (A-C). T-tests were calculated from each participant for each location and frequency band. Fields marked with a white circle were significant on the 0.05 level after FDR adjustment.

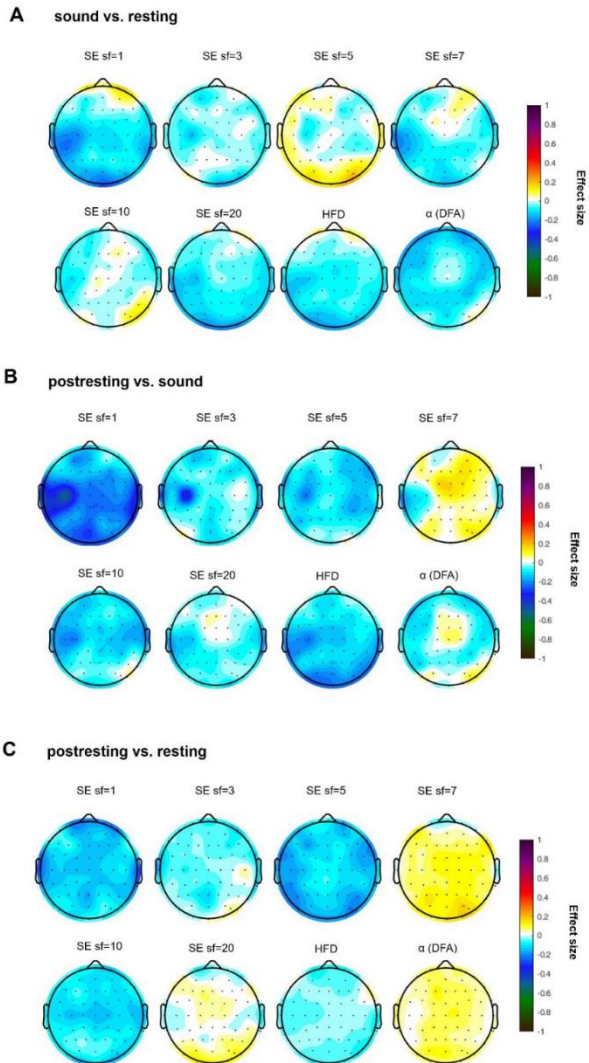


Figure 35: Topographical maps of differences in the effect sizes calculated for each complexity and criticality feature,

respectively. (A) Comparison between sound vs. resting, (B) postresting vs. sound, (C) postresting vs. resting.

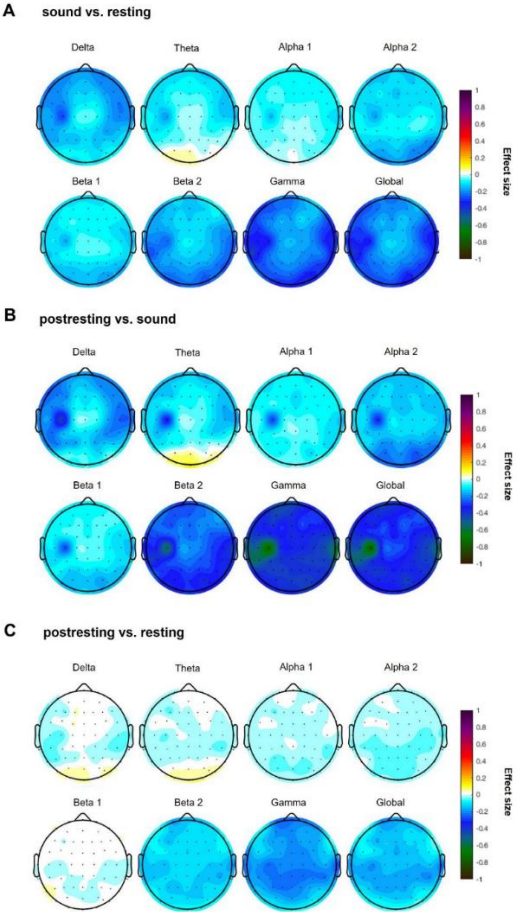


Figure 36: Topographical maps of differences in the effect sizes calculated for each frequency band, respectively. (A)

Comparison between sound vs. resting, (B) postresting vs. sound, (C) postresting vs. resting.

4.2.4 Complexity, criticality, and spectral features for each condition

For the distinct phases during the course of the singing bowl massage experiment, the sample entropy slightly decreased during the singing bowl massage (mean 1.479 ± 0.31) compared to the first resting state (mean 1.491 ± 0.37). The complexity captured with the entropy was further reduced in the second resting state (mean 1.459 ± 0.30). The same trend can be observed for the scale factor 3 and 10 of the multiscale entropy analysis (Figure 37). A decrease of complexity during the sound intervention was also found with the parameters SE $sf=7$ and SE $sf=20$, whereas here the complexity increased between the sound phase and the second resting state. Only the scale factor 5 of the sample entropy showed a different behaviour, with slightly increased value during the intervention compared to the first baseline (from a mean 0.131 ± 0.07 to 0.132 ± 0.06), while during the second resting state values further

decreased to 0.123 ± 0.05) (Figure 37). As depicted in Figure 38, the parameter HFD seems not be affected by the intervention with a mean value of 1.98 for all three phases. The scaling exponent resulting from the DFA slightly decreased from a mean of 0.336 ± 0.09 to 0.325 ± 0.08 between the first resting and the sound intervention, whereas no difference is found between the first and second resting state. The critical scaling exponent SNZ was higher during the intervention phase than in the first resting state (1.417 ± 0.08 compared to 1.379 ± 0.114) and further increased in the second resting state (1.433 ± 0.1) (Figure 38). Regarding the frequency bands, no differences in delta, theta and alpha 1 power was observed. Alpha 2 slightly decreased during the sound phase. For beta 1 values were slightly increased in the second resting state, whereas beta 2 power decreased. Gamma power slightly decreased during the course of the experiment from 4.061 ± 0.71 to 3.91 ± 0.60 (Figure 39).

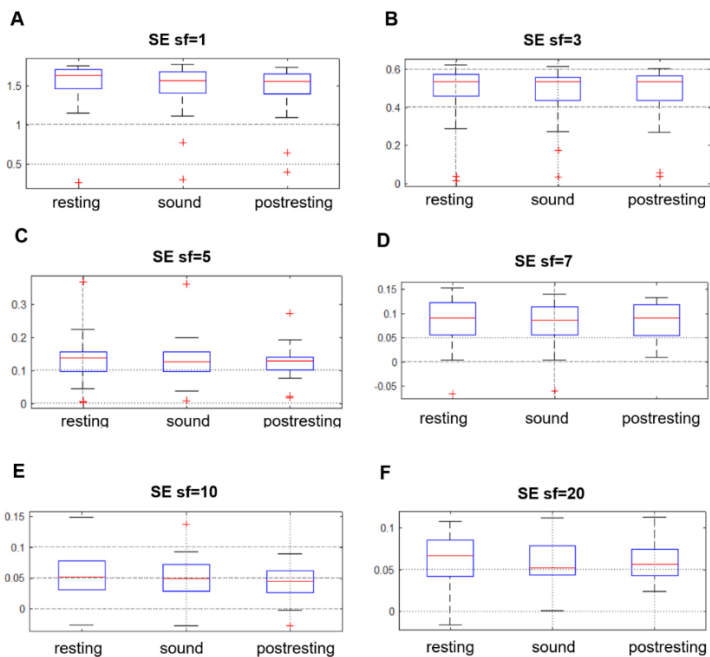


Figure 37: Resulting sample entropy (SE) values for the distinct scale factors (sf) are shown for each phase of the course of experiment (A-F).

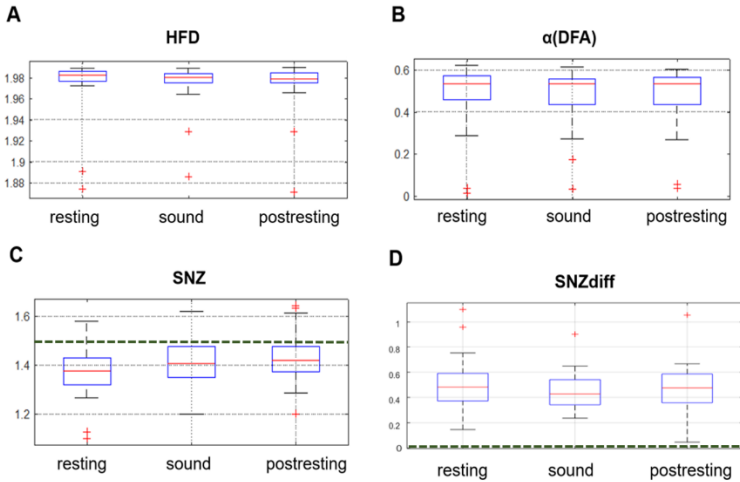
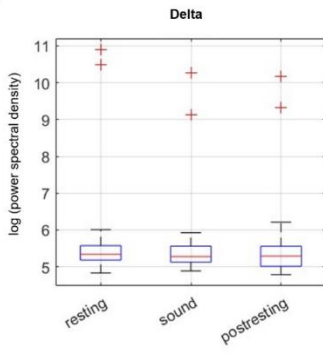
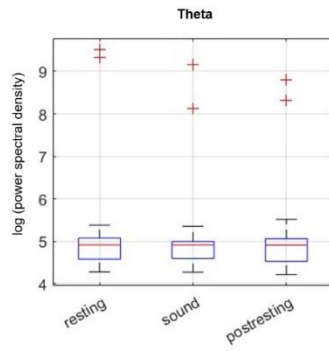
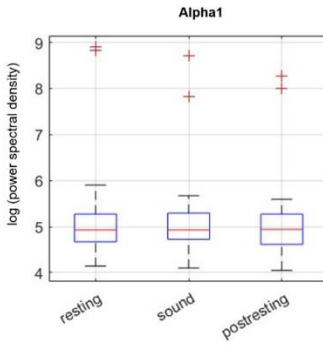
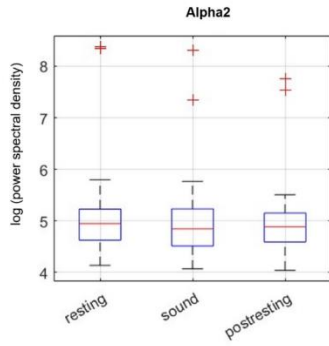
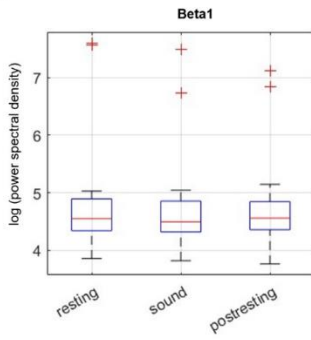
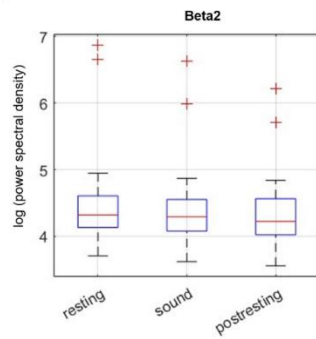


Figure 38: (A) Resulting Higuchi fractal dimension (HFD) values are shown for each condition. (B) Values from exponent resulting from detrended fluctuation analysis (DFA) are illustrated. (C) The critical exponents obtained from the neuronal avalanches are shown for each phase of the course of experiment. The hypothetical value is illustrated by the dark green dotted line (D) SNZdiff depicts the difference between the critical exponent resulting from the neuronal avalanches analysis and the scaling parameter obtained from the shape collapse function for each condition, respectively. The hypothetical value is illustrated by the dark green dotted line

A**B****C****D****E****F**

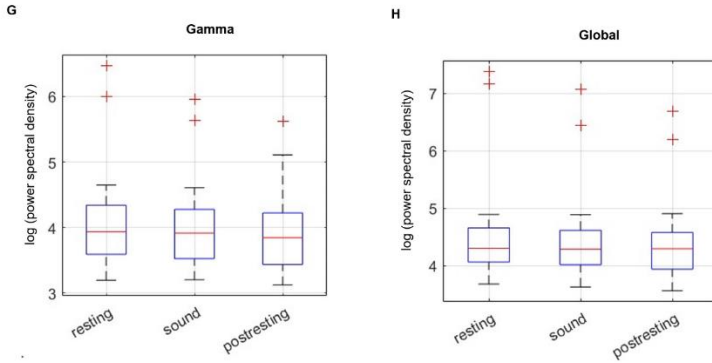


Figure 39: Power spectral density for each frequency band and condition, respectively. (A) shows the delta band, (B) the theta band, (C) alpha 1, (D) alpha 2, (E) beta 1, (F) beta 2, (G) the gamma band and (H) results on a global level.

4.2.5 Correlations between complexity, criticality, and spectral features

Spearman's rank correlations were calculated from the mean of the time series across participants after averaging over channels for each condition, respectively. Here, similar trends as shown in the first study (Table 6-Table 11) can be observed. The SNZ was significantly negatively correlated with the sample entropy, the scaling exponent resulting from

the DFA as well as the HFD in each condition. Also, a significant negative correlation with the gamma power was found (Table 19-Table 21).

Table 19: Spearman correlations of complexity and spectral parameter from the mean of the time series of the first resting state across participants after averaging over channels; n=30.
 **p<0.001, *p<0.01

rho	SE	SE sf=3	SE sf=5	SE sf=7	SE sf=10	SE sf=20	HFD	α (DFA)	SNZ
Delta	0.15	0.30	-0.55*	0.21	0.16	-0.02	0.00	0.38	-0.42
Theta	0.08	0.15	-0.65**	-0.02	-0.09	-0.28	0.14	-0.02	-0.36
Alpha1	-0.27	-0.18	-0.81**	-0.37**	-0.67**	-0.61**	-0.14	-0.44	0.06
Alpha2	-0.27	-0.22	-0.79**	-0.41	-0.47*	-0.52*	-0.11	-0.29	0.02
Beta 1	0.00	0.05	-0.77**	-0.12	-0.27	-0.36	0.14	-0.19	-0.24
Beta 2	0.10	0.05	-0.65**	-0.08	-0.28	-0.28	0.24	-0.17	-0.36
Gamma	0.36	0.35	-0.62**	0.23	-0.06	-0.01	0.38	0.03	-0.60**
Global	0.22	0.22	-0.69**	0.07	-0.17	-0.17	0.27	-0.08	-0.46*
SE	1.00	0.84**	0.11	0.88**	0.49*	0.80**	0.84**	0.11	-0.54*
SE sf=3	0.84**	1.00	-0.05	0.87**	0.48*	0.66**	0.58**	0.11	-0.36
SE sf=5	0.11	-0.05	1.00	0.13	0.50*	0.37	0.14	0.23	0.07
SE sf=7	0.88**	0.87**	0.13	1.00	0.54*	0.84**	0.59**	0.34	-0.46*
SE sf=10	0.49*	0.48*	0.50*	0.54*	1.00	0.57**	0.36	0.53*	-0.31
SE sf=20	0.80**	0.66**	0.37	0.84**	0.57**	1.00	0.53*	0.41	-0.41
HFD	0.84**	0.58**	0.14	0.59**	0.36	0.53*	1.00	-0.19	-0.45*
α (DFA)	0.11	0.11	0.23	0.34	0.53*	0.41	-0.19	1.00	-0.51*
SNZ	-0.54*	-0.36	0.07	-0.46*	-0.31	-0.41	-0.45*	-0.51*	1.00

Table 20: Spearman correlations of complexity and spectral parameter from the mean of the time series of singing bowl massage condition across participants after averaging over channels; n=30. **p<0.001, *p<0.01

rho	SE	SE sf=3	SE sf=5	SE sf=7	SE sf=10	SE sf=20	HFD	α(DFA)	SNZ
Delta	0.11	0.26	-0.54*	0.24	0.14	0.10	-0.08	0.35	-0.36
Theta	0.12	0.18	-0.51*	0.08	0.00	-0.10	0.09	0.05	-0.41
Alpha1	-0.25	-0.12	-0.75**	-0.33	-0.63**	-0.54*	-0.10	-0.43	0.02
Alpha2	-0.26	-0.19	-0.78**	-0.36	-0.53*	-0.42	-0.12	-0.35	-0.03
Beta 1	0.02	0.09	-0.75**	-0.06	-0.25	-0.20	0.12	-0.19	-0.30
Beta 2	0.17	0.10	-0.62**	-0.01	-0.20	-0.15	0.28	-0.19	-0.47*
Gamma	0.35	0.36	-0.62**	0.24	-0.04	0.10	0.35	-0.02	-0.61**
Global	0.23	0.26	-0.65**	0.12	-0.12	-0.04	0.25	-0.08	-0.49*
SE	1.00	0.83**	0.13	0.86**	0.56*	0.76**	0.84**	0.07	-0.64**
SE sf=3	0.83**	1.00	-0.07	0.87**	0.46*	0.66**	0.56**	0.08	-0.40*
SE sf=5	0.13	-0.07	1.00	0.06	0.50*	0.23	0.16	0.19	0.10
SE sf=7	0.86**	0.87**	0.06	1.00	0.57**	0.86**	0.54*	0.35	-0.52*
SE sf=10	0.56*	0.46*	0.50*	0.57**	1.00	0.64**	0.36	0.54*	-0.42
SE sf=20	0.76**	0.66**	0.23	0.86**	0.64**	1.00	0.45*	0.49	-0.57**
HFD	0.84**	0.56**	0.16	0.54*	0.36	0.45*	1.00	-0.27*	-0.54*
α(DFA)	0.07	0.08	0.19	0.35	0.54*	0.49*	-0.27	1.00	-0.40
SNZ	-0.64**	-0.40	0.10	-0.52*	-0.42	-0.57**	-0.54*	-0.40*	1.00

Table 21: Spearman correlations of complexity and spectral parameter from the mean of the time series of the second resting state across participants after averaging over channels; n=30. **p<0.001, *p<0.01

rho	SE	SE sf=3	SE sf=5	SE sf=7	SE sf=10	SE sf=20	HFD	α (DFA)	SNZ
Delta	0.00	0.29	-0.44	0.26	0.41	-0.08	-0.26	0.51*	-0.37
Theta	-0.02	0.17	-0.54*	0.10	0.17	-0.31	-0.14	0.20	-0.41
Alpha1	-0.18	0.00	-0.83**	-0.21	-0.31	-0.55*	-0.12	-0.23	-0.22
Alpha2	-0.30	-0.12	-0.81**	-0.38	-0.34	-0.54*	-0.21	-0.24	-0.13
Beta 1	-0.03	0.11	-0.72**	-0.03	-0.02	-0.36	0.00	-0.07	-0.42
Beta 2	0.16	0.18	-0.59**	0.10	0.01	-0.21	0.18	-0.07	-0.62**
Gamma	0.32	0.38	-0.53*	0.29	0.14	0.02	0.25	0.02	-0.72**
Global	0.19	0.32	-0.63**	0.20	0.09	-0.14	0.12	0.01	-0.61**
SE	1.00	0.69**	0.22	0.85**	0.45	0.71**	0.85**	-0.11	-0.58**
SE sf=3	0.69**	1.00	-0.03	0.78**	0.51*	0.55*	0.40	-0.03	-0.32
SE sf=5	0.22	-0.03	1.00	0.19	0.30	0.41	0.24	0.14	0.13
SE sf=7	0.85**	0.78**	0.19	1.00	0.66**	0.77**	0.52*	0.26	-0.52*
SE sf=10	0.45	0.51*	0.30	0.66**	1.00	0.53*	0.17	0.56*	-0.25
SE sf=20	0.71**	0.55*	0.41	0.77**	0.53*	1.00	0.47*	0.26	-0.41
HFD	0.85**	0.40	0.24	0.52*	0.17	0.47*	1.00	-0.44	-0.46*
α (DFA)	-0.11	-0.03	0.14	0.26	0.56*	0.26	-0.44	1.00	-0.23
SNZ	-0.58**	-0.32	0.13	-0.52*	-0.25	-0.41	-0.46*	-0.23	1.00

4.2.6 Phenomenological data

Regarding the subjective effects of the singing bowl massage, 91.2% of the participants felt more integrated, 97.1% more balanced and 76.5% more vitalized. The bodily feeling was rated as wider (85.3%), more intense (91.2%), more relaxed (91.2%), more comfortable (88.2%) as well as more powerful (70.6%). The emotional state appeared to be calmer for 82.4% of the participants and more balanced (97.1%). Further after the singing bowl application, participants reported to be happier (79.4%), satisfied (88.2%), more secure (82.4%) and connected (88.2%). Mentally, the majority of participants felt clearer (73.5%). Further, 47.1% of the participants were more extroverted and 76.5% satisfied. In total, 94.1% rated the contact with the singing bowl massage conductor as good and 32.4% stated that the duration of time was too short (Figure 40).

The mean TAS score was 69.4 ± 27.5 . The total TAS scores did not correlate significantly with age (*Spearman's* $\rho = .19$, $p = .271$), gender (*Spearman's*

$\rho = -.144$, $p = .417$) or the frequency of experiencing an altered state of consciousness (*Spearman's* $\rho = .317$, $p = .067$). However, significant positive correlations between the TAS score and the following items of the CSP-14 were found: body sensation narrow-wide (*Spearman's* $\rho = .340$, $p = .049$), body sensation uncomfortable-comfortable (*Spearman's* $\rho = .370$, $p = .031$), emotional state sad-happy (*Spearman's* $\rho = .414$, $p = .015$) and emotional state unsatisfied-satisfied (*Spearman's* $\rho = -.395$, $p = .021$).

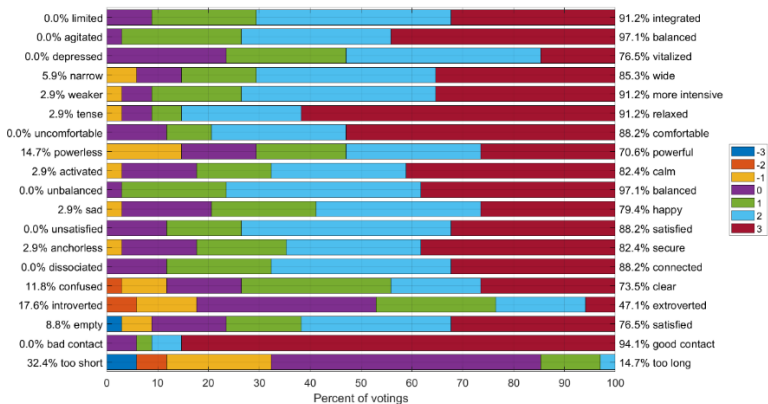


Figure 40: Results of the CSP-14 shown as percentages

Concerning the phenomenology of consciousness, participants scored highest in the dimensions

“openness”, “memory”, “introversion”, “timelessness”, “imagination” and “cognitive clarity” (Figure 41). The total TAS score was significantly correlated with the dimension “insights” (*Spearman's* $\rho = .457$, $p = .028$) and “introversion” (*Spearman's* $\rho = .472$, $p = .027$) of the PCI-K questionnaire. Interestingly, the mean TAS score was significantly negatively correlated with the SNZ during the first resting state as well as the second resting state (Figure 42, Figure 43).

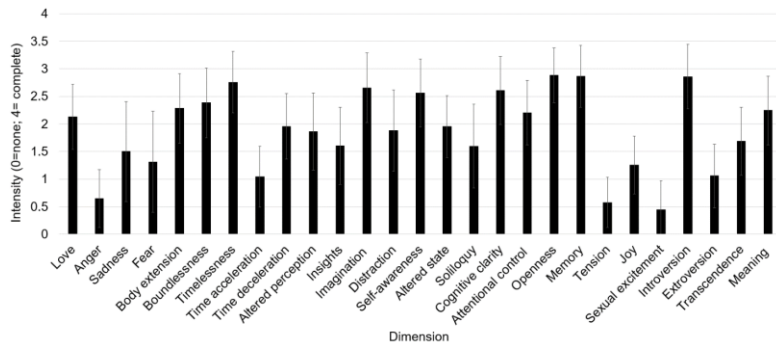


Figure 41: Results of the PCI-K shown as mean \pm SD for each dimension.

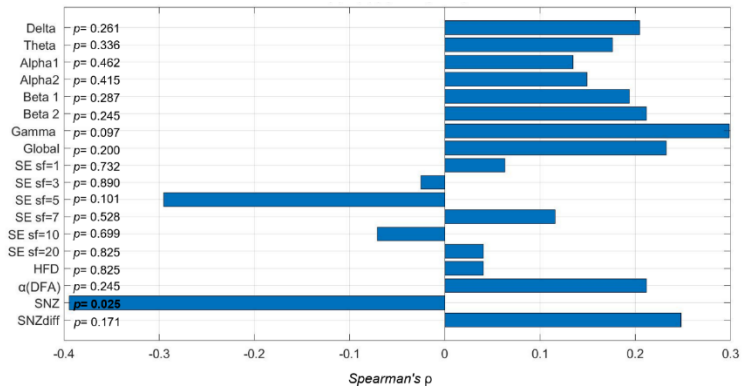


Figure 42: Spearman correlations of the TAS scores with the EEG features calculated from the mean of the time series of the first resting state averaged across participants.

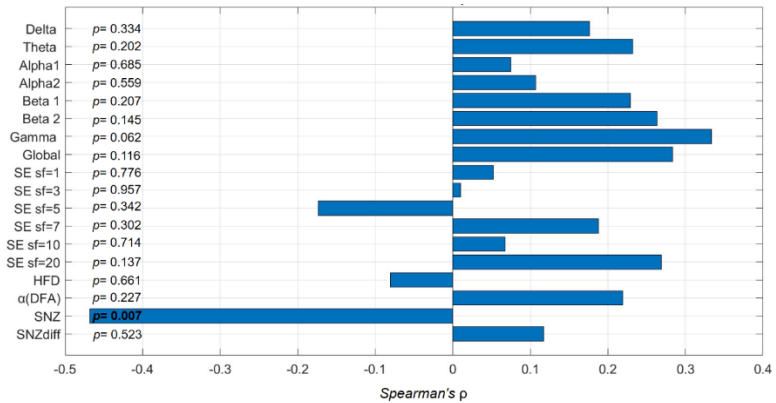


Figure 43: Spearman correlations of the TAS scores with the EEG features calculated from the mean of the time series of the second resting state averaged across participants.

4.3 Sensory processing sensitivity

4.3.1 Correlations between sensory processing sensitivity, complexity, criticality, and spectral features

To determine whether the scores on the HSPS-G scale are significantly associated with the estimated EEG features, Spearman's rank correlation was applied. Here, the summary scores did not significantly correlate with any of the spectral parameter nor with the complexity or criticality values. This was also observed for the subscale *Ease of Excitation* (EOE). However, the dimension *Low Sensory Threshold* (LST) was positively correlated with the scale factor 7 of the multiscale entropy (Spearman's $\rho = .20$, $p = .032$) and the HFD (Spearman's $\rho = .22$, $p = .021$). The subscale *Aesthetic Sensitivity* (AES) showed a positive correlation with beta 2 power (Spearman's $\rho = .20$, $p = .038$) (Table 22).

Table 22: Spearman correlations of complexity, criticality, and spectral parameter from the mean of the time series of the eyes closed resting state across participants after averaging over channels; n=116. *p<0.05.

rho	'HSPS-G_SUM'	'HSPS-G_EOE'	'HSPS-G_LST'	'HSPS-G_AES'
Delta	-0.129	-0.118	-0.146	-0.077
Theta	-0.098	-0.093	-0.119	-0.033
Alpha1	-0.047	0.008	-0.081	-0.021
Alpha2	-0.029	0.054	-0.104	0.035
Beta 1	0.125	0.131	0.084	0.153
Beta 2	0.176	0.183	0.131	0.195*
Gamma	0.110	0.099	0.091	0.089
Global	0.093	0.108	0.048	0.114
SE	0.080	0.027	0.122	0.015
SE sf=3	-0.008	0.003	0.015	-0.154
SE sf=5	-0.044	-0.091	-0.044	0.018
SE sf=7	0.140	0.059	0.201*	0.055
SE sf=10	-0.085	-0.178	-0.011	-0.087
SE sf=20	0.168	0.144	0.178	0.109
HFD	0.168	0.079	0.216*	0.137
α(DFA)	0.005	-0.087	0.066	-0.008
SNZ	0.042	0.099	-0.021	0.075
SNZdiff	0.093	0.160	0.032	0.091

4.3.2 Differences in frequency power spectra, complexity, and criticality features between highly sensitive and not sensitive participants

To examine whether highly sensitive and not sensitive participants show differences in frequency power spectra, complexity and criticality features, the cohort was grouped regarding the HSPS-G summary scores according to a latent class analysis performed by Lionetti et al. determining a frequency distribution of approximately 30% in the low-sensitivity, 40% in the medium-sensitivity and 30% in the high-sensitivity group [246]. EEG features were compared between the two groups applying a Wilcoxon signed-rank test.

The first group (highly sensitive, HS) consisted of $n=47$ participants (mean age 41.75 ± 12.7 years, 24 females/ 23 males), who scored in the range of 74-104 on the HSPS-G summary scale. The mean HSPS-G summary score was 85.14 ± 7.7 . The second group (not sensitive, NS) comprised $n=32$ participants (mean age 38.15 ± 5.1 years, 20 females/ 12 males) with a mean HSPS-G summary score of

22.97± 10.35 (range: 1- 40). The groups did not differ in respect to age ($p= 0.869$) and gender ($p= 0.649$). The NS group revealed lower beta 2 power (4.21 ± 0.17 vs. 4.38 ± 0.32 , $p= .014$), lower power in the gamma frequency band (4.00 ± 0.25 vs. 4.21 ± 0.37 , $p= .010$) as well as lower global EEG power (4.25 ± 0.17 vs. 4.38 ± 0.29 , $p= .041$) (Figure 44).

Regarding the complexity and criticality features, the only significant differences were found for the mean SE $sf=1$, which was lower in the NS group (1.77 ± 0.13 vs. 1.83 ± 0.10 , $p= .018$) and the mean SE $sf=5$, which was higher in the NS group (0.13 ± 0.05 vs. 0.08 ± 0.01 , $p= .004$) (Figure 45).

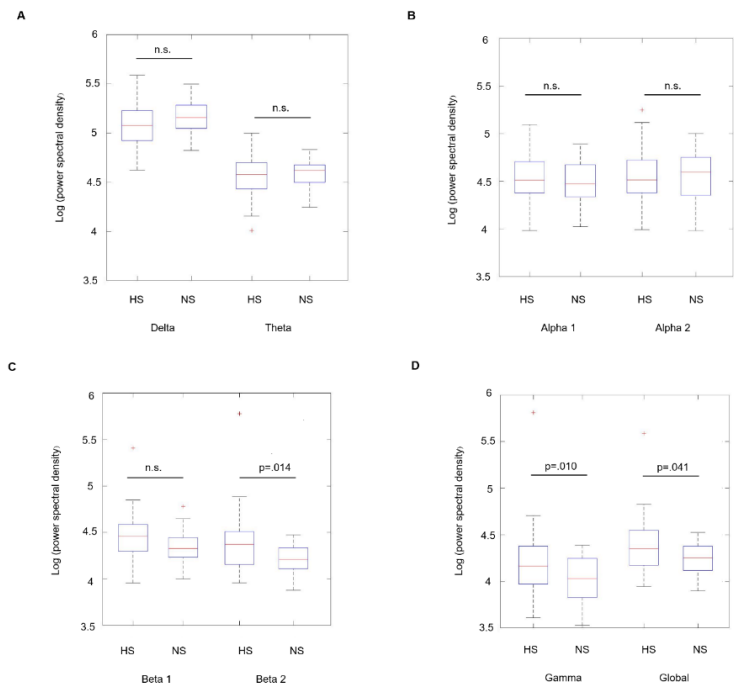


Figure 44: Comparison of power spectral density for each frequency band during resting with eyes closed between the highly sensitive and the not sensitive group. (A) shows the delta and the theta band, (B) alpha 1 and alpha 2, (C) beta 1 and beta 2 (D) the gamma band and results on a global level. *HS= highly sensitive, NS= not sensitive, n.s.= not significant.

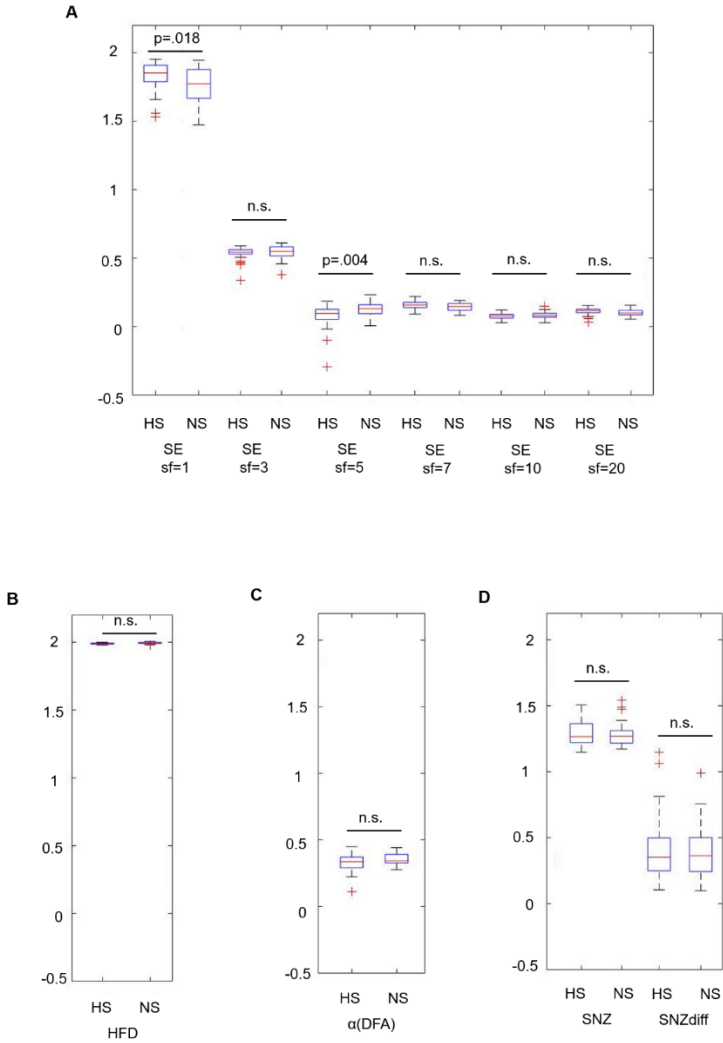


Figure 45: Comparison of complexity and criticality EEG features during resting with eyes closed between the highly

sensitive and the not sensitive group. (A) shows the results of the multiscale entropy, (B) HFD (C) scaling exponent resulting from the DFA (D) the critical exponent SNZ and the distance to the critical point (SNZdiff). *HS= highly sensitive, NS= not sensitive, n.s.= not significant.

5. Discussion

Consciousness has fascinated humankind since its very beginning and the question of how physical processes in the brain give rise to conscious experience still is a baffling for many researchers all over the world. Regarding the quest for specifying processes that underpin normal human consciousness, the nonlinear dynamical system approach has brought forward a variety of hypotheses on the relation between dynamics of neural activity and consciousness experiences. Hereby, contemporary proposals are that the complexity of brain dynamics is a fundamental property of consciousness. Thus, states of consciousness are quantifiable by the degree of neural complexity [247–249, 7]. In recent years, special attention has been given to the premise that neural dynamics might be governed by the phenomenon of self-organized criticality, referring to the ability of complex systems to dynamically evolve towards a second-order phase transition at which

interactions between system components give rise to scale-invariant behaviour. The premise of self-organized criticality is especially appealing as the observed scale-free patterns close to a phase transition imply the largest variability and thus, the largest number of configurations and repertoire of possible brain states. Accordingly, critical state dynamics have been attributed with optimized network functions of information processing such as input susceptibility, maximized dynamic range, storage capacity as well as computational power. Hence, critical dynamics were proposed as general gauges of information processing and features of healthy brain dynamics [250, 148, 251].

This thesis was based on the proposal that distinct states of consciousness are quantifiable by complexity and criticality measures serving as an index of the brain's information processing capacity. Such empirical measures suitable to discriminate states of consciousness could be important, inter alia, for clinical diagnostics and therapy [63, 61, 148, 51]. Here, a task-free baseline resting, a reading

condition and three meditation conditions (first study), a singing bowl experience (second study) as well as a task-free baseline resting obtained from participant with different sensory processing sensitivity (third study) were analysed applying analytical tools from criticality theory (detrended fluctuation analysis, neuronal avalanche analysis), complexity measures (multiscale entropy, Higuchi's fractal dimension) and power spectral density. Task conditions were contrasted, and effect sizes were compared to determine to what degree these EEG features reflect changes in the state of wakeful consciousness as well as temperament traits associated with information processing capacities.

5.1 The neurophysiology of meditative states

The results showed that state discriminations on the level of global field power could separate the meditation condition emptiness from focused attention and presence. Here, emptiness was associated with the highest reduction of overall EEG power. Delta and theta band power was significantly

decreased in all three meditation conditions compared to eyes closed resting. Also, beta band power was reduced during emptiness and focused attention meditation in comparison to resting, whereas gamma band power was significantly enhanced during focused attention. In line with these findings Cahn et al. associated meditation with a decrease in frontal delta power in long-term Vipassana meditators [252]. In contrast, Berman and Stevens reported significantly higher power in the delta, theta and alpha band during a nondual meditation compared to resting [253]. Also, Ahani et al. measured a cohort aged 50-75 years with high stress levels (perceived stress scale score ≥ 9 [254]) and no prior meditation experience. The authors reported increased beta and theta band power during meditation, whereas the alpha band had a slight increase in power in the right lateral and posterior locations during a sitting mindfulness meditation [255]. An evaluation of a Buddhist concentrative meditation revealed alpha power increases and enhanced theta power in a deep meditative state

[256]. Lagopoulos and colleagues carried out a nondirective meditation study. Compared to rest, they observed higher theta and alpha power during meditation on a global brain level. On a local level, the first was significantly increased in frontal and temporal-central brain areas, whereas the alpha band effect was found in the posterior region [257]. A comparison of novice and experienced meditators revealed a more integrated functional network topology determined based on a phase-lag index and a minimum spanning tree approach. For the theta and beta frequency bands no significant differences was found between the groups [258]. The observed increase in gamma power during focused attention meditation is in line with other studies. For instance, Lutz et al measured EEG in long-term Buddhist meditation practitioners and observed high amplitude gamma band oscillations and phase synchrony in frontoparietal electrodes. The authors concluded that their results suggest that meditation involves temporal integrative mechanism and may contribute to short- and long-term neural plasticity [259]. It has

also been suggested that the level of expertise significantly influences changes in the EEG. For instance, a positive correlation between gamma power during mind wandering and hours of practice was reported. However, such relationship could not be confirmed in other studies [260]. Here, only highly experienced meditators with an average of 20 years and 6498 hours of practice were included. Nonetheless, the practice duration and the level of proficiency are not necessarily proportional. In a systematic review Lomas et al. noted that no meta-analysis was possible as no more than three studies employed the same processing procedure [261]. In their work they found that enhanced alpha and theta power was associated with meditation in comparison to a eyes closed resting state, however such outcomes were not uniformly observed [261]. This emphasized the need of standardized approaches in meditation research as considerable inconsistencies in the literature hinder generalizations [262].

Further, higher neuronal complexity was found during the meditation conditions emptiness and

focused attention compared to resting with eyes closed as captured by the sample entropy and HFD values. The results also revealed significantly reduced LRTC in all three meditation conditions compared to the resting state. The critical scaling exponent yielded lower values for focused attention. SNZ values were further reduced during the reading condition compared to the meditation conditions, which may indicate a link between sustained attention and the critical regime.

It has previously been suggested that higher entropy states may represent an increased repertoire of potential configurations [263, 136, 249, 264] and that a loss of brain complexity may be associated with cognitive impairments [265]. In line with the presented results, Kakamanua et al., analysed EEG data of participants with different proficiencies during a Vipassana meditation and report increased HFD and permutation entropy in teachers and novices [266]. In addition, Huang and Lo estimated a higher complexity index, especially at occipital, temporal and anterior areas during Zen-meditation in

experienced practitioners compared to a control group, resting for the same amount of time [267]. Further, increased fractal dimension as determined by Sevcik's method was found in a calming meditation task [268]. Also, Vivot et al. analyzed an EEG dataset of experienced meditators following three different traditions. The meditation styles included Himalayan Yoga and Vipassana, which can be classified as focused attention, as well as Isha Yoga, classifiable as open monitoring. The authors reported an increase in the sample entropy during all practices [269]. In contrast, Young et al., obtained EEG from highly skilled meditators engaging in six different meditation styles. They reported lower Lempel-Ziv complexity scores during all meditation styles compared to a mind-wandering task, however no difference in the power spectra was observed [270]. Further, Aftanas and Golocheikine analyzed data of twenty experienced meditators during rest and Sahaja Yoga meditation, categorized as an open monitoring practice, using non-linear dimensional complexity (DCx). They report decreased DCx

estimates over midline frontal and central areas and a negative correlation with the alpha and theta frequencies bands, concluding that irrelevant networks might be deactivated for the maintenance of the focused internalized attention [271]. In accordance with these results, two studies showed decreased wavelet entropy during a mindful breathing meditation compared to an eyes closed resting state [272, 273].

On the other hand, the decline of LRTC was consistent in our findings among all three meditations. Also, Irmischer et al. showed that meditation practitioners exhibit weaker long-range temporal correlations during a focused attention meditation compared to rest by applying DFA to EEG data. The suppression of LRTCs could not be detected in participants without previous meditation experience. The authors interpreted the results as a shift towards a subcritical regime and argued that the reduced autocorrelation within the signal may be associated with fewer distractions from the task [274]. Here, the critical exponent was significantly

negatively correlated with the sample entropy, the HFD and the scaling exponent of the DFA consistently across the conditions. Thus, according to the critical exponent, our findings indicate a shift towards a subcritical regime during reading and the focused attention meditation. Also, Fagerholm et al. analysed neuronal avalanches during a visuomotor cognitive finger-tapping task in comparison to rest associating the task state and increased attentional load with a shift towards subcritical dynamics [215]. Further, Tomen and colleagues associated marginally subcritical dynamics with enhanced stimulus discriminability under attention. In their network model, entropy was maximized at the subcritical border under the assumption of a coarse observation scale [275]. Considering these nuances, post hoc interpretations of stronger LRTC as neural dynamics closer to the critical point [183] and subcritical dynamics as reduced information processing [274] require some caution. This finding is especially important for theories of consciousness, in which the concepts of complexity and criticality are

often used equivalently. For instance, in his entropic brain hypothesis informed by psychedelic research Carhart-Harris proposed that the entropy of brain activity indexes the informational richness of conscious states and equates higher entropic states with more flexible cognition and a shift towards supercritical dynamics. The author further entertain the idea that a supercritical regime may favor positive mood and creative thinking [276, 249]. To note, the proposal has been challenged [277] and the significant negative correlation between the critical scaling exponent and the sample entropy value in each meditation condition reported here, clearly shows that higher entropic state do not necessarily imply an attunement of brain activity towards the critical point. Thus, the relationship between different complexity and criticality features as a function of states of consciousness should be investigated meticulously, putting recent theories to experimental testing ground. Hereby, applying a combination of nonlinear methods seem to be of utmost importance [278]. Further, it has theoretically hypothesized that

meditation tunes the brain dynamics closer to a critical state [279], which has recently been supported by experimental research reporting that focused attention meditation shifts the scale-free dynamics towards the critical point [280]. These results seem to contrast the findings presented here, which may be explained by differences in the study design, e.g. experienced meditators measured with EEG vs. novices measured with MEG. Additionally, Dürschmid and colleagues used a frequency-specific criticality analysis, whereas in this study the data was not filtered into distinct frequency bands.

Additionally, our analysis showed significant correlations between that the complexity, criticality, and spectral measures. To date, the relationship between the complexity of EEG signals and their spectral properties is not fully understood [281]. The classification analysis revealed that the sample entropy, the HFD and the DFA yielded an accuracy over 70% in discriminating the conditions. Also, the global PSD and the gamma ban reached an accuracy of more than 75%. Addressing the question

to what extent nonlinear techniques capture phenomena that could not be assessed by spectral analysis, Mediano and colleagues performed a decomposition of spectral and phasic differences in the Lempel-Ziv complexity of an MEG dataset between a task and rest condition, reporting that the effect is mostly driven by spectral changes [282]. Further attempts have been made to determine whether observed complexity changes go beyond what would be expected from changes in the power spectrum. For instance, Schartner et al. (2017) measured lower dynamical complexity during non-rapid eye movement sleep compared to rapid eye movement sleep and wakeful rest. The differences could not be solely attributed to power spectral density changes between the conditions [283]. It has emphasized that each complexity measure gives additional information about the underlying data [278] and hence, the combination of EEG complexity and traditional measures such as power spectral density are deemed as fruitful for further investigations [281]. For a further discrimination and

classification of mental states, also other machine learning algorithms may yield promising results [284]. For instance, Hinterberger et al. successfully applied a linear classifier for staging of individual meditation sessions into a variety of predefined meditation states, whereby 83% of the epochs could be correctly classified to their originating task [234]. Also, Ahani et al established a classifier by applying a Support Vector Machine (SVM) algorithm to EEG data collected from novice meditators after a six-week meditation intervention. The authors further associated EEG with respiration, which resulted in a higher accuracy (85%) in the discrimination between meditation and control conditions compared to a classifier solely based on the EEG signal (78%) [285]. Additionally, Lee and colleagues reported an approach using SVM and an artificial neuronal network (ANN) to quantify meditation experience. Based on spectral features they classified three meditation groups categorized as novice, junior and senior achieving an accuracy rate >98% [286]. Further, Sharma et al aimed at discriminating

meditators and non-meditators. For this purpose, they collected EEG data before and after three months of regularly practice of combined yoga and meditation. Data was analysed by discrete wavelet transform. By applying ANN to statistical features of the frequency bands, 87% accuracy was achieved for classification [287]. Besides, approaches with fuzzy c-means and K-Nearest Neighbours algorithms for a classification of meditation states were reported [288, 289]. Goshvapour et al. compared the accuracy of different classification methods on EEG data recorded pre and post an meditation intervention, showing that Fisher discriminant and Parzen classifier yielded the best results [290].

5.2 Effects of a singing bowl experience

The intervention of a singing bowl massage found its way into various fields of applications such as prevention, therapy, wellness and education. In this study, neurophysiological effects as well as subjective changes of wellbeing were evaluated. The results showed an overall decrease of EEG power

during the singing bowl massage as well as afterwards. The effects were most pronounced in the beta 2 and gamma frequency band.

The neurophysiological changes may be interpreted as a refrain from specific cognitive processing such as mental conceptualization, which would be commensurate with the essential aspect of mindfulness, namely non-judgmental awareness of the moment-to-moment-experience [291]. This would be in line with the findings of the first study showing global decreased EEG activity as well as decreases in frontal beta and central and parietal gamma band, when highly experienced meditators entered a state of thoughtless emptiness [232]. Further, a decrease in power over all frequency bands was detected during a meditation characterized as “sacred, unified, egoless, and blessed” [288]. Also, Dor-Ziderman et al. distinguished between a state of “narrative” self-awareness and a “minimal” self-awareness in a MEG neurophenomenological study. The authors reported that the first involved frontal and medial prefrontal

gamma band power decrease while the latter was related to a beta band power decrease in a network including ventral medial prefrontal, medial posterior and lateral parietal regions. Furthermore, the authors linked an attenuation of beta band activity in the right inferior parietal lobule to a state of selflessness [292]. Compared to the findings of the meditation states study reported here, changes in neuronal complexity and criticality features due to the experimental condition were less pronounced (Table 17). Whereas the meditation states were associated with higher neuronal complexity, effect sizes of the sample entropy and fractal dimension were decreased in the second study, which was most pronounced in the comparison of the second and first resting state. Interestingly, the critical scaling exponent SNZ was suitable to discriminate all three phases of the course of the experiment, whereby values were closest to the critical point in the postresting condition. Also here, correlations revealed a significant negative correlation between the critical scaling exponent and the sample entropy, fractal dimension and the DFA

exponent and thus, verified the findings of the first study.

The reported positive psychological effects are in line with other findings in the literature. For instance, Goldsby et al. reported less tension, anger, fatigue, and depressed mood ($p < .001$) after a meditation with Tibetan singing bowl in healthy participants. Also, the feeling of spiritual well-being was significantly higher [293]. In addition, improvement in positive affect and a reduction in negative affect as captured by the Positive And Negative Affect Schedule (PANAS) questionnaire [294] was reported after a 40-minute-long sound meditation with singing bowls [295]. In the presented study, participants also reported to feel more vitalized, which is in accordance with another study determining that subjective sleepiness was lower after a 20-minute relaxation in during singing bowl sound compared to a silent relaxation ($p = .041$) [296]. Further, listening to singing bowl sound was shown to be an useful strategy to reduce anxiety in patients waiting for urologic surgery [297], which is consistent with high percentages of participants

reporting to be more relaxed, calm and balanced in this study. In addition, in a randomized controlled trial Landry compared the effects of a directed relaxation session with and without the use of Himalayan singing bowl sound, reporting a decline in systolic blood pressure ($p=.044$) and heart rate ($p=.003$) in the first group [298]. Also, a significant increase in heart rate variability was observed when applying singing bowl sound during a relaxation session compared to silent relaxation [299].

The presented findings suggest that the application of a singing bowl massage is beneficial on a physical and psychological level. Addressing the question whether the effects are also therapeutical, Wepner and colleagues investigated singing bowl massage interventions in patients with chronic unspecific pain. In their study, participants were divided into three groups, either receiving singing bowl therapy, a placebo intervention or no treatment. Both the placebo and the treatment group showed less pain intensities [300]. However, in a recent review it was concluded that more evidence is required to

recommend singing bowl therapies as numbers of studies eligible for inclusion were small ($n=4$) [301]. The revealed positive correlation between the TAS scores and psychological outcomes are in line with other findings suggesting that absorption, as a personality characteristic may be a predictor of outcomes in mind-body interventions [243, 318]. For instance, fibromyalgia patients with high levels of absorption reported more clinically relevant improvements after a guided imagery intervention in a randomized, controlled trial [302]. Interestingly, the critical exponent was significantly negatively correlated with the total TAS score. In line with this finding, Irmischer et al. demonstrated that participants with higher trait absorption showed more suppression of LRTC during a meditation task [274]. Also, it has been shown that persons scoring higher on the absorption scale are enabled to reach deeper meditative states faster [303]. Thus, trait absorption seems to contribute to a stable focus of attention reflected by a shift in critical brain dynamics.

5.3 Criticality and sensory processing sensitivity

Under the umbrella of theoretical frameworks on environmental sensitivity, providing models to elucidate individual differences in the capacity to process environmental stimuli, in the last 20 years sensory processing sensitivity (SPS) emerged as a topic of research [304]. As a continuum across humans, SPS reflects inter-individual differences in trait sensitivity to experiences [305, 245]. Hereby, SPS is proposed as a temperament trait defined by greater depth of information processing, enhanced awareness of environmental subtleties as well as an ease of overstimulation [306, 305, 307]. Importantly, according to the classification systems ICD-10 and DSM-5, high sensitivity does not constitute a psychopathological health disposition. Initially, Aron and Aron developed the Highly Sensitive Person Scale (HSPS) in 1997, a 27-item questionnaire designed to measure high sensitivity. In a series qualitative and quantitative of studies, high sensitivity was conceptualised as an unitary psychological construct composed of perceptual sensitivity as well

as cognitive and emotional responses to environmental stimuli [245]. Later, Smolewska et al. examined the questionnaire and obtained three factors, which they called Ease of Excitation (EOE), reflecting being easily overwhelmed by stimuli, Low Sensory Threshold (LST), characterising unpleasant sensory arousal in response to external stimuli, and Aesthetic Sensitivity (AES), e.g. being deeply moved by arts or music [308, 309, 304]. Consequently, the HSPS has been translated into several languages [305]. The German version of the HSPS-G questionnaire, which was used in this thesis, was evaluated by Konrad and Herzberg. Here, the three-factorial solution was essentially confirmed, although with a reduced number of items [244]. Other studies showed an association between EOE and LST with negative emotionality, anxiety and depression [310], whereas AES was reported to correlate with positive emotionality including positive affect and self-esteem as well as openness to experience and conscientiousness [311, 312]. It has been estimated that approximately 20-30% of the general population

score have a heightened sensory sensitivity [313, 246, 307]. Recently, a latent class analysis has been applied to HSPS results obtained from two samples consisting of $n= 451$ and $n= 540$ participants, respectively. The authors identifying a low, a medium and a highly sensitive group with a distribution of 29%- 40%- 31% [246]. The cut-off scores applied here for the grouping of participants was based on this finding, which was consistent across ages [246]. However, whereas SPS is captured based on questionnaires or behavioral observational assessment, its neurobiological basis has only been scarcely investigated. So far, no EEG study has been carried out determining neurophysiological signatures of SPS.

Nonetheless, to date, a few fMRI studies were conducted [314–318]. Taken together, the results support depths of information processing as an essential key feature to characterize SPS with increased activity in brain areas such as the precuneus, prefrontal cortex and the inferior frontal gyrus [305]. In addition, enhanced resting state

connectivity within the ventral attention, dorsal attention and limbic network was shown in association with higher SPS [319].

From a theoretical perspective, neural network models have shown that the critical brain state maximizes information processing capacities including enhanced input sensitivity to changes in external inputs [320, 321, 251, 187]. Explanations for the phenomenon include that nodes are more excitable in critical subpopulation and hence, can more effectively amplify weak stimuli [322].

Such findings led to the hypothesis, that scores on the HSPS-G scale might correlate with the dynamical regime captured by the critical scaling exponent and the DFA. However, the results of the third study did not validate this proposal, and an association between the critical state and SPS could not be proven.

5.4 Self-organized criticality as a neurodynamical correlate of consciousness

The conceptual nonlinear dynamical system framework in Neuroscience has produced a variety of approaches and hypotheses on the relation between dynamics of neural activity and conscious experience [323, 324]. Such notions are appealing considering that consciousness reflects an intrinsically dynamical phenomenon, a temporal process in its nature, notably described as the “stream of consciousness” [325].

Over the years an abundance of conceptual proposals with distinct philosophical foundations were published and straightforward comparisons can be challenging. Thus, hitherto, no current framework is univocally accepted on either theoretical or empirical grounds [326]. However, whereas all theories on how consciousness relates to the physical domain start from different premises, an explicit complexity-related framework is recently embraced [7]. Therefore, in the following the view of the brain’s function operating at the brink of criticality

will be cross linked to a “family resemblance” of theories of consciousness [324].

5.4.1 Consciousness as an order parameter

To start, the conjecture of self-organized criticality goes hand in hand with a huge body of literature published by Walter J. Freeman since the 1970s. According to Freeman, consciousness can be seen as an order parameter. Thus, it is measurable by the level of emergent global coherent neuronal activity. In his view “awareness is basically akin to the intervening state variable in a homeostatic mechanism, which is both a physical quantity, a dynamical operator, and the carrier of influence from the past into the future that supports the relation between a desired set point and an existing state” [327]. These thoughts were based on experiments including electrophysiological recordings of the olfactory system of rabbits. Here, scale-free dynamics and spatial patterns in amplitude and phase modulations of oscillations were observed. Interpreted within the framework of dynamical system theory, it was suggested that these are

generated by state transitions consistent with a critical regime and that sensory information are encoded in the spatiotemporal patterns [328–330]. The authors go further by proposing that the mechanism of self-organized local domains preceding the formation of global domains underlies Gestalt formation in perception [329].

Another proposal in this direction has been formulated by Francisco J. Varela, who worked on the “biophysics of being” until his death in 2001 [331]. Close to the notion of reverberant cell assemblies, labile sets of neurons transiently oscillating at the same frequency [323] formulated by Hebb (1949), which have been hypothesized to be the basis for short-term memory [153], Varela and colleagues pursued the idea of resonant cell assemblies [332]. By addressing how neural mechanisms account for “the flow of adapted and unified cognitive moments” [333, p. 229], the authors hypothesized that “for every cognitive act, there is a singular and specific large cell assembly that underlies its emergence and operation” [332]. In their “brain web” proposal the

authors argue that synchrony over multiple frequency bands, in particular the beta and gamma range, would be the most plausible candidate for temporal binding and large-scale integration across spatially distributed local brain regions [333]. Interestingly, the transient nature of the neural assemblies implies that the systems would represent metastable patterns of activity instead of attractor states [323]: “In the brain, there is no ‘settling down’ but an ongoing change marked only by transient coordination among populations, as the attractor itself changes owing to activity-dependent changes and modulations of synaptic connections” [333, p. 237]. Similarly to the work by Freeman, here, the balance of segregation and integration is considered to be a hallmark of the brain’s complexity and a plausible prerequisite for consciousness [323]. Interestingly, even though Varela and Thompsons’ proposal insinuates that conscious awareness can be mapped at the level of spatiotemporal patterns as an order parameter, the authors placed their work in a “radical embodiment” framework. Stating that

“consciousness depends crucially on the manner in which brain dynamics are embedded in the somatic and environmental context of the animal’s life” [334, p.425], they suggested that “processes crucial for consciousness cut across the brain–body–world divisions, rather than being brain-bound neural events“ [334, p.418].

5.4.2 Oscillatory synchrony

Alongside with the “brain web” proposal, extensive work was carried out over the last decades on oscillatory synchrony, defined as positive correlation between the spike timing of a neuronal population, as type of transient interaction between neural assemblies [323]. For instance, Treisman and Gelade (1980) published the hypothesis that neuronal synchrony might be a mechanism for mediating feature binding and attention [335]. Also, Von der Malsburg and Schneider (1986) suggested that the binding problem, the question how separate features are bound into a unified perceptual representation, is solvable by neurons firing

synchronously to encode and combine information [336]. From there on synchronous activity of neuronal assemblies and temporal binding was extensively explored as a candidate mechanism for conscious perception [337–339]. In particular, the working group of Wolf Singer brought forward the idea that there is a “temporary association of neurons into functionally coherent assemblies that as a whole represent a particular content whereby each individual neuron is tuned to one of the elementary features of composite perceptual objects” [340, p.1381]. Further, the “communication-through-coherence” hypothesis emerged with the idea of phase-locking amongst oscillations of neuronal assemblies as a gating mechanisms enabling effective communication by acting as windows of frequency-specific interactions [341]. Especially, the relation between synchrony in the gamma range and consciousness received much attention and has been regarded to be the “crowd’s favourite” [323, p. 733]. For instance, the highly influencing paper “Towards a neurobiological theory of

consciousness”, by Francis Crick and Christoph Koch (1990), proposing a theory of visual consciousness based on gamma band oscillations [47], sparked a new section of research on the neural correlates of consciousness, defined as “the minimal neuronal mechanisms jointly sufficient for any one consciousness percept” [342]. Also, transient phase locking during gamma oscillation was observed when participants reported perceiving a “gestalt” in figures [343]. Multiple studies were published associating attentional mechanisms with activity in the gamma frequency range. For example, Landau et al. reported effects on the gamma band (30-70 Hz) distinguishing between voluntary and involuntary attention measured with EEG [344]. Sokolov et al. measured MEG in the task of shifting selective attention between visual and auditory stimuli, showing an increased high gamma frequency response in cortical areas, observing a peak at 40 Hz [345]. An intracranial EEG study showed an increase of gamma band activity in the range of 60-200 Hz in the premotor cortex in the task of shifting attention

towards upcoming targets [346]. Intriguingly, as in this study enhanced gamma frequency in the context of reduced SOC during focused attention was found, an activity of 140-200 Hz was observed in rats at timepoints where the GABA system is switching from excitation to inhibition [347]. Additionally, in working memory task synchronous gamma oscillations are maintained even when the stimulus disappears. The phase-specific synaptic input of gamma frequency oscillations was suggested to facilitate synaptic plasticity and encoding of long-term memory [348]. Also, the degree of memory specificity was found to correlate with the magnitude of gamma activity [349] and Westpatat et al. reported that synaptic plasticity is modulated in respect to the phase of gamma frequency oscillation [350]. Stronger synaptic strengthening through neuronal synchronization in sensory and attentional areas was found to promote synaptic plasticity and a better flow of neural information [351]. However, it was shown that gamma synchronization can also occur in the absence of consciousness. For instance, gamma

synchrony was shown to increase during NREM sleep, anaesthesia or seizures [55–57]. Therefore, it has been concluded that “while synchronization and oscillatory patterning may be necessary conditions for activities to participate in generating awareness, they are certainly not sufficient” [352, p.492]. Also, it was suggested that oscillations, mostly studied in association with stationary and potential nonzero phase locking between cortical areas, are a rather rigid framework for such transient process. Instead, propagating waves [353, 354] or wave packets [355] were deemed as more natural for encoding temporal sequences [162]. In his manuscript “Corticonics”, Moshe Abeles coined the term “synfire chain” describing a particular type of neural synchronization characterized by the sequential activation of neuronal populations, similarly to a wave without any particular spatial ordering [356]. Thus, with “synfire chains” the neuronal avalanches at the level of spiking were described and this view basically outlined the idea of activity propagation in neuronal networks as the essential dynamical property [162].

However, if critical dynamics are in fact alternatives to “bind” features in cortical information processing through cascading activity, this opens up a few questions on how the dynamical concepts of oscillatory activity and neuronal avalanches can be brought together. For a reconciliation it has to be demonstrated that they coexist or even complement each other to improve information processing functions [162]. Indeed, the hypothesis that cortical dynamics resides at a critical point of optimized information processing, has refocused attempts to explain the tremendous variability in neuronal activity patterns observable in the brain [184, 250]. In the literature there seem to be a consensus that the cortical network is organizing close to a critical point with all temporal scales contributing to the dynamic [196, 357] and a fair amount of research has shown that neuronal avalanches and oscillations are related [250]. However, some aspects on the connection between oscillations and neuronal avalanches still need to be explored further. For instance, it is not fully understood yet how an avalanche can fit into a

continuous oscillation. If it would be the case that multiple cycles contribute to an avalanche, the cascades would represent recurrent activation of single cortical areas. This would be in contrast with findings showing that recurrent activations of sites are scarce [358, 162]. An emerging view is that transient phase locking of oscillations reflects the underlying organization of neuronal avalanches. Cortical neurons often propagate activity during nested oscillations, which occur during a coupling of the amplitude of a faster rhythm to the phase of a slower rhythm [359]. One study showed that nested theta and beta/ gamma oscillations organized as neuronal avalanches, as these were synchronized across cortical sites with a size distribution governed by a power law with a slope of -1.5 . Hence, nested oscillations seem to co-occur with neuronal avalanches [168]. Further, experimental findings suggest that neuronal avalanches seem to be a result of the alternation between Up and Down states [360]. It was found that the critical dynamic reflects Up states [361] and that Down states are

characterized by subcritical dynamic [362]. Hereby, the consequence of a large avalanche would be a hyperpolarization of the neurons involved, leading to a Down state, whereas small avalanches maintain the depolarization and the Up state, considering the Up state as a metastable state [360, 363]. Furthermore, it is suggested that small amplitude depolarizing potentials, resulting for example from spontaneous miniature synaptic release, emerge at higher frequencies, which can generate larger depolarization events and transitioning the network to the Up state [364, 365]. For instance, Lombardi et al. observed that the size of an avalanche and the silent time bins between avalanches are correlated and displayed the intermittency of oscillations, suggesting that neuronal avalanches exhibit characteristics of the frequency band oscillations [363]. Experimental findings also suggest that the diversity in broadband phase locking is maximized at criticality [366]. Here, Kitzbichler et al. investigated data recorded with MEG and fMRI, proposing a criticality as a broadband phenomenon. They found

critical dynamics during the phase lock interval and the duration of synchronization between a specific pair of time series in the low frequency measured with fMRI [367]. In this thesis neuronal avalanches analysis was consistently based on peaks and troughs identified on the broadband signal. To note, in a recent MEG study, it was asked whether the local minima of negative excursions or local maxima of positive excursions of the broadband signal are sufficiently sensitive events to detect certain phases of oscillations in narrow frequency bands. Hence, do these events represent only certain phases of *certain* frequency bands, or certain phases of *all* frequency bands? To outline whether peaks and troughs in the broad band signal are generated by band-limited processes, the authors filtered the broadband signal in 39 narrow frequency bands after events identifies as peak and trough time points beyond a threshold in the z-transformed time series were stored. Their results indicated that troughs and peaks derived from the broad band signal are more sensitive to troughs and peaks of low and high frequency bands but not

of intermediate frequencies as neuronal avalanches were only phase locked to oscillations in the frequency range $<50\text{Hz}$ and $>100\text{Hz}$. The authors then further analyzed cascade characteristics with a frequency-specific approach and reported a better goodness of fit to power-law scaling in the high frequency range ($>100\text{Hz}$) of the MEG, proposing high frequency activity as an ideal carrier of neural avalanches [280]. Also, it was demonstrated that the removal of gamma oscillations by bandpass filtering abolished the critical avalanche profile in high-density microelectrode array recordings from awake nonhuman primates. Thus, there seem to be an interdependence and coexistence of critical dynamics during intermittent oscillation periods [368].

To summarize, neuronal avalanches are suggested as a theoretical construct for the dynamic selection of neuronal groups into cell assemblies. However, the organizing principles of neuronal avalanches giving rise to cell assemblies has yet to be proven. However, based on several features such as the

large diversity of patterns and the stable recurrence in time critical dynamics as indicated by neuronal avalanches governed by power law behaviour are attractive as a candidate for the representation of cell assemblies [369].

5.4.3 Coordination dynamics

Groundwork for the self-organized criticality hypothesis was further laid by J.A. Scott Kelso, who developed the framework of coordination dynamics [370, 89, 88, 371]. Inspired by fundamental principles of synergetics [154], self-organized pattern formation pattern dynamics are in the focus of this approach. In the coordination dynamics' notion the brain is viewed as "a pattern forming self-organized system governed by potentially discoverable nonlinear dynamic laws [370, p. 257]. In this stance, cognitive processes "arise as metastable spatiotemporal patterns of brain activity that themselves are produced by cooperative interactions among neural cluster" (ibid). Further, it was proposed that "an order parameter isomorphism connects mind and body,

will and brain, mental and neural events. Mind itself is a spatiotemporal pattern that molds the metastable dynamic patterns of the brain” [370, p. 288]. Thus, with the framework of coordination dynamics it was aimed “to identify the key variables of coordination (defined as a functional ordering among interacting components) and their dynamics (rules that govern the stability and change of coordination patterns and the nonlinear coupling among components that give rise to them)” proposing that “ a crucial aspect of cognitive function, which can both integrate and segregate the activities of multiple distributed areas, is large-scale coordination governed by way of metastable dynamics” [372, p. 26, 30]. As illustrated in Figure 3B, metastability corresponds to a dynamical structure devoid of attractors and thus, any phase- and frequency-locking behaviour. However, segregation and integration tendencies still coexist [89]. To note, metastability as a basis for rapid switches among distinct operational modules is also the topic of multiple studies conducted by Fingelkurts and Fingelkurts [373, 374, 44]. Here,

metastability was associated with the assumption that each homogeneous segment within EEG frequency bands represents a temporary stable, also called “quasistable” microstate, which are suggested to be separable by sudden transitions in the vector of the maximal EEG global field power [324, 375, 376]. Importantly, Kelso and co-workers proposed that the switching between coordination states may be facilitated by criticality [89]. In favour of this interpretation, it was observed that metastable states are most numerous when the dynamics are tuned to the critical point in a computational neural network [192].

At the heart of theory of self-organized criticality in the brain lies the argument that nervous systems have to balance two seemingly opposing requirements. At the one hand, a certain degree of disorder is essential to enable flexibility and the capability of quick reorganization in order to efficiently interact with the environment and adapt in response. At the other hand a certain degree of order is needed to ensure coherent functioning and

maintain a resilience to external perturbations [377]. This goes hand in hand with the current two main theories of consciousness, namely the global workspace theory and the integrated information theory [378].

5.4.4 The global workspace theory

In the first formulation of the global workspace theory (GWT) in 1988 Bernard Baars used the metaphor of the theatre of the mind to describe a cognitive architecture. Here, the stage is the working memory with a spotlight on it representing consciously experienced event. The spotlight is controlled by selective attention with limited capacity [379]. Distinct to the Cartesian theatre with the implicit assumption of someone viewing, the audience as well as the director behind the scenes are in the dark and thus, unconscious in Baars' model. Hence, the central notion behind the GWT is that conscious content is globally available for diverse cognitive (unconscious) processes such as memory and attention and that consciousness might be a gateway enabling access

between otherwise separate neuronal functions (Figure 46) [380]. Thus, it posits that the function of conscious awareness is the broadcasting of information in the brain [381]. Later, Stanislas Dehaene and colleagues build on this fundament under the working title of “neuronal global workspace” [382]. At first, the authors emphasized the importance of distinguishing between the two related processes of conscious access and selective attention [383] citing William James’ definition of attention: “the taking possession by the mind, in clear and vivid form, of one out of what seem several simultaneously possible objects or trains of thought” [15]. Hereby, the authors refer access to the first part of the definition, consciously “taking possession of the mind”. Posing the question of conscious access, e.g. “How does an external or internal piece of information gain access to conscious processing, defined as a reportable subjective experience?” led to a number of empirical studies applying experimental paradigms such as masking, binocular rivalry, and inattention blindness to investigate a

minimal contrast between conscious and nonconscious (i.e. subliminal or preconscious) stimuli [383]. Dehaene et al. go further by postulating that information becomes conscious by the activation of long-distance connectivity of “workspace neurons”, which can make the information available to other modular cerebral networks processing information in an unconscious manner. Hence, in this view “this global availability of information (...) is what we subjectively experiences as a conscious state” [382]. Intriguingly, this stance comprises similarities to the idea of a “Dynamic Core” proposed by Edelman and Tononi: “When we become aware of something ... it is as if, suddenly, many different parts of our brain were privy to information that was previously confined to some specialized subsystem” [384 p. 148]. Whereas Edelman and Tononi hypothesized thalamocortical and corticocortical reentry as the basic mechanism facilitating the interaction among distant regions of the brain, GWT assumes that a non-linear network ignition associated with recurrent processing amplifies and

sustains a neural representation, which allows the global accesses by local processors [385]. The GWT further describes ignition as a sudden activation, which may be triggered by an external stimulus or may occur spontaneously and stochastically at rest [386]. Intriguingly, it has been suggested that the moment of ignition, when locally modular processing becomes generalized by the formation of a global workspace represents a phase transition driving cortical systems to the critical point [387]. More generally, Kitzbichler and colleagues proposed that “it may be that the self-organized criticality of spontaneous cortical dynamics favors rapid transitions between different states of the system, supporting the adaptive emergence and disappearance of global workspaces in response to changing demands, without tuning of an external driving parameter such as ascending neuromodulatory input” [387]. Thus, the abrupt activation facilitating conscious access may be attributed to self-organized criticality [388, 389].

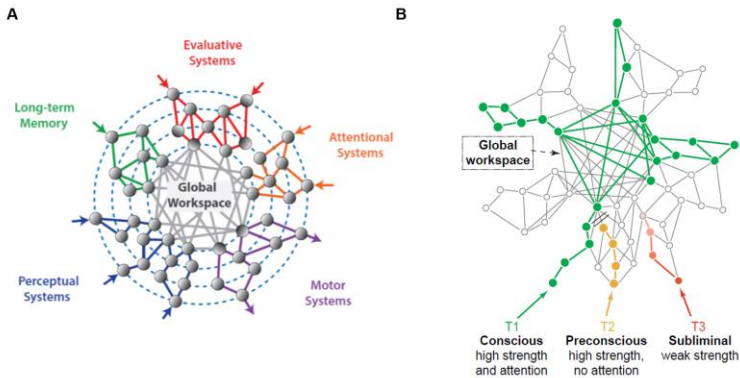


Figure 46: The global workspace theory. (A) Reproduced from [390], (B) reproduced from [391].

5.4.5 The integrated information theory

The integrated information theory (IIT) was historically the first theory that proposed precise quantitative predictions on the content and level of consciousness [392, 247]. Groundwork for the IIT can be traced back to early work on complexity and consciousness by Gerald Edelman, Giulio Tononi and Olaf Sporns [2, 377]. Due to its level of formalization as a theory, and especially “a calculus to evaluate whether a physical system is conscious”

[393], the IIT has triggered a lot of responses, debates, and criticisms. Therefore, it has been revised continually over the years [392, 394–396, 248]. Whereas two decades ago, Edelman and Tononi assigned the subtitle “how matter becomes imagination” to the book on their theory of consciousness [384], in later publications Tononi and colleagues emphasized that “IIT does not start from the brain and ask how it could give rise to experience; instead, it starts from the essential phenomenal properties of experience, or axioms, and infers postulates about the characteristics that are required of its physical substrate” [62, p. 450]. For Tononi, “every experience is whole, and the entire set of concepts that make up any particular experience – what makes the experience what it is and what it is not – are maximally interrelated” and that a “local maximum of integrated information is indeed identical with consciousness” [397, p.296]. Thus, according to the IIT, consciousness emerges from the interconnectedness of neural networks, i.e. more interaction among the neurons, the more one feels

conscious, even without sensory input [398]. Mathematically, the theory predicts a function which outputs are the contents of consciousness as an element of an experience space and the level of consciousness represented by a scalar value Φ [247]. In his formulation Tononi adopts a structural point of view, imagining three phases defined by the degree of regularity in the interactions. The intermediate regime in which segregation and integration occur simultaneously at its maximum would correspond to the conscious state. From a dynamical perspective, the three regimes are generated by changes in correlations. Accordingly, the structure of the brain connectivity will be the same, whereas completely different correlations can be exhibited. Thus, the conscious state would correspond to the critical state, whereas a loss of consciousness would be consistent with subcritical dynamics (Figure 47) [151, 247, 62].

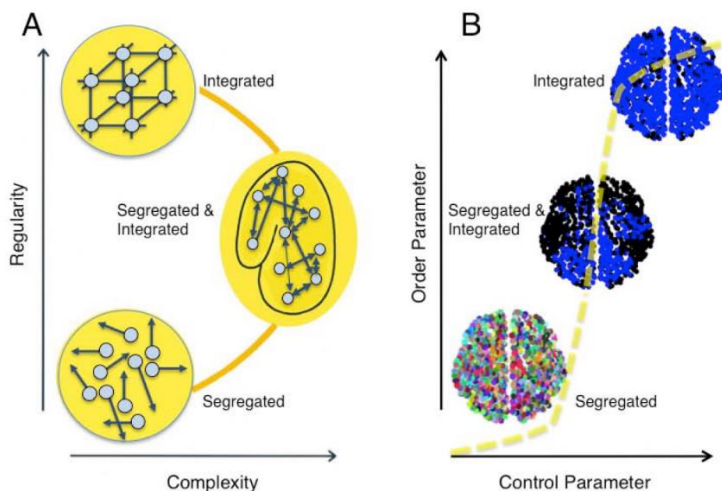


Figure 47: Consciousness as a function of (A) regularity and complexity and (B) self-organized criticality. Adapted from [151].

Recently, a few studies emerged connecting the IIT with the concept of criticality by investigation the explicit relationship between critical exponents and the amount of integrated information (Φ). For instance, Kim and Lee pursued three different approaches in their work [399]. First, they computed a large-scale human brain network model implementing a Kuramoto model on the scaffold of an anatomically informed human brain

network structure constructed from diffusion tensor imaging. The parameters for the models were set to simulate alpha oscillations in the brain. Arguing that criticality is associated with heightened susceptibility to external stimuli, the pair correlation function (PCF) was calculated as a surrogate measure for susceptibility [400] and defined as a parameter for criticality. Going further, the authors proposed a metric for Φ , defining integrated information as the effective information of the minimum information partition in a system, i.e. the partition of the system at which information loss caused by partitioning is minimized [401]. Then, the network model was modulated by systematically changing the coupling strength. The authors demonstrated that the Φ value was maximized at the point of maximized PCF. Second, they analysed previously published EEG data recorded from seven healthy participants [402]. During the recordings, sevoflurane, an anaesthetic agent, was applied, whereby the concentration was first increased from 0.4% to 0.6% to 0.8% and then gradually decreased. The level of consciousness

was assessed as the response rate to verbal commands. In comparison to the anaesthetic state, conscious resting states showed higher PCF and Φ . The authors concluded that a neural network in a critical regime is a necessary condition for information integration in the human brain [399]. Also, Popiel et al., simulated an Ising model on 159 randomly generated, positive weighted $n=5$ nodes network, which was tuned to a critical point. The parameter Φ was calculated as the effective information of the minimum information partition. The results indicated that subcritical regimes can generate high Φ values, whereby values were largest near the critical point. The authors concluded that the system would be most conscious, according to the definition given by the 3rd version of the IIT [248], in the critical regime [403].

Whereas the GWT and the ITT address distinct aspects of consciousness, the first conscious access closely related to the function of conscious awareness and the latter the phenomenology of consciousness, one notable study combined both in

the context of criticality [146]. Enzo Tagliazucchi constructed an anatomical connectivity network inferred from diffusion tensor imaging data. Their computational model represented a variant of the Greenberg-Hastings cellular automaton of excitable dynamics [404]. Hereby, each node of the network can be either be in an inactive, an active or a refractory state. Thus, the model only comprises two parameters, a threshold T , determining the difficulty of the activity to spread and the probability of transitioning from the refractory to the inactive state. For a given value of T (T_c) the model depicts a phase transition. Following the argument that Tononi et al. proposed the complexity as an indirect marker of the level of consciousness, the authors calculated neural complexity with the Lempel-Ziv algorithm [405]. Also, the amount of integrated information (Φ) was determined as the minimum amount of information that is lost when splitting the system into two- subsystems introduced by Barrett and Seth (2011) [406]. Further, metastability, defined as the repertoire of configurations that a system explores

throughout its temporal evolution was calculated by quantifying the level of global cohesion of the average time series. Then, to model the effect of backward masking, regions of interest chosen from 998 network nodes were serially activated with different delays between the activations. Here, both activations propagated at a certain T_c , whereby the probability of the second activation percolating through the network increased with the delay. Also, they simulated competing stimuli as in the paradigm of binocular rivalry by modelling the propagation threshold of each region of interest. The results reveal that the stimuli did not simultaneously percolate through the network, which the authors interpreted as a dichotomous access to the global network. Important to note, at the critical point of the model, maximal Φ and metastability was observed. This findings led the authors to conclude that the two influential theories GWT and IIT could be compatible and that the criticality hypothesis offers a framework in which experimental predications from both can co-exist [146].

5.5 Limitations

In all three EEG datasets, neuronal avalanches with power law distribution and long-range temporal correlations (LRTCs) in the broadband were identified. Recently, the quality of power-law fits to empirical data has been scrutinized by demonstrating that some claims of scale-free dynamics lack statistical significance. Hence, stringent statistical tests have been advocated in the detection of critical dynamics [71]. As an answer to these critiques, Clauset et al. provided a statistical framework combining maximum-likelihood fitting methods with goodness-of-fit tests which are based on Kolmogorov- Smirnov statistic and the analysis of likelihood ratios [407]. This was applied in this thesis to evidence power-law distribution in the EEG data. However, despite a growing body of research supporting the hypothesis of SOC in the brain and asserting the existence of scale-free statistics across a range of *in vitro* as well as *in vivo* neural recordings, the criticality still remains controversial [150, 408,

409]. The main pitfalls and caveats can be summarized as the following:

The universality of power laws: Debates on the significance of power laws have been hold for a long time in diverse areas of research [71, 410] and it remains discussable to what extent the idea of criticality can be generalized to biology [411]. Whereas at the one hand power laws were given the significance of universal and fundamental mechanisms, at the other hand these were regarded as largely uninformative [412] or even “more normal than normal” [413]. Importantly, power laws are one of the hallmarks of SOC but not a sufficient condition [150]. Hence, whereas all critical systems should exhibit $1/f$ noise, however not all $1/f$ noise is indicative of criticality [144, 148]. Also, power laws can emerge through several mechanisms and non-critical systems are also reported to display power law behaviour [414–416]. For instance, Friedman and Landsberg reported features of critical dynamics such as power-law distributions of avalanche sizes and durations in a network with hierarchical modular

structure even though underlying dynamical processes were not critical [417]. Further models of neural dynamics suggest that diverse neuronal avalanches can coexist simultaneously, although, the network does not operate in a regime at the edge of a phase transition [418]. Additionally, it might be the case that power law regimes may co-exist with others suggesting metastability [88] and that it might be possible that brain areas are driven to the critical point separately [144]. Addressing the issue that power laws are not unique to critical systems and the critique that power-law scaling may be a generic property of thresholded stochastic processes [419], Priesemann and Shriki elegantly investigated whether neuronal avalanches emerge when a common time-varying external drive is applied to a set of Poisson units. The authors showed that homogenous Poisson activity cannot give rise to power law distribution, whereas inhomogeneous Poisson activity generated approximate power laws with cutoffs [202]. Recently, Destexhe and Touboul reanalysed neural data recorded in various species,

which has previously been interpreted to represent a critical regime, based on a common scaling, even though the data ranged from freely moving to anesthetized animals and cultured slices of reptile and rat cortex [420]. Using two non-critical models, the Brunel network [421] and a stochastic surrogate [416], the authors confirmed the previous findings, underlining that the criticality hypothesis is yet to be established [409].

The choice of parameter: The main limitation is the issue of extracting binary data from the EEG (Figure 48). In the neuronal avalanche analysis, peaks and troughs beyond an applied threshold are identified as events. Based on these, the avalanche characteristics are calculated. Hence, the neuronal avalanches analysis is sensitive to the chosen threshold as a low value might lead to the detection of events related to noise and a larger one might not detect enough real events. The chosen threshold in this study is motivated by a previous publication, reporting a threshold of ± 3 SD to amount to $\sim 0.1\%$ false-positive detection probability [175]. Further, the

neuronal avalanche analysis depends on the chosen time bin for clustering the events and defining the size of the cascades. Even though it was shown that the power law fitting of the cascade size distribution is robust to varying time bins, the scaling exponent changes within the value of Δt . In their original publication, firstly reporting neuronal avalanches in neocortical circuits, Beggs and Plenz measured extracellular signals from acute coronal slices using time bins $\Delta t = 1, 2, 4, 8, \text{ or } 16 \text{ ms}$ and reported a dependence of the scaling exponent α on Δt in the relationship $\alpha(\Delta t) \sim \Delta t^{-0.16 \pm 0.01}$ [164].

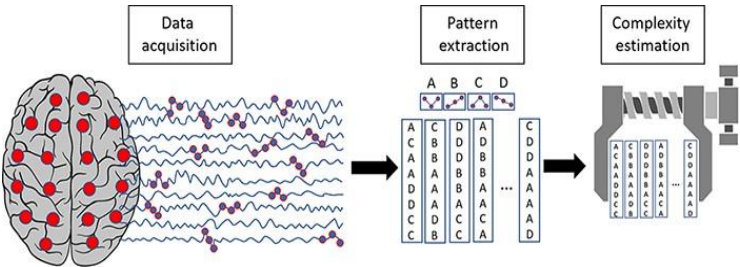


Figure 48: Schematic representation of one strategy for estimating temporal complexity as utilized in this work. Patterns of neuronal activity are directly extracted from the time series by applying methods such as signal binarization. Then, the degree of complexity and characteristics of neuronal avalanches

are estimated based on the extracted temporal patterns. Reproduced from [7].

Our understanding of the phenomenon of critical phase transitions is mostly informed by computational models of dynamic systems. The main classical models of criticality comprise the Ising model (Figure 9) and the Kuramoto model of phase coupled oscillators [422, 367, 423, 196]. In both models, the dynamics can be controlled by the manipulation of one parameter. For instance, the Ising model is tuned towards the critical point by changes of the temperature, whereby for the Kuramoto model increasing or decreasing the strength of coupling between oscillators led the system pass through a phase transition [367]. Instead by driving the system by an external modulation of a control parameter, self-organized critical systems spontaneously evolve towards a critical state without fine-tuning as explained in the original sandpile model from Bak, Tang and Wiesenfeld:” The scaling properties of the attractor are insensitive to the parameters of the model. This

robustness is essential in our explaining that no fine tuning is necessary to generate $1/f$ noise (and fractal structure) in nature” [161, p.381]. However, while some physical systems might be large enough that an asymptotically behaviour near the thermodynamic limit is assumable, it has been emphasized that biological systems would need to readjust a control parameter according to its size [424, 425]. Also, following the nonlinear dynamical system approach, changes from a control parameter would result in one or more bifurcations due to which a phase transition is likely to occur [426]. In later work of Bak’s group it has been established that self-organized criticality does not exclusively refer to self-tuning [427]. However, this opens up questions of potential control parameter, the biological mechanisms underlying the emergence of scale-free dynamics, and thus, how the critical state can be reached or remained [425, 428]. Addressing the first Chialvo and colleagues stated:” For a complex system like the brain, one might imagine that its control parameters be hard-wired genetically, selected by a long evolutionary

process to a critical point that is biologically most advantageous for survival” [425]. The authors further argued that “Darwinian evolution instead of furnishing a set of specific values for the control parameter must allow for a control mechanism such that systems can reach and stay close to a critical point” [425].

A biologically plausible control mechanisms would be a model of avalanche-related criticality with plastic connections [428]. Thus, it has been speculated that the target mechanisms might be neuromodulators, such as serotonin shifting the dynamic toward excitability or GABA, on the other hand, inducing inhibition [274]. In favour of this proposal are experimental findings suggesting that enhancement of inhibition or excitation is altering the dynamic of a neuronal network at criticality [365, 183, 429, 360]. Specifically, the level of inhibition has been investigated as a biological constraint for the branching parameter [149] (Figure 11). For instance, Massobrio et al. investigated ranges of E/I ratios on scale-free networks, reporting that critical dynamics

are achieved with 20-30% inhibitory nodes [184]. Further, Girardi-Schappo et al. used an *in silico* model observing the system's dynamic near the critical point when adding short-term depression in inhibitory synapses and firing threshold adaptation [430]. Simulating a 10,000 neuron, deterministic, plastic network of spiking neurons Stepp et al. also concluded that “the interplay of opposing forces from excitatory and inhibitory plasticity create a balance that allows self-tuning to take place” [431]. Zeraati et al. reported that applying short-term plasticity rules was generally resulting in hovering around the critical point. Also, long-term homeostatic plasticity created a global attractor at the critical state for some settings [428]. A number of studies explored how different types of plasticity may contribute to the tuning to the critical state in network models [432–434]. The current state of the art provides evidence that Hebbian plasticity produces critical dynamics, whereas homeostatic plasticity was shown to maintain the network activity [149, 361, 434, 435].

Terminology: In general, precise and clear terminology is important in every area of research. Especially, in the field of criticality, semantic issues and an inconsistent use of the term “critical” has been noted by several authors. In this thesis, criticality has been exclusively referred to avalanche dynamics of brain activity. However, variants of criticality and multiple paradigms such as “extended criticality”, “intermittent criticality”, “statistical criticality” or “quasi-critical” exist in the literature, leading to confusion. Therefore, the investigated concepts should be strictly defined in future to ensure comparability of findings [71, 408, 148]. Hence, it is important, that “criticality should not become a catch-all term for everything that is complex or variable” [92, p. 29].

6. Summary

In this thesis, I have explored the potential of the physics-derived concept of self-organized criticality as a neurodynamical correlate for consciousness.

The theoretical framework was tested in combination with nonlinear complexity measures and spectral analysing using two 64 channel EEG datasets comprising the induction of altered states of consciousness and one 64 channel EEG dataset obtained from participants with distinct degrees of sensory processing sensitivity.

To use the words of Dante Chialvo: “Understanding the brain is among the most challenging problems to which a physicist can be attracted. As a system with an astronomical number of elements, each one known to have plenty of nonlinearities, the brain exhibits collective dynamics that in many aspects resemble some of the classic problems well studied in statistical physics” [436]. In recent years the premise arose that self-organized criticality is a fundamental property of neural system and that “all human behaviors, including thoughts, undirected or goal oriented actions, or simply any state of mind, are the outcome of a dynamical system -the brain- at or near a critical state” [437]. Such framework is especially compelling as principles such as self-

organized criticality describing outcomes of collective phenomena in any complex dynamical system, provide a theory suitable to situate the phenomenon of consciousness within universal laws of the physical world [438]. Over the years some authors have claimed that consciousness is entirely beyond the reach of science and that “a purely materialist analysis of a living being, which focuses only on the structure and the function of the physical brain, will never reveal the content nor the origin of our consciousness” [439]. Even Galileo should have said that we have to put consciousness outside of the domain of physical science to then capture everything else in the language of mathematics and quantities [440]. Also, William James in his fundamental work on altered states of consciousness takes on a perspective in which consciousness does not originate in this physical world. Instead, it exists in another transcendental sphere and access to higher aspects of consciousness depends on an individual “threshold of consciousness”, which determines whether various characteristics of enhanced

consciousness are experienced [441]. While the pernicious perspective of 'mysterianism', the notion that a naturalized account of consciousness may exist but is inaccessible to humans as well as the notion of panpsychism, that consciousness is a fundamental feature in form of a ubiquitous field pervading the universe cannot be ruled out as a possibility [442, 443], within this thesis I hypothesize that consciousness is a biological phenomenon within the confines of the brain (although, not localized in some particular areas of the brain). Hereby, consciousness differs from other biological phenomena as it has a subjective or first-person ontology, but this does not prevent researchers from having an epistemically objective science of consciousness [444]. Thus, taking the view that the level of the brains organization is functionally isomorphic (i.e. a different realizations of the same kind) to consciousness [438], offers the possibility of empirically testing mathematical measures as neurophysiological indices for consciousness.

In this thesis, signatures of self-organized criticality in the form of neuronal avalanches with power law distribution and long-range temporal correlations in the amplitude of neural oscillations were identified on the level of the EEG in three distinct datasets. It was shown that criticality features are suitable to differentiate states in the spectrum of wakefulness consciousness and thus, to characterize electrophysiological correlates of altered states of consciousness. Further, the datasets were analyzed with two additional algorithms, multiscale entropy and Higuchi's fractal dimension, which quantify the self-similarity of the signal and hence, provide information about the degree of complexity of the brain dynamics. Also, traditional power spectral density analysis was carried out. In conclusion, electrophysiological correlates of three meditation categories, specifically thoughtless emptiness, presence monitoring and focused attention as well as of a singing bowl experience were determined. It was shown that the states of consciousness could be discriminated with nonlinear measures and

quantified by the degree of neuronal complexity, long-range temporal correlations, and power law distributions in neuronal avalanches. The results revealed an explicit relationship between nonlinear complexity, critical brain dynamics and spectral features. Finally, it was shown that the brain dynamics can be modified and shifted towards the critical point of a phase transition associated with optimized information processing functions by the practice of self-regulation and relaxation techniques. The framework of self-organized criticality as a neurodynamical correlate for consciousness is promising and in agreement with the current most influencing theories in the field of consciousness research.

7.a Appendix I: *t*-statistics

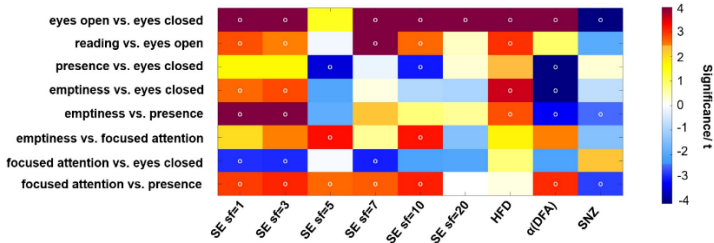


Figure A1: Color-coded differences of complexity parameters shown as *t*-values of the meditation task comparisons on a global level averaged over all electrodes. Fields marked with a white circle were significant on the 0.01 level after FDR adjustment.

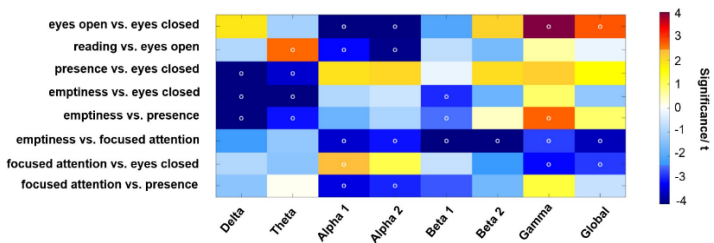
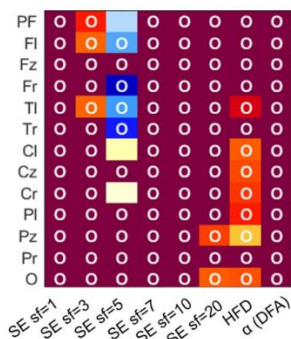
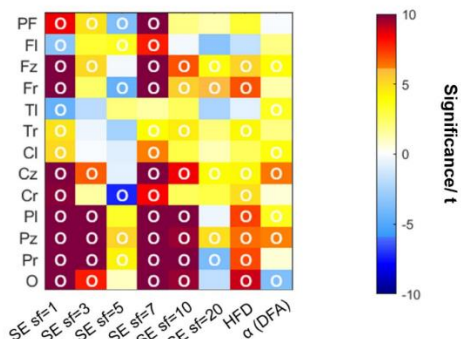


Figure A2: Color-coded differences of power spectral density shown as *t*-values of the task comparisons on a global level averaged over all electrodes. Fields marked with a white circle were significant on the 0.01 level after FDR adjustment over conditions and frequency bands.

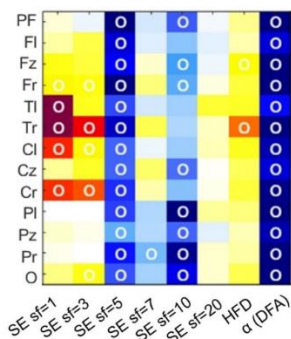
A eyes open vs. eyes closed



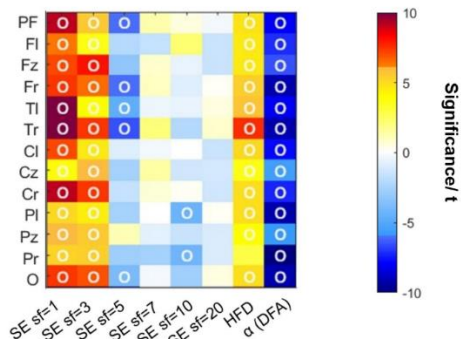
B reading vs. eyes open



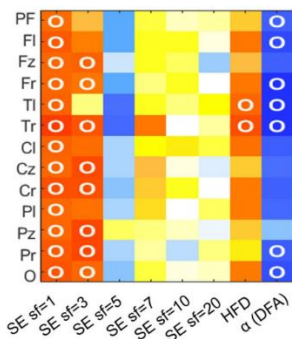
C presence vs. eyes closed



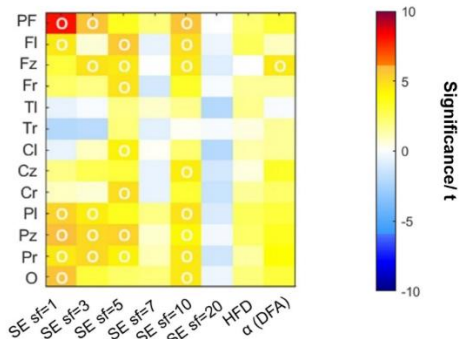
D emptiness vs. eyes closed



E focused attention vs. eyes closed



F emptiness vs. presence



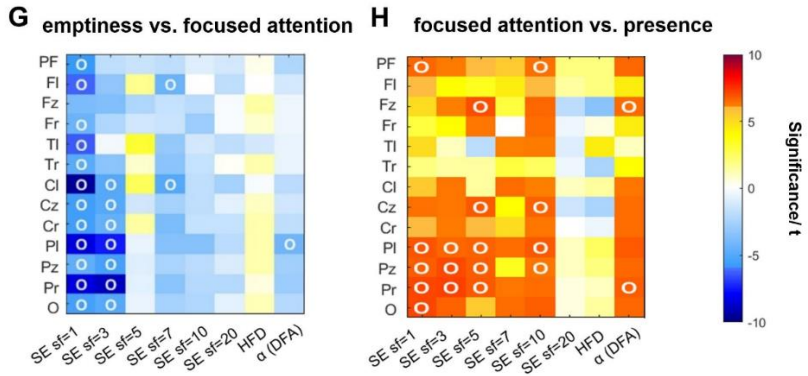
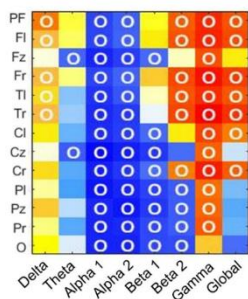
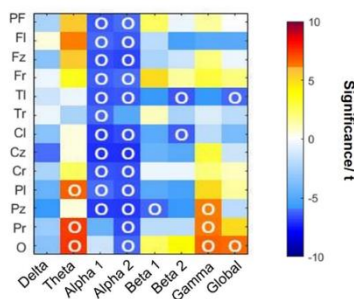
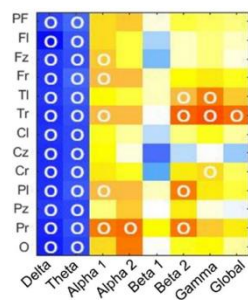
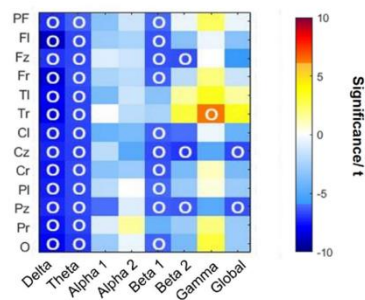
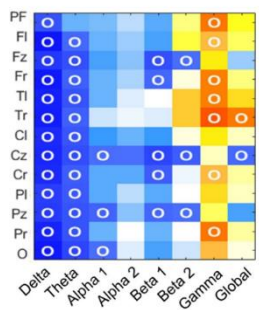
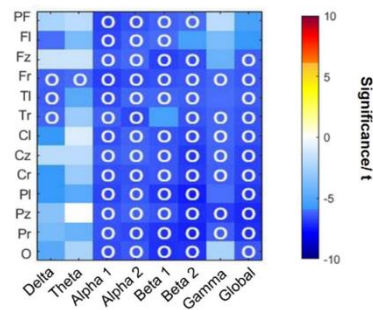


Figure A3: Color-coded complexity measure differences shown as t- values resulting from the task comparisons. (A) Comparison between eyes open and eyes closed, (B) reading vs. eyes open, (C) presence vs. eyes closed, (D) emptiness vs eyes closed, (E) focused attention vs. eyes closed, (F) emptiness vs. presence, (G) emptiness vs focused attention, (H) focused attention vs. presence. Fields marked with a white circle were significant on the 0.01 level after FDR adjustment over conditions and frequency bands.

A eyes open vs. eyes closed**B** reading vs. eyes open**C** presence vs. eyes closed**D** emptiness vs. eyes closed**E** focused attention vs. eyes closed**F** emptiness vs. presence

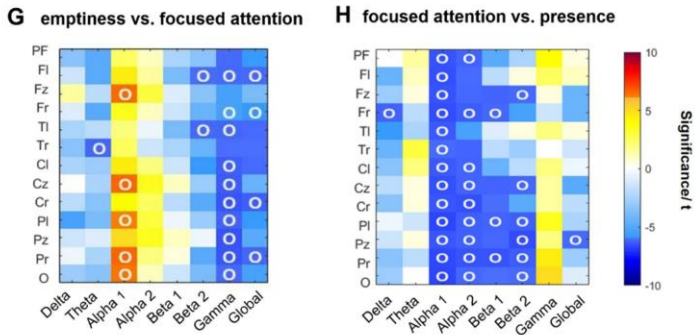
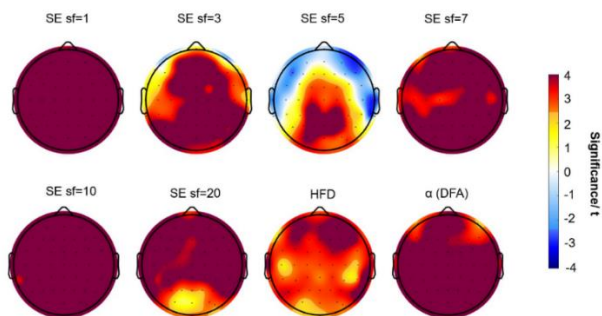
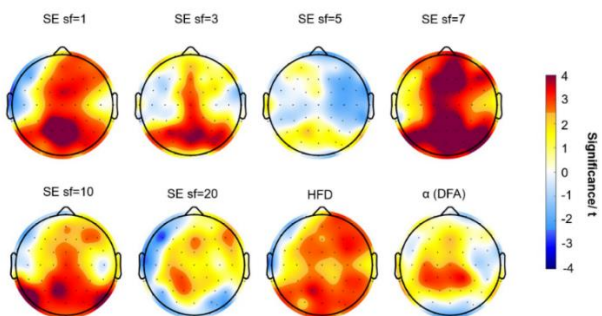


Figure A4: Color-coded complexity measure differences shown as t-values resulting from the task comparisons (A) Comparison between eyes open and eyes closed, (B) reading vs. eyes open, (C) presence vs. eyes closed, (D) emptiness vs eyes closed, (E) focused attention vs. eyes closed, (F) emptiness vs. presence, (G) emptiness vs focused attention, (H) focused attention vs. Presence. T-tests were calculated from each participant for each location and complexity parameter. Fields marked with a white circle were significant on the 0.05 level after FDR adjustment.

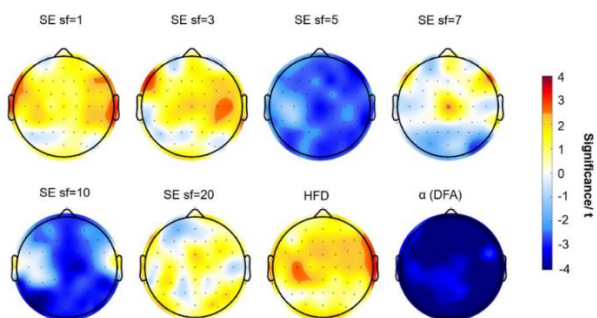
A eyes open vs. eyes closed



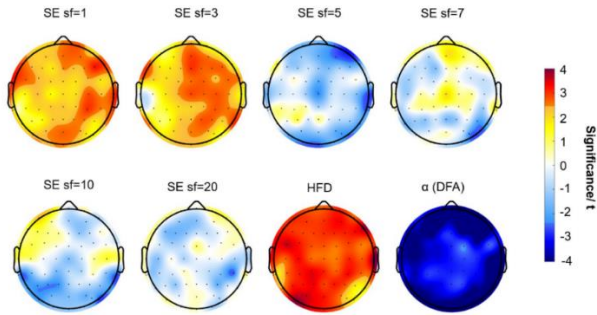
B reading vs. eyes open



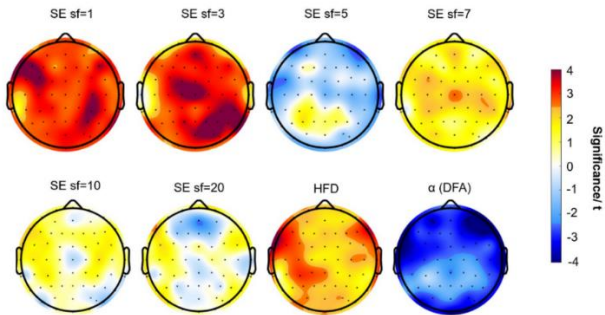
C presence vs. eyes closed



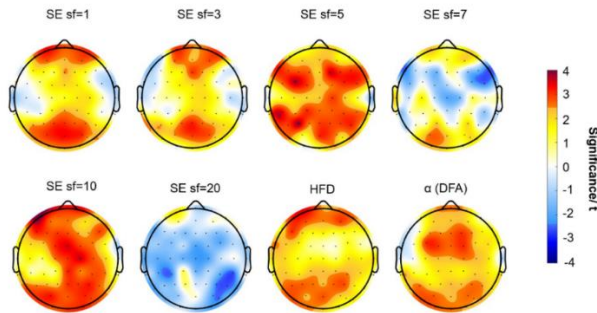
D emptiness vs. eyes closed



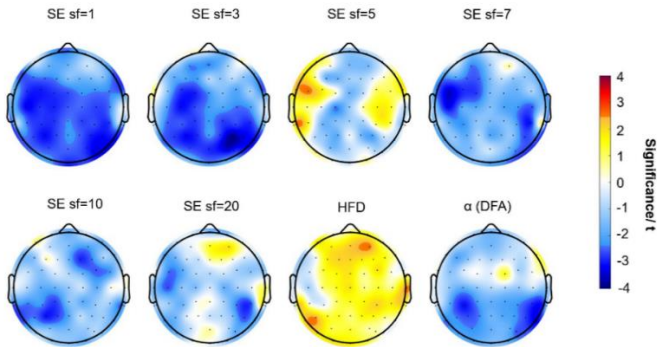
E focused attention vs. eyes closed



F emptiness vs. presence



G emptiness vs. focused attention



H focused attention vs. presence

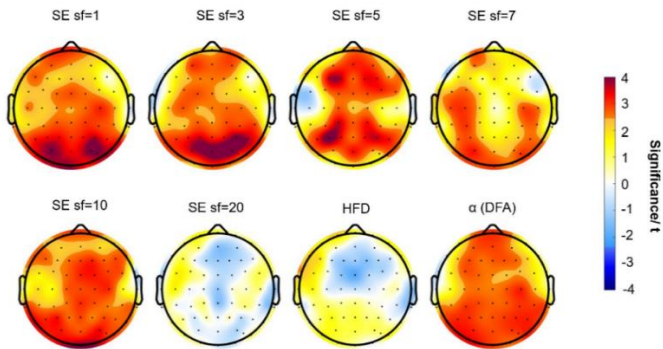
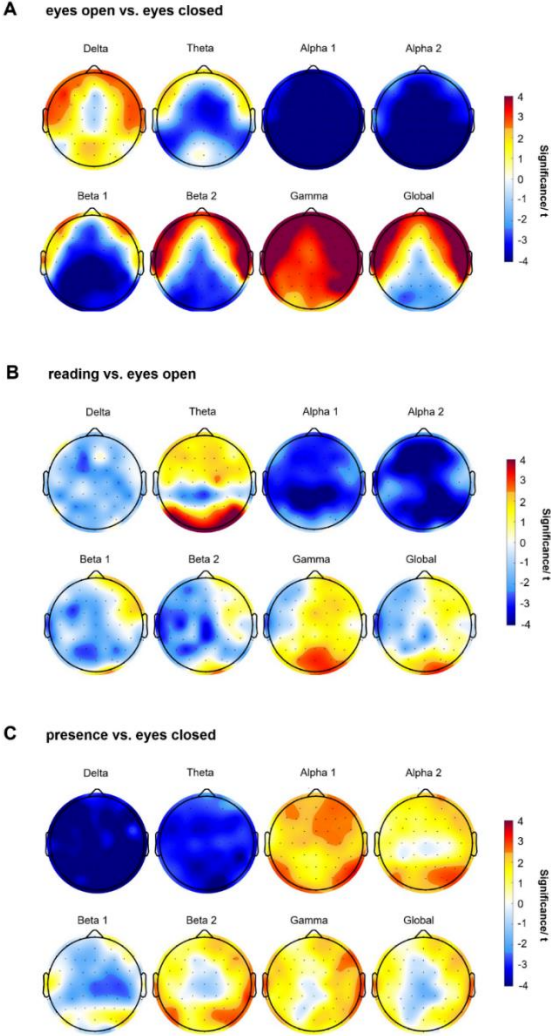
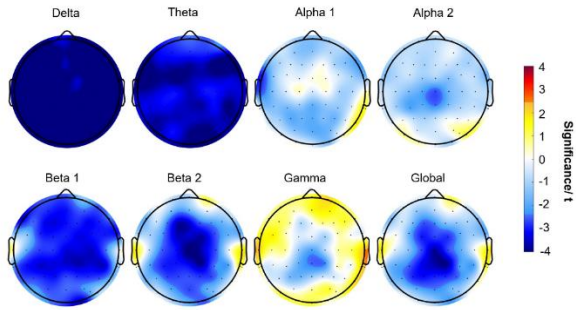


Figure A5: Topographical maps of differences in the t- values calculated for each complexity measure, respectively. (A) Comparison between eyes open and eyes closed, (B) reading vs. eyes open, (C) presence vs. eyes closed, (D) emptiness vs eyes closed, (E) focused attention vs. eyes closed, (F)

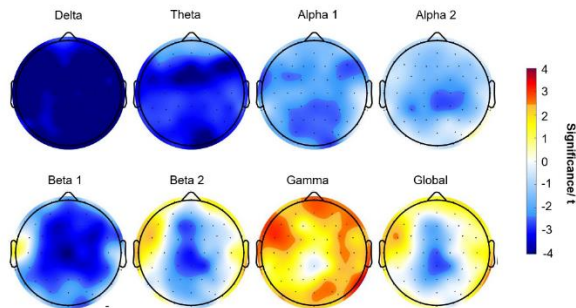
emptiness vs. presence, (G) emptiness vs focused attention, (H) focused attention vs. presence.



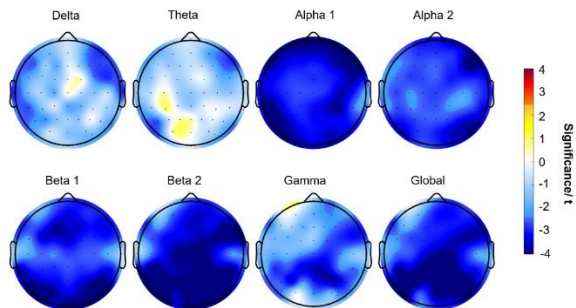
D emptiness vs. eyes closed



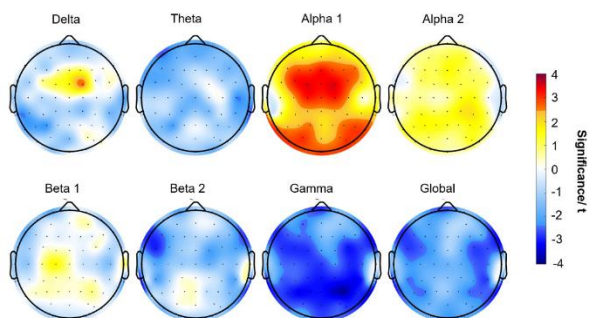
E focused attention vs. eyes closed



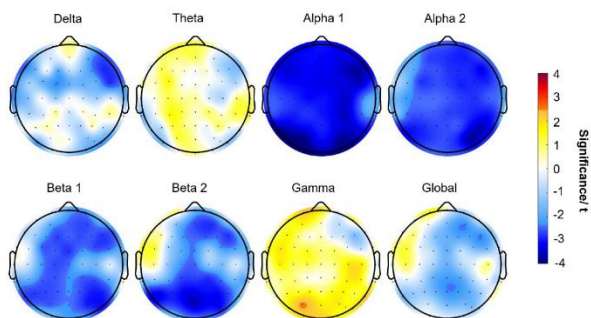
F emptiness vs. presence



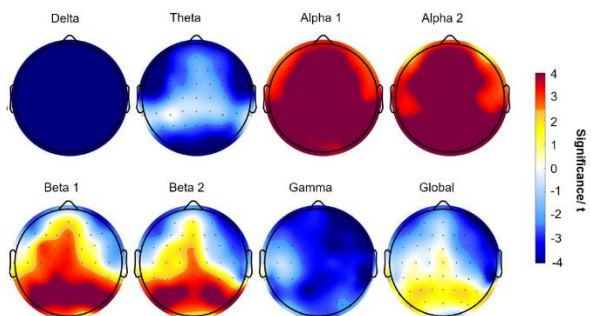
G emptiness vs. focused attention



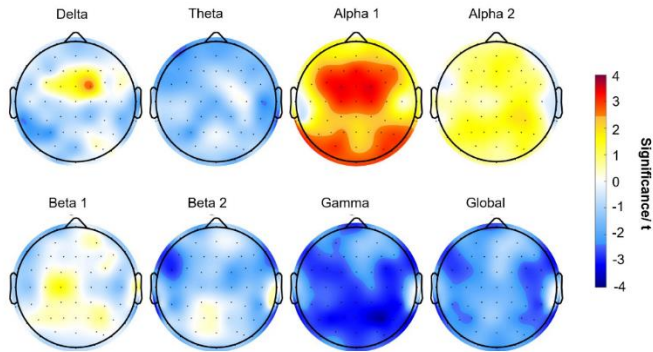
H focused attention vs. presence



I presence vs. reading



G emptiness vs. focused attention



H focused attention vs. presence

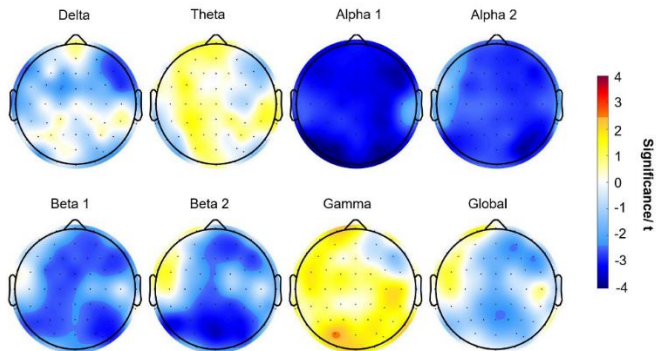


Figure A6: Topographical maps of differences in the t- values calculated for each frequency band, respectively. (A) Comparison between eyes open and eyes closed, (B) reading vs. eyes open, (C) presence vs. eyes closed, (D) emptiness vs eyes closed, (E) focused attention vs. eyes closed, (F)

emptiness vs. presence, (G) emptiness vs focused attention, (H) focused attention vs. presence.

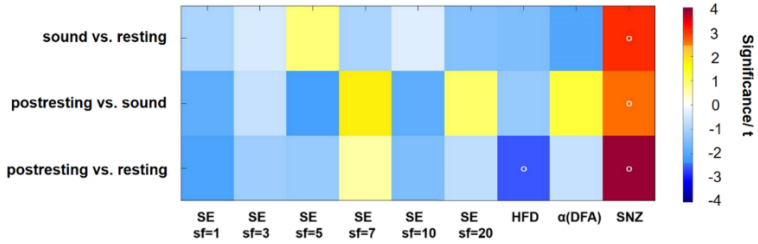


Figure A7: Color-coded differences of complexity parameters shown as t-values of the state comparisons on a global level averaged over all electrodes. Fields marked with a white circle were significant on the 0.05 level after FDR adjustment.

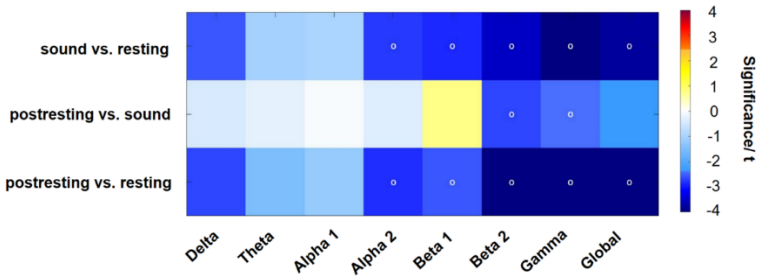


Figure A8: Color-coded differences of power spectral density shown as t-values of the state comparisons on a global level averaged over all electrodes. Fields marked with a white circle were significant on the 0.05 level after FDR adjustment over conditions and frequency bands.

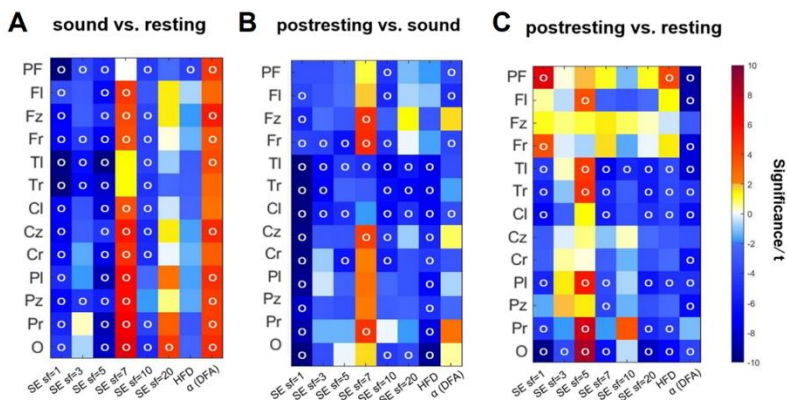


Figure A9: Color-coded complexity measure differences shown as t-values resulting from the task comparisons on a local level (A-C). T-tests were calculated from each participant for each location and complexity parameter. Fields marked with a white circle were significant on the 0.05 level after FDR adjustment.

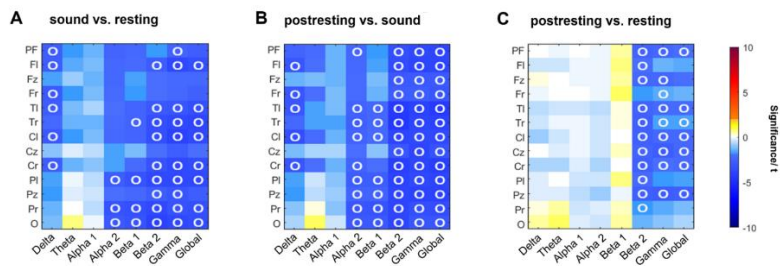


Figure A10 Color-coded power spectral density differences shown as t-values resulting from the task comparisons on a local level (A-C). T-tests were calculated from each participant for each location and complexity parameter. Fields marked with

a white circle were significant on the 0.05 level after FDR adjustment

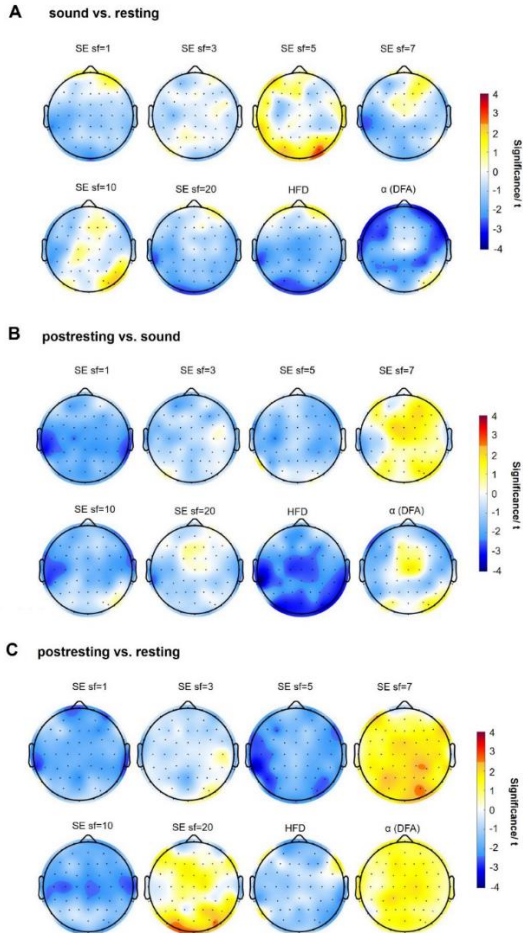


Figure A11: Topographical maps of differences in the t-value calculated for each complexity measure, respectively. (A)

Comparison between sound vs. resting, (B) postresting vs. sound, (C) postresting vs. resting.

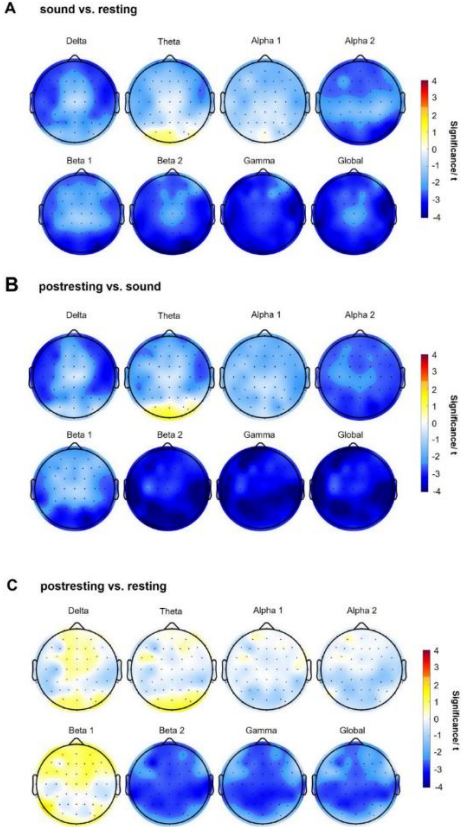


Figure A12: Topographical maps of differences in the t-value calculated for frequency band, respectively. (A) Comparison between sound vs. resting, (B) postresting vs. sound, (C) postresting vs. resting.

7.b Appendix II: Questionnaires

Inventar zur Phänomenologie des Bewusstseins (PCI-D-K)

Sehr geehrte Studienteilnehmerin, sehr geehrter Studienteilnehmer,

Bitte bewerten Sie Ihre Erfahrungen während der durchgeführten Intervention. Kreuzen Sie dazu im Fragebogen auf der Skala an, wie sehr die folgenden Aussagen auf Ihr Erleben zutreffen.

	Bitte bewerten Sie Ihr Erleben während und/oder nach der Intervention	Trifft				
		nicht zu	eher	teils/teils	eher zu	voll zu
1	Ich erfuhr Gefühle der Liebe					
2	Ich fühlte Wut					
3	Ich fühlte mich traurig					
4	Ich war angsterfüllt					
5	Meine Körpergefühle schienen sich auf die umgebende Welt auszudehnen					
6	Zwischen mir und der Umgebung lösten sich die Grenzen auf					
7	Ich hatte das Gefühl der Zeitlosigkeit					
8	Die Zeit schien sich zu beschleunigen					
9	Die Zeit schien sich zu verlangsamen					
10	Meine Wahrnehmung der Welt veränderte sich					
11	Ich erfuhr tiefgründige und leuchtende Einsichten					
12	Ich hatte bildhafte Vorstellungen					
13	Während der Zeit war ich abgelenkt					
14	Ich bewahrte die Bewusstheit meiner selbst					
15	Mein Bewusstseinszustand war ungewöhnlich					
16	Ich habe Selbstgespräche geführt					
17	Mein Denken war klar und verständlich					
18	Ich hatte Kontrolle darüber, worauf sich meine Aufmerksamkeit richtete					

19	Ich ließ die Kontrolle los und wurde empfänglich gegenüber dem, was ich erfuhr								
20	Ich kann mich erinnern, was ich erfuhr								
21	Ich fühlte mich angespannt und fest								
22	Ich fühlte mich ekstatisch voller Freude								
23	Ich erfuhr sexuelle Gefühle								
24	Meine Aufmerksamkeit war gerichtet auf meine eigene innere Erfahrung								
25	Meine Aufmerksamkeit war gerichtet auf die Welt um mich herum								
26	Meine Erfahrung würde ich als spirituell oder transzendental bezeichnen								
27	Ich empfand die Erfahrung als bedeutungsvoll								

Feedback- Fragebogen (CSP-14)

Sehr geehrte Studenteilehmerin, sehr geehrter Studenteilehmer,

Bitte bewerten Sie Ihr jetziges Befinden im Vergleich zu Ihrem Befinden vor Beginn der durchgeführten Sitzung.

Bitte tragen Sie dazu den entsprechenden Wert in das Kästchen ein. Je nachdem, wie sich ihr Zustand nach der Sitzung im Vergleich zu vorher verändert hat, kreuzen Sie bitte die Kästen von -3 (wesentlich schlechter) bis +3 (wesentlich besser) an. Haben Sie keine Veränderung festgestellt, kreuzen Sie bitte die „0“ an. Hier ist die Antwort +2 dargestellt.

Beispiel: Ich bin nach der Sitzung

angespannter |_-3_|_|_|_|_0_|_|_|_|_X_|_|_|_|_+3_|entspannter

Nachfolgende Daten werden nur pseudonymisiert weiterverwendet.

Geschlecht: männlich weiblich

Alter: _____

1. Mein Körperempfinden im Vergleich zu vorher ist jetzt

enger	_ _ _ _ _0_ _ _ _ _	weiter
schwächer	_ _ _ _ _0_ _ _ _ _	intensiver
angespannter	_ _ _ _ _0_ _ _ _ _	entspannter
schmerzhafter, unwohler	_ _ _ _ _0_ _ _ _ _	angenehmer
kraftloser	_ _ _ _ _0_ _ _ _ _	kraftvoller

2. Mein emotionaler Zustand ist jetzt

aufgewühlter	_ _ _ _ _0_ _ _ _ _	gelassener
unausgeglichen	_ _ _ _ _0_ _ _ _ _	ausgeglichen
trauriger	_ _ _ _ _0_ _ _ _ _	freudiger
unzufriedener	_ _ _ _ _0_ _ _ _ _	zufriedener
haltloser	_ _ _ _ _0_ _ _ _ _	geborgener
distanzierter	_ _ _ _ _0_ _ _ _ _	verbundener

3. Mein mentaler Zustand ist jetzt

müder, verwirrt	_ _ _ _ _0_ _ _ _ _	wacher, klarer
introvertierter	_ _ _ _ _0_ _ _ _ _	extrovertierter
leerer	_ _ _ _ _0_ _ _ _ _	erfüllter

4. Hat sie etwas gestört?

Ja Nein

Wenn ja was?

.....
.....

5. Ich hatte in dieser Veranstaltung zu der anleitenden Person einen

guten Kontakt _0_ schlechten Kontakt

6. Die Sitzung war zeitlich

zu kurz _0_ zu lang

Vielen Dank für Ihre Teilnahme!

TAS-D

Sehr geehrte Studienteilnehmerin, sehr geehrter Studienteilnehmer,

die folgenden Aussagen betreffen bestimmte Bereiche des Wahrnehmens und Erlebens. Diese können erfahrungsgemäß bei verschiedenen Personen sehr unterschiedlich ausgeprägt sein.

Bitte geben Sie zu jeder Aussage an, in welchem Ausmaß sie für Ihre Person zutrifft oder nicht zutrifft. Hierfür sind fünf Antwortmöglichkeiten vorgegeben, bitte entscheiden Sie sich bei jeder Aussage für eine davon. Behalten Sie dabei im Kopf, dass es letztlich keine richtigen oder falschen Antworten gibt.

	Trifft nicht zu	Trifft etwas zu	Trifft teilweise zu	Trifft überwiegend zu	Trifft völlig zu
1. Manchmal empfinde und erlebe ich die Dinge wie in meiner Kindheit					
2. Wortgewandte oder poetische Sprache kann mich stark beeindrucken					
3. Filme, Fernsehspiele oder Theaterstücke können mich so mitreißen, dass ich mich und alles um mich herum vergesse und die Geschichte erlebe, als wäre sie Realität und ich an ihr beteiligt					
4. Wenn ich ein Bild betrachte und danach wegsehe, habe ich manchmal ein Abbild davon, fast so, als ob ich das Bild selber noch sehen würde					
5. Manchmal habe ich das Gefühl, mein Geist könnte die ganze Welt umfassen					
6. Ich beobachte gerne, wie Wolken ihre Form verändern					
7. Wenn ich will, kann ich Tagträumen oder mir manche Dinge so lebhaft vorstellen, dass sie meine Aufmerksamkeit fesseln wie ein guter Film oder eine gute Geschichte					
8. Ich glaube, dass ich weiß, was manche Leute meinen, wenn sie von mystischen Erfahrungen sprechen					
9. Ich kann manchmal aus mir heraustreten und einen völlig anderen Seinszustand erfahren					
10. Stoffe – wie etwa Wolle, Sand oder Holz – erinnern mich manchmal an Farben oder Musik					
11. Manchmal erlebe ich die Dinge, als wären sie doppelt wirklich					
12. Wenn ich Musik höre, kann sie mich so gefangen nehmen, dass ich nichts anderes mehr beachte					
13. Wenn ich will, kann ich mir vorstellen, dass mein Körper so schwer ist, dass ich ihn nicht mehr bewegen kann, selbst wenn ich es wollte					
14. Oft kann ich die Gegenwart einer anderen Person spüren, noch bevor ich sie (oder ihn) wirklich sehe oder höre					
15. Das Knistern und die Flammen eines Holzfeuers regen meine Fantasie an					
16. Manchmal ist es mir möglich, mich völlig in Natur oder Kunst zu versenken, als ob sich mein Bewusstseinszustand vorübergehend verändert hätte					
17. Verschiedene Farben haben unterschiedliche und besondere Bedeutungen für mich					
18. Es kann mir passieren, dass ich während einer Routineaufgabe in Gedanken abschweife und dabei vergesse, was ich tue, bis ich nach einigen Minuten bemerke, dass ich die Aufgabe erledigt habe					
19. Ich kann mich manchmal an bestimmte Erfahrungen aus meiner Vergangenheit so lebhaft und klar erinnern, als ob ich sie noch einmal durchleben würde					
20. Dinge, die anderen bedeutungslos erscheinen mögen, haben für mich oft einen Sinn					
21. Ich glaube, wenn ich in einem Stück eine Rolle spielen würde, könnte ich die Gefühle des dargestellten Charakters tatsächlich empfinden und für diese Zeit als die betreffende Person wirklich leben, mich selbst und das Publikum vergessend					

	Trifft nicht zu	Trifft etwas zu	Trifft teil- weise zu	Trifft über- wie- gend zu	Trifft völlig zu
22. Meine Gedanken erscheinen oft nicht als Worte, sondern als Bilder					
23. Ich kann mich oft an kleinen Dingen erfreuen (wie die Farbe von Seifenblasen, oder ähnliches)					
24. Wenn ich mir Orgelmusik oder andere kraftvolle Musik anhöre, fühle ich mich manchmal wie in die Luft gehoben					
25. Manchmal kann ich Geräusche in Musik verwandeln, wenn ich auf eine bestimmte Art inhöre					
26. Einige meiner lebhaftesten Erinnerungen werden von Düften und Gerüchen geweckt					
27. Manche Musik erinnert mich an Bilder oder sich ändernde Farbmuster					
28. Oft weiß ich, was jemand sagen wird, noch bevor er (oder sie) es ausspricht					
29. Ich habe oft eine Art „körperliche Erinnerungen“, z. B. wenn ich geschwommen bin, kann ich danach immer noch das Gefühl haben, im Wasser zu sein					
30. Der Klang einer Stimme kann so faszinierend für mich sein, dass ich einfach nur zuhöre					
31. Manchmal fühle ich die Anwesenheit einer Person, die physisch überhaupt nicht da ist					
32. Manchmal kommen mir Gedanken und Bilder ohne das geringste Hinzutun					
33. Ich finde, dass verschiedene Gerüche verschiedene Farben haben					
34. Ein Sonnenuntergang kann mich tief berühren					

Hochsensibilitäts-Skala (HSPS-G)

Sehr geehrte Studienteilnehmerin, sehr geehrter Studienteilnehmer,

im Folgenden finden Sie 26 Aussagen, die das Ausmaß der Feinfühligkeit einer Person erfassen.

Wenn eine Aussage gar nicht auf Sie zutrifft, dann kreuzen Sie die Zahl 0 an, nur wenig auf Sie zutrifft, dann kreuzen sie die Zahl 1 an, doch teilweise auf Sie zutrifft, dann kreuzen Sie die Zahl 2 an, ziemlich gut auf Sie zutrifft, dann kreuzen Sie die Zahl 3 an, völlig auf Sie zutrifft, dann kreuzen Sie die Zahl 4 an. Bitte achten Sie darauf, dass Sie alle Aussagen zügig und aufrichtig beantworten. Es gibt keine „richtigen“ oder „falschen“ Antworten, sondern nur solche, die mehr oder weniger auf Sie zutreffen.

Aussagen	Trifft			
	nicht zu	wenig zu	teils zu	gut zu
	0	1	2	3
1 Ich fühle mich durch starke Sinneseindrücke wie Riechen überfordert				
2 Ich habe eine feine Wahrnehmung für unterschwellige Dinge in meiner Umgebung.				
3 Wenn ich mit anderen Menschen konkurrieren muss, werde ich nervös, so dass ich viel schlechter abschneide, als ich eigentlich könnte.				
4 Stimmungen anderer Menschen beeinflussen mich.				
5 Ich fühle mich leicht überwältigt von intensiven Reizen, wie starke Gerüche.				
6 Ich habe an stressigen Tagen das starke Bedürfnis, mich an einen Ort zurückzuziehen, wo ich alleine bin und mich erholen kann.				
7 Ich fühle mich leicht überwältigt von intensiven Reizen, wie hellem Licht.				
8 Ich habe ein reiches und vielfältiges Innenleben.				
9 Ich fühle mich durch starke Sinneseindrücke wie Schmecken überfordert.				
10 Laute Geräusche empfinde ich als sehr unangenehm.				
11 Bestimmte Musik berührt mich sehr stark.				
12 Ich fühle mich leicht überwältigt von intensiven Reizen, wie starkem Lärm (z. B. durch laute Sirenen in der Nähe).				
13 Ich fühle mich leicht überwältigt von intensiven Reizen, wie grober oder kratziger Kleidung.				
14 Ich fühle mich durch starke Sinneseindrücke wie Sehen überfordert.				
15 Ich erschrecke leichter als andere Menschen.				
16 Ich werde sehr unruhig, wenn ich in kurzer Zeit viel zu tun habe.				
17 Ich fühle mich genervt, wenn sich um mich herum viel abspielt.				
18 Ich fühle mich durch starke Sinneseindrücke wie Fühlen überfordert.				
19 Veränderungen in meinem Leben bringen mich merklich durcheinander.				
20 Ich nehme feine Düfte deutlich wahr und genieße sie.				
21 Ich empfinde es als sehr unangenehm, wenn ich mich mit vielen Dingen gleichzeitig beschäftigen muss.				
22 Für mich ist es wichtig, aufregende oder überfordernde Situationen in meinem Leben zu vermeiden.				
23 Starke Reize, wie laute Geräusche oder chaotische Szenen, stören mich sehr.				
24 Wenn ich während der Durchführung einer Aufgabe beobachtet werde, werde ich nervös, so dass ich viel schlechter abschneide, als ich eigentlich könnte.				
25 Ich fühle mich durch starke Sinneseindrücke wie Hören überfordert.				
26 Ich nehme Kunstwerke deutlich wahr und genieße sie.				

8. References

1. Chalmers DJ. Facing up to the problem of consciousness. *Journal of Consciousness* 1995; 3(1):200–19.
2. Tononi G, Edelman GM. Consciousness and complexity. *Science* 1998; 282(5395):1846–51.
3. Searle JR. The problem of consciousness. *Ciba Found Symp* 1993; 174:61-9; discussion 70-80.
4. Laureys S, Owen AM, Schiff ND. Brain function in coma, vegetative state, and related disorders. *The Lancet Neurology* 2004; 3(9):537–46.
5. Berlucchi G, Marzi CA. Neuropsychology of Consciousness: Some History and a Few New Trends. *Front Psychol* 2019; 10:50.
6. Garcia-Romeu AP, Tart CT. Altered States of Consciousness and Transpersonal Psychology. In: Friedman HL, Hartelius G, editors. *The Wiley-Blackwell Handbook of Transpersonal Psychology*. Wiley; 2013. p. 121–40.
7. Sarasso S, Casali AG, Casarotto S, Rosanova M, Sinigaglia C, Massimini M. Consciousness and complexity: a consilience of evidence. *Neuroscience of Consciousness* 2021.
8. Ustinova Y. Consciousness alteration practices in the West from prehistory to late antiquity. In: Cardeña E, Winkelmann M, editors. *Altering consciousness: Multidisciplinary perspectives*. Santa Barbara, Calif.: Praeger; 2011. p. 45–72.

9. James W. The varieties of religious experience. New York: Random House; 1929.
10. Cambiaghi M, Sacchetti B. Ivan Petrovich Pavlov (1849-1936). *J Neurol* 2015; 262(6):1599–600.
11. Todd JT, Morris EK. The early research of John B. Watson: Before the behavioral revolution. *Behav Anal* 1986; 9(1):71–88.
12. Morris EK, Smith NG, Altus DE. B. F. Skinner's contributions to applied behavior analysis. *Behav Anal* 2005; 28(2):99–131.
13. Molnar M. Sigmund Freud (1856-1939): life and work. *J Med Biogr* 1996; 4(4):236–43.
14. Ansbacher HL. Alfred Adler, pioneer in prevention of mental disorders. *J Prim Prev* 1990; 11(1):37–68.
15. Lieberman EJ. Rankian will. *Am J Psychoanal* 2012; 72(4):320–5.
16. Jones RA. Jung's "Psychology with the Psyche" and the Behavioral Sciences. *Behav Sci (Basel)* 2013; 3(3):408–17.
17. ROGERS CR. Significant aspects of client-centered therapy. *Am Psychol* 1946; 1(10):415–22.
18. Maslow AH. *Toward a psychology of being*. First Sublime edition. Floyd, Virginia: Sublime Books; 2014.
19. D'Sa N. Trajectory of the Mind - Transpersonal Psychology in Context [cited 2021 Jun 20]. Available from: URL: https://www.academia.edu/10855954/Trajectory_of_the_Mind_Transpersonal_Psychology_in_Context.
20. Ludwig AM. Altered states of consciousness. *Arch Gen Psychiatry* 1966; 15(3):225–34.

21. Grof S. Brief History of Transpersonal Psychology. *IJTS* 2008; 27(1):46–54.
22. Lajoie DH, Shapiro SI. Definitions of transpersonal psychology: The first twenty-three years. *Journal of Transpersonal Psychology* 1992; (24):79–98.
23. Tart CT. *Altered states of consciousness: A book of readings*. New York: Wiley; 1969.
24. Tart CT. *States of consciousness*. New York: Dutton; 1975. (A Dutton paperback; vol 406).
25. Tart CT. *Transpersonal psychologies*. El Cerrito, Calif.: Psychological Processes; 1983.
26. Walsh R. *Asian Psychotherapies*. In: Corsini RJ, Wedding D, editors. *Current psychotherapies*. 9th ed. Belmont, CA: Brooks/Cole; 2011.
27. Grof S, Grof C. *Holotropic breathwork: A new approach to self-exploration and therapy*. Albany: State University of New York Press; 2010. (SUNY series in transpersonal and humanistic psychology). Available from: URL: <http://search.ebscohost.com/login.aspx?direct=true&scope=sit e&db=nlebk&db=nlabk&AN=333449>.
28. Farthing GW. *The psychology of consciousness*. Englewood Cliffs, N.J: Prentice Hall; 1992.
29. Fischer R. A cartography of the ecstatic and meditative states. *Science* 1971; 174(4012):897–904.
30. Flor-Henry P, Shapiro Y, Sombrun C. Brain changes during a shamanic trance: Altered modes of consciousness,

hemispheric laterality, and systemic psychobiology. *Cogent Psychology* 2017; 4(1):1313522.

31. Vaitl D, Birbaumer N, Gruzelier J, Jamieson GA, Kotchoubey B, Kübler A et al. Psychobiology of altered states of consciousness. *Psychol Bull* 2005; 131(1):98–127.

32. Tabatabaeian S, Jennings CD. Toward a neurophysiological foundation for altered states of consciousness. *Behav Brain Sci* 2018; 41:e87.

33. Rock AJ, Krippner S. Does the Concept of “Altered States of Consciousness” Rest on a Mistake? *IJTS* 2007; 26(1):33–40.

34. Revonsuo A, Kallio S, Sikka P. What is an altered state of consciousness? *Philosophical Psychology* 2009; 22(2):187–204.

35. Dittrich A, Arx S von, Staub S. International study on altered states of consciousness (ISASC). *German Journal of Psychology* 1985; (9):319–39.

36. Dittrich A. The standardized psychometric assessment of altered states of consciousness (ASCs) in humans. *Pharmacopsychiatry* 1998; 31 Suppl 2:80–4.

37. Studerus E, Gamma A, Vollenweider FX. Psychometric evaluation of the altered states of consciousness rating scale (OAV). *PLoS One* 2010; 5(8):e12412.

38. Pekala RJ. *Quantifying Consciousness*. Boston, MA: Springer US; 1991.

39. Barrett FS, Johnson MW, Griffiths RR. Validation of the revised Mystical Experience Questionnaire in experimental

sessions with psilocybin. *J Psychopharmacol* 2015; 29(11):1182–90.

40. Nour MM, Evans L, Nutt D, Carhart-Harris RL. Ego-Dissolution and Psychedelics: Validation of the Ego-Dissolution Inventory (EDI). *Front Hum Neurosci* 2016; 10:269.

41. Schmidt TT, Berkemeyer H. The Altered States Database: Psychometric Data of Altered States of Consciousness. *Front Psychol* 2018; 9:1028.

42. Wittmann M. *Altered states of consciousness: Experiences out of time and self*. Cambridge, MA: MIT Press; 2018.

43. Berkovich-Ohana A, Dor-Ziderman Y, Glicksohn J, Goldstein A. Alterations in the sense of time, space, and body in the mindfulness-trained brain: a neurophenomenologically-guided MEG study. *Front Psychol* 2013; 4:912.

44. Fingelkurts AA, Fingelkurts AA. Timing in cognition and EEG brain dynamics: discreteness versus continuity. *Cogn Process* 2006; 7(3):135–62.

45. Varela F. Neurophenomenology: A methodological remedy for the hard problem. *Journal of Consciousness Studies* 1996; (3):330–49.

46. Berkovich-Ohana A, Dor-Ziderman Y, Trautwein F-M, Schweitzer Y, Nave O, Fulder S et al. The Hitchhiker's Guide to Neurophenomenology - The Case of Studying Self Boundaries With Meditators. *Front Psychol* 2020; 11:1680.

47. Crick F, Koch C. Towards a neurobiological theory of consciousness. *Seminars in the Neurosciences* 1990; (2):263–75.
48. Sousa A de. Towards an integrative theory of consciousness: part 1 (neurobiological and cognitive models). *Mens Sana Monogr* 2013; 11(1):100–50.
49. Seth A. Models of consciousness. *Scholarpedia* 2007; 2(1):1328.
50. Fries P. Rhythms for Cognition: Communication through Coherence. *Neuron* 2015; 88(1):220–35.
51. Seth AK, Izhikevich E, Reeke GN, Edelman GM. Theories and measures of consciousness: an extended framework. *Proc Natl Acad Sci U S A* 2006; 103(28):10799–804.
52. Nagel T. What Is It Like to Be a Bat? *The Philosophical Review* 1974; 83(4):435.
53. Seth AK. Consciousness: The last 50 years (and the next). *Brain Neurosci Adv* 2018; 2:2398212818816019.
54. Schmidt TT. WORKSHOP: The empirical study of altered states of consciousness - common standards in the psychometric assessment of subjective experiences; 2018.
55. Koch C, Massimini M, Boly M, Tononi G. Neural correlates of consciousness: progress and problems. *Nat Rev Neurosci* 2016; 17(5):307–21.
56. Pockett S, Holmes MD. Intracranial EEG power spectra and phase synchrony during consciousness and unconsciousness. *Conscious Cogn* 2009; 18(4):1049–55.

57. Murphy M, Bruno M-A, Riedner BA, Boveroux P, Noirhomme Q, Landsness EC et al. Propofol anesthesia and sleep: a high-density EEG study. *Sleep* 2011; 34(3):283-91A.
58. Sitt JD, King J-R, El Karoui I, Rohaut B, Faugeras F, Gramfort A et al. Large scale screening of neural signatures of consciousness in patients in a vegetative or minimally conscious state. *Brain* 2014; 137(Pt 8):2258–70.
59. Faugeras F, Rohaut B, Weiss N, Bekinschtein TA, Galanaud D, Puybasset L et al. Probing consciousness with event-related potentials in the vegetative state. *Neurology* 2011; 77(3):264–8.
60. Kotchoubey B. Event-related potential measures of consciousness: two equations with three unknowns. In: *The Boundaries of Consciousness: Neurobiology and Neuropathology*. Elsevier; 2005. p. 427–44 (Progress in Brain Research).
61. Arsiwalla XD, Verschure P. Measuring the Complexity of Consciousness. *Front Neurosci* 2018; 12:424.
62. Tononi G, Boly M, Massimini M, Koch C. Integrated information theory: from consciousness to its physical substrate. *Nat Rev Neurosci* 2016; 17(7):450–61.
63. Demertzi A, Tagliazucchi E, Dehaene S, Deco G, Barttfeld P, Raimondo F et al. Human consciousness is supported by dynamic complex patterns of brain signal coordination. *Sci Adv* 2019; 5(2):eaat7603.

64. Vaitl D. *Veränderte Bewusstseinszustände: Grundlagen - Techniken - Phänomenologie*. Stuttgart: Schattauer; 2012. (Körperpsychotherapie, Verhaltenstherapie). Available from: URL: http://sub-hh.ciando.com/book/?bok_id=328213.
65. Nardini-Bubols M, Da Silva DS, Dos Santos-Silva A, Stagnaro OK, Irigaray TQ, Alminhana LO. The Altered States of Consciousness in Transpersonal Approach Psychotherapy: Systematic Review and Guidelines for Research and Clinical Practice. *J Relig Health* 2019; 58(6):2175–94.
66. Kabat-Zinn J, Lipworth L, Burney R. The clinical use of mindfulness meditation for the self-regulation of chronic pain. *J Behav Med* 1985; 8(2):163–90.
67. Hofmann SG, Gómez AF. Mindfulness-Based Interventions for Anxiety and Depression. *Psychiatr Clin North Am* 2017; 40(4):739–49.
68. Schiepek G, editor. *Neurobiologie der Psychotherapie: Mit Geleitworten von Hermann Haken, Wolf Singer und Felix Unger*. 2., vollständig neu bearbeitete und erweiterte Auflage. s.l.: Schattauer GmbH Verlag für Medizin und Naturwissenschaften; 2010. (Psychotherapie). Available from: URL: http://www.content-select.com/index.php?id=bib_view&ean=9783608266214.
69. Kennedy D, Norman C. What don't we know? *Science* 2005; 309(5731):75.
70. Schrödinger E. *What is life?: The physical aspect of the living cell*. Cambridge: Cambridge Univ. Press; 1944.

71. Muñoz MA. Colloquium : Criticality and dynamical scaling in living systems. *Rev. Mod. Phys.* 2018; 90(3).
72. St. Louis E, Frey L, Britton J, Hopp J, Korb P, Koubeissi M et al. *Electroencephalography (EEG): An Introductory Text and Atlas of Normal and Abnormal Findings in Adults, Children, and Infants.* American Epilepsy Society; 2016.
73. Niedermeyer E, Da Lopes Silva FH, editors. *Electroencephalography: Basic principles, clinical applications, and related fields.* 5. ed. Philadelphia: Lippincott Williams & Wilkins; 2005. Available from: URL: <http://www.loc.gov/catdir/enhancements/fy0712/2004056721-d.html>.
74. Di Ieva A, Esteban FJ, Grizzi F, Klonowski W, Martín-Landrove M. Fractals in the neurosciences, Part II: clinical applications and future perspectives. *Neuroscientist* 2015; 21(1):30–43.
75. Başar E, Başar-Eroglu C, Karakaş S, Schürmann M. Gamma, alpha, delta, and theta oscillations govern cognitive processes. *International Journal of Psychophysiology* 2001; 39(2-3):241–8.
76. Cannon J, McCarthy MM, Lee S, Lee J, Börgers C, Whittington MA et al. *Neurosystems: brain rhythms and cognitive processing.* *Eur J Neurosci* 2014; 39(5):705–19.
77. Stam CJ. Nonlinear dynamical analysis of EEG and MEG: review of an emerging field. *Clin Neurophysiol* 2005; 116(10):2266–301.

78. Ižikevič EM. Dynamical systems in neuroscience: the geometry of excitability and bursting. 1. MIT Press paperback ed. Cambridge, Mass.: MIT Press; 2010. (Computational neuroscience).
79. He F, Yang Y. Nonlinear System Identification of Neural Systems from Neurophysiological Signals. *Neuroscience* 2021; 458:213–28.
80. Klonowski W. From conformons to human brains: an informal overview of nonlinear dynamics and its applications in biomedicine. *Nonlinear Biomed Phys* 2007; 1(1):5.
81. Klonowski W. Everything you wanted to ask about EEG but were afraid to get the right answer. *Nonlinear Biomed Phys* 2009; 3(1):2.
82. Henry B, Lovell N, Camacho F. Nonlinear Dynamics Time Series Analysis. In: Akay (Hg.) 2000 – Nonlinear Biomedical Signal processing, Volume 2: Dynamic Analysis and modeling. p. 1–39.
83. Kantz H, Schreiber T. Nonlinear time series analysis. Transfer. to digital printing. Cambridge: Cambridge University Press; 2004. (Cambridge nonlinear science series; vol 7).
84. Lorenz EN. Deterministic Nonperiodic Flow. *J. Atmos. Sci.* 1963; 20(2):130–41.
85. Kuznetsov NV, Mokaev TN, Kuznetsova OA, Kudryashova EV. The Lorenz system: hidden boundary of practical stability and the Lyapunov dimension. *Nonlinear Dyn* 2020; 102(2):713–32.

86. Friston KJ, Stephan KE. Free-energy and the brain. *Synthese* 2007; 159(3):417–58.
87. Werner G. Fractals in the nervous system: conceptual implications for theoretical neuroscience. *Front Physiol* 2010; 1:15.
88. Kelso JAS. Multistability and metastability: understanding dynamic coordination in the brain. *Philos Trans R Soc Lond B Biol Sci* 2012; 367(1591):906–18.
89. Tognoli E, Kelso JAS. The metastable brain. *Neuron* 2014; 81(1):35–48.
90. Briggman KL, Kristan WB. Multifunctional pattern-generating circuits. *Annu Rev Neurosci* 2008; 31:271–94.
91. Deco G, Jirsa VK. Ongoing cortical activity at rest: criticality, multistability, and ghost attractors. *J. Neurosci.* 2012; 32(10):3366–75.
92. Cocchi L, Gollo LL, Zalesky A, Breakspear M. Criticality in the brain: A synthesis of neurobiology, models and cognition. *Prog Neurobiol* 2017; 158:132–52.
93. Di Ieva A, Grizzi F, Jelinek H, Pellionisz AJ, Losa GA. Fractals in the Neurosciences, Part I: General Principles and Basic Neurosciences. *Neuroscientist* 2014; 20(4):403–17.
94. Pritchard WS. The brain in fractal time: 1/f-like power spectrum scaling of the human electroencephalogram. *Int J Neurosci* 1992; 66(1-2):119–29.
95. La Torre FC-D, González-Trejo JI, Real-Ramírez CA, Hoyos-Reyes LF. Fractal dimension algorithms and their

- application to time series associated with natural phenomena. *J. Phys.: Conf. Ser.* 2013; 475:12002.
96. He BJ. Scale-free brain activity: past, present, and future. *Trends Cogn Sci* 2014; 18(9):480–7.
97. He BJ, Zempel JM, Snyder AZ, Raichle ME. The temporal structures and functional significance of scale-free brain activity. *Neuron* 2010; 66(3):353–69.
98. Sejdić E, Lipsitz LA. Necessity of noise in physiology and medicine. *Comput Methods Programs Biomed* 2013; 111(2):459–70.
99. Gao J, Hu J, Tung W-W. Complexity measures of brain wave dynamics. *Cogn Neurodyn* 2011; 5(2):171–82.
100. Packard NH, Crutchfield JP, Farmer JD, Shaw RS. Geometry from a Time Series. *Phys Rev Lett* 1980; 45(9):712–6.
101. Grassberger P, Procaccia I. Characterization of Strange Attractors. *Phys Rev Lett* 1983; 50(5):346–9.
102. Wolf A, Swift JB, Swinney HL, Vastano JA. Determining Lyapunov exponents from a time series. *Physica D: Nonlinear Phenomena* 1985; 16(3):285–317.
103. Katz MJ. Fractals and the analysis of waveforms. *Computers in Biology and Medicine* 1988; 18(3):145–56.
104. Petrosian A. Kolmogorov complexity of finite sequences and recognition of different preictal EEG patterns. *Proceedings of the 8th IEEE Symposium on Computer-Based Medical Systems* 1995; (6):212–7.

105. Higuchi T. Approach to an irregular time series on the basis of the fractal theory. *Physica D: Nonlinear Phenomena* 1988; 31(2):277–83.
106. Esteller R, Vachtsevanos G, Echauz J, Litt B. A comparison of waveform fractal dimension algorithms. *IEEE Trans Circ Sys* 2001; (48(2)):177–83.
107. Kesić S, Spasić SZ. Application of Higuchi's fractal dimension from basic to clinical neurophysiology: A review. *Comput Methods Programs Biomed* 2016; 133:55–70.
108. Khoa TQD, Ha VQ, van Toi V. Higuchi fractal properties of onset epilepsy electroencephalogram. *Comput Math Methods Med* 2012; 2012:461426.
109. Anier A, Lipping T, Melto S, Hovilehto S. Higuchi fractal dimension and spectral entropy as measures of depth of sedation in intensive care unit. *Conf Proc IEEE Eng Med Biol Soc* 2004; 2006:526–9.
110. Negahbani E, Amirfattahi R, AHMADI B, Dehnavi AM, Rouzbeh M, Zaghari B et al. Electroencephalogram Fractal Dimension as a Measure of Depth of Anesthesia. In: 2008 3rd International Conference on Information and Communication Technologies: From Theory to Applications. IEEE; 042008. p. 1–5.
111. AHMADI B, AMIRFATTAHI R. Comparison of Correlation Dimension and Fractal Dimension in Estimating BIS index. *WSN* 2010; 02(01):67–73.

112. Klonowski W, Olejarczyk E, Stepien R, Jalowiecki P, Rudner R. Monitoring the depth of anaesthesia using fractal complexity method. In: *Complexus Mundi*. WORLD SCIENTIFIC; 012006. p. 333–42.
113. Cusenza M, Accardo A, Orsini A. EEG fractal dimension combined with burst suppression ratio as a measure of depth of anesthesia. In: Long M, editor. *World Congress on Medical Physics and Biomedical Engineering May 26-31, 2012, Beijing, China*. Berlin, Heidelberg: Springer Berlin Heidelberg; 2013. p. 497–500 (IFMBE proceedings).
114. Susmáková K, Krakovská A. Discrimination ability of individual measures used in sleep stages classification. *Artif Intell Med* 2008; 44(3):261–77.
115. Koley B, Dey D. An ensemble system for automatic sleep stage classification using single channel EEG signal. *Computers in Biology and Medicine* 2012; 42(12):1186–95.
116. Ferenets R, Lipping T, Suominen P, Turunen J, Puumala P, Jäntti V et al. Comparison of the properties of EEG spindles in sleep and propofol anesthesia. *Conf Proc IEEE Eng Med Biol Soc* 2006; 2006:6356–9.
117. Accardo A, Affinito M, Carrozzi M, Bouquet F. Use of the fractal dimension for the analysis of electroencephalographic time series. *Biol Cybern* 1997; 77(5):339–50.
118. Jouny CC, Bergey GK. Characterization of early partial seizure onset: frequency, complexity and entropy. *Clin Neurophysiol* 2012; 123(4):658–69.

119. Bao FS, Gao J-M, Hu J, Lie DY-C, Zhang Y, Oommen KJ. Automated Epilepsy Diagnosis Using Interictal Scalp EEG; 2009 Apr 24. Available from: URL: <http://arxiv.org/pdf/0904.3808v2>.
120. Al-Nuaimi AH, Jammeh E, Sun L, Ifeachor E. Higuchi fractal dimension of the electroencephalogram as a biomarker for early detection of Alzheimer's disease. *Annu Int Conf IEEE Eng Med Biol Soc* 2017; 2017:2320–4.
121. Smits FM, Porcaro C, Cottone C, Cancelli A, Rossini PM, Tecchio F. Electroencephalographic Fractal Dimension in Healthy Ageing and Alzheimer's Disease. *PLoS One* 2016; 11(2):e0149587.
122. Staudinger T, Polikar R. Analysis of complexity based EEG features for the diagnosis of Alzheimer's disease. *Annu Int Conf IEEE Eng Med Biol Soc* 2011; 2011:2033–6.
123. Solhjo S, Motie Nasrabadi A, Hashemi Golpayegani MR. EEG-Based Mental Task Classification in Hypnotized and Normal Subjects. *Conf Proc IEEE Eng Med Biol Soc* 2005; 2005:2041–3.
124. Ibáñez-Molina AJ, Iglesias-Parro S. Fractal characterization of internally and externally generated conscious experiences. *Brain Cogn* 2014; 87:69–75.
125. Baghdadi G, Nasrabadi AM. Comparison of different EEG features in estimation of hypnosis susceptibility level. *Computers in Biology and Medicine* 2012; 42(5):590–7.

126. Liu Y, Sourina O, Nguyen MK. Real-Time EEG-Based Emotion Recognition and Its Applications. In: Gavrilova ML, Tan CJK, Sourin A, Sourina O, editors. Transactions on Computational Science XII. Berlin, Heidelberg: Springer Berlin Heidelberg; 2011. p. 256–77 (Lecture Notes in Computer Science).
127. Shannon CE. A Mathematical Theory of Communication. Bell System Technical Journal 1948; 27(3):379–423.
128. Grassberger P, Procaccia I. Measuring the strangeness of strange attractors. Physica D: Nonlinear Phenomena 1983; 9(1-2):189–208.
129. Grassberger P, Procaccia I. Estimation of the Kolmogorov entropy from a chaotic signal. Phys Rev A Gen Phys 1983; 28(4):2591–3.
130. Costa M, Goldberger AL, Peng C-K. Multiscale entropy analysis of biological signals. Phys Rev E Stat Nonlin Soft Matter Phys 2005; 71(2 Pt 1):21906.
131. Pincus SM. Approximate entropy as a measure of system complexity. Proc Natl Acad Sci U S A 1991; 88(6):2297–301.
132. Richman JS, Moorman JR. Physiological time-series analysis using approximate entropy and sample entropy. Am J Physiol Heart Circ Physiol 2000; 278(6):H2039-49.
133. Zhou R, Yang C, Wan J, Zhang W, Guan B, Xiong N. Measuring Complexity and Predictability of Time Series with Flexible Multiscale Entropy for Sensor Networks. Sensors (Basel) 2017; 17(4).

134. Goldberger AL, Peng C-K, Lipsitz LA. What is physiologic complexity and how does it change with aging and disease? *Neurobiology of Aging* 2002; 23(1):23–6.
135. Costa M, Goldberger AL, Peng C-K. Multiscale entropy analysis of complex physiologic time series. *Phys Rev Lett* 2002; 89(6):68102.
136. Keshmiri S. Entropy and the Brain: An Overview. *Entropy (Basel)* 2020; 22(9).
137. Miskovic V, MacDonald KJ, Rhodes LJ, Cote KA. Changes in EEG multiscale entropy and power-law frequency scaling during the human sleep cycle. *Hum Brain Mapp* 2019; 40(2):538–51.
138. Liu Q, Chen Y-F, Fan S-Z, Abbod MF, Shieh J-S. EEG Signals Analysis Using Multiscale Entropy for Depth of Anesthesia Monitoring during Surgery through Artificial Neural Networks. *Comput Math Methods Med* 2015; 2015:232381.
139. Takahashi T, Cho RY, Mizuno T, Kikuchi M, Murata T, Takahashi K et al. Antipsychotics reverse abnormal EEG complexity in drug-naive schizophrenia: a multiscale entropy analysis. *Neuroimage* 2010; 51(1):173–82.
140. Mizuno T, Takahashi T, Cho RY, Kikuchi M, Murata T, Takahashi K et al. Assessment of EEG dynamical complexity in Alzheimer's disease using multiscale entropy. *Clin Neurophysiol* 2010; 121(9):1438–46.
141. McDonough, Letang, Erwin, Kana. Evidence for Maintained Post-Encoding Memory Consolidation Across the

Adult Lifespan Revealed by Network Complexity. *Entropy* 2019; 21(11):1072.

142. Angsuwatanakul T, O'Reilly J, Ounjai K, Kaewkamnerdpong B, Iramina K. Multiscale Entropy as a New Feature for EEG and fNIRS Analysis. *Entropy (Basel)* 2020; 22(2).

143. Bak P. *How Nature Works*. New York, NY: Springer New York; 1996.

144. Hesse J, Gross T. Self-organized criticality as a fundamental property of neural systems. *Front Syst Neurosci* 2014; 8:166.

145. Shew WL, Plenz D. The functional benefits of criticality in the cortex. *Neuroscientist* 2013; 19(1):88–100.

146. Tagliazucchi E. The signatures of conscious access and its phenomenology are consistent with large-scale brain communication at criticality. *Conscious Cogn* 2017; 55:136–47.

147. Roli A, Villani M, Filisetti A, Serra R. Dynamical Criticality: Overview and Open Questions. *J Syst Sci Complex* 2018; 31(3):647–63.

148. Zimmern V. Why Brain Criticality Is Clinically Relevant: A Scoping Review. *Front Neural Circuits* 2020; 14:54.

149. Heiney K, Huse Ramstad O, Fiskum V, Christiansen N, Sandvig A, Nichele S et al. Criticality, Connectivity, and Neural Disorder: A Multifaceted Approach to Neural Computation. *Front Comput Neurosci* 2021; 15:611183.

150. Beggs JM, Timme N. Being critical of criticality in the brain. *Front Physiol* 2012; 3:163.
151. Chialvo DR. Life at the Edge: Complexity and Criticality in Biological Function. *Acta Phys. Pol. B* 2018; 49(12):1955.
152. TURING AM. I.—Computing Machinery and Intelligence. *Mind* 1950; LIX(236):433–60.
153. Hebb DO. The organization of behavior: A neuropsychological theory. 11. [print.]. New York: Wiley; 1949.
154. Haken H. Synergetics. *Scholarpedia* 2007; 2(1):1400.
155. Haken H, Kelso JA, Bunz H. A theoretical model of phase transitions in human hand movements. *Biol Cybern* 1985; 51(5):347–56.
156. Kauffman SA. The origins of order: Self-organization and selection in evolution. New York: Oxford Univ. Press; 1993. Available from: URL: <http://www.loc.gov/catdir/enhancements/fy0602/91011148-d.html>.
157. Hopfield JJ. Neural networks and physical systems with emergent collective computational abilities. *Proc Natl Acad Sci U S A* 1982; 79(8):2554–8.
158. Langton CG. Computation at the edge of chaos: Phase transitions and emergent computation. *Physica D: Nonlinear Phenomena* 1990; 42(1-3):12–37.
159. Packard NH. Adaptation towards the edge of chaos. In: *Dynamic Patterns in Complex Systems*. WORLD SCIENTIFIC; 1988. p. 293–301.

160. Crutchfield JP, Young K. *Computation at the Onset of Chaos, Complexity, Entropy, and Physics of Information*. New Jersey, USA: Addison Wesley; 1990.
161. Bak, Tang, Wiesenfeld. Self-organized criticality: An explanation of the $1/f$ noise. *Phys Rev Lett* 1987; 59(4):381–4.
162. Plenz D. Criticality in Cortex: Neuronal Avalanches and Coherence Potentials. In: Plenz D, Niebur E, editors. *Criticality in Neural Systems*. Weinheim, Germany: Wiley-VCH Verlag GmbH & Co. KGaA; 2014. p. 5–42.
163. Tateno T, Kawana A, Jimbo Y. Analytical characterization of spontaneous firing in networks of developing rat cultured cortical neurons. *Phys Rev E Stat Nonlin Soft Matter Phys* 2002; 65(5 Pt 1):51924.
164. Beggs JM, Plenz D. Neuronal Avalanches in Neocortical Circuits. *J. Neurosci.* 2003; 23(35):11167–77.
165. Eurich CW, Herrmann JM, Ernst UA. Finite-size effects of avalanche dynamics. *Phys Rev E Stat Nonlin Soft Matter Phys* 2002; 66(6 Pt 2):66137.
166. Beggs JM, Plenz D. Neuronal avalanches are diverse and precise activity patterns that are stable for many hours in cortical slice cultures. *J. Neurosci.* 2004; 24(22):5216–29.
167. Stewart CV, Plenz D. Inverted-U profile of dopamine-NMDA-mediated spontaneous avalanche recurrence in superficial layers of rat prefrontal cortex. *J. Neurosci.* 2006; 26(31):8148–59.

168. Gireesh ED, Plenz D. Neuronal avalanches organize as nested theta- and beta/gamma-oscillations during development of cortical layer 2/3. *Proc Natl Acad Sci U S A* 2008; 105(21):7576–81.
169. Plenz D, Ribeiro TL, Miller SR, Kells PA, Vakili A, Capek EL. Self-Organized Criticality in the Brain; 2021 Feb 18. Available from: URL: <http://arxiv.org/pdf/2102.09124v1>.
170. Petermann T, Thiagarajan TC, Lebedev MA, Nicolelis MAL, Chialvo DR, Plenz D. Spontaneous cortical activity in awake monkeys composed of neuronal avalanches. *Proc Natl Acad Sci U S A* 2009; 106(37):15921–6.
171. Hahn G, Petermann T, Havenith MN, Yu S, Singer W, Plenz D et al. Neuronal avalanches in spontaneous activity in vivo. *J Neurophysiol* 2010; 104(6):3312–22.
172. Klaus A, Yu S, Plenz D. Statistical analyses support power law distributions found in neuronal avalanches. *PLoS One* 2011; 6(5):e19779.
173. Ribeiro TL, Copelli M, Caixeta F, Belchior H, Chialvo DR, Nicolelis MAL et al. Spike avalanches exhibit universal dynamics across the sleep-wake cycle. *PLoS One* 2010; 5(11):e14129.
174. Linkenkaer-Hansen K, Nikouline VV, Palva JM, Ilmoniemi RJ. Long-Range Temporal Correlations and Scaling Behavior in Human Brain Oscillations. *J. Neurosci.* 2001; 21(4):1370–7.

175. Shriki O, Alstott J, Carver F, Holroyd T, Henson RNA, Smith ML et al. Neuronal avalanches in the resting MEG of the human brain. *J. Neurosci.* 2013; 33(16):7079–90.
176. Priesemann V, Valderrama M, Wibral M, van Quyen M. Neuronal avalanches differ from wakefulness to deep sleep--evidence from intracranial depth recordings in humans. *PLoS Comput Biol* 2013; 9(3):e1002985.
177. Priesemann V, Wibral M, Valderrama M, Pröpper R, van Quyen M, Geisel T et al. Spike avalanches in vivo suggest a driven, slightly subcritical brain state. *Front Syst Neurosci* 2014; 8:108.
178. Priesemann V. Self-organization to sub-criticality. *BMC Neurosci* 2015; 16(S1).
179. Wilting J, Priesemann V. Quantifying the distance to criticality under subsampling. *BMC Neurosci* 2015; 16(S1).
180. Tagliazucchi E, Balenzuela P, Fraiman D, Chialvo DR. Criticality in large-scale brain fMRI dynamics unveiled by a novel point process analysis. *Front Physiol* 2012; 3:15.
181. Beggs J. Neuronal avalanche. *Scholarpedia* 2007; 2(1):1344.
182. Harris TE. *The Theory of branching processes*. Mineola: Dover Publications; 2002.
183. Poil S-S, Hardstone R, Mansvelder HD, Linkenkaer-Hansen K. Critical-state dynamics of avalanches and oscillations jointly emerge from balanced excitation/inhibition in neuronal networks. *J. Neurosci.* 2012; 32(29):9817–23.

184. Massobrio P, Pasquale V, Martinoia S. Self-organized criticality in cortical assemblies occurs in concurrent scale-free and small-world networks. *Sci Rep* 2015; 5:10578.
185. Heiney K, Ramstad OH, Sandvig I, Sandvig A, Nichele S. Assessment and manipulation of the computational capacity of in vitro neuronal networks through criticality in neuronal avalanches. In: 2019 IEEE Symposium Series on Computational Intelligence (SSCI). IEEE; 122019. p. 247–54.
186. Kello CT, Brown GDA, Ferrer-I-Cancho R, Holden JG, Linkenkaer-Hansen K, Rhodes T et al. Scaling laws in cognitive sciences. *Trends Cogn Sci* 2010; 14(5):223–32.
187. Kinouchi O, Copelli M. Optimal dynamical range of excitable networks at criticality. *Nature Phys* 2006; 2(5):348–51.
188. Larremore DB, Shew WL, Restrepo JG. Predicting criticality and dynamic range in complex networks: effects of topology. *Phys Rev Lett* 2011; 106(5):58101.
189. Shew WL, Yang H, Petermann T, Roy R, Plenz D. Neuronal avalanches imply maximum dynamic range in cortical networks at criticality. *J. Neurosci.* 2009; 29(49):15595–600.
190. Gautam SH, Hoang TT, McClanahan K, Grady SK, Shew WL. Maximizing Sensory Dynamic Range by Tuning the Cortical State to Criticality. *PLoS Comput Biol* 2015; 11(12):e1004576.
191. Bertschinger N, Natschläger T. Real-time computation at the edge of chaos in recurrent neural networks. *Neural Comput* 2004; 16(7):1413–36.

192. Haldeman C, Beggs JM. Critical branching captures activity in living neural networks and maximizes the number of metastable States. *Phys Rev Lett* 2005; 94(5):58101.
193. Del Papa B, Priesemann V, Triesch J. Criticality meets learning: Criticality signatures in a self-organizing recurrent neural network. *PLoS One* 2017; 12(5):e0178683.
194. Shew WL, Yang H, Yu S, Roy R, Plenz D. Information capacity and transmission are maximized in balanced cortical networks with neuronal avalanches. *J. Neurosci.* 2011; 31(1):55–63.
195. Fagerholm ED, Scott G, Shew WL, Song C, Leech R, Knöpfel T et al. Cortical Entropy, Mutual Information and Scale-Free Dynamics in Waking Mice. *Cereb Cortex* 2016; 26(10):3945–52.
196. Botcharova M, Farmer SF, Berthouze L. Markers of criticality in phase synchronization. *Front Syst Neurosci* 2014; 8:176.
197. Peng CK, Buldyrev SV, Havlin S, Simons M, Stanley HE, Goldberger AL. Mosaic organization of DNA nucleotides. *Phys Rev E Stat Phys Plasmas Fluids Relat Interdiscip Topics* 1994; 49(2):1685–9.
198. Kantelhardt JW, Koscielny-Bunde E, Rego HH, Havlin S, Bunde A. Detecting long-range correlations with detrended fluctuation analysis. *Physica A: Statistical Mechanics and its Applications* 2001; 295(3-4):441–54.

199. Hardstone R, Poil S-S, Schiavone G, Jansen R, Nikulin VV, Mansvelder HD et al. Detrended fluctuation analysis: a scale-free view on neuronal oscillations. *Front Physiol* 2012; 3:450.
200. Eke A, Herman P, Kocsis L, Kozak LR. Fractal characterization of complexity in temporal physiological signals. *Physiol Meas* 2002; 23(1):R1-38.
201. Marshall N, Timme NM, Bennett N, Ripp M, Lautzenhiser E, Beggs JM. Analysis of Power Laws, Shape Collapses, and Neural Complexity: New Techniques and MATLAB Support via the NCC Toolbox. *Front Physiol* 2016; 7:250.
202. Priesemann V, Shriki O. Can a time varying external drive give rise to apparent criticality in neural systems? *PLoS Comput Biol* 2018; 14(5):e1006081.
203. Friedman N, Ito S, Brinkman BAW, Shimono M, DeVille REL, Dahmen KA et al. Universal critical dynamics in high resolution neuronal avalanche data. *Phys Rev Lett* 2012; 108(20):208102.
204. Timme NM, Marshall NJ, Bennett N, Ripp M, Lautzenhiser E, Beggs JM. Criticality Maximizes Complexity in Neural Tissue. *Front Physiol* 2016; 7:425.
205. Alonso LM, Proekt A, Schwartz TH, Pryor KO, Cecchi GA, Magnasco MO. Dynamical criticality during induction of anesthesia in human ECoG recordings. *Front Neural Circuits* 2014; 8:20.

206. Thiery T, Lajnef T, Combrisson E, Dehgan A, Rainville P, Mashour GA et al. Long-range temporal correlations in the brain distinguish conscious wakefulness from induced unconsciousness. *Neuroimage* 2018; 179:30–9.
207. Cook MJ, Varsavsky A, Himes D, Leyde K, Berkovic SF, O'Brien T et al. The dynamics of the epileptic brain reveal long-memory processes. *Front Neurol* 2014; 5:217.
208. Parish LM, Worrell GA, Cranstoun SD, Stead SM, Pennell P, Litt B. Long-range temporal correlations in epileptogenic and non-epileptogenic human hippocampus. *Neuroscience* 2004; 125(4):1069–76.
209. Worrell GA, Cranstoun SD, Echaz J, Litt B. Evidence for self-organized criticality in human epileptic hippocampus. *Neuroreport* 2002; 13(16):2017–21.
210. Arviv O, Medvedovsky M, Sheintuch L, Goldstein A, Shriki O. Deviations from Critical Dynamics in Interictal Epileptiform Activity. *J Neurosci* 2016; 36(48):12276–92.
211. Meisel C, Storch A, Hallmeyer-Elgner S, Bullmore E, Gross T. Failure of adaptive self-organized criticality during epileptic seizure attacks. *PLoS Comput Biol* 2012; 8(1):e1002312.
212. Stam CJ, Montez T, Jones BF, Rombouts SARB, van der Made Y, Pijnenburg YAL et al. Disturbed fluctuations of resting state EEG synchronization in Alzheimer's disease. *Clin Neurophysiol* 2005; 116(3):708–15.
213. West T, Farmer S, Berthouze L, Jha A, Beudel M, Foltynie T et al. The Parkinsonian Subthalamic Network: Measures of

Power, Linear, and Non-linear Synchronization and their Relationship to L-DOPA Treatment and OFF State Motor Severity. *Front Hum Neurosci* 2016; 10:517.

214. Tinker J, Velazquez JLP. Power law scaling in synchronization of brain signals depends on cognitive load. *Front Syst Neurosci* 2014; 8:73.

215. Fagerholm ED, Lorenz R, Scott G, Dinov M, Hellyer PJ, Mirzaei N et al. Cascades and cognitive state: focused attention incurs subcritical dynamics. *J. Neurosci.* 2015; 35(11):4626–34.

216. Ouyang G, Hildebrandt A, Schmitz F, Herrmann CS. Decomposing alpha and 1/f brain activities reveals their differential associations with cognitive processing speed. *Neuroimage* 2020; 205:116304.

217. Dimitriadis SI, Laskaris NA, Simos PG, Micheloyannis S, Fletcher JM, Rezaie R et al. Altered temporal correlations in resting-state connectivity fluctuations in children with reading difficulties detected via MEG. *Neuroimage* 2013; 83:307–17.

218. Kwok EYL, Cardy JO, Allman BL, Allen P, Herrmann B. Dynamics of spontaneous alpha activity correlate with language ability in young children. *Behav Brain Res* 2019; 359:56–65.

219. Ezaki T, Fonseca Dos Reis E, Watanabe T, Sakaki M, Masuda N. Closer to critical resting-state neural dynamics in individuals with higher fluid intelligence. *Commun Biol* 2020; 3(1):52.

220. Linkenkaer-Hansen K, Monto S, Rytsälä H, Suominen K, Isometsä E, Kähkönen S. Breakdown of long-range temporal

correlations in theta oscillations in patients with major depressive disorder. *J. Neurosci.* 2005; 25(44):10131–7.

221. Lee J-S, Yang B-H, Lee J-H, Choi J-H, Choi I-G, Kim S-B. Detrended fluctuation analysis of resting EEG in depressed outpatients and healthy controls. *Clin Neurophysiol* 2007; 118(11):2489–96.

222. Gärtner M, Irrmischer M, Winnebeck E, Fissler M, Huntenburg JM, Schroeter TA et al. Aberrant Long-Range Temporal Correlations in Depression Are Attenuated after Psychological Treatment. *Front Hum Neurosci* 2017; 11:340.

223. Leistedt S, Dumont M, Coumans N, Lanquart J-P, Jurysta F, Linkowski P. The modifications of the long-range temporal correlations of the sleep EEG due to major depressive episode disappear with the status of remission. *Neuroscience* 2007; 148(3):782–93.

224. Leistedt S, Dumont M, Lanquart J-P, Jurysta F, Linkowski P. Characterization of the sleep EEG in acutely depressed men using detrended fluctuation analysis. *Clin Neurophysiol* 2007; 118(4):940–50.

225. Nikulin VV, Jönsson EG, Brismar T. Attenuation of long-range temporal correlations in the amplitude dynamics of alpha and beta neuronal oscillations in patients with schizophrenia. *Neuroimage* 2012; 61(1):162–9.

226. Moran JK, Michail G, Heinz A, Keil J, Senkowski D. Long-Range Temporal Correlations in Resting State Beta Oscillations are Reduced in Schizophrenia. *Front Psychiatry* 2019; 10:517.

227. Pettersson-Yeo W, Allen P, Benetti S, McGuire P, Mechelli A. Dysconnectivity in schizophrenia: where are we now? *Neurosci Biobehav Rev* 2011; 35(5):1110–24.
228. Friston K, Brown HR, Siemerikus J, Stephan KE. The dysconnection hypothesis (2016). *Schizophr Res* 2016; 176(2-3):83–94.
229. Ros T, J Baars B, Lanius RA, Vuilleumier P. Tuning pathological brain oscillations with neurofeedback: a systems neuroscience framework. *Front Hum Neurosci* 2014; 8:1008.
230. Zhigalov A, Kaplan A, Palva JM. Modulation of critical brain dynamics using closed-loop neurofeedback stimulation. *Clin Neurophysiol* 2016; 127(8):2882–9.
231. Colombo MA, Wei Y, Ramautar JR, Linkenkaer-Hansen K, Tagliazucchi E, van Someren EJW. More Severe Insomnia Complaints in People with Stronger Long-Range Temporal Correlations in Wake Resting-State EEG. *Front Physiol* 2016; 7:576.
232. Hinterberger T, Schmidt S, Kamei T, Walach H. Decreased electrophysiological activity represents the conscious state of emptiness in meditation. *Front Psychol* 2014; 5:99.
233. Travis F, Shear J. Focused attention, open monitoring and automatic self-transcending: Categories to organize meditations from Vedic, Buddhist and Chinese traditions. *Conscious Cogn* 2010; 19(4):1110–8.

234. Hinterberger T, Kamei T, Walach H. Psychophysiological classification and staging of mental states during meditative practice. *Biomed Tech (Berl)* 2011; 56(6):341–50.
235. Hinterberger T, Kübler A, Kaiser J, Neumann N, Birbaumer N. A brain–computer interface (BCI) for the locked-in: comparison of different EEG classifications for the thought translation device. *Clin Neurophysiol* 2003; 114(3):416–25.
236. Cohen J. *Statistical Power Analysis for the Behavioral Sciences*. Routledge; 2013.
237. Benjamini Y, Hochberg Y. Controlling the false discovery rate: a practical and powerful approach to multiple testing. *J. R. Statist. Soc. B* 1995; (57):289–300.
238. Rosipal R, Krämer N. Overview and Recent Advances in Partial Least Squares. In: Saunders C, Grobelnik M, Gunn S, Shawe-Taylor J, editors. *Subspace, Latent Structure and Feature Selection*. Berlin, Heidelberg: Springer Berlin Heidelberg; 2006. p. 34–51 (Lecture Notes in Computer Science).
239. Hanley JA, McNeil BJ. The meaning and use of the area under a receiver operating characteristic (ROC) curve. *Radiology* 1982; 143(1):29–36.
240. Tellegen A, Atkinson G. Openness to absorbing and self-altering experiences ("absorption"), a trait related to hypnotic susceptibility. *J Abnorm Psychol* 1974; 83(3):268–77.

241. Hinterberger T, Walter N. Rhythmic Mechanical Body Stimulation Improves Physical and Mental Wellbeing and Alters States of Consciousness. *AJBSR* 2020; 9(2):132–6.
242. Kihlstrom JF, Register PA, Hoyt IP, Albright JS, Grigorian EM, Heindel WC et al. Dispositional correlates of hypnosis: a phenomenological approach. *Int J Clin Exp Hypn* 1989; 37(3):249–63.
243. Menzies V, Taylor AG, Bourguignon C. Absorption: an individual difference to consider in mind-body interventions. *J Holist Nurs* 2008; 26(4):297–302.
244. Konrad S, Herzberg PY. Psychometric Properties and Validation of a German High Sensitive Person Scale (HSPS-G). *European Journal of Psychological Assessment* 2019; 35(3):364–78.
245. Aron EN, Aron A. Sensory-processing sensitivity and its relation to introversion and emotionality. *J Pers Soc Psychol* 1997; 73(2):345–68.
246. Lionetti F, Aron A, Aron EN, Burns GL, Jagiellowicz J, Pluess M. Dandelions, tulips and orchids: evidence for the existence of low-sensitive, medium-sensitive and high-sensitive individuals. *Transl Psychiatry* 2018; 8(1):24.
247. Tononi G. An information integration theory of consciousness. *BMC Neurosci* 2004; 5:42.
248. Oizumi M, Albantakis L, Tononi G. From the phenomenology to the mechanisms of consciousness:

- Integrated Information Theory 3.0. *PLoS Comput Biol* 2014; 10(5):e1003588.
249. Carhart-Harris RL. The entropic brain - revisited. *Neuropharmacology* 2018; 142:167–78.
250. Massobrio P, Arcangelis Ld, Pasquale V, Jensen HJ, Plenz D. Criticality as a signature of healthy neural systems. *Front Syst Neurosci* 2015; 9:22.
251. Fekete T, Hinrichs H, Sitt JD, Heinze H-J, Shriki O. Multiscale criticality measures as general-purpose gauges of proper brain function. *Sci Rep* 2021; 11(1):14441.
252. Cahn BR, Delorme A, Polich J. Occipital gamma activation during Vipassana meditation. *Cogn Process* 2010; 11(1):39–56.
253. Berman AE, Stevens L. EEG manifestations of nondual experiences in meditators. *Conscious Cogn* 2015; 31:1–11.
254. Cohen S, Kamarck T, Mermelstein R. A global measure of perceived stress. *J Health Soc Behav* 1983; 24(4):385–96.
255. Ahani A, Wahbeh H, Miller M, Nezamfar H, Erdogmus D, Oken B. Change in physiological signals during mindfulness meditation. *Int IEEE EMBS Conf Neural Eng* 2013:1738-1381.
256. DeLosAngeles D, Williams G, Burston J, Fitzgibbon SP, Lewis TW, Grummett TS et al. Electroencephalographic correlates of states of concentrative meditation. *Int J Psychophysiol* 2016; 110:27–39.
257. Lagopoulos J, Xu J, Rasmussen I, Vik A, Malhi GS, Eliassen CF et al. Increased theta and alpha EEG activity during

nondirective meditation. *J Altern Complement Med* 2009; 15(11):1187–92.

258. van Lutterveld R, van Dellen E, Pal P, Yang H, Stam CJ, Brewer J. Meditation is associated with increased brain network integration. *Neuroimage* 2017; 158:18–25.

259. Lutz A, Greischar LL, Rawlings NB, Ricard M, Davidson RJ. Long-term meditators self-induce high-amplitude gamma synchrony during mental practice. *Proc Natl Acad Sci U S A* 2004; 101(46):16369–73.

260. Fucci E, Abdoun O, Caclin A, Francis A, Dunne JD, Ricard M et al. Differential effects of non-dual and focused attention meditations on the formation of automatic perceptual habits in expert practitioners. *Neuropsychologia* 2018; 119:92–100.

261. Lomas T, Ivtzan I, Fu CHY. A systematic review of the neurophysiology of mindfulness on EEG oscillations. *Neurosci Biobehav Rev* 2015; 57:401–10.

262. Deolindo CS, Ribeiro MW, Aratanha MA, Afonso RF, Irrmischer M, Kozasa EH. A Critical Analysis on Characterizing the Meditation Experience Through the Electroencephalogram. *Front Syst Neurosci* 2020; 14:53.

263. Wang DJJ, Jann K, Fan C, Qiao Y, Zang Y-F, Lu H et al. Neurophysiological Basis of Multi-Scale Entropy of Brain Complexity and Its Relationship With Functional Connectivity. *Front Neurosci* 2018; 12:352.

264. Tagliazucchi E, Carhart-Harris R, Leech R, Nutt D, Chialvo DR. Enhanced repertoire of brain dynamical states during the

- psychedelic experience. *Hum Brain Mapp* 2014; 35(11):5442–56.
265. Hager B, Yang AC, Brady R, Meda S, Clementz B, Pearlson GD et al. Neural complexity as a potential translational biomarker for psychosis. *J Affect Disord* 2017; 216:89–99.
266. Kakumanu RJ, Nair AK, Venugopal R, Sasidharan A, Ghosh PK, John JP et al. Dissociating meditation proficiency and experience dependent EEG changes during traditional Vipassana meditation practice. *Biol Psychol* 2018; 135:65–75.
267. Huang H-Y, Lo P-C. EEG dynamics of experienced Zen meditation practitioners probed by complexity index and spectral measure. *J Med Eng Technol* 2009; 33(4):314–21.
268. Vyšata O, Schätz M, Kopal J, Burian J, Procházka A, Jiří K et al. Non-Linear EEG Measures in Meditation. *JBiSE* 2014; 07(09):731–8.
269. Martínez Vivot R, Pallavicini C, Zamberlan F, Vigo D, Tagliazucchi E. Meditation Increases the Entropy of Brain Oscillatory Activity. *Neuroscience* 2020; 431:40–51.
270. Young JH, Arterberry ME, Martin JP. Contrasting Electroencephalography-Derived Entropy and Neural Oscillations With Highly Skilled Meditators. *Front Hum Neurosci* 2021; 15:628417.
271. Aftanas LI, Golocheikine SA. Non-linear dynamic complexity of the human EEG during meditation. *Neuroscience Letters* 2002; 330(2):143–6.

272. Gao J, Fan J, Wu BWY, Zhang Z, Chang C, Hung Y-S et al. Entrainment of chaotic activities in brain and heart during MBSR mindfulness training. *Neuroscience Letters* 2016; 616:218–23.
273. Sik HH, Gao J, Fan J, Wu BWY, Leung HK, Hung YS. Using Wavelet Entropy to Demonstrate how Mindfulness Practice Increases Coordination between Irregular Cerebral and Cardiac Activities. *J Vis Exp* 2017; (123).
274. Irmischer M, Houtman SJ, Mansvelder HD, Tremmel M, Ott U, Linkenkaer-Hansen K. Controlling the Temporal Structure of Brain Oscillations by Focused Attention Meditation. *Hum Brain Mapp* 2018; 39(4):1825–38.
275. Tomen N, Rotermund D, Ernst U. Marginally subcritical dynamics explain enhanced stimulus discriminability under attention. *Front Syst Neurosci* 2014; 8:151.
276. Carhart-Harris RL, Leech R, Hellyer PJ, Shanahan M, Feilding A, Tagliazucchi E et al. The entropic brain: a theory of conscious states informed by neuroimaging research with psychedelic drugs. *Front Hum Neurosci* 2014; 8:20.
277. Papo D. Commentary: The entropic brain: a theory of conscious states informed by neuroimaging research with psychedelic drugs. *Front Hum Neurosci* 2016; 10:423.
278. Burns T, Rajan R. Combining complexity measures of EEG data: multiplying measures reveal previously hidden information. *F1000Res* 2015; 4:137.

279. Hankey A, Shetkar R. Self-transcending meditation is good for mental health: why this should be the case. *Int Rev Psychiatry* 2016; 28(3):236–40.
280. Dürschmid S, Reichert C, Walter N, Hinrichs H, Heinze H-J, Ohi FW et al. Self-regulated critical brain dynamics originate from high frequency-band activity in the MEG. *PLoS One* 2020; 15(6):e0233589.
281. Frohlich J, Toker D, Monti MM. Consciousness among delta waves: a paradox? *Brain* 2021; 144(8):2257–77.
282. Mediano PAM, Rosas FE, Barrett AB, Bor D. Decomposing Spectral and Phasic Differences in Nonlinear Features between Datasets. *Phys Rev Lett* 2021; 127(12):124101.
283. Schartner M, Seth A, Noirhomme Q, Boly M, Bruno M-A, Laureys S et al. Complexity of Multi-Dimensional Spontaneous EEG Decreases during Propofol Induced General Anaesthesia. *PLoS One* 2015; 10(8):e0133532.
284. Kora P, Meenakshi K, Swaraja K, Rajani A, Raju MS. EEG based interpretation of human brain activity during yoga and meditation using machine learning: A systematic review. *Complement Ther Clin Pract* 2021; 43:101329.
285. Ahani A, Wahbeh H, Nezamfar H, Miller M, Erdogmus D, Oken B. Quantitative change of EEG and respiration signals during mindfulness meditation. *J Neuroeng Rehabil* 2014; 11:87.

286. Lee Y-H, Hsieh Y-J, Shiah Y-J, Lin Y-H, Chen C-Y, Tyan Y-C et al. A cross-sectional evaluation of meditation experience on electroencephalography data by artificial neural network and support vector machine classifiers. *Medicine (Baltimore)* 2017; 96(16):e6612.
287. Sharma H, Raj R, Juneja M. EEG signal based classification before and after combined Yoga and Sudarshan Kriya. *Neuroscience Letters* 2019; 707:134300.
288. CHANG K-M, LO P-C. Meditation EEG interpretation based on novel fuzzy-merging strategies and wavelet features. *Biomed. Eng. Appl. Basis Commun.* 2005; 17(04):167–75.
289. Jadhav N, Manthalkar R, Joshi Y. Effect of meditation on emotional response: An EEG-based study. *Biomedical Signal Processing and Control* 2017; 34:101–13.
290. Goshvarpour A, Goshvarpour A. Classification of Electroencephalographic Changes in Meditation and Rest: using Correlation Dimension and Wavelet Coefficients. *IJITCS* 2012; 4(3):24–30.
291. Keng S-L, Smoski MJ, Robins CJ. Effects of mindfulness on psychological health: a review of empirical studies. *Clin Psychol Rev* 2011; 31(6):1041–56.
292. Dor-Ziderman Y, Berkovich-Ohana A, Glicksohn J, Goldstein A. Mindfulness-induced selflessness: a MEG neurophenomenological study. *Front Hum Neurosci* 2013; 7:582.

293. Goldsby TL, Goldsby ME, McWalters M, Mills PJ. Effects of Singing Bowl Sound Meditation on Mood, Tension, and Well-being: An Observational Study. *J Evid Based Complementary Altern Med* 2017; 22(3):401–6.
294. Watson D, Clark LA, Tellegen A. Development and validation of brief measures of positive and negative affect: the PANAS scales. *J Pers Soc Psychol* 1988; 54(6):1063–70.
295. Panchal S, Irani F, Trivedi GY. Impact of Himalayan Singing Bowls Meditation Session on Mood and Heart Rate Variability – An Observational Study. *IJPR* 2019; 1(4):20–30.
296. Bergmann M, Riedinger S, Stefani A, Mitterling T, Holzknecht E, Grassmayr P et al. Effects of singing bowl exposure on Karolinska sleepiness scale and pupillographic sleepiness test: A randomised crossover study. *PLoS One* 2020; 15(6):e0233982.
297. Cotoia A, Dibello F, Moscatelli F, Sciusco A, Polito P, Modolo A et al. Effects of Tibetan Music on Neuroendocrine and Autonomic Functions in Patients Waiting for Surgery: A Randomized, Controlled Study. *Anesthesiol Res Pract* 2018; 2018:9683780.
298. Landry JM. Physiological and psychological effects of a Himalayan singing bowl in meditation practice: a quantitative analysis. *Am J Health Promot* 2014; 28(5):306–9.
299. Trivedi GY, Saboo B. A Comparative Study of the Impact of Himalayan Singing Bowls and Supine Silence on Stress Index and Heart Rate Variability. *JBTM* 2018; 2(1):40–50.

300. Wepner F, Hahne J, Teichmann A, Berka-Schmid G, Hördinger A, Friedrich M. Quarzklangschalenterapie bei Wirbelsäulenbeschwerden und chronobiologische Vorgänge - eine randomisierte kontrollierte Studie. *Forsch Komplementmed* 2008; 15(3):130–7.
301. Stanhope J, Weinstein P. The human health effects of singing bowls: A systematic review. *Complement Ther Med* 2020; 51:102412.
302. Menzies V, Taylor AG, Bourguignon C. Effects of guided imagery on outcomes of pain, functional status, and self-efficacy in persons diagnosed with fibromyalgia. *J Altern Complement Med* 2006; 12(1):23–30.
303. Hölzel BK, Ott U. Relationships between meditation depth, absorption, meditation practice, and mindfulness: A latent variable approach. *Journal of Transpersonal Psychology* 2006; (38):179-99.
304. Pluess M. Individual Differences in Environmental Sensitivity. *Child Dev Perspect* 2015; 9(3):138–43.
305. Greven CU, Lionetti F, Booth C, Aron EN, Fox E, Schendan HE et al. Sensory Processing Sensitivity in the context of Environmental Sensitivity: A critical review and development of research agenda. *Neurosci Biobehav Rev* 2019; 98:287–305.
306. Homberg JR, Schubert D, Asan E, Aron EN. Sensory processing sensitivity and serotonin gene variance: Insights into

mechanisms shaping environmental sensitivity. *Neurosci Biobehav Rev* 2016; 71:472–83.

307. Aron EN, Aron A, Jagiellowicz J. Sensory processing sensitivity: a review in the light of the evolution of biological responsiveness. *Pers Soc Psychol Rev* 2012; 16(3):262–82.

308. Smolewska KA, McCabe SB, Woody EZ. A psychometric evaluation of the Highly Sensitive Person Scale: The components of sensory-processing sensitivity and their relation to the BIS/BAS and “Big Five”. *Personality and Individual Differences* 2006; 40(6):1269–79.

309. Lionetti F, Pastore M, Moscardino U, Nocentini A, Pluess K, Pluess M. Sensory Processing Sensitivity and its association with personality traits and affect: A meta-analysis. *Journal of Research in Personality* 2019; 81:138–52.

310. Liss M, Mailloux J, Erchull MJ. The relationships between sensory processing sensitivity, alexithymia, autism, depression, and anxiety. *Personality and Individual Differences* 2008; 45(3):255–9.

311. Sobocko K, Zelenski JM. Trait sensory-processing sensitivity and subjective well-being: Distinctive associations for different aspects of sensitivity. *Personality and Individual Differences* 2015; 83:44–9.

312. Ahadi B, Basharpour S. Relationship Between Sensory Processing Sensitivity, Personality Dimensions and Mental Health. *J. of Applied Sciences* 2010; 10(7):570–4.

313. Pluess M, Assary E, Lionetti F, Lester KJ, Krapohl E, Aron EN et al. Environmental sensitivity in children: Development of the Highly Sensitive Child Scale and identification of sensitivity groups. *Dev Psychol* 2018; 54(1):51–70.
314. Acevedo BP, Aron EN, Aron A, Sangster M-D, Collins N, Brown LL. The highly sensitive brain: an fMRI study of sensory processing sensitivity and response to others' emotions. *Brain Behav* 2014; 4(4):580–94.
315. Acevedo B, Aron E, Pospos S, Jessen D. The functional highly sensitive brain: a review of the brain circuits underlying sensory processing sensitivity and seemingly related disorders. *Philos Trans R Soc Lond B Biol Sci* 2018; 373(1744).
316. Jagiellowicz J, Xu X, Aron A, Aron E, Cao G, Feng T et al. The trait of sensory processing sensitivity and neural responses to changes in visual scenes. *Soc Cogn Affect Neurosci* 2011; 6(1):38–47.
317. Aron A, Ketay S, Hedden T, Aron EN, Rose Markus H, Gabrieli JDE. Temperament trait of sensory processing sensitivity moderates cultural differences in neural response. *Soc Cogn Affect Neurosci* 2010; 5(2-3):219–26.
318. Chen C, Chen C, Moyzis R, Stern H, He Q, Li H et al. Contributions of dopamine-related genes and environmental factors to highly sensitive personality: a multi-step neuronal system-level approach. *PLoS One* 2011; 6(7):e21636.
319. Acevedo BP, Santander T, Marhenke R, Aron A, Aron E. Sensory Processing Sensitivity Predicts Individual Differences

- in Resting-State Functional Connectivity Associated with Depth of Processing. *Neuropsychobiology* 2021; 80(2):185–200.
320. Shriki O, Yellin D. Optimal Information Representation and Criticality in an Adaptive Sensory Recurrent Neuronal Network. *PLoS Comput Biol* 2016; 12(2):e1004698.
321. Yu S, Yang H, Shriki O, Plenz D. Universal organization of resting brain activity at the thermodynamic critical point. *Front Syst Neurosci* 2013; 7:42.
322. Gollo LL. Coexistence of critical sensitivity and subcritical specificity can yield optimal population coding. *J R Soc Interface* 2017; 14(134).
323. Cosmelli D, Lachaux J-P, Thompson E. Neurodynamical Approaches to Consciousness. In: Zelazo PD, Moscovitch M, Thompson E, editors. *The Cambridge Handbook of Consciousness*. Cambridge: Cambridge University Press; 2007. p. 731–72.
324. Werner G. Metastability, criticality and phase transitions in brain and its models. *Biosystems* 2007; 90(2):496–508.
325. James W. *The principles of psychology*. Unabridged and unaltered republ. of the work first publ. ... 1890. New York, NY: Dover-Publ; 1950. (Dover books Dover-books on biology, psychology and medicineT381).
326. Signorelli CM, Szczotka J, Prentner R. Explanatory profiles of models of consciousness - towards a systematic classification. *Neuroscience of Consciousness* 2021; 2021(2):niab021.

327. Freeman WJ. Consciousness, intentionality and causality. *Journal of Consciousness Studies* 1999:143–72.
328. Skarda CA, Freeman WJ. How brains make chaos in order to make sense of the world. *Behav Brain Sci* 1987; 10(2):161–73.
329. Freeman WJ. A field-theoretic approach to understanding scale-free neocortical dynamics. *Biol Cybern* 2005; 92(6):350–9.
330. Freeman WJ. *How Brains Make up Their Minds* London: Weidenfeld & Nicolson; 1999. 190
331. Rudrauf D, Lutz A, Cosmelli D, Lachaux J-P, van Quyen M. From autopoiesis to neurophenomenology: Francisco Varela's exploration of the biophysics of being. *Biol Res* 2003; 36(1):27–65.
332. Varela FJ. Resonant cell assemblies: a new approach to cognitive functions and neuronal synchrony. *Biol Res* 1995; 28(1):81–95.
333. Varela F, Lachaux JP, Rodriguez E, Martinerie J. The brainweb: phase synchronization and large-scale integration. *Nat Rev Neurosci* 2001; 2(4):229–39.
334. Thompson E, Varela FJ. Radical embodiment: neural dynamics and consciousness. *Trends Cogn Sci* 2001; 5(10):418–25.
335. Treisman AM, Gelade G. A feature-integration theory of attention. *Cognitive Psychology* 1980; 12(1):97–136.

336. Malsburg C von der, Schneider W. A neural cocktail-party processor. *Biol Cybern* 1986; 54(1):29–40.
337. Engel AK, Fries P, König P, Brecht M, Singer W. Temporal binding, binocular rivalry, and consciousness. *Conscious Cogn* 1999; 8(2):128–51.
338. Engel AK, Fries P, Singer W. Dynamic predictions: oscillations and synchrony in top-down processing. *Nat Rev Neurosci* 2001; 2(10):704–16.
339. Engel AK, Singer W. Temporal binding and the neural correlates of sensory awareness. *Trends Cogn Sci* 2001; 5(1):16–25.
340. Singer W. Consciousness and the structure of neuronal representations. *Philos Trans R Soc Lond B Biol Sci* 1998; 353(1377):1829–40.
341. Fries P. A mechanism for cognitive dynamics: neuronal communication through neuronal coherence. *Trends Cogn Sci* 2005; 9(10):474–80.
342. Chalmers DJ. What is a neural correlate of consciousness? In: Metzinger T, editor. *Neural correlates of consciousness: Empirical and conceptual questions*. MIT Press; 2000. p. 17–39.
343. Eckhorn R, Bauer R, Jordan W, Brosch M, Kruse W, Munk M et al. Coherent oscillations: a mechanism of feature linking in the visual cortex? Multiple electrode and correlation analyses in the cat. *Biol Cybern* 1988; 60(2):121–30.

344. Landau AN, Esterman M, Robertson LC, Bentin S, Prinzmetal W. Different effects of voluntary and involuntary attention on EEG activity in the gamma band. *J. Neurosci.* 2007; 27(44):11986–90.
345. Sokolov A, Pavlova M, Lutzenberger W, Birbaumer N. Reciprocal modulation of neuromagnetic induced gamma activity by attention in the human visual and auditory cortex. *Neuroimage* 2004; 22(2):521–9.
346. Brovelli A, Lachaux J-P, Kahane P, Boussaoud D. High gamma frequency oscillatory activity dissociates attention from intention in the human premotor cortex. *Neuroimage* 2005; 28(1):154–64.
347. Buhl DL, Buzsáki G. Developmental emergence of hippocampal fast-field "ripple" oscillations in the behaving rat pups. *Neuroscience* 2005; 134(4):1423–30.
348. Jensen O, Kaiser J, Lachaux J-P. Human gamma-frequency oscillations associated with attention and memory. *Trends Neurosci* 2007; 30(7):317–24.
349. Weinberger NM, Miasnikov AA, Chen JC. The level of cholinergic nucleus basalis activation controls the specificity of auditory associative memory. *Neurobiol Learn Mem* 2006; 86(3):270–85.
350. Wespapat V, Tennigkeit F, Singer W. Phase sensitivity of synaptic modifications in oscillating cells of rat visual cortex. *J. Neurosci.* 2004; 24(41):9067–75.

351. Salinas E, Sejnowski TJ. Correlated neuronal activity and the flow of neural information. *Nat Rev Neurosci* 2001; 2(8):539–50.
352. Sewards TV, Sewards MA. On the correlation between synchronized oscillatory activities and consciousness. *Conscious Cogn* 2001; 10(4):485–95.
353. Rubino D, Robbins KA, Hatsopoulos NG. Propagating waves mediate information transfer in the motor cortex. *Nat Neurosci* 2006; 9(12):1549–57.
354. Takahashi K, Saleh M, Penn RD, Hatsopoulos NG. Propagating waves in human motor cortex. *Front Hum Neurosci* 2011; 5:40.
355. Freeman WJ. The wave packet: an action potential for the 21st century. *J Integr Neurosci* 2003; 2(1):3–30. 192
356. Abeles M. *Corticonics: Neural circuits of the cerebral cortex*. Cambridge: Cambridge Univ. Press; 1991. Available from: URL: <http://www.loc.gov/catdir/description/cam024/90002035.html>.
357. Yu S, Klaus A, Yang H, Plenz D. Scale-invariant neuronal avalanche dynamics and the cut-off in size distributions. *PLoS One* 2014; 9(6):e99761.
358. Yu S, Yang H, Nakahara H, Santos GS, Nikolić D, Plenz D. Higher-order interactions characterized in cortical activity. *J. Neurosci.* 2011; 31(48):17514–26.
359. Penny WD, Duzel E, Miller KJ, Ojemann JG. Testing for nested oscillation. *J Neurosci Methods* 2008; 174(1):50–61.

360. Lombardi F, Herrmann HJ, Perrone-Capano C, Plenz D, Arcangelis L de. Balance between excitation and inhibition controls the temporal organization of neuronal avalanches. *Phys Rev Lett* 2012; 108(22):228703.
361. Levina A, Herrmann JM, Geisel T. Dynamical synapses causing self-organized criticality in neural networks. *Nature Phys* 2007; 3(12):857–60.
362. Millman D, Mihalas S, Kirkwood A, Niebur E. Self-organized criticality occurs in non-conservative neuronal networks during Up states. *Nature Phys* 2010; 6(10):801–5.
363. Lombardi F, Herrmann HJ, Plenz D, Arcangelis Ld. On the temporal organization of neuronal avalanches. *Front Syst Neurosci* 2014; 8:204.
364. Timofeev I, Grenier F, Bazhenov M, Sejnowski TJ, Steriade M. Origin of slow cortical oscillations in deafferented cortical slabs. *Cereb Cortex* 2000; 10(12):1185–99.
365. Lombardi F, Herrmann HJ, Arcangelis L de. Balance of excitation and inhibition determines 1/f power spectrum in neuronal networks. *Chaos* 2017; 27(4):47402.
366. Yang H, Shew WL, Roy R, Plenz D. Maximal variability of phase synchrony in cortical networks with neuronal avalanches. *J. Neurosci.* 2012; 32(3):1061–72.
367. Kitzbichler MG, Smith ML, Christensen SR, Bullmore E. Broadband criticality of human brain network synchronization. *PLoS Comput Biol* 2009; 5(3):e1000314.

368. Miller SR, Yu S, Plenz D. The scale-invariant, temporal profile of neuronal avalanches in relation to cortical γ -oscillations. *Sci Rep* 2019; 9(1):16403.
369. Plenz D, Thiagarajan TC. The organizing principles of neuronal avalanches: cell assemblies in the cortex? *Trends Neurosci* 2007; 30(3):101–10.
370. Kelso JAS, Haken H. *Dynamic patterns: The self-organization of brain and behavior*. Cambridge, Massachusetts, London, England: MIT Press; 1995. (A Bradford book).
371. Kelso JAS, Tognoli E. Toward a Complementary Neuroscience: Metastable Coordination Dynamics of the Brain. In: Perlovsky LI, Kozma R, editors. *Neurodynamics of Cognition and Consciousness*. Berlin, Heidelberg: Springer Berlin Heidelberg; 2007. p. 39–59 (Understanding Complex Systems).
372. Bressler SL, Kelso J. Cortical coordination dynamics and cognition. *Trends Cogn Sci* 2001; 5(1):26–36.
373. Fingelkurts AA, Fingelkurts AA. Operational architectonics of the human brain biopotential field: Towards solving the mind-brain Problem. *Brain and Mind* 2001; 2(3):261–96.
374. Fingelkurts AA, Fingelkurts AA. Making complexity simpler: multivariability and metastability in the brain. *Int J Neurosci* 2004; 114(7):843–62.
375. Lehmann D, Strik W, Henggeler B, Koenig T, Koukkou M. Brain electric microstates and momentary conscious mind states as building blocks of spontaneous thinking: I. Visual

imagery and abstract thoughts. *International Journal of Psychophysiology* 1998; 29(1):1–11.

376. Lehmann D, Faber PL, Gianotti LRR, Kochi K, Pascual-Marqui RD. Coherence and phase locking in the scalp EEG and between LORETA model sources, and microstates as putative mechanisms of brain temporo-spatial functional organization. *J Physiol Paris* 2006; 99(1):29–36.

377. Sporns O, Tononi G, Edelman G. Connectivity and complexity: the relationship between neuroanatomy and brain dynamics. *Neural Networks* 2000; 13(8-9):909–22.

378. Michel M, Fleming SM, Lau H, Lee ALF, Martinez-Conde S, Passingham RE et al. An Informal Internet Survey on the Current State of Consciousness Science. *Front Psychol* 2018; 9:2134.

379. Baars BJ. *In the Theater of Consciousness*. Oxford University Press; 1997.

380. Baars BJ. The conscious access hypothesis: origins and recent evidence. *Trends Cogn Sci* 2002; 6(1):47–52.

381. Baars BJ. *A cognitive theory of consciousness*. 1. paperback ed. Cambridge: Cambridge Univ. Press; 1993. 194

382. Dehaene S. Towards a cognitive neuroscience of consciousness: basic evidence and a workspace framework. *Cognition* 2001; 79(1-2):1–37.

383. Dehaene S, Changeux J-P. Experimental and theoretical approaches to conscious processing. *Neuron* 2011; 70(2):200–27.

384. Edelman GM, Tononi G. A universe of consciousness: How matter becomes imagination. 1. paperback ed., [Nachdr.]. New York, NY: Basic Books; 2001.
385. Mashour GA, Roelfsema P, Changeux J-P, Dehaene S. Conscious Processing and the Global Neuronal Workspace Hypothesis. *Neuron* 2020; 105(5):776–98.
386. Dehaene S, Changeux J-P. Ongoing spontaneous activity controls access to consciousness: a neuronal model for inattentional blindness. *PLoS Biol* 2005; 3(5):e141.
387. Kitzbichler MG, Henson RNA, Smith ML, Nathan PJ, Bullmore ET. Cognitive effort drives workspace configuration of human brain functional networks. *J. Neurosci.* 2011; 31(22):8259–70.
388. Werner G. Brain dynamics across levels of organization. *J Physiol Paris* 2007; 101(4-6):273–9.
389. Werner G. Consciousness related neural events viewed as brain state space transitions. *Cogn Neurodyn* 2009; 3(1):83–95.
390. Krauss P, Maier A. Will We Ever Have Conscious Machines? *Front Comput Neurosci* 2020; 14:556544.
391. Dehaene S, Changeux J-P, Naccache L, Sackur J, Sergent C. Conscious, preconscious, and subliminal processing: a testable taxonomy. *Trends Cogn Sci* 2006; 10(5):204–11.
392. Kleiner J, Hoel E. Falsification and consciousness. *Neuroscience of Consciousness* 2021; 2021(1):niab001.

393. Tononi G, Koch C. Consciousness: here, there and everywhere? *Philos Trans R Soc Lond B Biol Sci* 2015; 370(1668).
394. Kleiner J, Tull S. The Mathematical Structure of Integrated Information Theory. *Front. Appl. Math. Stat.* 2021; 6.
395. Barrett AB, Mediano PAM. The Phi measure of integrated information is not well-defined for general physical systems. *Journal of Consciousness Studies*. Available from: URL: <http://arxiv.org/pdf/1902.04321v1>.
396. Cerullo MA. The Problem with Phi: A Critique of Integrated Information Theory. *PLoS Comput Biol* 2015; 11(9):e1004286.
397. Tononi G. Integrated information theory of consciousness: an updated account. *Arch Ital Biol* 2012; 150(2-3):56–90.
398. Reardon S. Rival theories face off over brain's source of consciousness. *Science* 2019; 366(6463):293.
399. Kim, Lee. Criticality as a Determinant of Integrated Information Φ in Human Brain Networks. *Entropy* 2019; 21(10):981.
400. Yoon S, Sorbaro Sindaci M, Goltsev AV, Mendes JFF. Critical behavior of the relaxation rate, the susceptibility, and a pair correlation function in the Kuramoto model on scale-free networks. *Phys Rev E Stat Nonlin Soft Matter Phys* 2015; 91(3).
401. Kitazono J, Kanai R, Oizumi M. Efficient Algorithms for Searching the Minimum Information Partition in Integrated Information Theory. *Entropy (Basel)* 2018; 20(3).

402. Blain-Moraes S, Tarnal V, Vanini G, Alexander A, Rosen D, Shortal B et al. Neurophysiological Correlates of Sevoflurane-induced Unconsciousness. *Anesthesiology* 2015; 122(2):307–16.
403. Popiel NJM, Khajehabdollahi S, Abeyasinghe PM, Riganello F, Nichols ES, Owen AM et al. The Emergence of Integrated Information, Complexity, and 'Consciousness' at Criticality. *Entropy (Basel)* 2020; 22(3).
404. Greenberg JM, Hastings SP. Spatial Patterns for Discrete Models of Diffusion in Excitable Media. *SIAM J. Appl. Math.* 1978; 34(3):515–23.
405. Lempel A, Ziv J. On the Complexity of Finite Sequences. *IEEE Trans. Inform. Theory* 1976; 22(1):75–81.
406. Barrett AB, Seth AK. Practical measures of integrated information for time-series data. *PLoS Comput Biol* 2011; 7(1):e1001052.
407. Clauset A, Shalizi CR, Newman MEJ. Power-law distributions in empirical data. *SIAM Rev.* 2009; 51(4):661–703. Available from: URL: <http://arxiv.org/pdf/0706.1062v2>.
408. Wilting J, Priesemann V. 25 years of criticality in neuroscience - established results, open controversies, novel concepts. *Curr Opin Neurobiol* 2019; 58:105–11. 196
409. Destexhe A, Touboul JD. Is There Sufficient Evidence for Criticality in Cortical Systems? *eNeuro* 2021; 8(2).
410. Reed WJ, Hughes BD. From gene families and genera to incomes and internet file sizes: why power laws are so common

in nature. *Phys Rev E Stat Nonlin Soft Matter Phys* 2002; 66(6 Pt 2):67103.

411. Gisiger T. Scale invariance in biology: coincidence or footprint of a universal mechanism? *Biol Rev Camb Philos Soc* 2001; 76(2):161–209.

412. Stumpf MPH, Porter MA. Mathematics. Critical truths about power laws. *Science* 2012; 335(6069):665–6.

413. Willinger W, Alderson D, Doyle JC, Li L. More "Normal" Than Normal: Scaling Distributions and Complex Systems. In: *Proceedings of the 2004 Winter Simulation Conference, 2004*. IEEE; 2004. p. 124–35.

414. Mitzenmacher M. A Brief History of Generative Models for Power Law and Lognormal Distributions. *Internet Mathematics* 2004; 1(2):226–51.

415. Faqeeh A, Osat S, Radicchi F, Gleeson JP. Emergence of power laws in noncritical neuronal systems. *Phys Rev E* 2019; 100(1-1):10401.

416. Touboul J, Destexhe A. Power-law statistics and universal scaling in the absence of criticality. *Phys Rev E* 2017; 95(1-1):12413.

417. Friedman EJ, Landsberg AS. Hierarchical networks, power laws, and neuronal avalanches. *Chaos* 2013; 23(1):13135.

418. Martinello M, Hidalgo J, Maritan A, Di Santo S, Plenz D, Muñoz MA. Neutral Theory and Scale-Free Neural Dynamics. *Phys. Rev. X* 2017; 7(4).

419. Touboul J, Destexhe A. Can power-law scaling and neuronal avalanches arise from stochastic dynamics? *PLoS One* 2010; 5(2):e8982.
420. Fontenele AJ, Vasconcelos NAP de, Feliciano T, Aguiar LAA, Soares-Cunha C, Coimbra B et al. Criticality between Cortical States. *Phys Rev Lett* 2019; 122(20):208101.
421. Brunel N. Dynamics of sparsely connected networks of excitatory and inhibitory spiking neurons. *J Comput Neurosci* 2000; 8(3):183–208.
422. Acebrón JA, Bonilla LL, Pérez Vicente CJ, Ritort F, Spigler R. The Kuramoto model: A simple paradigm for synchronization phenomena. *Rev. Mod. Phys.* 2005; 77(1):137–85. 197
423. Kuramoto Y. Self-entrainment of a population of coupled non-linear oscillators. In: Araki H, editor. *International Symposium on Mathematical Problems in Theoretical Physics*. Berlin/Heidelberg: Springer-Verlag; 1975. p. 420–2 (Lecture Notes in Physics).
424. Attanasi A, Cavagna A, Del Castello L, Giardina I, Melillo S, Parisi L et al. Finite-size scaling as a way to probe near-criticality in natural swarms. *Phys Rev Lett* 2014; 113(23):238102.
425. Chialvo DR, Cannas SA, Grigera TS, Martin DA, Plenz D. Controlling a complex system near its critical point via temporal correlations. *Sci Rep* 2020; 10(1):12145.
426. Perez Velazquez JL, Cortez MA, Snead O, Wennberg R. Dynamical regimes underlying epileptiform events: role of

- instabilities and bifurcations in brain activity. *Physica D: Nonlinear Phenomena* 2003; 186(3-4):205–20.
427. Paczuski, Maslov, Bak. Avalanche dynamics in evolution, growth, and depinning models. *Phys Rev E Stat Phys Plasmas Fluids Relat Interdiscip Topics* 1996; 53(1):414–43.
428. Zeraati R, Priesemann V, Levina A. Self-organization toward criticality by synaptic plasticity. *Front. Phys.* 2021; 9:364. Available from: URL: <http://arxiv.org/pdf/2010.07888v1>.
429. Li J, Shew WL. Tuning network dynamics from criticality to an asynchronous state. *PLoS Comput Biol* 2020; 16(9):e1008268.
430. Girardi-Schappo M, Brochini L, Costa AA, Carvalho TTA, Kinouchi O. Synaptic balance due to homeostatically self-organized quasicritical dynamics. *Phys. Rev. Research* 2020; 2(1).
431. Stepp N, Plenz D, Srinivasa N. Synaptic plasticity enables adaptive self-tuning critical networks. *PLoS Comput Biol* 2015; 11(1):e1004043.
432. Rubinov M, Sporns O, Thivierge J-P, Breakspear M. Neurobiologically realistic determinants of self-organized criticality in networks of spiking neurons. *PLoS Comput Biol* 2011; 7(6):e1002038.
433. Zierenberg J, Wilting J, Priesemann V. Homeostatic Plasticity and External Input Shape Neural Network Dynamics. *Phys. Rev. X* 2018; 8(3).

434. Ma Z, Turrigiano GG, Wessel R, Hengen KB. Cortical Circuit Dynamics Are Homeostatically Tuned to Criticality In Vivo. *Neuron* 2019; 104(4):655-664.e4.
435. Naudé J, Cessac B, Berry H, Delord B. Effects of cellular homeostatic intrinsic plasticity on dynamical and computational properties of biological recurrent neural networks. *J. Neurosci.* 2013; 33(38):15032–43.
436. Chialvo DR. Emergent complex neural dynamics. *Nature Phys* 2010; 6(10):744–50.
437. Chialvo DR. The brain near the edge. In: Marro J, Garrido PL, Torres JJ, editors. Cooperative behavior in neural systems:ninth Granada lectures. Maryland, USA: American Institute of Physics; 2007.
438. Fingelkurts AA, Fingelkurts AA, Neves CF. Consciousness as a phenomenon in the operational architectonics of brain organization: Criticality and self-organization considerations. *Chaos, Solitons & Fractals* 2013; 55:13–31.
439. van Lommel P. Non-local Consciousness:A Concept Based on Scientific Research on Near-Death Experiences During Cardiac Arrest. *Journal of Consciousness Studies* 2013; (20(1-2)):1–2.
440. Goff P. Galileo's Error: Foundations for a New Science of Consciousness. New York, USA: Vintage; 2020.
441. James W. Human Immortality. Boston, USA: Houghton Mifflin; 1898.
442. Seth AK. The grand challenge of consciousness. *Front Psychol* 2010; 1:5.
443. Keppler J, Shani I. Cosmopsychism and Consciousness Research: A Fresh View on the Causal Mechanisms Underlying Phenomenal States. *Front Psychol* 2020; 11:371.
444. Searle JR. Consciousness. *Annu Rev Neurosci* 2000; 23:557–78.

9. List of acronyms, figures, and tables

Abbreviation	Description
AD	Alzheimer's disease
AES	Aesthetic sensitivity
ANN	Artificial neural network
ASC	Altered state of consciousness
AUC	Area under the curve
BIS	Bispectral index
Cl	Left central
Cr	Right central
Cz	Central
DFA	Detrended fluctuation analysis
EEG	Electroencephalography
E/I	Excitation/inhibition
EOE	Ease of excitation
FDR	False discovery rate
FFT	Fast Fourier transform
fMRI	Functional neuroimaging
Fl	Left frontal
Fr	Right frontal
Fz	Frontal
GWT	Global Workspace Theory
HFD	Higuchi's fractal dimension
HSPS	High sensitive person scale
IIT	Information Integration Theory

LFP	Local field potential
LRTC	Longe-range temporal correlateion
LST	Low sensory threshold
MDD	Major depressive disorder
MEG	Magnetoencephalography
MSE	Multiscale entropy
NCC	Neural correlates of consciousness
NREM	Non-rapid eye movement
O	Occipital
REM	Rapid eye movement
PCF	Pair correlation function
PCI	Phenomenology of Consciousness Inventory
Pf	Prefrontal
Pl	Left parietal
Pr	Right parietal
PSD	Power spectral density
Pz	Parietal
ROC	Receiver operating characteristic
SE	Sample entropy
SF	Scale factor
SOC	Self-organized criticality
SVM	Support vector machine
TAS	Tellegen Absorption Scale
Tl	Left temporal
Tr	Right temporal

Figure 1: Neuroscientific approach to measure altered states of consciousness. To associate phenomenological changes to underlying neuronal mechanisms, ASCs can be induced experimentally. For this, besides substance-based approaches, a variety of non-pharmacological induction methods such as breathing techniques, meditation practices or sensory deprivation can be utilized. By investigating phenomenological states and electrophysiological patterns simultaneously, subjective experience can be mapped onto brain functions. Comparisons across studies capturing a broad range of ASC experiences may lead to the identification of common structures shared by differently induced ASCs. Modified from [54].20

Figure 2: Numerical visualization of the Lorenz attractor as example of a three-dimensional nonlinear dynamical systems which shows chaotic behaviour with the parameters $p = 28$, $\sigma = 10$, $b = 83$. Modified from [85].30

Figure 3: Coordinated system dynamics. (A) Multistable systems can switch between attractors. As the system is briefly dwelling in each attractor basin, time series are characterized by long-tailed distributions (here shown on a logarithmic scale). (B) Metastable systems do not have attractors, rather a sequence of unstable fixed points and time series are associated with gamma distributions (here shown in linear coordinates). Modified from [92].32

Figure 4: Examples of geometrically self-similar fractals. (A) The Mandelbrot set. (A) the curve and (B) the snowflake

described by Niels F.H. von Koch. (C) shows the Sierpinski triangle. Modified from [93].....34

Figure 5: Examples of noise processes. (A) white noise, (B) pink noise, (C) Brownian noise. Adapted from [98].....36

Figure 6: Simulated time series to illustrate the procedure of calculation the sample entropy for the case $m = 2$ and a given positive real value r [130].....47

Figure 7: Schematic illustration of the coarse-gaining procedure. Adapted from [130].....49

Figure 8: MSE analysis of simulated white and $1/f$ noise time series. The value of the sample entropy is plotted against the scale factor, which specifies the number of data points averaged to obtain each element of the coarse-grained time series [130].50

Figure 9: (A) Diagram of the spins in the Ising model in an ordered state at low temperature, a complex state at critical temperature and a disordered state at high temperature, adapted from [150]. (B) Simulation of a 2D Ising model with length = 256 in subcritical, critical and supercritical states as temperatures increases from left to right panels. Black areas reflect a spin pointed up and white square represent spins down, adapted from [148]. (C) modified from [151].57

Figure 10: A binary cellular automaton represents an n -dimensional array of binary cells. The states are update synchronously in discrete time steps, whereby each state $t+1$ depends on the state of the cells at time t . Langton (1990)

identified different classes corresponding to different dynamical regimes characterized by the ratio of transitions to an arbitrary state selected as the “quiescent state” (parameter λ). Class IV depicts a transitional state analogous to complex behavior arising in the critical regime. Taken from Heiney et al (2021), adapted from Langton (1990) [149, 158].....59

Figure 11: Schematic illustration of the branching ratio. Adapted from [149] and [181]. Blue nodes represent active ones and gray nodes are inactive. The middle regime of $\sigma= 1$ corresponds to the critical state, in which activity is self-sustained. The case of $\sigma < 1$ corresponds to a subcritical state in which activity will die out over time. A supercritical state is indicated by a $\sigma > 1$, in which activity will increase with time.67

Figure 12: Stepwise explanation of the detrended fluctuation analysis. (A) shows an original time series taken from a 1/f signal sampled at 5 Hz with a duration of 100 s. (B) The cumulative sum of the time series. (C) Removal of the linear trend from the signal for each time window. (D) Plot of the mean fluctuation per window size against window size on a logarithmic scale. In this example the scaling exponent is $\alpha=1$, estimated as the slope of the best fit line. Adapted from [199].71

Figure 13: (A) Schematic illustration of the event identification process. Adapted from [175]. (B) Avalanche definition. Neuronal avalanches are defined as a contiguous sequence of time bins of activity preceded, ending with at least one time bin

of quiescence. Modified from [202]. (C) Probability distribution of the relationship between size and likelihood of avalanches shown in double logarithmic coordinates. At criticality a scale-free process yields a power law relationship with a critical exponent of $-3/2$. Adapted from [92].73

Figure 14: Shape collapse procedure [149]. First, raw avalanche shapes are determined by averaging the profile of all avalanches with a given duration. Then, the avalanches are scaled to a uniform length and finally, the scaling parameter is estimated by using a quadratic polynomial. Adapted from [201].75

Figure 15: Illustration of long-range temporal correlations (LRTC) as a function of criticality in different conditions. Adapted from [231] and [148]. The grey area represents the physiological range of brain dynamics. Black arrays show the deviations towards a subcritical regime (left) or a supercritical regime (right) according to findings in the literature [148]. Double arrays imply contradictory evidence for both increases and decreases in LRTC.....81

Figure 16: Experimental procedure. Modified from [232].91

Figure 17: Scheme of the analysis workflow. PSD= power spectral density, DFA= detrended fluctuation analysis, HFD= Higuchi's fractal dimension, MSE= multiscale entropy, SE= sample entropy, sf=scale factor.....97

Figure 18: Reduction scheme into 13 major topographic regions. Adapted from [232].98

Figure 19: Experimental procedure.....105

Figure 20: Topographical maps of chi-square values resulting from the Kruskal-Wallis test over all conditions for the complexity and criticality features.115

Figure 21: Topographical maps of chi-square values resulting from the Kruskal-Wallis test over all conditions for the spectral bands.....115

Figure 22: Color-coded differences of complexity parameters shown as effect sizes (Cohen's d) of the meditation task comparisons on a global level averaged over all electrodes. Fields marked with a white circle were significant on the 0.05 level after FDR adjustment.....119

Figure 23: Color-coded differences of power spectral density shown as effect sizes (Cohen's d) of the task comparisons on a global level averaged over all electrodes. Fields marked with a white circle were significant on the 0.01 level after FDR adjustment over conditions and frequency bands.119

Figure 24: Color-coded feature differences shown as effect sizes (Cohen's d) resulting from the task comparisons. (A) Comparison between eyes open and eyes closed, (B) reading vs. eyes open, (C) presence vs. eyes closed, (D) emptiness vs eyes closed, (E) focused attention vs. eyes closed, (F) emptiness vs. presence, (G) emptiness vs focused attention, (H) focused attention vs. presence. T-tests were calculated from each participant for each location and complexity

parameter. Fields marked with a white circle were significant on the 0.05 level after FDR adjustment.129

Figure 25: Color-coded power spectral density differences shown as effect sizes (Cohen's d) resulting from the task comparisons. (A) Comparison between eyes open and eyes closed, (B) reading vs. eyes open, (C) presence vs. eyes closed, (D) emptiness vs eyes closed, (E) focused attention vs. eyes closed, (F) emptiness vs. presence, (G) emptiness vs focused attention, (H) focused attention vs. presence. T-tests were calculated from each participant for each location and complexity parameter. Fields marked with a white circle were significant on the 0.05 level after FDR adjustment.131

Figure 26: Topographical maps of differences in the effect sizes calculated for each complexity and criticality feature, respectively. (A) Comparison between eyes open and eyes closed, (B) reading vs. eyes open, (C) presence vs. eyes closed, (D) emptiness vs eyes closed, (E) focused attention vs. eyes closed, (F) emptiness vs. presence, (G) emptiness vs focused attention, (H) focused attention vs. presence.....134

Figure 27: Topographical maps of differences in the effect sizes calculated for each frequency band, respectively. (A) Comparison between eyes open and eyes closed, (B) reading vs. eyes open, (C) presence vs. eyes closed, (D) emptiness vs eyes closed, (E) focused attention vs. eyes closed, (F) emptiness vs. presence, (G) emptiness vs focused attention, (H) focused attention vs. presence.137

Figure 28: Resulting sample entropy (SE) values for the distinct scale factors (sf) are shown for each condition (A-F).140

Figure 29: (A) Resulting Higuchi fractal dimension (HFD) values are shown for each condition. (B) Values from exponent resulting from detrended fluctuation analysis (DFA) are illustrated. (C) The critical exponents obtained from the neuronal avalanches analysis are shown for each condition. The hypothetical value is illustrated by the dark green dotted line. (D) SNZdiff depicts the difference between the critical exponent resulting from the neuronal avalanches analysis and the scaling parameter obtained from the shape collapse function for each condition, respectively. The hypothetical value is illustrated by the dark green dotted line.....141

Figure 30: Power spectral density for each frequency band and condition, respectively. (A) shows the delta band, (B) the theta band, (C) alpha 1, (D) alpha 2, (E) beta 1, (F) beta 2, (G) the gamma band and (H) results on a global level.....143

Figure 31: Color-coded differences of complexity and criticality features shown as effect sizes (Cohen's d) of the comparisons between the phases of the experiment on a global level averaged over all electrodes. Fields marked with a black circle were significant on the 0.05 level after FDR adjustment.....159

Figure 32: Color-coded differences of power spectral density shown as effect sizes (Cohen's d) of the task comparisons on a global level averaged over all electrodes. Fields marked with a

black circle were significant on the 0.05 level after FDR adjustment over conditions and frequency bands.159

Figure 33: Color-coded complexity and criticality feature differences shown as effect sizes (Cohen's d) resulting from the task comparisons (A-C). T-tests were calculated from each participant for each location and complexity parameter. Fields marked with a white circle were significant on the 0.05 level after FDR adjustment.163

Figure 34: Color-coded power spectral density differences shown as effect sizes (Cohen's d) resulting from the task comparisons (A-C). T-tests were calculated from each participant for each location and frequency band. Fields marked with a white circle were significant on the 0.05 level after FDR adjustment.164

Figure 35: Topographical maps of differences in the effect sizes calculated for each complexity and criticality feature, respectively. (A) Comparison between sound vs. resting, (B) postresting vs. sound, (C) postresting vs. resting.....165

Figure 36: Topographical maps of differences in the effect sizes calculated for each frequency band, respectively. (A) Comparison between sound vs. resting, (B) postresting vs. sound, (C) postresting vs. resting.166

Figure 37: Resulting sample entropy (SE) values for the distinct scale factors (sf) are shown for each phase of the course of experiment (A-F).....169

Figure 38: (A) Resulting Higuchi fractal dimension (HFD) values are shown for each condition. (B) Values from exponent resulting from detrended fluctuation analysis (DFA) are illustrated. (C) The critical exponents obtained from the neuronal avalanches are shown for each phase of the course of experiment. The hypothetical value is illustrated by the dark green dotted line (D) SNZdiff depicts the difference between the critical exponent resulting from the neuronal avalanches analysis and the scaling parameter obtained from the shape collapse function for each condition, respectively. The hypothetical value is illustrated by the dark green dotted line170

Figure 39: Power spectral density for each frequency band and condition, respectively. (A) shows the delta band, (B) the theta band, (C) alpha 1, (D) alpha 2, (E) beta 1, (F) beta 2, (G) the gamma band and (H) results on a global level.....172

Figure 40: Results of the CSP-14 shown as percentages ...177

Figure 41: Results of the PCI-K shown as mean \pm SD for each dimension.178

Figure 42: Spearman correlations of the TAS scores with the EEG features calculated from the mean of the time series of the first resting state averaged across participants.179

Figure 43: Spearman correlations of the TAS scores with the EEG features calculated from the mean of the time series of the second resting state averaged across participants.....179

Figure 44: Comparison of power spectral density for each frequency band during resting with eyes closed between the highly sensitive and the not sensitive group. (A) shows the delta and the theta band, (B) alpha 1 and alpha 2, (C) beta 1 and beta 2 (D) the gamma band and results on a global level. *HS= highly sensitive, NS= not sensitive, n.s.= not significant.....184

Figure 45: Comparison of complexity and criticality EEG features during resting with eyes closed between the highly sensitive and the not sensitive group. (A) shows the results of the multiscale entropy, (B) HFD (C) scaling exponent resulting from the DFA (D) the critical exponent SNZ and the distance to the critical point (SNZdiff). *HS= highly sensitive, NS= not sensitive, n.s.= not significant.....185

Figure 46: The global workspace theory. (A) Reproduced from [390], (B) reproduced from [391].....232

Figure 47: Consciousness as a function of (A) regularity and complexity and (B) self-organized criticality. Adapted from [151].235

Figure 48: Schematic representation of one strategy for estimating temporal complexity as utilized in this work. Patterns of neuronal activity are directly extracted from the time series by applying methods such as signal binarization. Then, the degree of complexity and characteristics of neuronal avalanches are estimated based on the extracted temporal patterns. Reproduced from [7].244

Table 1: EEG spectral bands.....	27
Table 2: Chi-Square values for each complexity, criticality and spectral feature resulting from the Kruskal-Wallis-Test calculated over all conditions. **p<.001, *p<.01	113
Table 3: Chi-Square values for each complexity, criticality and spectral feature resulting from the Kruskal-Wallis-Test calculated over the three meditation conditions.	114
Table 4: Values of the effect size and p-values resulting from the comparison between conditions. All p-values were corrected for multiple comparison.....	120
Table 5: Values of the effect size and p-values resulting from the comparison between conditions. All p-values were corrected for multiple comparison.....	121
Table 6: Spearman correlations of complexity and spectral parameter from the mean of the time series of the condition eyes open across participants after averaging over channels; n=30. **p<0.001, *p<0.01	145
Table 7: Spearman correlations of complexity and spectral parameter from the mean of the time series of the condition eyes closed across participants after averaging over channels; n=30. **p<0.001, *p<0.01	146
Table 8: Spearman correlations of complexity and spectral parameter from the mean of the time series of the reading condition across participants after averaging over channels; n=30. **p<0.001, *p<0.01	147

Table 9: Spearman correlations of complexity and spectral parameter from the mean of the time series of the presence meditation condition across participants after averaging over channels; n=30. **p<0.001, *p<0.01	148
Table 10: Spearman correlations of complexity and spectral parameter from the mean of the time series of the emptiness meditation condition across participants after averaging over channels; n=30. **p<0.001, *p<0.01	149
Table 11: Spearman correlations of complexity and spectral parameter from the mean of the time series of the focused attention meditation condition across participants after averaging over channels; n=30. **p<0.001, *p<0.01	150
Table 12: Accuracy of classification of the frequency bands determined by partial least square regression and ROC analysis.	152
Table 13: Accuracy of the complexity and criticality features in classification determined by partial least square regression and ROC analysis.....	153
Table 14: Values of the area under the curve (AUC) for ROC analysis for the frequency bands.....	154
Table 15: Values of the area under the curve (AUC) for ROC analysis for the complexity parameter.	155
Table 16: Chi-Square values for each complexity, criticality and spectral features resulting from the Kruskal-Wallis-Test.....	156
Table 17: Values of the effect size and p-values resulting from the comparison of complexity and criticality features between	

the three phases of the experiment. All p-values were corrected for multiple comparison.	160
Table 18: Values of the effect size and p-values resulting from the comparison of frequency band power between the three phases of the experiment. All p-values were corrected for multiple comparison.	161
Table 19: Spearman correlations of complexity and spectral parameter from the mean of the time series of the first resting state across participants after averaging over channels; n=30. **p<0.001, *p<0.01.....	173
Table 20: Spearman correlations of complexity and spectral parameter from the mean of the time series of singing bowl massage condition across participants after averaging over channels; n=30. **p<0.001, *p<0.01	174
Table 21: Spearman correlations of complexity and spectral parameter from the mean of the time series of the second resting state across participants after averaging over channels; n=30. **p<0.001, *p<0.01	175
Table 22: Spearman correlations of complexity, criticality, and spectral parameter from the mean of the time series of the eyes closed resting state across participants after averaging over channels; n=116. *p<0.05.	181

Danksagung

Mein größter Dank gilt meinem Doktorvater, Herrn Prof. Dr. rer. nat. Thilo Hinterberger, für die Annahme des komplexen Themas, die ausgezeichnete Betreuung und die enorme Unterstützung bei der Umsetzung der gesamten Arbeit inklusive der Bereitstellung von EEG-Daten und MATLAB-Skripten. Darüber hinaus danke ich für die stetige Bereitschaft, mir bei Fragen oder Problemen jeglicher Art mit fachlicher Expertise Hilfestellung zu geben, sowie die Bestärkung meiner Begeisterung für die Bewusstseinsforschung und die Verbindung von Wissenschaft und Spiritualität.

Ebenso danke ich Herrn Prof. Dr. med. Thomas Loew für die fortwährende Förderung dieser Arbeit, sowie für die Möglichkeit meine wissenschaftlichen, als auch medizinischen Qualifikationen vielfältig zu erweitern. Bei dieser Gelegenheit möchte ich mich auch bei Herrn Prof. Dr. phil. Stefan Schmidt bedanken für die Mentorenschaft.

Auch möchte ich Frau Dr. Christina Koller und dem internationalen Fachverband für Klang-Massage-Therapie e.V. meinen Dank aussprechen für den Beitrag bei der Durchführung der Klangschalenstudie.

Für die kollegiale Zusammenarbeit an der Hochsensibilitätsstudie danke ich Nicole-Meinersen Schmidt und dem Institut für Psychologie der Universität der Bundeswehr, München.

Außerdem möchte ich mich bei Herrn Dr. Ralf Girg bedanken, der mich in dem Forschungsprozess mit wertvollen Gesprächen begleitet hat, sowie Frau Sonja Zimmermann für den inspirierenden Austausch.

Mein tiefster Dank gebührt meiner Familie und meinem Partner für all die Liebe und das Verständnis, den Rückhalt und die Fürsorge, die Ermutigungen und den unerschütterlichen Glauben an den Erfolg dieser Dissertation.

M.Sc. Nike Walter

CURRICULUM VITAE



M.Sc. Nike Walter

Universitätsklinikum Regensburg
Klinik und Poliklinik für Unfallchirurgie
Franz-Josef-Strauß-Allee 11
93053 Regensburg
Telefon: 0941 944-6799
Email: nike.walter@ukr.de

M.Sc. Nike Walter

Persönliche Daten

Name	Nike Walter
Geburtsdaten	05. September 1991 in Braunschweig
Familienstand	Ledig

Schulbildung

2004-2011	Gymnasium Kleine Burg in Braunschweig
	Abitur: Note 1,8

Akademische Ausbildung

10/2011- 09/2014	Bachelorstudium Biotechnologie an der Technischen Universität Braunschweig
10/2014- 09/2017	Masterstudium Biotechnologie an der Technischen Universität Braunschweig Titel der Masterarbeit: Self- organized criticality in a meditative brain state: High gamma MEG activity during focused attention (Note 1,6)

M.Sc. Nike Walter

Seit 02/2019

Anfertigung einer
Dissertation in der Abteilung
für Psychosomatische
Medizin,
Universitätsklinikum
Regensburg zur Erlangung
des
humanwissenschaftlichen
Doktorgrades Dr. sc. hum.

Seit 10/2021

Studium der Humanmedizin
an der Universität
Regensburg

Universitäre Tätigkeit

Vertretung der
Promovierenden im
Leitungsgremium und im
Beirat des Zentrums zur
Förderung des
wissenschaftlichen
Nachwuchses der
Universität Regensburg

Mitwirkung beim Aufbau
des Landesnetzwerks der
Promovierendenvertretungen
in Bayern (LaProBay)

M.Sc. Nike Walter

Wissenschaftliche Tätigkeit

Seit 02/2020

Klinik und Poliklinik für
Unfallchirurgie,
Universitätsklinikum
Regensburg unter der
Leitung von Prof. Dr. Dr. V.
Alt

08/2018-
02/2020

Abteilung für
Psychosomatische Medizin,
Universitätsklinikum
Regensburg unter der
Leitung von Prof. Dr. T.
Loew

04/2017-
08/2018

Abteilung für
Verhaltensneurologie,
motorisches Lernen und
Hirn-Maschine Interaktion,
Leibniz Institut für
Neurobiologie, Magdeburg
unter der Leitung von Prof.
Dr. H.-J. Heinze

10/2016 –
01/2017

Abteilung Regulation in der
Infektionsbiologie, Max-
Planck-Institut für
Infektionsbiologie, Berlin
unter der Leitung von Prof.
Dr. E. Charpentier

M.Sc. Nike Walter

Fortbildungen

12/2021	Erwerb Zertifikat Hochschullehre Bayern (Universität Regensburg)
02/2020	Zuteilung der Erlaubnis zur berufsmäßigen Ausübung der Heilkunde beschränkt auf das Gebiet der Psychotherapie (Gesundheitsamt Regensburg)
04/2017- 08/2018	Funktionelle Entspannung“- tiefenpsychologische orientierte Körpertherapie (Abteilung für Psychosomatische Medizin, Universitätsklinikum Regensburg)
10/2016 – 01/2017	Psychodynamische Psychotherapie (Abteilung für Psychosomatische Medizin, Universitätsklinikum Regensburg)

M.Sc. Nike Walter

Mitgliedschaften

Deutsche Gesellschaft für
Orthopädie und
Unfallchirurgie

Deutsche Gesellschaft für
Unfallchirurgie

Deutsche Gesellschaft für
Psychiatrie und
Psychotherapie,
Psychosomatik und
Nervenheilkunde

Gesellschaft für
Bewusstseinswissenschaften
und Bewusstseinskultur